



HAL
open science

Disparity, an unified metric to compare the responses of biodiversity to past and current crises : a test with dragonfly wings

Isabelle Deregnaucourt

► To cite this version:

Isabelle Deregnaucourt. Disparity, an unified metric to compare the responses of biodiversity to past and current crises : a test with dragonfly wings. Populations and Evolution [q-bio.PE]. Sorbonne Université, 2020. English. NNT : 2020SORUS202 . tel-03905216

HAL Id: tel-03905216

<https://theses.hal.science/tel-03905216>

Submitted on 18 Dec 2022

HAL is a multi-disciplinary open access archive for the deposit and dissemination of scientific research documents, whether they are published or not. The documents may come from teaching and research institutions in France or abroad, or from public or private research centers.

L'archive ouverte pluridisciplinaire **HAL**, est destinée au dépôt et à la diffusion de documents scientifiques de niveau recherche, publiés ou non, émanant des établissements d'enseignement et de recherche français ou étrangers, des laboratoires publics ou privés.



Sorbonne Université

Ecole doctorale 398 – Géosciences, ressources naturelles et environnement

UMR 7207 – Centre de Recherche en Paléontologie - Paris

UMR 7204 – Centre d'Ecologie et des Sciences de la Conservation

La disparité, une métrique unifiée pour comparer les réponses de la biodiversité aux crises passées et actuelles : un test avec les ailes de libellules

Par Isabelle Deregnacourt

Thèse de doctorat en Paléontologie & Biologie de la Conservation

Dirigée par Loïc Villier & Romain Julliard

Présentée et soutenue publiquement le 17 décembre 2020

Devant le jury composé de :

M. Luc Abbadie	Professeur, Sorbonne Université	Examineur
M. Alexander Blanke	Professeur, Universität Bonn	Rapporteur
M ^{me} Carolin Haug	Research associate, Ludwig-Maximilians-Universität München	Rapporteur
M. Adrien Perrard	Maître de conférences, Université Paris-Diderot	Examineur
M. Jérémie Bardin	Ingénieur d'études, Sorbonne Université	Co-encadrant
M. Olivier Béthoux	Maître de conférences, Muséum National d'Histoire Naturelle	Co-encadrant
M. Romain Julliard	Directeur de Recherche, Muséum National d'Histoire Naturelle	Co-directeur
M. Loïc Villier	Professeur, Sorbonne Université	Co-directeur

Remerciements

Cette thèse a été possible grâce aux financements de l'Association Sorbonne Université (anciennement, Sorbonne Universités). Je remercie le Centre de Recherche en Paléontologie - Paris, le Centre d'Ecologie et des Sciences de la Conservation, l'Ecole Doctorale 398 et Sorbonne Université de m'avoir permis d'effectuer ma thèse dans de bonnes conditions.

Tout d'abord, merci aux rapporteurs Carolin Haug et Alexander Blanke d'avoir accepté de relire mon travail ainsi qu'aux deux examinateurs Luc Abbadie et Adrien Perrard.

Merci aux DAAD de m'avoir permis de partir un mois à Cologne dans le cadre du programme de financement "Forschungsstipendien - Kurzstipendien, 2019". Merci à Alexander Blanke d'avoir partagé ses données avec moi dans ce cadre et merci aussi à son équipe, Carina, Melina et Peter pour leur accueil si chaleureux.

Merci à Lars Hendrich de m'avoir permis d'accéder aux collections de Munich (Zoologische Staatssammlung, München), de photographier et d'emprunter de nombreux spécimens. Merci à Tony Robillard, André Nel et à Laurent Albenga de m'avoir permis d'accéder aux collections d'entomologie du Muséum National d'Histoire Naturelle de Paris, d'emprunter et de photographier de nombreux spécimens.

Merci à Rosser Garrison pour l'envoi d'ailes d'odonates, à Dmitry Vassilenko pour les photos de spécimens fossiles et à John Anderson pour sa collaboration dans les manuscrits d'article. Un immense merci à Alexandre Lethiers pour tous ses dessins. Merci aussi à Sylvain Gerber pour ses conseils.

Merci à Benoît Fontaine pour son aide précieuse sur ces domaines et logiciels où je ne connaissais rien. Merci à Axel Dehalleux, Thomas Bitsch, Pascal Guy et Paul Chatelain de m'avoir initié si gentiment aux sorties naturalistes et à l'identification des odonates. Merci à Charlotte Giordano d'avoir participé à la collection de travail.

Merci à mes directeurs et encadrants de m'avoir fait confiance pour mener à bien ce projet de thèse. Merci à Romain Julliard de m'avoir permis de mettre un pied dans la biologie de la conservation. Merci de t'être montré disponible tout au long de ces trois ans. Merci Loïc Villier et Jérémie Bardin d'avoir toujours été présents, d'avoir pris le temps de répondre à mes questions, même les plus bêtes. Merci pour tous vos conseils, toutes vos corrections, même le soir et le week-end, et merci aussi pour les conseils oenologiques. Merci Olivier Béthoux d'avoir initié et rendu ce projet possible. Merci de t'être montré si disponible et encourageant. J'ai beaucoup appris à vos côtés. J'ai eu beaucoup de chance

de vous avoir comme encadrants et j'espère avoir l'occasion de continuer à travailler avec vous dans les années à venir.

Je souhaite également remercier tous les habitants du 46-56 5ème étage, les permanents mais aussi ceux de passage au cours de ces trois dernières années. Merci pour vos conseils, vos encouragements et toutes les discussions pendant les pauses café. Merci à Sylvie Crasquin de m'avoir accueillie au sein du laboratoire.

A mes amis, merci pour votre soutien et tous les verres partagés. Merci Anne-Hélène, Kelly et Sarah. Merci aussi à ceux toujours disponibles pour aider, papoter ou juste décompresser, Marjorie, Louise, Paul, Alexis, Margot, Mélanie et à ceux que j'oublie. Merci à la team com'event de Doc'Up, Djamila, Guillaume et surtout Antoine.

A mes co-bureaux, un merci tout particulier. Merci Marine pour toutes ces discussions, tes conseils et ton soutien. Merci à Béatrice pour ta bonne humeur à toute épreuve qui remonte toujours le moral. Enfin, merci Laura. Ce fut un honneur de partager ces trois ans avec toi du premier au dernier jour. Merci pour ces longues soirées de travail, ces samedis, ces discours inspirants et ces karaokés improvisés. Merci d'être une si bonne amie.

Je tiens également à remercier ma famille pour m'avoir soutenue durant ces trois années et de s'être intéressée sincèrement à ce que je fais. Merci aussi à Nina pour le réconfort. Enfin, un immense merci à mon conjoint. Merci pour ton soutien sans faille. Merci de m'avoir supporté et nourri durant ces trois années. Je n'en serais pas arrivé jusque là sans toi.

Pour finir, merci à toutes les odonates sacrifiées au cours de mon projet. J'espère faire en sorte que ce ne soit pas en vain et d'avoir pu, au moins à mon échelle, sensibiliser à votre sujet.

Contents

Introduction	1
1 Ascertaining homologies, a prerequisite to an accurate description of disparity	7
1.1 Historical context	7
1.2 The case of the Protomyrmeleontoidea	11
1.2.1 Abstract	11
1.2.2 Introduction	12
1.2.3 Material and Methods	12
1.2.4 Systematic Palaeontology	15
1.2.5 Discussion	20
1.3 Vein fusion altering the usual vein elevation	21
1.4 Distinguishing main vs. intercalary veins	21
1.5 Remaining uncertainties	22
1.6 Operational homology scheme for morphometrics	23
2 From specimens to morphospace and disparity measures	27
2.1 From specimens to pictures	28
2.1.1 Specimen collection & conservation	28
2.1.2 Wing pictures acquisition	29
2.1.3 Fossil specimen pictures	31
2.2 From pictures to landmarks	32
2.2.1 Wing shape description	32
2.2.2 Landmarks selection	32
2.2.3 Comparison between sliding semi-landmarks and fixed landmarks approaches	35
2.2.4 Sliding landmarks parametrization	37
2.3 Morphospace and species reference shape: an example with French odonates	41
2.3.1 Inventory data and species lists	41
2.3.2 Reference shapes for each species	43
2.4 Disparity	46

3	Odonata disparity in Ile-de-France	49
3.1	Introduction	49
3.2	Material & Methods	52
3.2.1	Sites selection	52
3.2.2	Landscape structure	52
3.2.3	Diversity	55
3.2.4	Disparity	56
3.3	Results	58
3.3.1	Sensitivity analysis and choice of parameters	61
3.3.2	Disparity & Diversity	67
3.3.3	Landscape structure	70
3.3.4	Forecast of diversity loss in urban environments	72
3.4	Discussion & Conclusion	74
3.4.1	Robustness of the Steli data and parametrisation of disparity analyses	74
3.4.2	Diversity and disparity patterns	74
3.4.3	Perspectives	77
4	Odonata disparity during the Permian and the Triassic	79
4.1	Introduction	79
4.2	Fossils species selection	83
4.3	New data on Triassic odonates	83
4.3.1	New gondwanian Triassic material	83
4.3.2	A new Zygophlebiida from Molteno reconstructed	84
4.3.3	Reconstruction of <i>Moltenagrion koningskroonensis</i>	98
4.3.4	Completing Triassic dataset with retro-deformed Madygen material	99
4.4	Disparity analysis	101
4.4.1	Material & Method	101
4.4.2	Results	104
4.4.3	Discussion	107
	General conclusion	111
	The challenge of comparing Recent and fossil biodiversity	111
	Could the effect of landscape artificialization be compared to the effects of the major mass extinction of the Permo-Triassic transition, 250 My ago? . . .	112
	Perspectives	113
	Bibliography	115
	Annexes	129
	List of Figures	169
	List of Tables	171

Introduction

It has been demonstrated that the community composition and variety of organisms through time has been dramatically affected by five major crises during the past 500 million years (Alroy, 2008). The recent alarming loss of species induced by human activities has sparked the proclamation of a sixth one (Myers and Knoll, 2001). However, it is still difficult to compare selectivity and severity of recent with past extinctions. The fossil record samples a very limited amount of the initial diversity of organisms. Fossil datasets are also subject to enhanced sampling biases, and individual samples may represent various temporal and spatial resolutions. Diversity estimates like “species richness” are especially sensitive to analytical difficulties and to sampling biases (Foote, 2001). Estimates of species richness cannot be applied in the same way for extant and fossil assemblages without an alteration of the data resolution on the Recent. Metrics allowing to formally test hypotheses on similar properties (or not) of historical crises with the current one, such as the intensity, selectivity and recomposition processes at stake, need to be investigated.

Gould (1989) developed the idea that the diversity of morphologies might be a relevant approach, complementary to taxonomic diversity. His main idea was that, in the early history of a group, body plans, and thus morphological diversity, rise while taxonomic richness keeps limited. Such a decoupling of disparity and diversity was understood as a major feature of evolutionary radiations. Foote (1993a, 1997a,b) and Wills et al. (1994, Wills, 1998) formalized the metrics aiming to quantify morphologic diversity, called "disparity". Several disparity metrics are available that can be gathered into three categories, whether they describe size of the occupied morphospace, density of observations within the morphospace, and position of the observations within the morphospace (Foote, 1993b; Ciampaglio et al., 2001; Guillerme et al., 2020). Those different metrics have different levels of robustness and explore different aspect of disparity. They can help characterizing changes in morphospace occupation, trends in disparity, like expansion, change of shape of a taxa distribution by exploring their spread and spacing within the morphospace (Ciampaglio et al., 2001; Hopkins and Gerber, 2017). The contrast between morphological and taxonomic diversity has been recognized as a powerful tool to address macroevolutionary questions. Disparity temporal trends have been used to described evolutionary radiations but also to characterize the properties of extinction events in the fossil record

(Foote, 1993b).

Taxonomic diversity increases through diversification events but disparity may remain constant if morphological constraint stay high (Fig. 1A). In such case, size metric and position may remain constant, whereas dispersion decreases. Because of the morphological constraint new taxa have close morphologies, less dispersed within the morphospace. Disparity can increase before diversity, a case revealing of an early diversification event, which matches the initial idea of Gould (Fig. 1B). As an example, the scenario of fast growing disparity is favoured by Labandeira et al. (2000) in the interpretation of insect mouthpart evolution. In such a scenario, size and density metrics would increase early and then range could increase slowly while density could slightly decrease. Disparity and diversity can also increase more or less concurrently, revealing the absence of major morphological constrains (Fig. 1C). In that case, the range increases concurrently with diversity whereas dispersion and position remain constant. When taxonomic diversity decreases, i.e. when extinction overcomes appearance numbers, disparity may, or not, decrease cogently. The disappearance of large regions of the morphospace is expected when functional traits are negatively selected. The selection can target extreme morphologies (Fig. 1D). The size metric would decrease while position and density remain constant. This scenario can be related to a loss of niche specialists. If there is a selection on large peculiar regions of the morphospace, size metric would decrease. In this scenario the position is of particular relevance, being strongly impacted (Fig. 1E), in the contrary of what would be observed for extreme morphologies selection. If disparity is steady or increases while diversity decreases, then it can be revealing of a morphologically non-selective extinction, either driven by traits independent of the morphospace or simply resulting in a random sorting (Fig. 1F). Under such scenario, size metric and position should remain steady while dispersion increases. These trends of the different metrics of disparity, with potentially a more important increase in dispersion, could be revealing of a loss of intermediate morphologies (Fig. 1G).

According to Foote (1993b), when compared to diversity, disparity can provide insights into evolutionary processes, but analysis of disparity itself allows documentation and interpretation of the evolution, success and demise of a group. Metrics of morphological diversity are much less sensitive to sampling heterogeneity than species richness. The only limitation is that different conformations of the morphospace may result in similar disparity values.

Quantification of disparity requires building of relevant morphospace. Theoretical morphospace have been proposed for some group of organisms (McGhee, 1999) but in most cases only empirical morphospaces, based on observed records, are available and most often appropriate (Eble, 2000b). Several ways of quantifying morphology are commonly used. Numbers of morphotypes, or discretely-coded morphological characters, which can be extracted from character matrices used in phylogenetic studies, have been

used (Briggs et al., 1992; Foote, 1992). However, morphometric data are considered as the most objective measure (Wills et al., 1994). Morphometric geometry is of standard use when landmarks, point homologies, can be recognized in all forms under comparison (Briggs et al., 1992). As far as the descriptive methods properly sample morphology, the reconstructed trends in disparity patterns are likely to sample a similar story (Villier and Korn, 2004; Romano et al., 2017).

Despite their potential, disparity studies and contrast between diversity and disparity have rarely been applied to address biogeographic patterns, the effect of anthropogenic pressures, or in conservation biology (Roy et al., 2001; Neige, 2003; McClain et al., 2004; Neustupa et al., 2009).

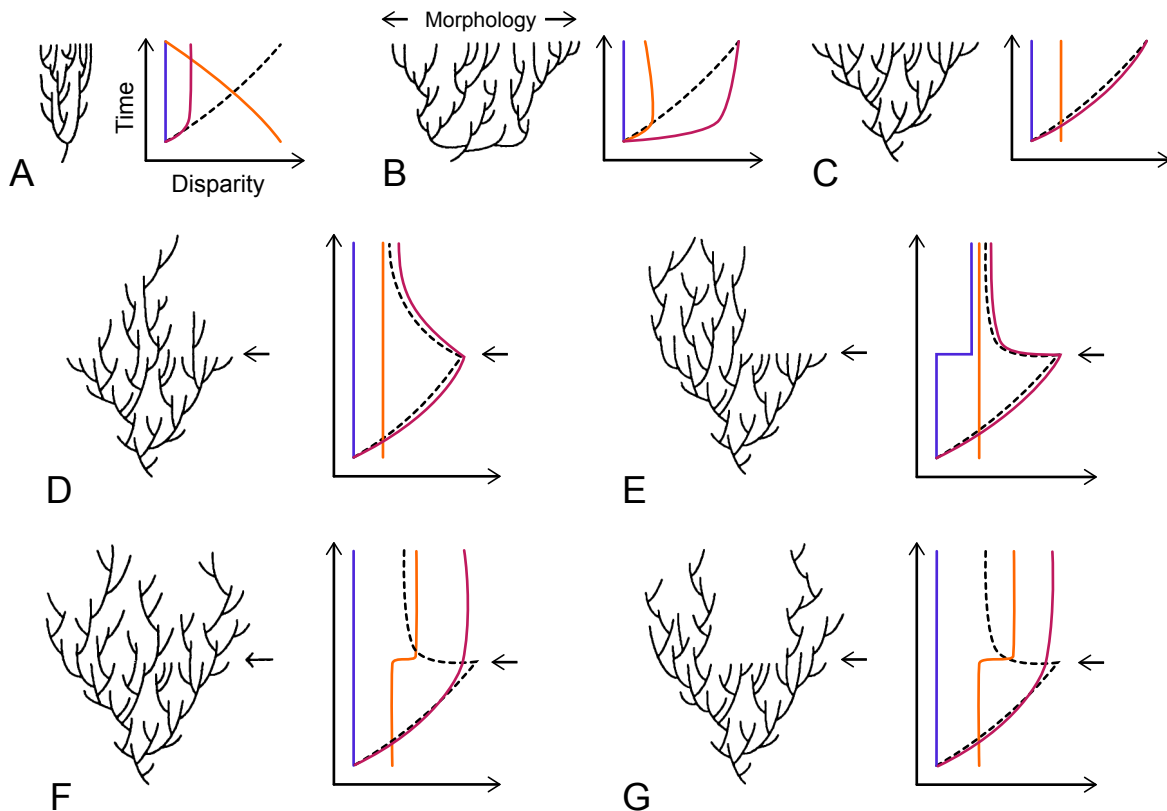


Figure 1 – Idealized diversity histories (modified from Foote, 1993b, Fig. 1, p. 192) and the corresponding potential diversity and disparity curves over time. The evolution of three metrics of disparity is represented: size, dispersion and position. **A-C**, diversification events; **D-G**, extinction events. Dotted black line correspond to diversity; red line corresponds to size metric, orange line to dispersion and violet line to position; arrows (on **D-G**) indicate time of maximal taxonomic diversity.

My PhD aims at comparing patterns of past and extant biodiversity crises on a model group, the odonates, using the theoretical framework of disparity studies. The goal is to address the following questions:

- How patterns of disparity of odonates are impacted by:
 - habitat perturbation due to human imprint;
 - a past mass extinction event, such as the Permian-Triassic one?
- Is there a consistency between these variation patterns? Can we infer common recomposition processes of diversity specific to biological crises conditions?

Even though insects represent the most speciose taxon on earth, their past disparity has been seldom investigated (Labandeira et al., 2000; Stockmeyer-Lofgren et al., 2003; Nel et al., 2018). The insect order Odonata, including dragonflies (Anisoptera; with the closely-related Epiophlebiidae), damselflies (Zygoptera) and fossil stem-groups, was found to be particularly suitable for this project. Odonates are represented nowadays by about 6000 living species (Dijkstra et al., 2013) and by about 1000 fossil species (Paleobiology Database, 2019). Odonata wing venation homologies are complex and have been securely identified (Riek and Kukalová-Peck, 1984; Bechly, 1996; Béthoux, 2015), which provide a large number of landmarks useful for morphometric analyses. Odonates have been existing for 320 million years (Carpenter, 1992; Grimaldi and Engel, 2005; Petrusevičius and Gutiérrez, 2016), a period covering three of the five main historical extinctions. Moreover, ecology of extant species is well known and dispersal ability of the majority is important: community composition might be considered fitted to environmental conditions. Finally, the group is considered threatened. As a consequence, it is subject to protective measures and monitoring, in part realised by citizen sciences programs.

Herein, we are investigating odonates disparity through their wing morphology, which are the predominantly found structures in the odonate fossil records. To accurately quantify wing morphology it is essential to rely on well-ascertained wing homologies. In the first chapter, we are presenting the main consensus on wing venation homologies. Some peculiar cases are discussed and a basic pattern of wing venation homologies, applicable to both extant and fossil species, is presented.

To investigate disparity we are using a morphometric geometric approach based on this pattern of homologies. In the second chapter we are detailing the steps leading from actual specimens to the computation of their disparity. Outcomes of an exploration of different approaches to quantify wing shapes are presented and the selected metrics of disparity are detailed.

In the third chapter, human impact on taxonomic diversity and disparity of extant odonates is explored focusing on artificialization in the urbanised Ile-de-France Region. An important citizen sciences network for odonates monitoring (Steli) provides occurrence

data of highest quality for statistical analyses, for several sites, ranging from the Paris centre to the country-side margins of the region. The primary working hypotheses would be that a selective pressure induced by anthropization should induce correlation between diversity and disparity along environmental gradients. A selective sorting of species should favour generalist shapes and eliminate the more specialized ones (Clavel et al., 2011), therefore reducing disparity. On the opposite, if morphospace occupation keeps grossly the same among samples, even in low diversity ecosystems, then the signal would mimic the pattern regarded as typical of a mass extinction (Foote, 1993b).

The effects of the Permo-Triassic mass extinction is explored as an historical reference in the fourth chapter. This crisis is especially interesting, being the one that have the most impacted insects' diversity (Béthoux et al., 2005; Ponomarenko, 2016). However, the patterns of extinction on insects and more particularly on odonates keeps poorly understood. Studies on insect functional disparity using characters related to feeding ecology (i.e. mouthparts; Labandeira et al., 2000; Nel et al., 2018) have shown no impact of this crisis on morphological diversity. Here we focus on odonates wing disparity through the crisis as the majority of the fossil record consists of wings.

Chapter 1

Ascertaining homologies, a prerequisite to an accurate description of disparity

Contents

1.1	Historical context	7
1.2	The case of the Protomyrmeleontoidea	11
1.2.1	Abstract	11
1.2.2	Introduction	12
1.2.3	Material and Methods	12
1.2.4	Systematic Palaeontology	15
1.2.5	Discussion	20
1.3	Vein fusion altering the usual vein elevation	21
1.4	Distinguishing main vs. intercalary veins	21
1.5	Remaining uncertainties	22
1.6	Operational homology scheme for morphometrics	23

1.1 Historical context

To accurately quantify wing morphology it is essential to rely on well-ascertained wing venation homologies (or, more accurately, conjectures of primary homology). Insect wing venation is composed of a primary branching pattern, composed of "main veins", usually corresponding to the tracheal network, and of a secondary branching pattern, composed of "cross-veins", usually free of trachea. Based on these premises, attempts were made

to derive wing venation homologies for the entire winged insects, early accounts including Redtenbacher (1886) and Brongniart (1893), among many others. The discussion continues nowadays for various insect orders.

As for dragon- and damselflies (Odonata), wing venation homologies remained a matter of debate for most of the 20th century. Despite the ancient Meganeuridae being known, attempts to relate the wing venation of stem- and crown-Odonata to other insect groups abutted to a number of issues. Among them was the propensity, in odonate wings, of cross-veins to convert into main-vein-like elements, including so-called "intercalary veins", which can prove difficult to distinguish from surrounding genuine main veins, even though they display an elevation reversed with respect to them. Confusion also arose from persisting gaps in the documentation of venation patterns which later proved to have experienced intense modifications since the Pennsylvanian, including multiple fusions of main veins.

An important step in the debate was the proposal made by Tillyard (1925) who, that time, adopted the view that the insect wing venation groundplan is composed of a number of primary veins sharing the same branching pattern, specifically a convex, anterior branch and a concave posterior one (nowadays called the "serial pattern"). With some minor discrepancies, Tillyard (1925) used a terminology consistent with Lameere's proposal (Lameere, 1922, 1923). This terminology was later formalized by Kukalová-Peck (1991), that most subsequent works adopted: ScP, posterior Subcosta; R, Radius; RA, anterior Radius; RP, posterior Radius; RP1+2, anterior branch of RP (to be further divided into RP1 and RP2); RP3+4, posterior branch of RP (to be further divided into RP3 and RP4); M, Media; MA, anterior Media; MP, posterior Media; Cu, Cubitus; CuA, anterior Cubitus; CuP, posterior Cubitus; AA, anterior Analis. This nomenclature is used hereafter for the main veins, complemented by Deregnaucourt et al. (2017) for the terminology to apply to intercalary veins. In details, Irp_1-rp_2 is the intercalary vein occurring between RP1 and RP2 (also termed "IR1"), and $Irp_{1+2}-rp_{3+4}$ that occurring between RP1+2 and RP3+4 (also termed "IR2").

The key point in Tillyard's thesis is the presumed loss of MP and CuA as free veins, beyond the wing base. He derived this view from the study of a remarkable specimen of Meganeuridae recovered from Elmo (Early Permian; Kansas, USA; Fig. 1.1). Unlike previously known Meganeuridae, vein elevations were preserved in a pristine manner in this material. Tillyard recognized a fusion of M with R, owing to the occurrence, after ScP, of two closely adjoining veins. The resulting vein further splitting into a convex vein (certainly RA), a concave vein (certainly RP) and a convex vein (likely MA), the concave MP had to have vanished. He observed what he believed was a remnant of it (red thick arrow in Fig. 1.1D) but this observation was not corroborated. He also noted a loop, near the wing base, he regarded as formed by CuA and CuP diverging and fusing shortly afterwards. The resulting vein being concave, the convex CuA had to have vanished. Finally, a strong oblique structure, his "anal crossing", located between CuP (his "Cu2")

and AA (his "1A"), was not regarded as part of the main veins scheme, despite its strength. This proposal was further formalized in Tillyard and Fraser (1938) and was followed for decades, including prominent textbooks (e.g., Carpenter, 1992; Rohdendorf, 1962).

It is important to mention that even though Tillyard (1925: p.42) stressed that "Protodonata" (including, to his opinion, Meganeuridae and a few other species) and Odonata were two clearly distinct taxa, he also stated that MP and CuA (his "Cu1") were not present as free veins beyond the wing base in the Meganeuridae, but also in species he regarded as stem-Zygoptera, i.e. crown-Odonata. It follows that Tillyard, in some respect, regarded a subset of "Protodonata" as stem-Odonata (and see Tillyard and Fraser, 1938).

This paradigm was challenged by Riek and Kukalová-Peck (1984) who described two early Pennsylvanian fossils (herein referred to as "geropteromorphs", a grade) which decisively demonstrated that Tillyard's "anal crossing" was actually composed of secondarily fused CuA and CuP, this stem then fusing with AA (Fig. 1.1C,F). Another important input from specimens described by Riek and Kukalová-Peck's is that four veins occur between ScP and AA at the wing base (there are three in Meganeuridae, two in extant Odonata). These authors interpreted them as RA, RP, M and Cu, successively. It was then derived that MP fuses with Cu in Odonata other than "geropteromorphs". This made Tillyard's CuP and AA available for being interpreted as the supposedly missing MP and CuA, respectively. This definitely reconciled the wing venation of Odonata with the serial insect wing venation groundplan: all extant Odonata possess a R+MA stem and a MP+Cu (or MP+Cu+AA) stem at the wing base. This proposal was applied at the scale of the entire order by Bechly (1995) and was confirmed by detailed analysis of wing base structures in extant Odonata (Jacquelin et al., 2018). It is widely accepted nowadays. However, some aspects remained unclear, notably the actual course of MA in "geropteromorphs".

Béthoux (2015) proposed an alternative to Riek and Kukalová-Peck's interpretation of the four veins located between ScP and AA, at the wing base, in "geropteromorphs", as follows: RA (as opposed to R), MA (as opposed to RP), MP (as opposed to M) and Cu. In other words, instead of assuming an R system splitting into RA and RP at the very wing base, as proposed by Riek and Kukalová-Peck, Béthoux assumed that the M system, instead, is split. This was more consistent with the conclusion of Riek and Kukalová-Peck that, in extant Odonata, MA is fused with R, and MP with Cu, from the wing base (which implies a very early split of the M system). Another alternative was proposed by Petrulvičius and Gutiérrez (2016), with RA, RP+MA, MP and Cu composing the four veins of interest, but this implies that both R and M systems are split at the wing base. These aspects are of minor importance, as they concern "geropteromorphs" only.

Ultimately, the recent proposal by Trueman and Rowe (2019a, and see associated debate, Nel et al., 2019; Trueman and Rowe, 2019b) lacks relevance as a consequence of

ignoring "geropteromorphs", arguably the most important species to address the question of wing venation homologies in Odonata.

Even if a consensus has been reached for most of Odonata there are still some peculiar cases that required further discussion, in the context of this project.

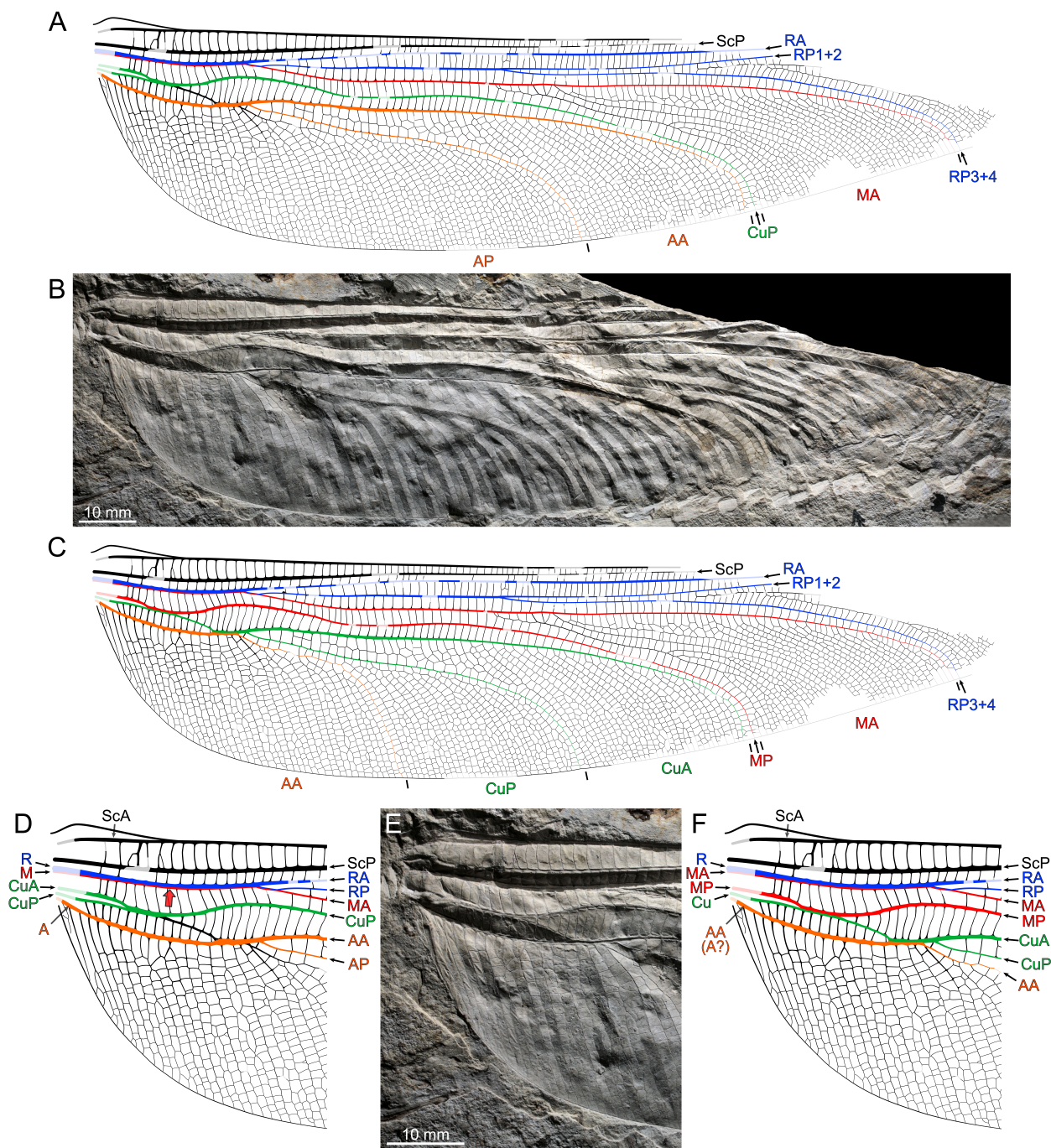


Figure 1.1 – *Megatypus schucherti* Tillyard, 1925 from the Elmo locality (Early Permian, Kansas, USA). **A**, **D**, wing venation interpretation according to Tillyard (1925), overview (**A**) and details of the base (**D**); **C**, **F**, wing venation interpretation according to Riek and Kukalová-Peck (1984), overview (**C**) and details of the base (**F**); **B**, photograph, overview; **E**, photograph of the wing base. Red arrow on D corresponds to the location of a supposed distinct MP according to Tillyard (1925). From Béthoux et al. (*in prep.*).

1.2 The case of the Protomyrmeleontoidea

The Protomyrmeleontoidea are a Mesozoic group of damselfly-like Odonata. Their peculiar wing shape and occurrence during the Triassic made them of particular importance for the part of the project focusing on the evolution of disparity during the Permo-Triassic transition (see Chapter 4). Two competing interpretations of Protomyrmeleontoidea wing venation homologies (Zessin, 1991; Nel and Henrotay, 1992) jeopardized their inclusion in disparity analyses. In details, they disagreed on the position of the anterior stem of RP3+4, a vein portion used in the quantification of shape, and thus disparity (see Chapter 2). We investigated a remarkable specimen from the Molteno Formation (Triassic; South Africa) which led us to derive a third interpretation, allowing an adequate treatment of the Protomyrmeleontoidea in the morphometric analysis. This part consist of a paper manuscript published as an online preprint in *Historical Biology*:

**The wing venation of the Protomyrmeleontidae (Insecta:
Odonoptera) reconsidered thanks to a new specimen from
Molteno (Triassic; South Africa)**

Historical Biology, 2019

Deregnacourt, I., Wappler, T., Anderson, J. M., and Béthoux, O.

<https://doi.org/10.1080/08912963.2019.1616291>

Supplementary file available at: <https://doi.org/10.5061/dryad.jh3m624>

<http://zoobank.org//urn:lsid:zoobank.org:pub:6AF81E13-E57B-4EF8-BBBB-5392EF439E87>

1.2.1 Abstract

Wing venation homologies of the Protomyrmeleontidae, a widespread group of damselfly-like stem-Odonata during the Triassic, are debated. The two main interpretations, by Zessin (1991) and Nel and Henrotay (1992), essentially disagree on the identification of RP branches. Indeed, Protomyrmeleontidae display a very complex wing venation necessarily involving, in a way or another, fusions of the concave RP branches with the convex intercalary veins. As a consequence, vein elevations in the radial area are challenging to interpret. Here, we present a new Triassic specimen from the Molteno Formation (Karoo Basin, South Africa), *Moltenagrion koningskroonensis* gen. et sp. nov.. It displays a unique venation pattern supporting a new, alternative interpretation involving a pair of supplementary intercalaries. The systematic implications of this wing venation interpretation are then discussed. The new species is assigned to the new family Moltenagrionidae fam. nov., itself considered sister-group of the family Protomyrmeleontidae, as previously delimited, both composing the super-family Protomyrmeleontoidea. Diagnoses of these taxa are revised according to our new interpretation.

Keywords: Molteno Formation; Triassic; wing venation; Protomyrmeleontidae; stem-Odonata

1.2.2 Introduction

Insect wing venation is a topic which has been the focus of numerous debates. In the early 20th century, the wing venation of Odonoptera (dragon- and damselflies and their stem-relative –some of which called griffenflies–; i.e. total-Odonata), in the context of the serial insect wing venation groundplan (Lameere, 1922, 1923), remained a contentious issue (Needham, 1903; Tillyard, 1925; Carpenter, 1992; among others; and see Bechly, 1996). In this context the discovery of early Odonoptera displaying a full set of veins consistent with the serial pattern, and the associated interpretation by Riek and Kukalová-Peck (1984) was a breakthrough. This interpretation is consensually accepted nowadays, with some minor adjustments (Bechly, 1997; Béthoux, 2015; and see Jacquelin et al., 2018). However, wing venation homologies of a few groups within Odonoptera remain obscure.

This is the case of the Protomyrmeleontidae. The earliest representatives of this extinct group of damselfly-like Odonoptera are from the Triassic, when they already had a wide distribution [Europe (Geinitz, 1887; Tillyard, 1925; Bode, 1953; Zessin, 1991; Nel and Henrotay, 1992; Martínez-Delclós and Nel, 1996; Bechly, 1997; Nel and Jarzembowski, 1998, see); Asia (Martynov, 1927; Nel et al., 2005, see); Australia (Tillyard, 1922; Henrotay et al., 1997, see); and Africa, herein]. The group is known from the Mesozoic era only. There are two main interpretations of the wing venation of this family. One essentially assumes that two branches of RP, namely RP2 and RP3, fuse (or, are fused and display a clear fork; Zessin, 1991; Fig. 1.2A, B). This proposal then assumes that RP3+4 is forked in Protomyrmeleontidae. The other interpretation assumes that RP2 has a genuine fork (resulting into RP2a and RP2b; Nel and Henrotay, 1992; Nel and Jarzembowski, 1998; Nel et al., 2005; Fig. 1.2C, D). The fact that known Protomyrmeleontidae display wing venation patterns which accumulated several transformations (including fusions of RP branches –concave– and intercalary vein –convex– into a convex common stems) makes it impossible to favour one interpretation over the other.

Herein we describe a new Upper Triassic specimen from the Molteno Formation (Karoo Basin, South Africa) displaying a unique venation pattern that prompted us to propose a third interpretation (Fig. 1.2E, F), involving a pair of supplementary intercalary veins, a structure commonly occurring among extant crown-Odonata.

1.2.3 Material and Methods

The specimen PRE/F/10334 is housed at Evolutionary Studies Institute (formerly ‘Bernard Price Institute for Palaeontology’), University of the Witwatersrand, Johannesburg, South Africa. We also studied the specimen MNHN.F.A40897 (belonging to *Protomyrmeleon brunonis* Geinitz, 1887), housed at the Muséum National d’Histoire Naturelle, Paris.

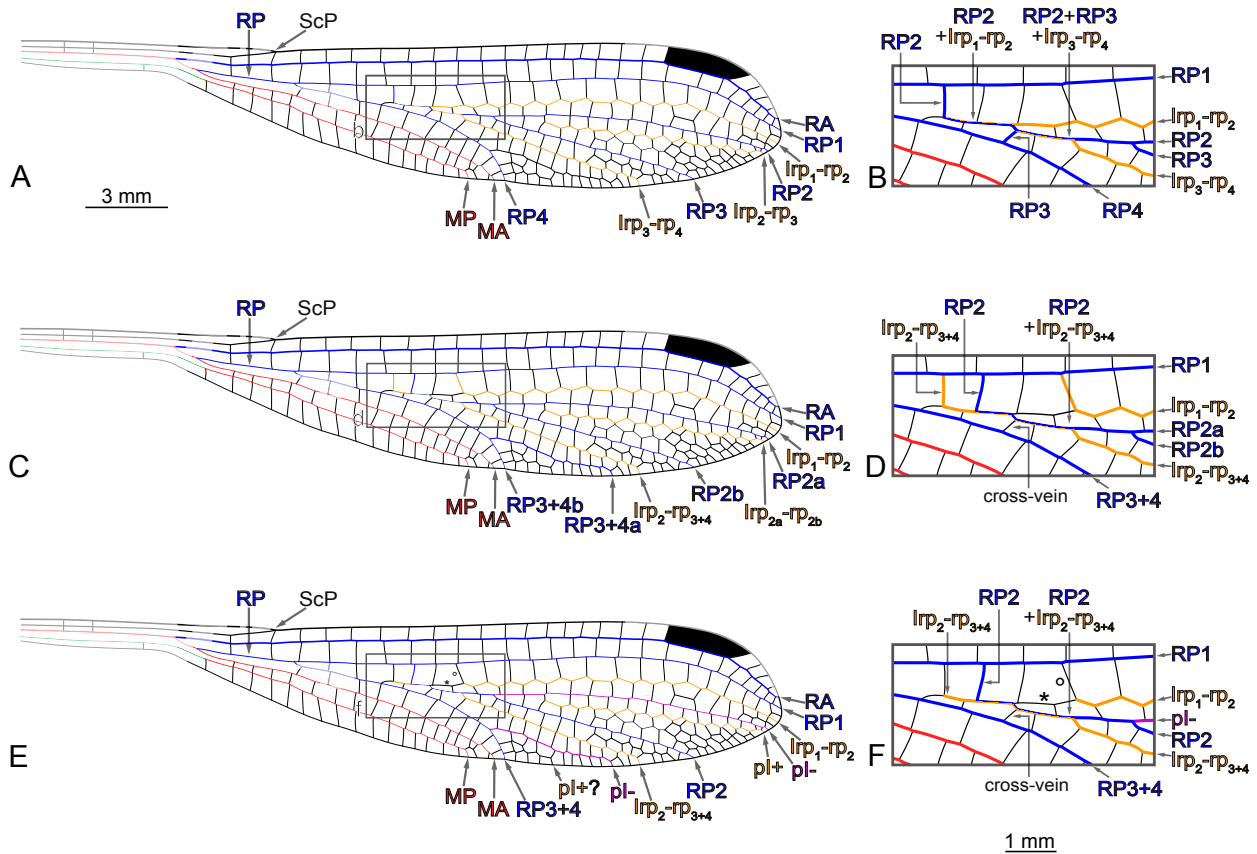


Figure 1.2 – †*Protomyrmeleon brunonis* Geinitz, 1887, specimen MNHN.F.A40897 (one of the two overlapping wings represented, left wing; all drawings flipped horizontally); Toarcian (Jurassic), Bascharage, Grand Duchy of Luxembourg. **A, B**, wing venation interpretation according to Zessin (1991), overview (**A**) and details of the radial area as located on **A** (**B**), main veins thickness increased for clarity; **C, D**, wing venation interpretation according to Nel and Henrotay (1992), overview (**C**) and details of the radial area as located on **C** (**D**), main veins thickness increased for clarity; **E, F**, new interpretation, overview (**E**) and details of the radial area as located on **E** (**F**), main veins thickness increased for clarity.

Draft drawings were prepared with the aid of a Zeiss SterEO Discovery V8 Stereomicroscope equipped with a pair of W-PL 10x/23 eye pieces, a Plan Apo S 1.0x FWD objective, and a drawing tube (Jena, Germany). Photographs were taken using a Canon EOS 5D Mark III equipped with Canon 50 mm or MP-E 65 mm macro lenses. Photographs were optimized using Adobe Photoshop CS6 (Adobe Systems, San Jose, CA, USA). Draft drawings were inked using Adobe Illustrator CS6 (Adobe Systems, San Jose, CA, USA) using both scanned draft drawings and photographs. Missing parts were reconstructed based on data on conspecific specimens (for *P. brunonis*), and data on *Obotritagrion petersi* Zessin, 1991 for the newly described species. A Procrustes superimposition has been realized to find which species of the Protomyrmeleontidae (among the ones represented by a complete wing) minimizes the distance between the ends of ScP, RP3, RP4, MA and MP.

In order to better appreciate and document the configuration of ‘supplementary sectors’ (sensu Garrison et al., 2010 below, ‘pI’), we computed RTI files of fore- and hind wings of three extant damselfly species (for details on the used RTI setting, see Béthoux et al., 2016). We provide an online Dryad dataset, cited below as ‘Deregnacourt et al. (2019b)’, in which the RTI files are available. Photographs composing Fig. 1.3 were extracted from these files.

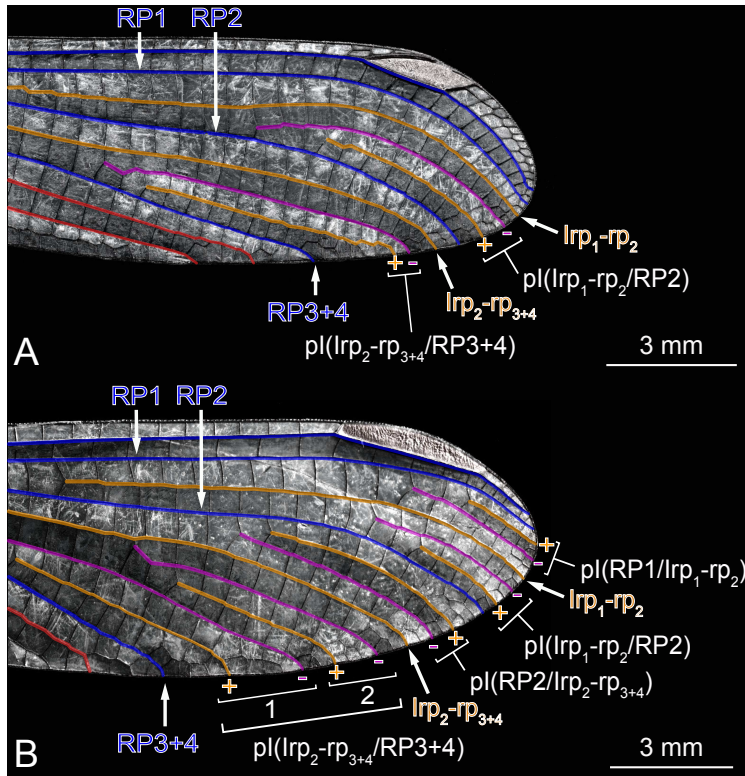


Figure 1.3 – Proposed terminology for paired intercalaries (pI), based on RTI extracts of extant Zygoptera wing apices, specular enhancement (see text for details; Rosser W. Garrison collection). **A**, right hindwing in dorsal view of a male *Dimeragrion percutibile* Calvert, 1913; **B**, right hindwing in dorsal view of a male *Heliocharis amazona* Selys, 1853.

We follow the serial insect wing venation ground pattern (Lameere, 1922, 1923). The corresponding wing venation nomenclature (Kukalová-Peck, 1991) is repeated for convenience: ScP, posterior Subcosta; R, Radius; RA, anterior Radius; RP, posterior Radius; RP1+2, anterior branch of RP (to be further divided into RP1 and RP2); RP3+4, posterior branch of RP (to be further divided into RP3 and RP4); MA, anterior Media; MP, posterior Media; Cu, Cubitus; CuA, anterior Cubitus; CuP, posterior Cubitus; AA, anterior Analis. We follow Deregnacourt et al. (2017) for the terminology to apply to intercalary veins. Additionally it proved necessary to be able to refer to intercalary veins occurring in addition to $l_{rp_1-rp_2}$ and $l_{rp_2-rp_{3+4}}$. Therefore we propose the following terminology and rationale. Based on observations made on a variety of extant representatives of Zygoptera (Fig. 1.3), we noticed that these supplementary intercalaries always occur by pairs, and that veins composing a pair have opposed elevation (i.e. one is convex, the other concave). Given the orderly alternation of convex and concave veins/intercalaries characteristic of odonate wings, the addition of intercalaries of opposite elevation, by pair, is to be expected, because it allows this order to be maintained. We then propose the terms ‘pI’, accounting for ‘paired intercalaries’. It might prove necessary to indicate

particular areas in which a pI occurs. Then, for example, for a pI occurring in the area between Irp_1-rp_2 and RP_2 , we propose the term ‘pI(Irp_1-rp_2/RP_2)’ (see Fig. 1.3A). If several pI occur in a given area, they could be numbered, starting with the longest one [see the case of pI(Irp_2-rp_{3+4}/RP_{3+4}) in Fig. 1.3B]. Finally, elevation can be mentioned to indicate a particular intercalary within a pair (pI+ and pI-). Finally, it proved also necessary to be able to refer to cross-veins connecting with an intercalary at its origin (forming, together, a horizontally-oriented Y), in the current case Irp_1-rp_2 . The cross-veins located on the anterior side, and the posterior side, are referred to as cv° and cv^* , respectively (‘ $^\circ$ ’ and ‘ * ’, respectively, on Figs. 1.2E, F, 1.5, 1.6A, C).

1.2.4 Systematic Palaeontology

The proposed classification is summarized in Fig. 1.4.

Order **Odonata** Fabricius, 1793
 Taxon **Pandiscoidalia** Nel et al., 2001
 Taxon **Discoïdalia** Bechly, 1996
 Taxon **Stigmoptera** Bechly, 1996
 Taxon †**Archizygoptera** Handlirsch, 1906
 Superfamily †**Protomyrmeleontoidea** Handlirsch, 1906
 Taxon †**Terskejoptera** tax. nov.

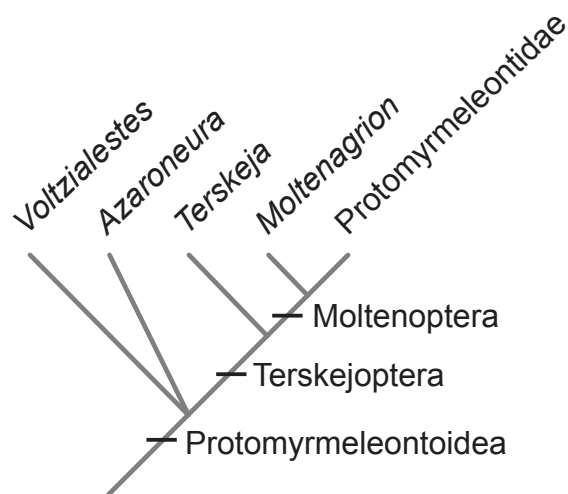


Figure 1.4 – Proposed summarized phylogeny of Protomyrmeleontoidea.

Diagnosis. In the area between Irp_1-rp_2 and RP_2 , occurrence of a pair of supplementary intercalaries of opposed elevation [i.e. occurrence of a pI(Irp_1-rp_2/RP_2)].

Composition. *Terskeja* Pritykina, 1981 and Moltenoptera tax. nov.

Remarks. The genus *Terskeja* is considered by Nel et al. (2012) as a member of the Voltzialesidae, itself sister-group of the Protomyrmeleontidae. However our comparative analysis demonstrates that this genus possess a pI(Irp₁-rp₂/RP2) (Fig. 1.5), alike *Moltenagrion* gen. nov. (Fig. 1.6A–D), *Protomyrmeleon* Geinitz, 1887 (Fig. 1.2E, F) and other Moltenoptera tax. nov. This derived structure is absent in *Voltziales* Nel et al., 1996 and *Azaroneura* Nel et al., 2012.

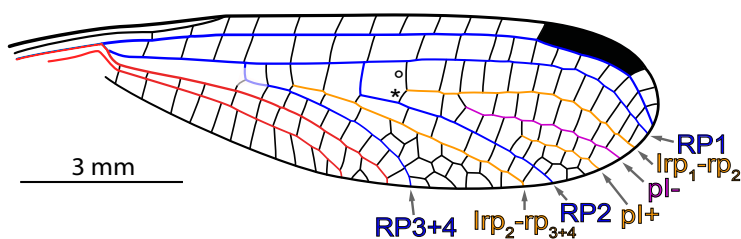


Figure 1.5 – †*Terskeja pumilio* Pritykina, 1981, redrawn with minor modifications from Pritykina (1981: fig. 25).

Taxon †**Moltenoptera** tax. nov.

Diagnosis. RP2 fused with Irp₂-rp₃₊₄ for short distance, shortly after its origin.

Composition. Protomyrmeleontidae Handlirsch, 1906 and Moltenagrionidae fam. nov.

Remarks. The occurrence of a fusion of RP2 with Irp₂-rp₃₊₄, is deduced from the fact that a portion of RP2 is convex. Given that RP2 is usually concave, it implies that it is fused with another structure. Additionally, given that RP2 becomes concave distal to the point of origin of (the free part of) Irp₂-rp₃₊₄, it implies that the ‘additional structure’ is Irp₂-rp₃₊₄. The occurrence of this fusion is easily observable in *Moltenagrion koningskroonensis* gen. et sp. nov. (see Fig. 1.6D), but the available documentation of veins elevation in this area is insufficient to assess the occurrence of the state in other Protomyrmeleontoidea.

The actual origin of RP2 in representatives of Moltenoptera is not totally evident. In Fig. 1.2E, F, it could be ‘one cross-vein more basally’. In any case a fusion with Irp₂-rp₃₊₄ occurs.

Family †**Moltenagrionidae** fam. nov.

Type genus. *Moltenagrion* gen. nov.

Included genera. Type genus only.

Diagnosis. By monotypy, as for the type genus.

Genus †**Moltenagrion** gen. nov.

Type species. *Moltenagrion koningskroonensis* sp. nov.

Diagnosis. By monotypy, as for the type species.

Remarks. The genus *Moltenagrion* can be confidently assigned to the Protomyrmeleontoidea owing the occurrence of the diagnostic character of this taxon (see above).

†***Moltenagrion koningskroonensis*** sp. nov.

(Fig. 1.6)

Diagnosis. At its origin, pI(Irp₁-rp₂/RP₂)⁺ separated from RP₂ by a convex cross-vein.

Derivation of name. From the name of the type locality, "Konings Kroon".

Material. Holotype specimen PRE/F/10334 (positive imprint only).

Description (holotype). Two-thirds of a right wing, apex missing; wing total length unknown, about 30.5 mm (27.5 mm as preserved), maximum width 4.6 mm; wing narrow, strongly petiolated; no preserved antenodals; ScP fused with the anterior wing margin basally, slightly before the separation of RP into RP₁+₂ and RP₃+₄; RA and RP+MA diverging opposite the petiole end (R+MA and RA aligned); anterior wing margin, ScP and RA bent towards the posterior wing margin between the petiole end and the nodus (possible deformation); distal to the nodus, RA parallel to the anterior wing margin, with a single row of cells between them; at its origin, RP+MA sharply diverging from RA; RP+MA divided into RP and MA shortly after the petiole end; as preserved, RA, RP₁ and Irp₁-rp₂ parallel and separated by only one row of cells; occurrence of pI between Irp₁-rp₂ and RP₂; RP₂ and pI⁻ approaching each other at the point of origin of pI⁻; RP₂ shortly fused with Irp₂-rp₃₊₄ (resulting composite vein convex); RP₂ clearly concave at its point of divergence from Irp₂-rp₃₊₄ (itself remaining convex); Irp₂-rp₃₊₄ parallel to RP₂ after their divergence; areas between RP₂ and Irp₂-rp₃₊₄, and between Irp₂-rp₃₊₄ and RP₃+₄, with a single row of cells, and 1–3 rows of cells, respectively; RP₃+₄, simple, parallel to MA with only one row of cells between them; up to two rows of cells between MA and MP; in the petiole, a single preserved cross-vein occurs between MP+Cu/MP and the posterior wing margin (it is probably CuA, possibly fused with CuP, or CuP and AA); occurrence of a linear and convex structure between MP+CuA (dotted line in Fig. 1.6A) which origin and termination are not preserved, and which cannot be detected under ethanol (it is therefore likely a crease in the membrane).

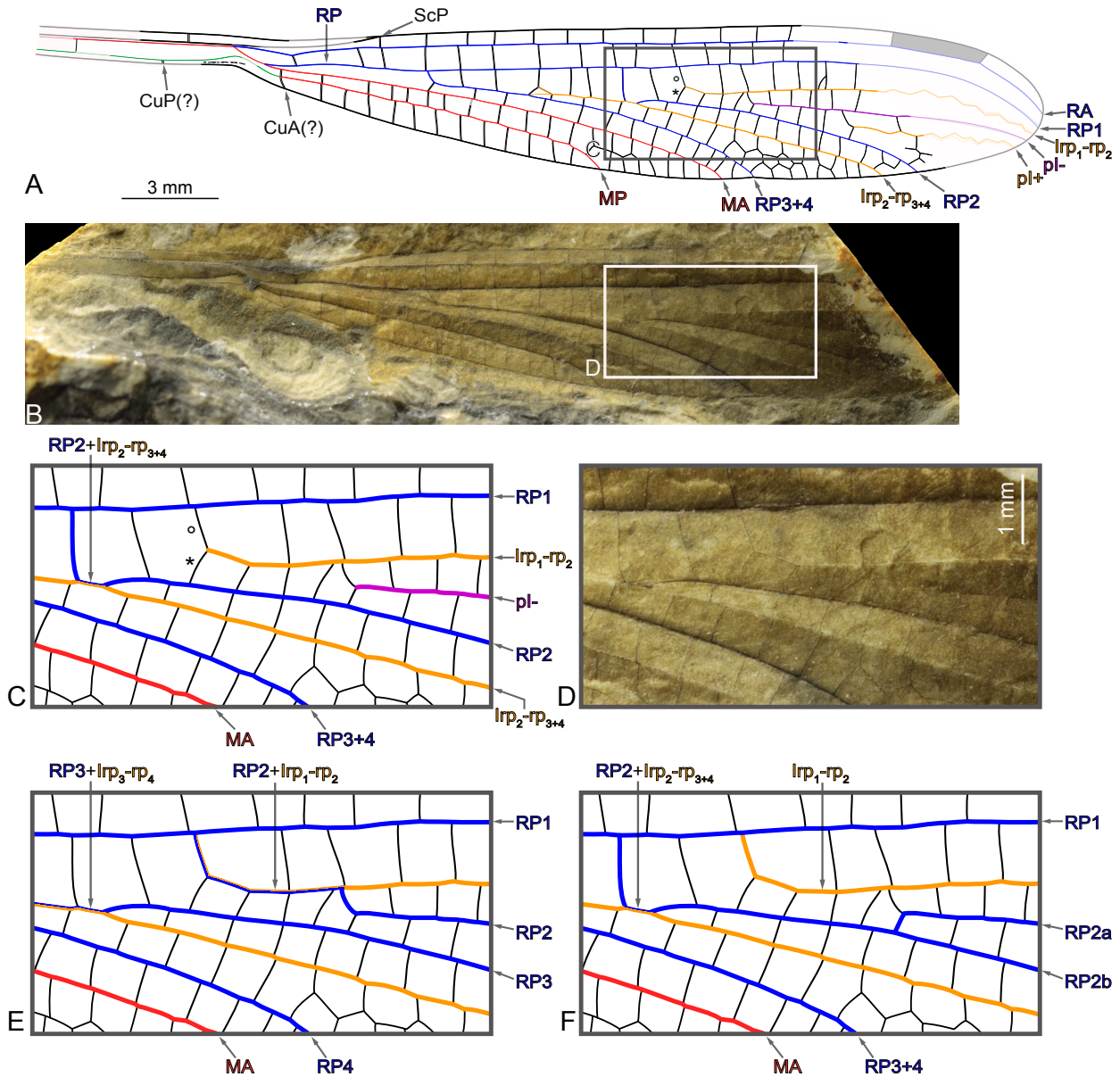


Figure 1.6 – †*Moltenagrion koningskroonensis* gen. et sp. nov., specimen PRE/F/10334 (right wing); Carnian (Triassic), Konings Kroon, Molteno Formation, Karoo Basin, South Africa. **A**, drawing, wing venation interpretation favoured herein; **B**, photograph; **C–E**, details of the radial area (drawings, main veins thickness increased for clarity); **C**, wing venation interpretation favoured herein; **D**, photograph, as located on **B**; **E**, wing venation interpretation according to Zessin (1991); **F**, wing venation interpretation according to Nel and Henrotay (1992).

Locality and horizon. Konings Kroon (locality code "Kon 222" in Anderson and Anderson (1984), Karoo basin, South Africa; Molteno Formation; Carnian, Triassic (Anderson et al., 1998).

Remarks. Minor preparation was conducted by one of us (OB) on the specimen, complementing a former preparation. A small portion of the area between RP+MA and the posterior wing margin, just basal of the RP+MA fork, was left unexposed due to a risk of damage to the specimen. The assumed position of the origin of RP2 is deduced thanks

the configuration in *Terskeja* spp. The rationale underlying our new interpretation is provided in the Discussion section.

The diagnostic character state of the species (and, as a consequence of monotypy, of the genus and family containing the species) is a plesiomorphy (it is present in *Terskeja*). Due to a lack of known, closely-related species, and to the position of the species within Terskejoptera, it proved impossible to recover any derived character state.

Family †**Protomyrmeleontidae** Handlirsch, 1906

Diagnosis. Origin of pI(Irp₁-rp₂/RP2)- (vein purple-coloured in Figure 1.2E, F, Figure 1.6A, C) indistinct from RP2.

Composition. Triassagrioninae Tillyard, 1922 (including *Triassagrion* Tillyard, 1922) and Protomyrmeleontinae Handlirsch, 1906 (including *Ferganagrion* Nel et al., 2005, *Italomyrmeleon* Bechly, 1997, *Malmomyrmeleon* Martínez-Delclós and Nel, 1996, *Mongolagrion* Nel et al., 2005, *Obotritagrion* Zessin, 1991, *Paraobotritagrion* Nel et al., 2005, *Protomyrmeleon* Geinitz, 1887, *Saxomyrmeleon* Nel and Jarzembowski, 1998, *Tillyardomyrmeleon* Henrotay et al., 1997).

Remarks. According to Nel et al. (2005), the only synapomorphy of the family is RP2 being forked, differentiating it from the Voltzialesidae, its assumed sister-group within the Protomyrmeleontoidea (Nel et al., 2012). However, under the interpretation we favour herein, RP2 is simple (a plesiomorphy in this context), and instead the distinctive trait of the family is the origin of pI(Irp₁-rp₂/RP2) - being indistinct from RP2 (as a consequence, RP2 seemingly has a fork indeed).

Most genera listed above display a RP3+4 with an anterior pseudo-branch. It is interpreted as a branch of RP3+4 by Nel et al. (2005). As seen above, odonates often evolve secondary intercalaries from cross-veins, and it is very likely the case here. We tentatively consider the ‘anterior branch of RP3+4’ as part of a pI (see Fig. 1.2E). The monotypic *Triassagrion* has been regarded as sister-group of the remaining Protomyrmeleontidae (hence its assignment to a distinct subfamily), owing to the purported occurrence of a long CuA. However, (1) this vein is very short in all ‘basal’ members of Protomyrmeleontoidea, and it would therefore represent an apomorphy; and (2) photographs of the only known specimen of the type species reveal that preservation is average in the corresponding area. Therefore, a proper revision of the original material appears necessary. We provisionally maintain the systematic proposal by Bechly (1996), already considered weakly supported by Nel et al. (2005).

1.2.5 Discussion

The newly described species allows a re-assessment of wing venation homologies for Moltenoptera (as delimited above). Homologies proposed by Zessin [1991; according which we made tentative interpretations of *Protomyrmeleon brunonis* (Fig. 1.2A, B) and of *Moltenagrion koningskroonensis* (Fig. 1.6E)] assume a forked RP3+4. This would imply that (1) the Moltenoptera are related to the Triadophlebiomorpha and Triadotypomorpha, which share this trait (Nel et al., 2001; Deregnaucourt et al., 2017), but which would then imply homoplasy on other characters, or that (2) the fork of RP3+4 itself is homoplastic. The alternative interpretation, which assumes a forked RP2 (Nel and Henrotay, 1992; Nel and Jarzembowski, 1998; Nel et al., 2005; see Fig. 1.2C, D for *Protomyrmeleon brunonis* and Fig. 1.6F for *Moltenagrion koningskroonensis*), is challenged by the fact that the then supposed origin of RP2a (see Fig. 1.6F) is convex, just as any cross-vein (see Fig. 1.6D), in *Moltenagrion koningskroonensis*, while it shall be concave. Moreover, a forked RP2 would be a unique character among Odonatoptera. In summary, none of these proposals are satisfactory.

Compared to these, our new interpretation for Moltenoptera minimizes the amount of transformations that has to be assumed to explain differences between the known morphologies. Its core element is the identification of a pI between Irp_1 - rp_2 and RP2, a trait present in *Terskeja* spp. (see Pritykina, 1981; Fig. 1.5), a taxon previously identified as related to the Protomyrmeleontidae (Nel et al., 2012; and references therein). Note that, in many extant Zygoptera, pI occur in various areas of the wings, such as *Dimeragrion percubitale* Calvert, 1913 and *Heliocharis amazona* Sélys, 1853 [Fig. 1.3; and see Deregnaucourt et al. (2019b) for original RTI files, and data on *Polythore derivata* (McLachlan, 1881)]. The veins RP3+4 and RP2 are both considered simple, as in the vast majority of Odonatoptera. We assume a fusion between RP2 and Irp_2 - rp_{3+4} , which represents a minor modification with respect to *Terskeja* spp., in which the two structures are separated by a very short cross-vein (see Pritykina, 1981; Fig. 1.5). The transition from *Moltenagrion koningskroonensis* to the Protomyrmeleontidae also involves few transformations. Firstly, the cv^* at the origin of Irp_1 - rp_2 aligns with Irp_1 - rp_2 [i.e. it becomes parallel to the main axis of the wing] and forms (part of) the ‘bridge’ sensu Nel and Henrotay (1992; and see Nel et al. 2005). Secondly, pI- [precisely, pI(Irp_{1+2} /RP2)-] and RP2 connect (i.e. pI- seemingly emerges from RP2), and RP2 diverges obliquely at their point of contact.

Moltenagrion koningskroonensis then turns out to be a key element to solve the question of the wing venation homologies of the Protomyrmeleontidae. In turn, the systematic position of the Protomyrmeleontoidea is obvious: as proposed by Nel et al. (2012), they represent a highly specialized group of the Archizygoptera and, as a matter of fact, the only representatives of the group during the Mesozoic.

1.3 Vein fusion altering the usual vein elevation

Vein elevation has proved a very useful criterion to establish vein homologies in odonates. In dorsal view, anterior sectors of mains veins (such as RA, MA and CuA) are convex (i.e. positive) while their posterior counterparts (such as RP, MP and CuP) are concave (i.e. negative) (Riek and Kukalová-Peck, 1984; Kukalová-Peck, 1991, among others). However, this general pattern has exceptions, in particular when main veins and/or intercalary veins of opposed elevation fuse, often resulting in a convex portion of vein which can then be interpreted in different ways. This kind of fusion can be found in extant species, for example in the Calopterygidae (Fig. 1.7), in which RP1+2 (concave) is bent towards RA (convex) from its origin, fuses with it for a short distance, and then diverges from it. The merge portion of RA and RP1+2 is convex.

Fusions of main veins and/or intercalary veins of opposed elevation occur also in fossil groups, including the Protomyrmeleontoidea and Zygophlebiida, two cases investigated in detail in the course of this study (see section 1.2 and Chapter 4, respectively).

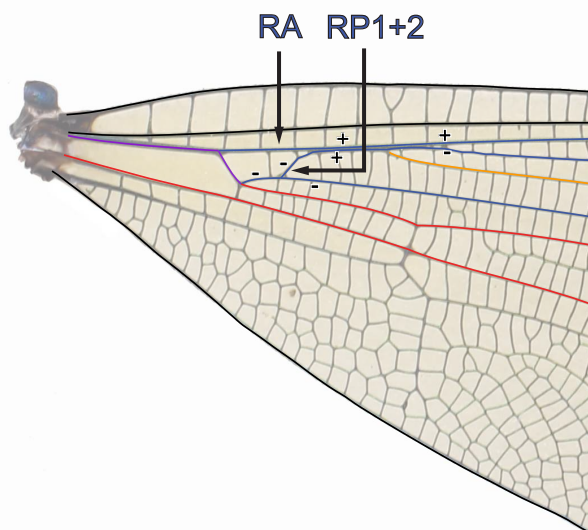


Figure 1.7 – Hindwing base of a male *Calopteryx splendens* (Harris, 1780)

1.4 Distinguishing main vs. intercalary veins

Whether a particular main vein is forked, or simple but provided with multiple intercalary veins seemingly diverging from it and sharing the same elevation, can also be difficult to assess. It relates to the propensity of intercalary veins to evolve main-vein-like features (such as strength and/or an orientation lined up with a genuine main vein). It is, however, essential to address the corresponding cases in order to conduct a morphometric analysis including the corresponding species and structures. Indeed, only one branch among two (or more) can be taken into account if species displaying a single branch are included. A good example is the case of the first concave element posterior to Irp_1-rp_2 in Proto-

myrmeleontoidea, interpreted either as RP2 (Zessin, 1991) or the anterior branch of RP2 (Nel and Henrotay, 1992), and which turned out to be an intercalary vein (see section 1.2).

Whether MA, CuA, CuP and AA possess genuine posterior branches in Meganisoptera can also be discussed (Fig. 1.1B, C, E, F). A seemingly branched RP3+4 occurs in Triadotypomorpha (Deregnacourt et al., 2017) and Triadophlebiomorpha (see Chapter 4). In both cases the concerned main veins were considered posteriorly pectinate or simple which, in both cases, provides the anterior stem as an homologous segment.

Another confusing case is the seemingly branched $Irp_{1+2}-rp_{3+4}$ present in some Aeschnidae, such as *Aeshna isoceles* (Müller, 1767) (Fig. 1.8A). Judging from the morphology of *Aeshna caerulea* (Störm, 1783) (Fig. 1.8B), the seemingly anterior branch clearly evolved from a structure weaker than genuine main veins. In other words, it is an intercalary vein that evolved strength and orientation usually indicative of a main vein.

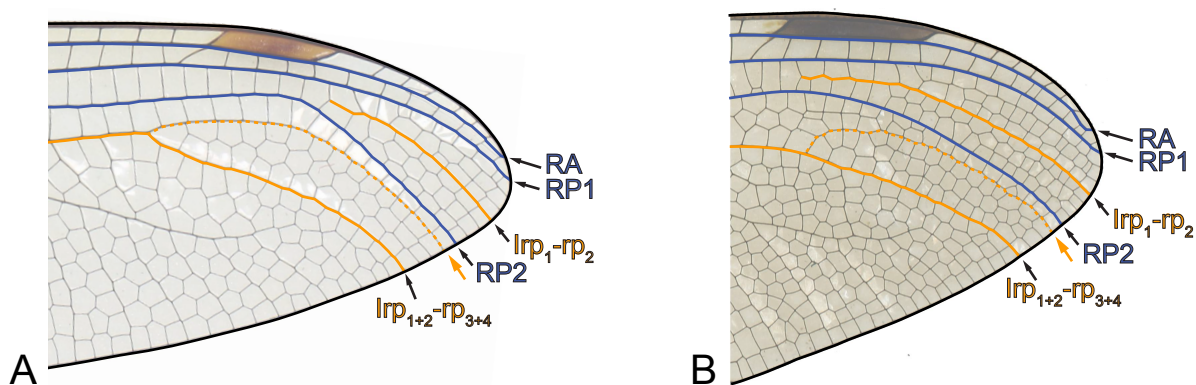


Figure 1.8 – Hindwings apex of **A**, a male *Aeshna isoceles* (Müller, 1767) with a seemingly branched $Irp_{1+2}-rp_{3+4}$; **B**, a female *Aeshna caerulea* (Störm, 1783) with a simple $Irp_{1+2}-rp_{3+4}$. Orange dotted line correspond to the seemingly anterior branch of $Irp_{1+2}-rp_{3+4}$, orange arrow indicate its end.

1.5 Remaining uncertainties

The course of some of the main veins in the postero-basal area of the wing remains difficult to assess. In particular, CuA, CuP and AA are not always clearly recognizable. For example, in many odonates (fossil and extant) the ending of CuA is difficult to identify with certainty (Fig. 1.9). CuA is even absent (or fused with AA) in extant Protoneuridae (a family not represented in France) and in the Permian species *Engellestes chekardensis* Nel et al., 2012. The course of CuP is virtually untraceable in crown-odonates, and is a matter of debate for several stem-groups, including the Triassic *Mesophlebia* spp. (see Annex A.1). Indeed, CuP is well developed only in early stem-odonates, such as Meganisoptera (Fig. 1.1C; and see Bechly, 1996). Expectedly, the case of AA, located

posteriorly with respect to CuP, is equally challenging. Because several interpretations are equally plausible, we choose not to take CuA and CuP in consideration for morphometric analyses.

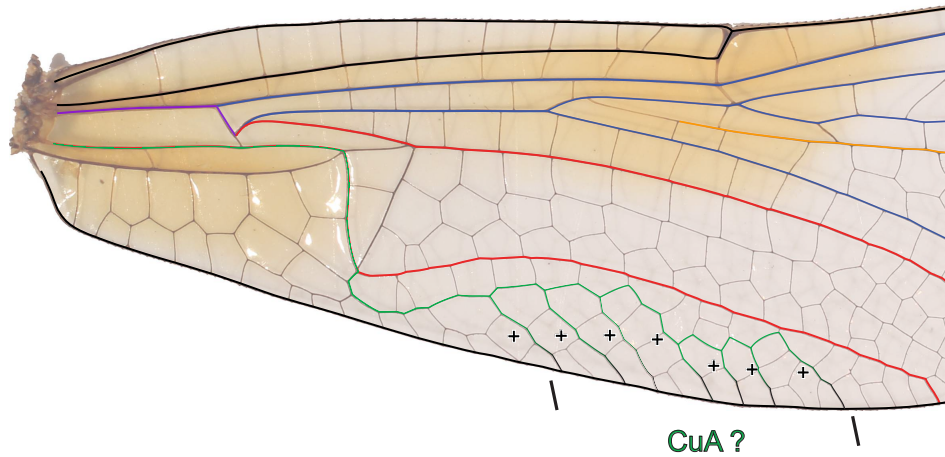


Figure 1.9 – Forewing base of a male *Sympetrum flaveolum* (Linnaeus, 1758) with all the possible courses of CuA represented.

1.6 Operational homology scheme for morphometrics

A pattern of vein homologies that could be applied to the entire odonates (i.e. all known stem-groups and crown-group) and that fulfill the requirements of a morphometric analysis (same structures shared by all species taken into consideration), has been adopted for all further analyses. It is summarized in Fig. 1.10A and examples of application to various odonates morphotypes are illustrated on Figs 1.10, 1.11.

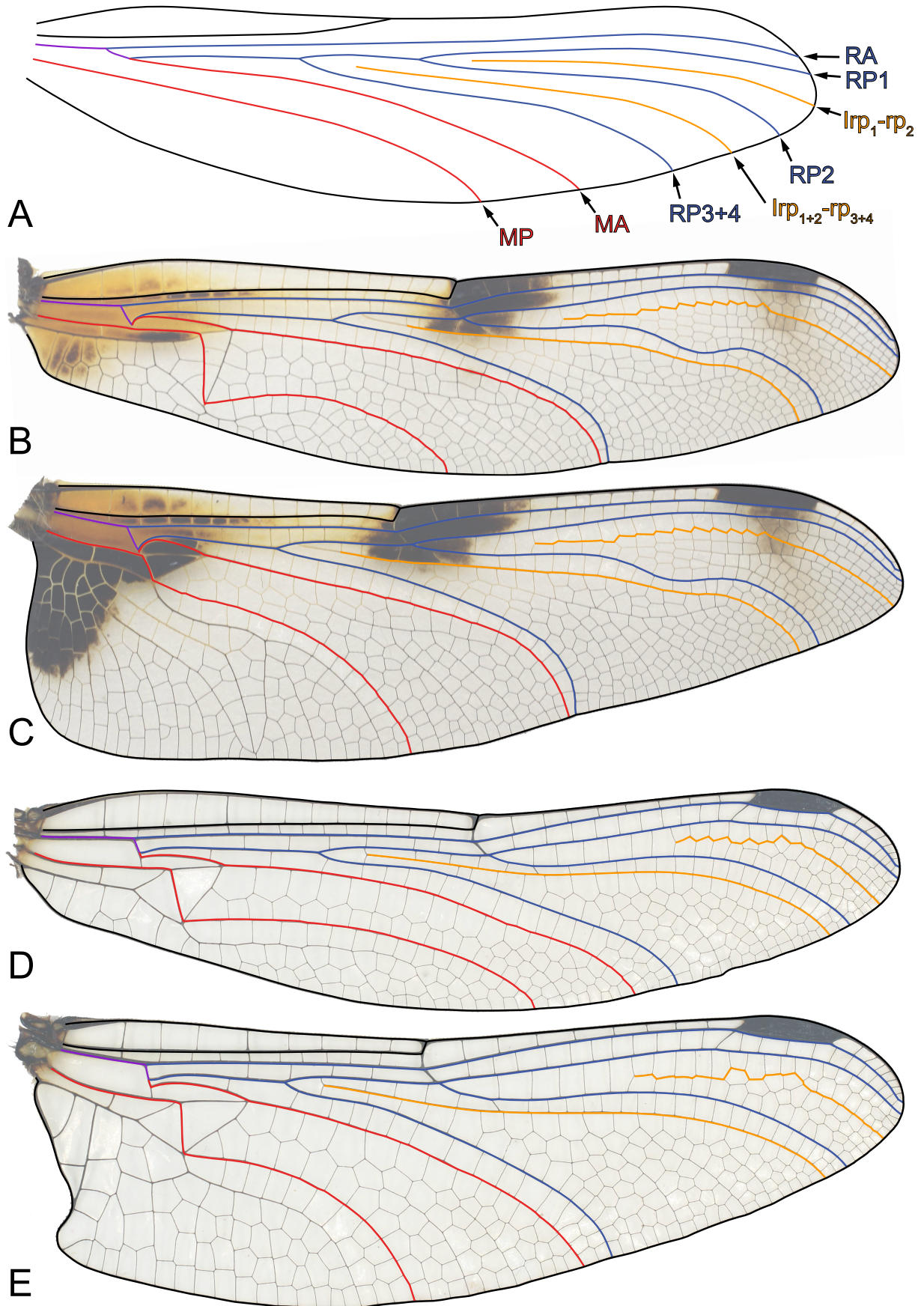


Figure 1.10 – A, basic pattern of homologous main veins on odonates wings applied to: B, C, forewing and hindwing of a male *Libellula quadrimaculata* (Linnaeus, 1758; D, E, forewing and hindwing of a male *Onychogomphus forcipatus* (Linnaeus, 1758).

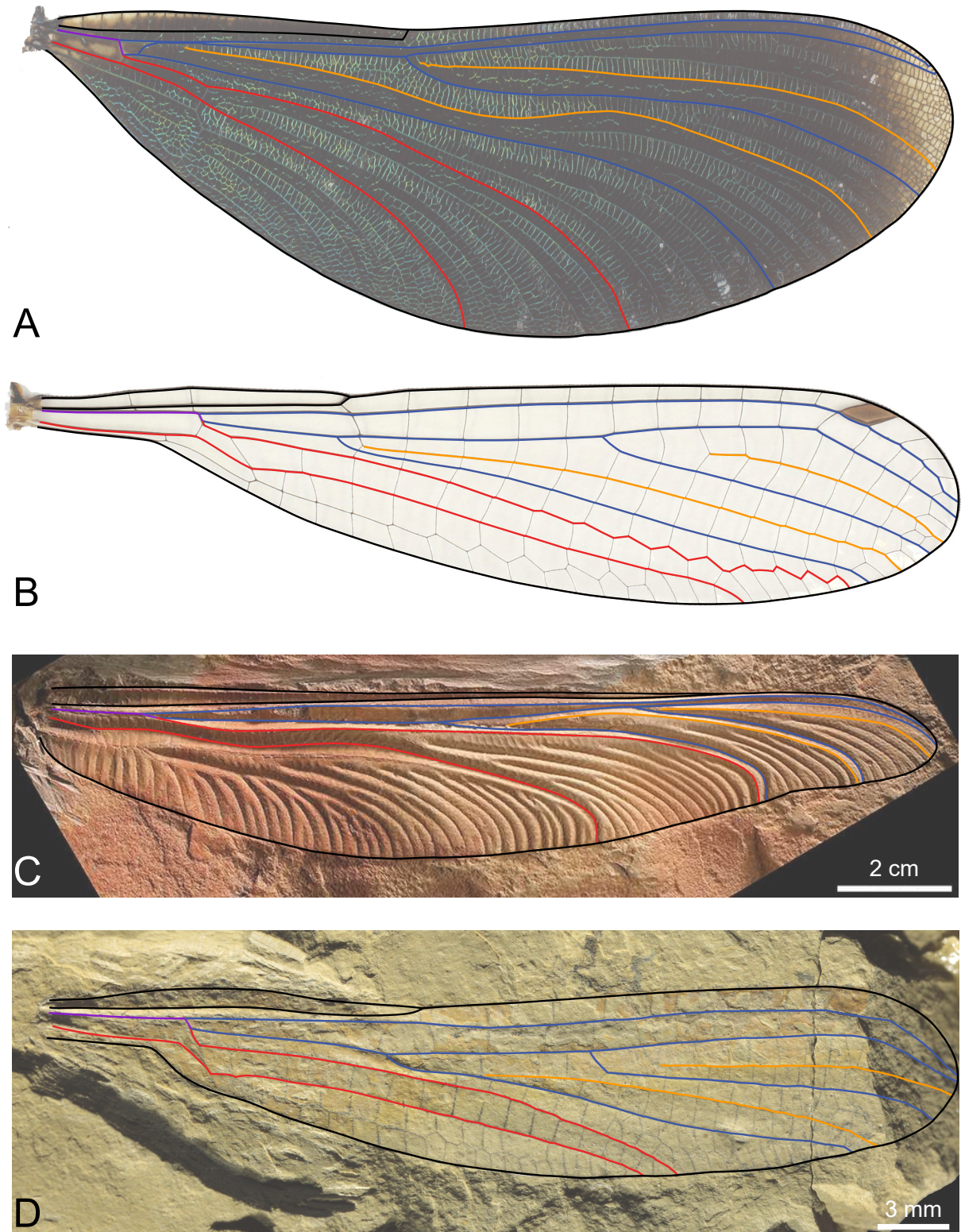


Figure 1.11 – Basic pattern of homologous main veins on odonates wings applied to: **A**, hindwing of a male *Calopteryx virgo* (Linnaeus, 1758); **B**, hindwing of a female *Ceriagrion tenellum* (Villers, 1789); **C**, *Tupus gracilis* Carpenter, 1947, photo of the specimen PALE-4819 from the MCZbase; **D**, imprint of specimen PRE/F/10442a from the Molteno formation, apex completed by the counterprint PRE/F/10442b.

Chapter 2

From specimens to morphospace and disparity measures

Contents

2.1	From specimens to pictures	28
2.1.1	Specimen collection & conservation	28
2.1.2	Wing pictures acquisition	29
2.1.3	Fossil specimen pictures	31
2.2	From pictures to landmarks	32
2.2.1	Wing shape description	32
2.2.2	Landmarks selection	32
2.2.3	Comparison between sliding semi-landmarks and fixed landmarks approaches	35
2.2.4	Sliding landmarks parametrization	37
2.3	Morphospace and species reference shape: an example with French odonates	41
2.3.1	Inventory data and species lists	41
2.3.2	Reference shapes for each species	43
2.4	Disparity	46

Once a pattern of vein homologies applicable to all extant and fossil odonate wings has been elaborated, its use to accurately quantify shapes and their disparity still need to be determined. In this chapter the steps leading from actual specimens to the computation of their disparity are detailed. First are detailed specimens collection, conservation, pictures acquisition and drawings. We then present the landmark-based geometric morphometrics approach used to build the morphospace. In such analyses, it is important to have a

tight control of potential biases. In our case, those biases can be induced by both picture acquisition and drawing making. We thus tested the variance introduced by these steps. Then we tested different parameters of landmark positioning and density, aiming to find those optimal to quantify wing shapes for the geometric morphometrics analyses, based on the pattern of vein homologies presented in the above chapter. Thanks to all these steps, morphospace can be computed, and we present here an example with the French odonate species. Finally, we discuss how to extract disparity measures that will summarize complementary aspects on shape distribution within a morphospace.

2.1 From specimens to pictures

2.1.1 Specimen collection & conservation

A working collection of extant odonate wings was built based on new collects and complemented by specimens from institutional collections. As mentioned above, geometric morphometrics requires a tight control of potential measurement biases. Therefore, wing preparation requires a careful flattening (Perrard et al., 2012), which is easier to obtain with detached wing. The flattening allows reduction of the potential deformation due to drying or other preparation processes. Flattened wings can easily be set perfectly perpendicular to the camera lens axis, minimizing any deformation potentially induced at this stage. The need to remove wings from specimens body precluded the use of most specimens from institutional collections, this is why the elaboration of a working collection was favoured.

The specimens were gathered by volunteers and myself. We solicited citizen sciences participants but obtained a single positive reply (namely, Charlotte Giordano). Naturalists helped throughout several outings with capture and identification (of which Thomas Bitsch and Axel Dehalleux). Specimens were identified thanks to Dijkstra (2015) and Grand et al. (2014). Most specimens of the working collection were captured by Loïc Villier and myself.

Specimens were collected using a butterfly net with a diameter of 35 mm and a handle of 1 m. Some of the specimens were stored in tracing paper envelopes, with wings folded over their back. They were left for approximately 24 hours in these envelopes to allow emptying of their gut, thus preventing rotting of the abdomen and color loss. Then individuals were killed using acetone vapour. Other specimens were put into 70° ethanol directly after capture. Most of the specimens were then spread, pinned and let to dry. Those with neither pruinescence nor metallic colors were pinned then spread with the ventral side up on a perforated metal plate. Wings were maintained with tracing paper and magnets. They were then dried in an acetone bath to preserve the colors of the body in an airtight container. This method was adapted from that described in Dommanget

(1999). Other specimens were pinned, spread on polystyrene and let to dry two to three weeks. Spread specimens were finally stored in entomological boxes. Some specimens were kept in cellophane envelope, especially Zygoptera species that were collected in high numbers. Eighty-one of the specimens used in the analyses were from this working collection (as well as the 27 used to tests for biases due to data acquisition). Other used specimens are from the Zoologische Staatssammlung of Munich (190 specimens) and from the Museum National d'Histoire Naturelle of Paris (90 specimens; see Annex A.2). Protected species were documented from institutional collections.

2.1.2 Wing pictures acquisition

All wings were photographed flattened under a cover glass. Wherever possible wings were separated from the body for convenience. Specimens from institutional collections were photographed without separating the wings from the body, following a method adapted from Perrard et al. (2012). The specimens were relaxed with water vapour for a couple of hours before manipulation. For each specimens, a forewing and a hindwing were photographed. All pictures were made using with a Canon EOS 700D equipped with Canon 50 mm macro lens and, occasionally, an elongation tube. Alignment of the camera and the wing mounting device was checked each time.

Free wings set-up

It has been possible to separate wings from bodies for the working collection and for 102 specimens of the Zoologische Staatssammlung (Munich). Free forewings and hindwings were placed on a plastic white background. Then they were covered by a glass with nylon thread glued on two opposite sides to prevent excessive compression. Indeed, nylon threads maintain a 1mm space between the background and the glass. Light weights were placed on both side of the glass to flatten the wings to a minimal thickness, even with comparatively thick Anisoptera wing. Photographed wings were then stored in envelopes.

Set for specimens from institutional collection

The device allowing the flattening of wings without removal from the body is composed of a thin, white plastic plate and a glass plate on which nylon thread were glued on two opposite sides, creating a 1mm space in which the wing is constrained. The two parts are maintained together thanks to a wooden peg. The glass plate was cut along a curved line so that the basal side could be inserted very close to the pin holding specimen without having basal parts of the wings left uncovered. The use of a thin white plastic plate allows insertion of this white background between wings for specimens in envelopes and also between the hindwing and the abdomen for both pinned and enveloped specimens.

This assembly, mounted on a stand, was open, placed around the wing and closed on the other side thanks to an other peg (Fig. 2.1).

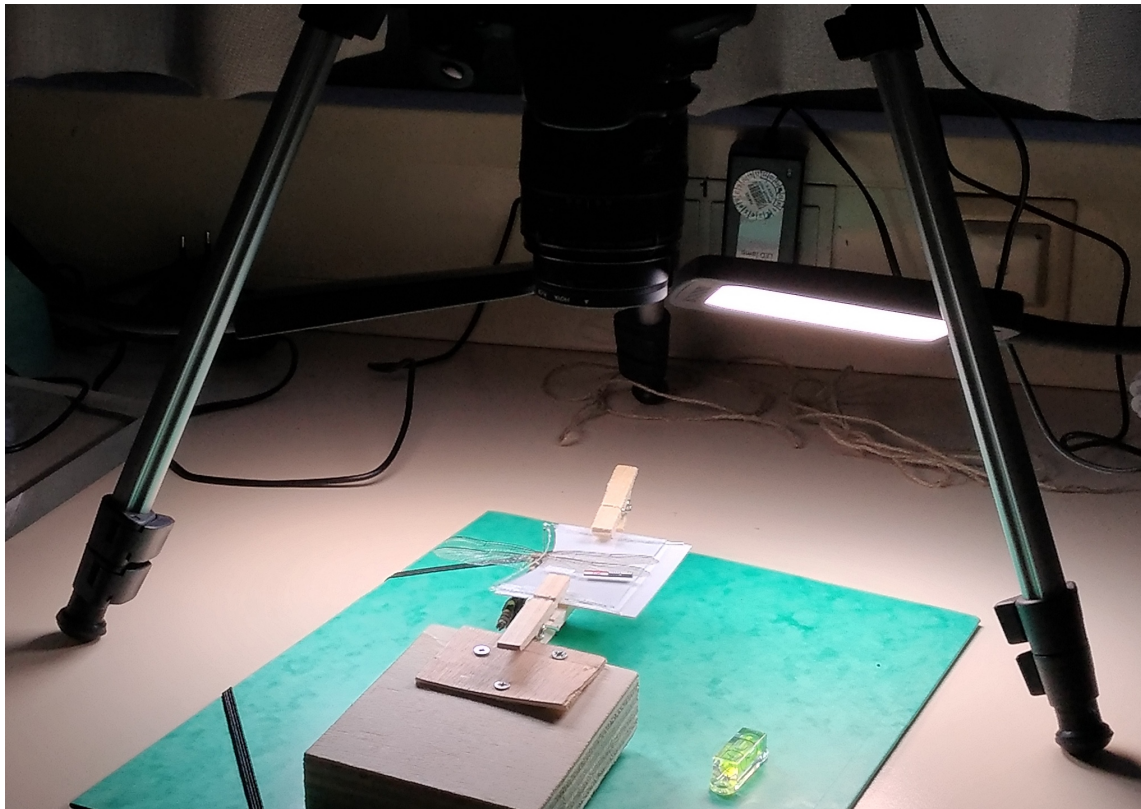


Figure 2.1 – Mounting adapted from Perrard et al. (2012) used to picture odonate wings. Specimen in the picture is a pinned *Macromia splendens* (Pictet, 1843) male from the Zoologische Staatssammlung München.

Testing for biases between pictures from different set-ups

Using pictures acquired using two different protocols may introduce bias. In order to assess the effect of this bias in regard to the disparity analysis, we appreciated how its variance compares to that documented between specimens.

To conduct this testing, 15 specimens of *Sympetrum striolatum* (Charpentier, 1840) and 20 specimens of *Sympetrum sanguineum* (Müller, 1764) from the working collection were used. These species were selected because their hindwing have a broad postero-basal area, bent ventrally when dry, and therefore likely to display an important variance when compressed using different set-ups. This would not be the case with wings of Zygoptera, for example.

Right forewings and hindwings of each specimen were pictured attached to the body, using the dedicated set-up, and then removed and pictured using the "free wings set-up". Vector line drawings were then prepared by a single operator. The procedure allowing an automated landmarks positioning (see section 2.2) was then applied.

The potential biases linked to the two distinct photographic processes are investigated

using MANOVA. The effect of the set-ups may be different for forewings and hindwings. We thus tested for a potential bias for each separately. The obtained R^2 are equal to 0.00101 and to 0.00189 for forewings and hindwings, respectively, indicating that the variation induced by photographing free or attached wings is negligible. Data acquired from the two acquisition processes can therefore be used jointly in morphological analysis.

For wings photographed while still attached to the body, some specimens were stored in envelopes and some other were pinned. The ones in envelopes are maintained with the wings folded over their back. The wings are therefore exposed and photographed in ventral view, whereas they are in dorsal view for pinned specimens. We tested the potential impact of the wing side view comparing the same 13 left wings of *Sympetrum striolatum*. The MANOVA test resulted in R^2 values of 0.03028 and to 0.002012 for forewings and hindwings, respectively. The impact of ventral vs. dorsal views on both forewings and hindwings can therefore be considered negligible. Both dorsal or ventral views can be confidently used in a single morphological analysis.

The variance added by considering left and right wings of each individual was also tested on 13 pinned specimens of *Sympetrum striolatum*. R^2 is equal to 0.01462 and to 0.01152 for forewings and hindwings respectively. Thus, both right and left wings can also be combined in morphological analyses.

The potential sources of precision and resolution losses throughout the pictures acquisition protocols have all shown very low variances and thus negligible effects. We can thus consider that our whole dataset for extant species is consistent. To think in the long term, this is also encouraging for large database constitution as some flexibility on protocols seems to be acceptable.

2.1.3 Fossil specimen pictures

For our fossil species dataset, pictures have been in majority extracted from bibliographic sources. Data for a few specimens from the Molteno Formation are based on drawings and photographs made by Olivier Béthoux and which are still unpublished (see details in Chapter 4, Table 4.1)).

Some biases might be induced by the use of drawings from diverse bibliographic sources. Indeed, some specimens might have been idealised by the authors and/or slight reconstructions might not be specified. Even to a limited extent, some degree of subjectivity is to be expected from human-produced drawings. However it was not possible to test for such biases. That would require that different experts investigate the same set of specimens, which was unachievable. However, drawings were confronted with photographs, if available, to appreciate their accuracy.

2.2 From pictures to landmarks

2.2.1 Wing shape description

Vector line drawings were derived for each wing photograph. Wings outlines were automatically detected using Adobe Photoshop CS6 (Adobe Systems, San Jose, CA, USA) and then vectorised using Adobe Illustrator CS6 (Adobe Systems, San Jose, CA, USA). The rest of the adopted pattern was drawn by operators under Adobe Illustrator CS6.

For extant species, three operators made the drawings, namely Alexandre Lethiers (CR2P lab graphic designer), Olivier Béthoux and myself. In total 304 pairs of wings were drawn for the analyses and an additional 116 to test for potential biases (see section 2.1.2). Among the 304 pairs of wings used in the analyses, 143 were drawn by Alexandre Lethiers, 24 by Olivier Béthoux and 137 by myself. Additional drawings were made by Alexandre Lethiers. The impact of the operators on variance was tested using 10 specimens belonging to the family Libellulidae. They were drawn by Alexandre Lethiers and by myself. The MANOVA test returned a R^2 equal to 0.0009536 and 0.004272 for forewings and hindwings, respectively. The drawings done by the different operators can thus be included in the same analyses without considering their differences.

2.2.2 Landmarks selection

Several types of landmarks can be used (Bookstein, 1991; MacLeod, 2011): type I landmarks are specific points corresponding to biological homology; type II landmarks correspond to geometric homology and not necessarily biologic one; and type III landmarks are points whose location depends on that of other landmarks and/or specimen orientation (maximum bending of a curve for example, or maximum distance between two veins). Herein, type I landmarks are the homologous points corresponding to the beginning and end of each vein or vein portion, usually corresponding to points of vein divisions.

On odonates wings, specific vein bending (marked angle to more or less marked curvature) are very common. For example, a strong bending of RP2 towards the end of the pterostigma occurs in Aeshnidae and can help distinguishing the genera *Anax* Leach, 1815 and *Hemianax* Selys, 1883 (Fig. 2.2; Grand et al. 2014). Another relevant example, only occurring in extant species such as Anisoptera, are the marked angle along MA and MP at the point where they connect with the cross-vein delimiting the triangle and the supertriangle (Fig. 2.2). Thus, we considered relevant the use of veins curvature information to characterize wing shapes. Type II landmarks are placed along the veins to take into account these features. More specifically, type II landmarks are semi-landmarks allowed to slide along the curves during the Procrustes superimposition, in order to reduce the distance between these semi-landmarks on the specimens. We do not use type III

landmarks.

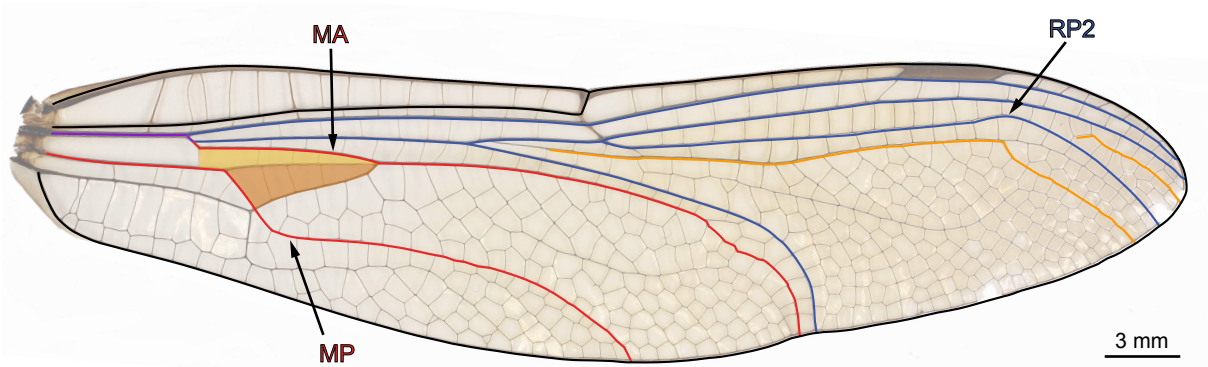


Figure 2.2 – Forewing of a male of *Anax parthenope* (Selys, 1839). Light orange structure is the supertriangle; dark orange structure is the triangle.

Acquisition of homologous landmarks and geometric morphometrics analyses were conducted under R (R Core Team, 2018). Landmarks of types I and II were automatically placed thanks to a dedicated script developed under R, which avoids the manual placement of each points. Veins are directly drawn on the pictured wing for extant species and on drawings or pictures available in the bibliography for the fossils ones. A specific RGB color-coding was attributed to each vein or portion of veins. Color-coding was inspired by colors used in literature (Béthoux, 2015; Deregnaucourt et al., 2017) and is specified in Table 2.1 (and see Fig. 2.3). Veins which are not forked (viz. RA, MA, MP, Irp_1-rp_2 and $Irp_{1+2}-rp_{3+4}$) were represented by a single object. The only bifurcating veins, namely RP, was split into several objects. The portion of RP from its origin to its division into RP1+2 and RP3+4 was treated as a single object, as well as as the portion of RP1+2 from its origin to its division into RP1 and RP2, RP2 (from its origin to its end along the wing margin), and RP3+4 (from its origin to its end along the wing margin), each being assigned a specific color coding.

Table 2.1 – RGB color-codes used for each vein or portion of vein on vector lines drawings.

Major veins	Outline	ScP	RA	RP	RP1+2	RP1
Color-code	#000000	#030303	#3F59A7	#3F59A5	#3F59A6	#3F59A8
Major veins	RP2	RP3+4	MA	MP	Irp_1-rp_2	Irp_2-rp_3+4
Color-code	#3F59A9	#3F59A0	#EA2727	#EA2728	#FF9900	#FF9901

From an anatomical perspective, specialists usually recognized fusion of veins. For geometric morphometrics, fused portions of veins can be considered running aside each other, and therefore treated as two different curves (thus superimposed) or the fused portion can be treated as a single object. Herein, fused portion of veins are considered superimposed for the geometric morphometrics analyses. For example, in some extant species of Libellulidae and Corduliidae, the divergence of RP and MA (from RP+MA) is not always clear, these two veins can be contiguous for a short distance (Fig. 2.3).

Thus, we consider that RP and MA originate at the arculus, as for other species, and the potentially fused portions of RP and MA after this points are superimposed.

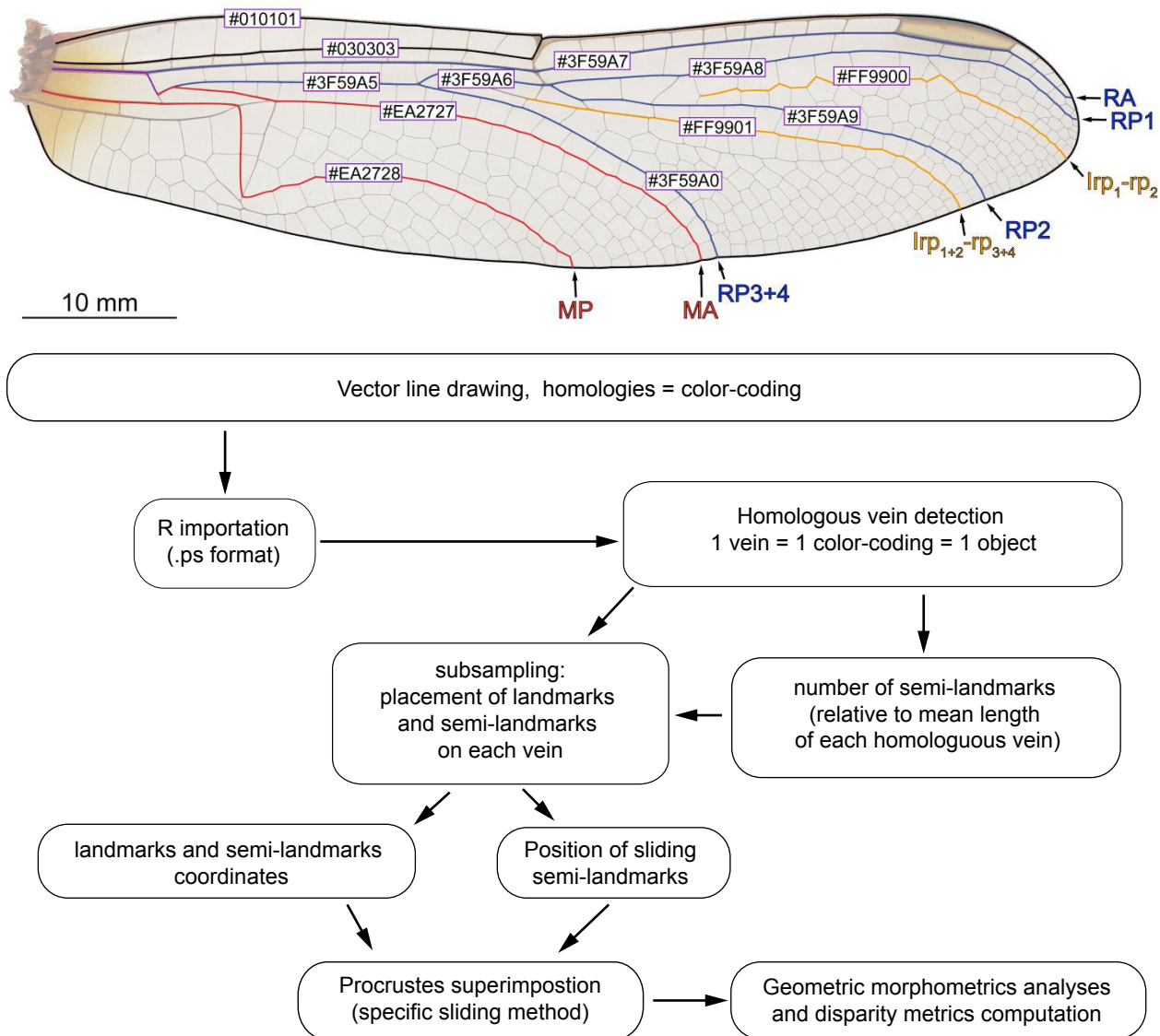


Figure 2.3 – Forewing of a male of *Crocothemis erythraea* (Brullé, 1832). Photograph and vector line drawing of veins and vein portions with the associated color-code, followed by a flow-chart summarizing the steps of the R script designed to place landmarks and semi-landmarks automatically, based on color-code, to be further used for geometric morphometrics analyses. Violet frame on the wing: RGB color-codes.

The fused portions of R and MA (R+MA), and of RP and MA (RP+MA) were initially treated as single objects (distinct from RA, RP and MA; purple veins in Fig. 2.2 and 2.3), because they occur in all odonates considered in the morphological analyses. However, their reduced length, in most of the wings, prevented placement of semi-landmarks. Moreover, the beginnings of RA of one hand, and of RP and MA on the other, also accounted for the endings of R+MA, and of RP+MA, respectively. As a consequence, R+MA and RP+MA were ignored.

MP, in its basal portion, is fused with Cu. However, we do not take into account Cu, therefore its origin was traced from the wing base.

The elaborated R script imports a vector line drawing, itself exported in postscript format (.ps), thanks to the package `grImport` v. 0.9-1 (Murrell, 2009). Each curve (vein or vein portion) is then identified thanks to its color-coding information, contained in the postscript file. Then, each object is sub-sampled thanks to the function `digit.curves` from the package `geomorph` v.3.0.7 (Adams and Otárola-Castillo, 2013). In other words, type I landmarks are placed at the beginning and end of each curve and semi-landmarks are automatically placed equidistantly along each curve. The number of semi-landmarks is defined according to the relative mean length of each vein (see subsection 2.2.4). The returning object of the scripted function contains the coordinates of all the wings, of each landmarks and semi-landmarks, the number of landmarks, and a matrix specifying which landmarks are semi-landmarks, thus, allowed to slide. Each of these steps are summarized in Fig. 2.3. This automated script could further be used on any insect wings or 2D object with curves.

2.2.3 Comparison between sliding semi-landmarks and fixed landmarks approaches

The most commonly used approach to quantify insect wing shape in geometric morphometrics is to use fixed landmarks (Perrard et al., 2012; Barour and Baylac, 2016; Blanke, 2018). This approach can be used to take into consideration structures that are known to bear, in extant forms (or some of them), important shape information, such as the oblique ‘o’ cross-vein, the pterostigma, the nodus and the triangle and supertriangle. However, these structures are not present in all extant and fossil forms we considered.

We thus investigated if using our sliding semi-landmarks approach, applicable to all extant and fossil species, carries the same information than an approach based on an exhaustive set of type I landmarks designed for extant species. To do so, we used the dataset of Blanke (2018) composed of 121 homologous landmarks (60 on the forewing and 61 on the hindwing) applied to 189 species of Anisoptera. This dataset takes into account the specific structures cited earlier and also all the major veins and other relevant cross-veins. We focused on a subset of 15 male forewings. Vector drawings were prepared based on the exact same pictures than the ones used by Blanke (2018). For this test RP, RP1+2 and RP1 were combined into a single object, the division in vein portions being adopted afterwards. Two sets of sliding semi-landmarks were tested, one with maximised number of semi-landmarks [301 for the outline, 53 for ScP, 110 for MA, 121 for RP/RP1+2/RP1, 39 for RP2, 44 for RP3+4, 6 for Irp₁-rp₂ (a small number because this vein is strongly reduced in Aeshnidae), 65 for Irp₁₊₂-rp₃₊₄, 71 for MA and 78 for MP] and another with a minimal number (6 sliding semi-landmarks on each vein). During the Procrustes su-

perimposition, two optimisation criteria were tested for the sliding semi-landmarks, one minimizing Bending Energy (BE) between semi-landmarks and the other minimizing the Procrustes distances. These methods are presented and discussed in subsection 2.2.4.

A Procrustes superimposition (GPA) was performed for each dataset to correct for the effects of rotation, translation and size (Rohlf and Slice, 1990). Correlation between the aligned landmarks coordinates was then computed thanks to a two-block partial least square analysis (Rohlf and Corti, 2000; Fig. 2.4). A good correlation was found between the landmarks dataset of Blanke (2018) and the minimal set of sliding semi-landmarks, under both sliding methods ($R^2 > 0.7$ and $p\text{-value} < 0.05$). The correlation is stronger when using the maximum number of sliding semi-landmarks and the Procrustes sliding method ($R^2 > 0.8$; Fig. 2.4). Using the maximum number of sliding semi-landmarks in association with the BE sliding method resulted in a pile of dots rather than realistic wing shapes, an issue further considered below (subsection 2.2.4).

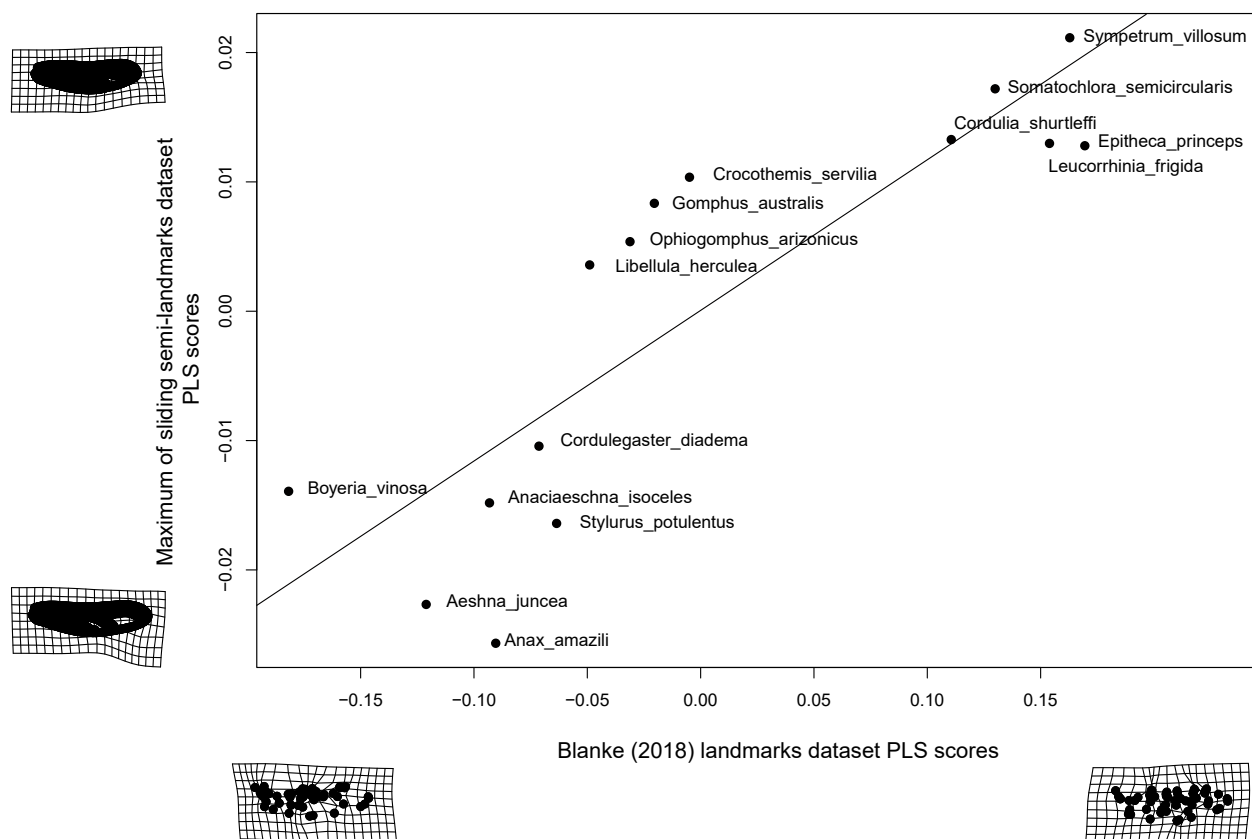


Figure 2.4 – Two Block-Partial Least Squares between two different landmarks datasets on the same 15 forewings of male Anisoptera. Along x axis: PLS scores of Blanke (2018) dataset of 60 landmarks; along y axis: PLS scores of our dataset with a maximum of sliding semi-landmarks and using sliding method minimizing Procrustes distances.

These results suggest that the sliding semi-landmarks approach quantify a morphological information nearly equivalent to the fixed homologous points approach. In other words, the discarding of notable structures present in extant species does not lead to an important information loss. However, the sliding semi-landmarks approach has the significant advantage of being applicable to both fossil and extant species.

2.2.4 Sliding landmarks parametrization

Within the methodological comparison presented above we also tested the two possible sliding methods. The two gave different results and computational issues were faced when using the BE method with a high number of semi-landmarks. Superposition resulted in a pile of dots rather than wing shapes. A balance had to be found between the sliding method and the number of semi-landmarks.

Sliding method

Sliding landmarks are semi-landmarks that are allowed to slide along a curve (here the veins) until they match, as well as possible, the position of corresponding points on reference curves (Adams et al., 2004). Two main methods are used to allow points to slide, one minimizing Procrustes distances and one minimizing the Bending Energy (BE) (Perez et al., 2006; Fig.2.5). The method minimizing Procrustes distances requires low computational power and thus can be used with a large number of semi-landmarks, whereas the BE one requires much more computational power. However, for very different shapes, the first one can lead to unwanted distortions, whereas the second one ensures a smoother sliding in any case (Zheng et al., 2017b). Both method were tested to find the one best suited for our problematic.

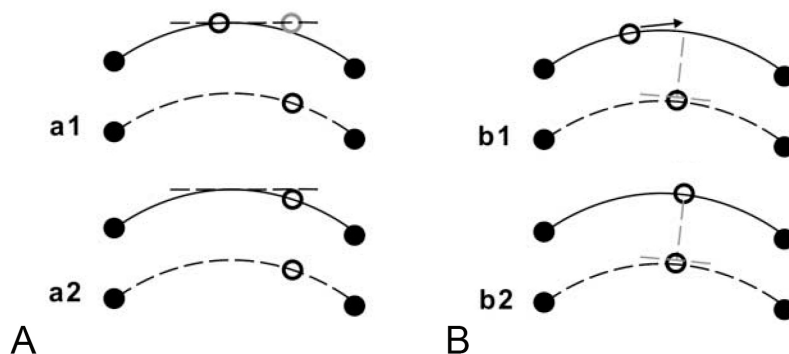


Figure 2.5 – Illustration of the sliding methods. **A.** Minimum Bending Energy criterion: (a1) semi-landmarks slide along an outline tangent (a2) and are projected onto the outline after relaxation step. **B.** Minimum Procrustes distances criterion: semi-landmarks (b1) before and (b2) after sliding towards the line perpendicular to the edge of the corresponding semi-landmarks of the reference. Modified from Perez et al. (2006).

The two methods were also used during the elaboration of the wing reconstruction method presented in Chapter 4. The use of Procrustes distances led to unwanted distortion of the wings, with landmarks positions, after the superposition, not reflecting the observable wing shape anymore. Such distortion was not observed with the BE method (Fig. 2.6). Thus, and given the diversity of odonates wing shape, the BE method was favoured for the analyses because it appeared best suited for important shape variations.

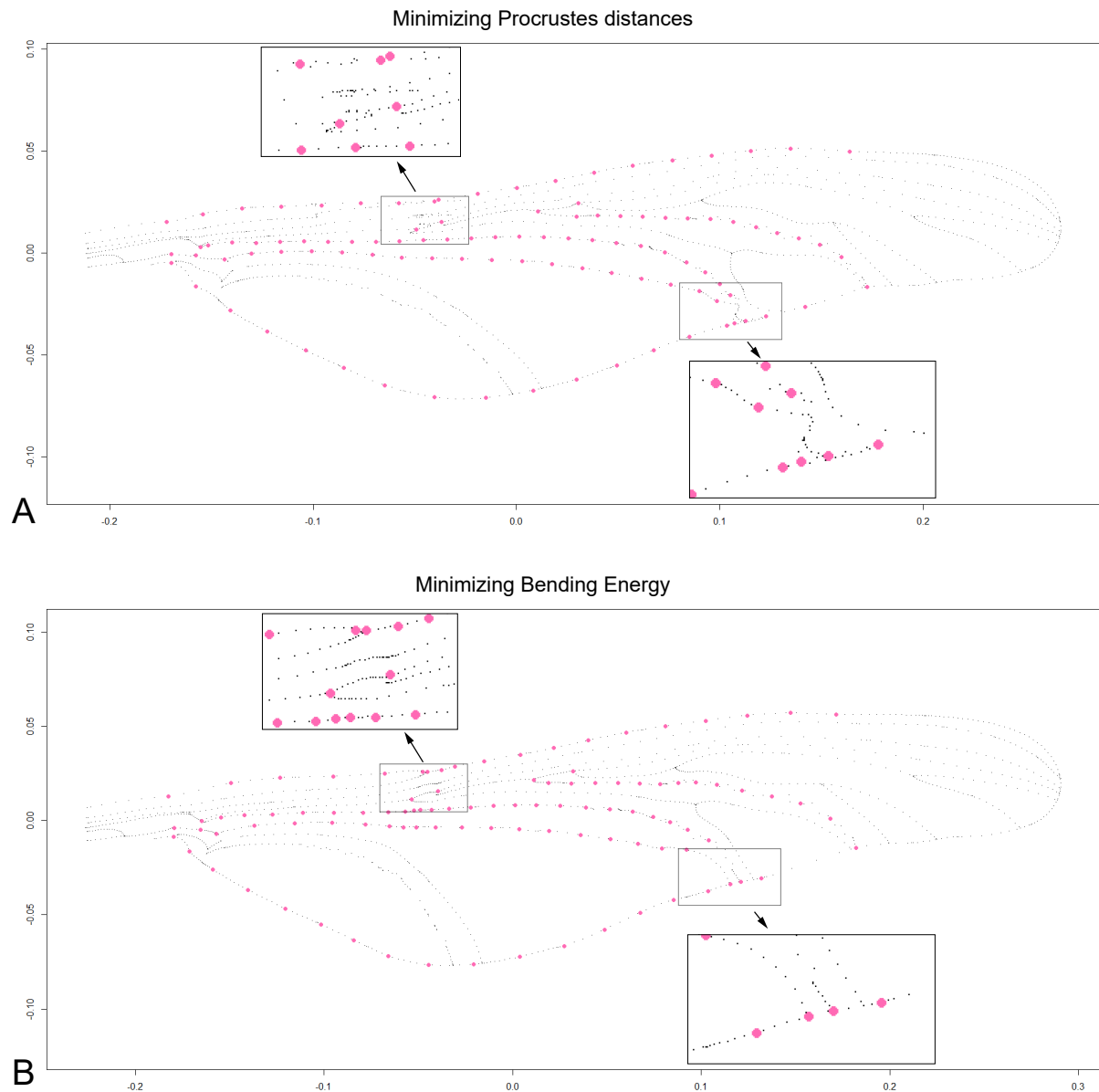


Figure 2.6 – Thin plate Spline deformation of *Zygophlebia ramosa* Pritykina, 1981 onto *Moltenophlebia lindae* Deregnacourt et al., *in review* after Procrustes superimposition sliding semi-landmarks under two different criteria: **A.** minimizing Procrustes distances, **B.** minimizing Bending Energy. Boxes correspond to zoom on areas showing unwanted distortion under the minimizing Procrustes distances criterion.

Number of sliding semi-landmarks

In the analyses presented in subsection 2.2.3, we found that too many landmarks is not necessarily the best choice with BE. Indeed, using a large number of landmarks does not necessarily add substantial morphological information, unnecessarily increases computation time and can lead to unwanted distortions of wings shapes.

Therefore an optimal number of semi-landmarks was searched for. This number needs to be sufficient to quantify as much morphological information as possible but, at the same time, allowing computation in an acceptable time and, most importantly, avoiding distortion. The variation of the number of semi-landmarks has been investigated on the dataset of French extant species elaborated as described in section 2.1. The number of semi-landmarks was set as a proportion of the mean length of each vein or vein portion. This proportion is defined by a chosen coefficient. Several coefficient were tested, from 0.0004 to 0.0008 every 0.0002 and from 0.001 to 0.003 every 0.001. A GPA was been realised for each and a principal component analyses computed (Fig. 2.7).

Starting from 0.002, too many semi-landmarks lead to unrealistic deformations of the grids (Fig. 2.7E). Therefore the optimal number of semi-landmarks selected is obtained with a coefficient of 0.001 for the analysis. Applying this coefficient to extant species provided 76 semi-landmarks for the outline ("O"), 14 for ScP, 31 for RA, 5 for RP, 6 for RP1+2, 18 for RP1, 17 for RP2, 17 for RP3+4, 11 for MA, 20 for MP, 21 for Irp₁-rp₂ and 22 for Irp₁₊₂-rp₃₊₄.

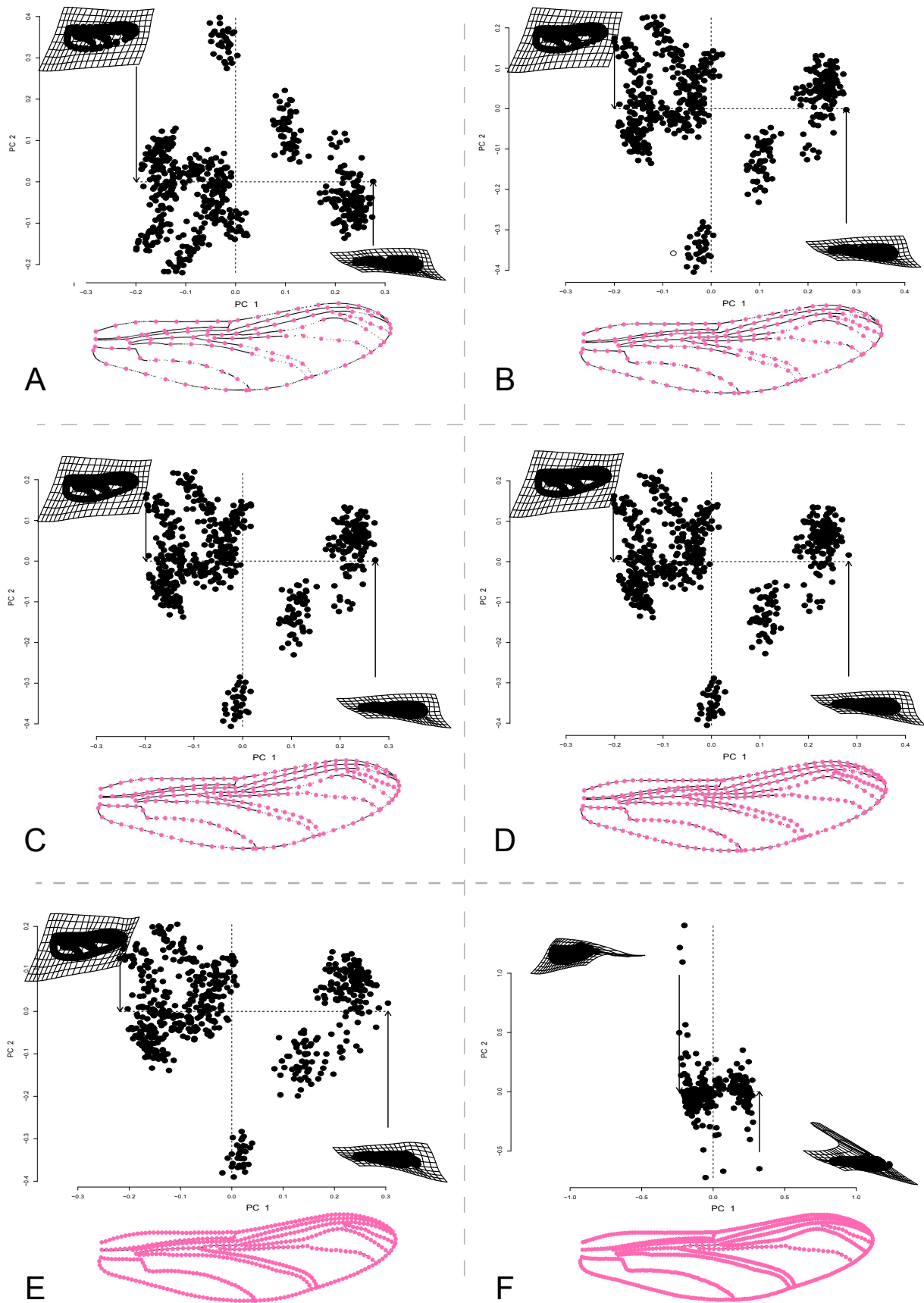


Figure 2.7 – Principal component analyses and a representation of the placement of the landmarks and semi-landmarks on the anterior wing of *Aeshna affinis* for each tested coefficient defining the number of semi-landmarks. Unrealistic distortions appear starting from subfigure **E** (coefficient 0.002). **A.** coefficient of 0.0004, **B.** 0.0006, **C.** 0.0008, **D.** 0.001, **E.** 0.002, **F.** 0.003

2.3 Morphospace and species reference shape: an example with French odonates

2.3.1 Inventory data and species lists

Odonate diversity is very well documented in France. It has been monitored for decades by several groups and programs involving both professional and non-professional, entomologists. A list of extant species and their occurrences were extracted from the Steli database, a citizen sciences monitoring program developed by the CESCO (<http://odonates.pnaopie.fr/steli>). Contributors follow a standardised field inventory protocol so that, although not exhaustive, the data are of high standards and are well suited for statistical comparisons. I used observations data collected from 2011, the starting year of the program, to 2019. The list of all the 79 observed species in mainland France is given in Table 2.2.

For the morphological analyses, the morphology of each species is summarized by a collection of reference specimens. To do so, I used two females and two males of each species in order to take into account the intraspecific variabilities (i.e. eight wings per species; Annex A.2).

Table 2.2 – Species observed in France from 2011 to 2019 in the STELI database

Suborder	Families	Species
	Aeshnidae	<i>Aeshna affinis</i> (Vander Linden, 1820)
		<i>Aeshna cyanea</i> (Müller, 1764)
		<i>Aeshna grandis</i> (Linnaeus, 1758)
		<i>Aeshna isoceles</i> (Müller, 1767)
		<i>Aeshna juncea</i> (Linnaeus, 1758)
		<i>Aeshna mixta</i> (Latreille, 1805)
		<i>Aeshna subarctica</i> Walker, 1908
		<i>Anax imperator</i> (Leach, 1815)
		<i>Anax parthenope</i> (Selys, 1839)
		<i>Boyeria irene</i> (Fonscolombe, 1838)
		<i>Brachytron pratense</i> (Müller, 1764)
		<i>Hemianax ephippiger</i> (Burmeister, 1839)
		Cordulegastridae
<i>Cordulegaster boltonii</i> (Donovan, 1807)		
Corduliidae	<i>Cordulia aenea</i> (Linnaeus, 1758)	
	<i>Epithea bimaculata</i> (Charpentier, 1825)	
	<i>Oxygastra curtisii</i> (Dale, 1834)	
	<i>Somatochlora arctica</i> (Zetterstedt, 1840)	
	<i>Somatochlora flavomaculata</i> (Vander Linden, 1825)	
<i>Somatochlora metallica</i> (Vander Linden, 1825)		

Table 2.2 – Continued on next page

Table 2.2 – Continued from previous page

Anisoptera	Gomphidae	<i>Gomphus graslinii</i> (Rambur, 1842) <i>Gomphus pulchellus</i> (Selys, 1840) <i>Gomphus simillimus</i> (Selys, 1840) <i>Gomphus vulgatissimus</i> (Linnaeus, 1758) <i>Onychogomphus forcipatus</i> (Linnaeus, 1758) <i>Onychogomphus uncatus</i> (Charpentier, 1840) <i>Ophiogomphus cecilia</i> (Fourcroy, 1785)
	Libellulidae	<i>Crocothemis erythraea</i> (Brullé, 1832) <i>Leucorrhinia albifrons</i> (Burmeister, 1839) <i>Leucorrhinia caudalis</i> (Charpentier, 1840) <i>Leucorrhinia dubia</i> (Vander Linden, 1825) <i>Leucorrhinia pectoralis</i> (Charpentier, 1825) <i>Libellula depressa</i> (Linnaeus, 1758) <i>Libellula fulva</i> (O. F. Müller, 1764) <i>Libellula quadrimaculata</i> (Linnaeus, 1758) <i>Orthetrum albistylum</i> (Selys, 1848) <i>Orthetrum brunneum</i> (Fonscolombe, 1837) <i>Orthetrum cancellatum</i> (Linnaeus, 1758) <i>Orthetrum coerulescens</i> (Fabricius, 1798) <i>Sympetrum danae</i> (Sulzer, 1776) <i>Sympetrum depressiusculum</i> (Selys, 1841) <i>Sympetrum flaveolum</i> (Linnaeus, 1758) <i>Sympetrum fonscolombii</i> (Selys, 1840) <i>Sympetrum meridionale</i> (Selys, 1841) <i>Sympetrum pedemontanum</i> (Müller in Allioni, 1766) <i>Sympetrum sanguineum</i> (Müller, 1764) <i>Sympetrum striolatum</i> (Charpentier, 1840) <i>Sympetrum vulgatum</i> (Linnaeus, 1758) <i>Trithemis annulata</i> (Palisot de Beauvois, 1807)
Zygoptera	Calopterygidae	<i>Calopteryx haemorrhoidalis</i> (Vander Linden, 1825) <i>Calopteryx splendens</i> (Harris, 1780) <i>Calopteryx virgo</i> (Linnaeus, 1758) <i>Calopteryx xanthostoma</i> (Charpentier, 1825)
	Coenagrionidae	<i>Ceriagrion tenellum</i> (Villers, 1789) <i>Coenagrion caerulescens</i> (Boyer de Fonscolombe, 1838) <i>Coenagrion hastulatum</i> (Charpentier, 1825) <i>Coenagrion lunulatum</i> (Charpentier, 1840) <i>Coenagrion mercuriale</i> (Charpentier, 1840) <i>Coenagrion ornatum</i> (Selys, 1850) <i>Coenagrion puella</i> (Linnaeus, 1758) <i>Coenagrion pulchellum</i> (Vander Linden, 1825) <i>Coenagrion scitulum</i> (Rambur, 1842) <i>Enallagma cyathigerum</i> (Charpentier, 1840) <i>Erythromma lindenii</i> (Selys, 1840) <i>Erythromma najas</i> (Hansemann, 1823)

Table 2.2 – Continued on next page

Table 2.2 – Continued from previous page

		<i>Erythromma viridulum</i> (Charpentier, 1840) <i>Ischnura elegans</i> (Vander Linden, 1820) <i>Ischnura pumilio</i> (Charpentier, 1825) <i>Pyrrhosoma nymphula</i> (Sulzer, 1776)
	Lestidae	<i>Chalcolestes viridis</i> (Vander Linden, 1825) <i>Lestes barbarus</i> (Fabricius, 1798) <i>Lestes dryas</i> (Kirby, 1890) <i>Lestes macrostigma</i> (Eversmann, 1836) <i>Lestes sponsa</i> (Hansemann, 1823) <i>Lestes virens</i> (Charpentier, 1825) <i>Sympecma fusca</i> (Vander Linden, 1820)
	Platycnemididae	<i>Platycnemis acutipennis</i> (Selys, 1841) <i>Platycnemis latipes</i> (Rambur, 1842) <i>Platycnemis pennipes</i> (Pallas, 1771)

2.3.2 Reference shapes for each species

We performed a principal component analysis (PCA) for all the 79 species monitored in France by the Steli program during the interval 2011-2019 (Fig. 2.8). The 304 pairs of wings sample 2 females and 2 males for almost all the species. For *Aeshna subartica* Walker, 1908, *Gomphus graslinii* (Rambur, 1842), *Libellula quadrimaculata* (Linnaeus, 1758), *Orthetrum coerulescens* (Fabricius, 1798), *Sympetrum flaveolum* (Linnaeus, 1758), *Coenagrion hastalum* (Charpentier, 1825) and *Coenagrion lunulatum* (Charpentier, 1840), a female is missing, two for *Coenagrion caerulescens* (Boyer de Fonscolombe, 1838). For *Aeshna affinis* (Vander Linden, 1820), *Orthetrum albistylum* (Selys, 1848) and *Ischnura pumilio* (Charpentier, 1825) a male is missing. This PCA is used as global morphospace in Chapter 3.

The first two axes explain 80.5% of the total variance (values of the variance explained by the 6 first axes are available in Annex A.3). Anisoptera and Zygoptera occupy clearly distinct areas of the morphospace. Within Anisoptera, forewing and hindwing are well differentiated. This is less clear for Zygoptera. There is no notable sexual dimorphism for any suborder. Within Zygoptera the different families occupy clearly distinct areas of the morphospace except for the Platycnemididae and Coenagrionidae, which are superposed when considering the first two axes (Fig. 2.8). The Calopterygidae occupy a peculiar area. Within Coenagrionidae, *Pyrrhosoma nymphula* (Sulzer, 1776) (in yellow in Fig. 2.8) is stepping out, highlighting a distinctive wing shape within the family. As for Anisoptera, only the families Aeshnidae and Libellulidae do not overlap.

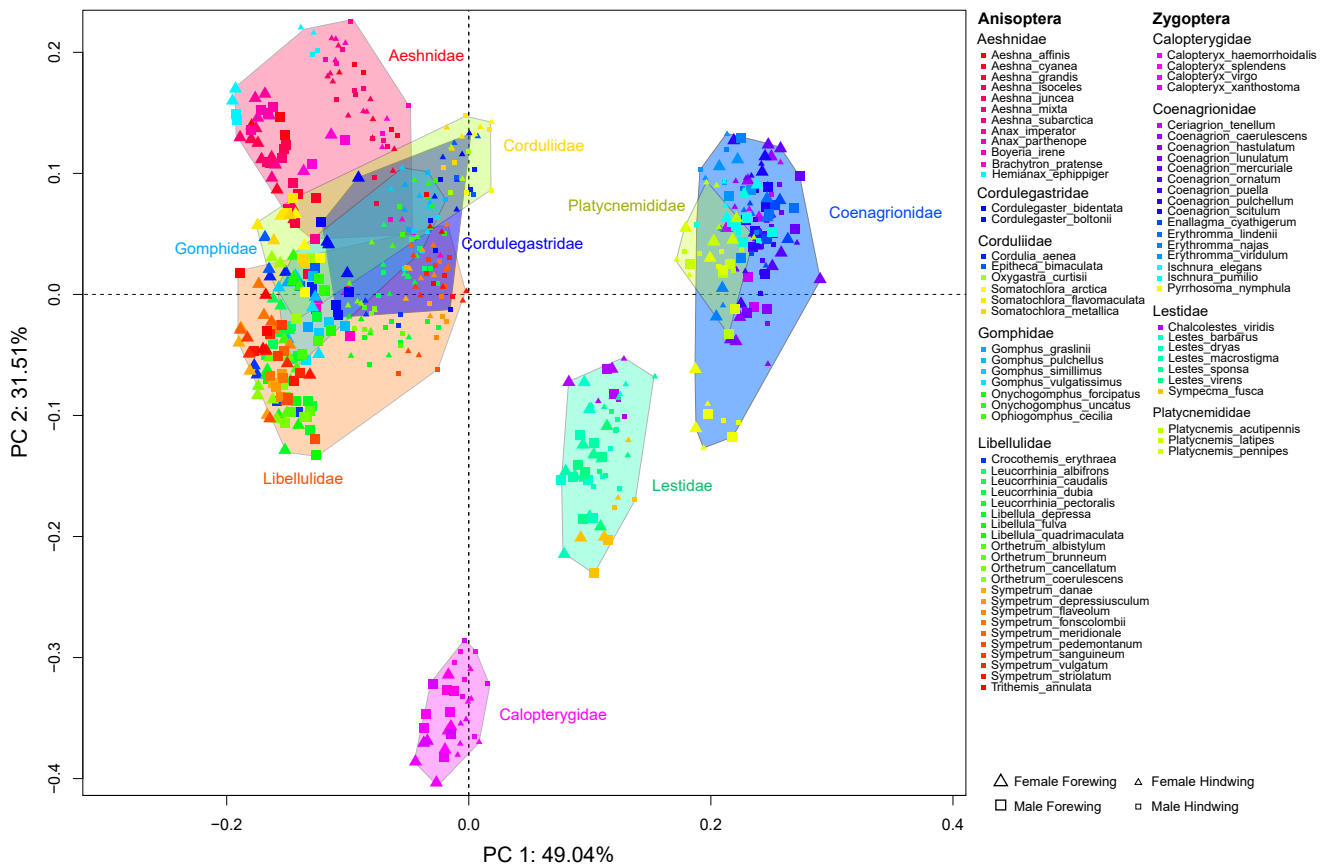


Figure 2.8 – Principal component analysis of the 304 wing pairs considered as reference for species monitored in mainland France by the Steli program. Observations are coloured by species. Coloured areas delimit families. Large and small triangles represent female forewings and hindwings, respectively, while large and small squares represent male forewings and hindwings, respectively.

Several analyses were performed on the first six principal components (PC) scores which explain more than 99% of the total variance. A paired Hotelling t^2 test were realised to test for difference between forewing and hindwing, male and female, within Odonata and within Zygoptera and Anisoptera taken separately. To do so, shape differences between forewings and hindwings and between male and female were computed by subtracting PC scores from one to the other. The normality of the distribution of each PCs for these differences were checked thanks to Shapiro-Wilk normality tests. The multivariate normality was also checked thanks to the package MVN (Korkmaz et al., 2014). The differences of these six variables were not always normally distributed. The different test and their results are shown in Table 2.3. The Hotelling t^2 test was then performed on the differences on R, thanks to the ICSNP package (Nordhausen et al., 2018). According to these tests, there is a significant difference between male and female within odonates as a whole. The Hotelling t^2 assumes normality of distances between each compared pairs of individuals. As the distribution is not normal for the difference between forewings and hindwings the results might not be reliable. The distribution is bimodal for the first five PCs, and for the four first PCs this bimodal distribution reflects the distribution of

Zygoptera and Anisoptera as mentioned earlier. Within Zygoptera, there is a significant difference between forewings and hindwings. Within Anisoptera, the distribution was still not normal. Thus we tested other subgroups. Only the difference between the male and female hindwings have a normal distribution and are tested significantly different. In summary, these Hotteling t^2 tests seem to highlight sexual dimorphism within odonates and significant difference between forewings and hindwings. However multivariate normal distribution was not always checked, therefore the reliability of this results can be questioned.

Table 2.3 – Results of the paired Hotteling t^2 test realised on the scores of the 6 first principal components. The column "Group" indicate the group on which the test has been performed, the "Comparison" one the parameters that have been compared, the "MVN" one indicate the results of the Multivariate Normality tests. * refers to significant values. FW = forewing; HW =hindwing.

Group	Comparison	Nomality of each PC	MVN	p-values
Odonata (FW & HW)	F vs. M	Yes (PC 1:5); No (PC 6)	No	1.053e-12 *
Odonata (F & M)	FW vs. HW	No (PC 1:5); Yes (PC 6)	No	<2.2e-16 *
Zygoptera (F & M)	FW vs. HW	Yes	Yes	3.978e-13 *
Anisoptera (F & M)	FW vs. HW	No (PC 1,5); Yes (PC 2:4,6)	No	<2.2e-16 *
Anisoptera FW	F vs. M	Yes (PC 1:2,4:6); No (PC 3)	No	4.18e-07 *
Anisoptera HW	F vs. M	Yes	Yes	1.608e-13 *
Anisoptera Female	FW vs. HW	No(PC 1,5); Yes (PC 2:4,6)	No	<2.2e-16 *
Anisoptera Male	FW vs. HW	No(PC 1,5,6); Yes (PC 2:4)	No	<2.2e-16 *

As mentionned above, four reference specimens are used to represent each monitored species in the computation of the morphospace. Considering that units of interest are not isolated wings but species, a single reference mean shape was computed for each species. The erection of a reference shape also avoid biases that could be induced by the few species not fully documented. To do so, we took the PC scores means of all wings of a species (i.e. the forewing and hindwings of the males and females; Fig. 2.9). However, preliminary tests suggest that there are significant differences between forewings and hindwings and between males and females. The intra-specific variations due to sex and wing segment was therefore compared to inter-specific variations in order to assess the consistency of the erection of such reference shapes.

The variance due to the sex and the wing segment within each species have been tested thanks to a nested permutational MANOVA. This test is equivalent to a Multivariate Analysis of Variance (MANOVA) but it is based on permutations of euclidean distance matrices. Given that our data are not normally distributed we choose to use this non-parametric test rather than a nested-MANOVA. This test was performed on R thanks to the package *vegan* (Oksanen et al., 2016). The obtained R^2 equals 0.883 for the species (p-value= 0.001), 0.007 for sex within species (p-value= 0.001), 0.099 for wing segment within species (p-value= 0.001) and 0.001 for the interaction of sex and wing segment within species (p-value= 1). Therefore, there is an important inter-specific dissimilarity. There are significant differences between sexes and between wing segments within species,

however we consider, given the obtained R^2 , that the intra-specific variations of sex and wing segment are negligible compared to the inter-specific variations. In that respect we assumed that the erection of a reference shape for each species, as the average shape, is consistent with our problematic.

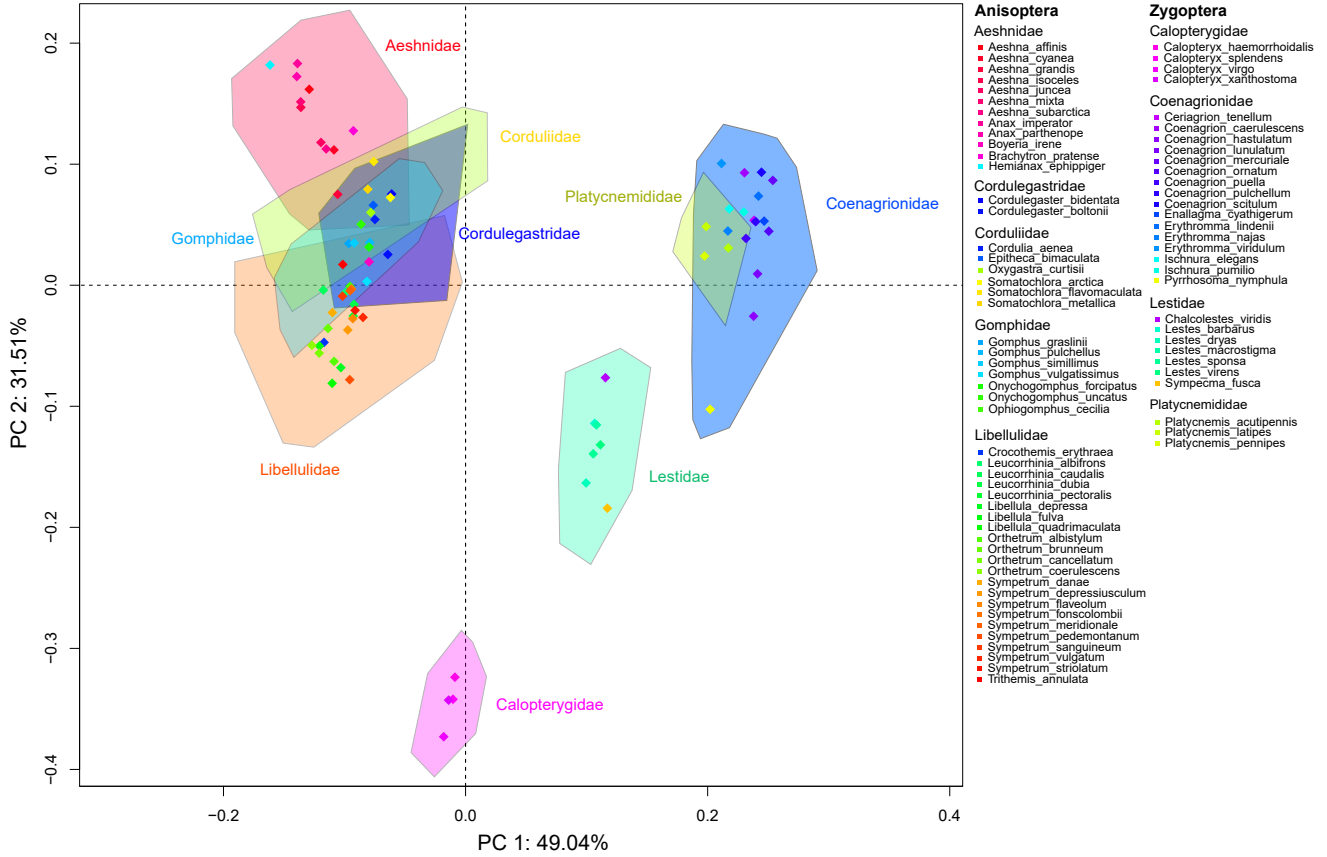


Figure 2.9 – Distribution of reference shape for each species in the global morphospace. Observations are coloured by species. Coloured areas as in Fig. 2.8 delimit the space occupied by each families prior to the computation of species reference shape.

2.4 Disparity

Disparity is the quantification of the diversity of morphologies (Gould, 1989; Foote, 1993b) and can be described based on several data types (e.g. linear measurements, cladistic matrices). Here we are resorting to geometric morphometrics, considered as the most objective assessment of shape differences (Briggs et al., 1992; Wills et al., 1994). Coordinates of species in a morphospace are used as raw variables to compute disparity measures. In practice, the variables are the PC scores obtained from the PCA.

Disparity can be described by three, different and complementary metrics types, namely size, density and position. These different types of metrics provide different and complementary information (Foote, 1993b; Ciampaglio et al., 2001; Guillerme et al., 2020). The size approximates the amount of space occupied. Larger values indicate the presence

of more extreme shape combinations. Density metrics approximates the distribution of the observations. This metric informs on the average distances between shapes. The position metrics informs on the location of the observations in the global morphospace.

For each type, numerous estimates can be found in the literature. Here the size is quantified as the sum of ranges. The range is defined as the maximal euclidean distance between two specimens on each variable. It corresponds to the maximum minus the minimum values observed along the axes and therefore takes into account only extreme shapes (Ciampaglio et al., 2001; Foote, 1992; Neige, 2003). This estimates is thus very sensitive to outliers (Guillerme et al., 2020). Moreover, the sum of ranges is also sensitive to sample size (Foote, 1993b). An important size heterogeneity of the samples leads to important biases. Therefore, this estimate and the others were bootstrapped to a minimal number of species in the following analyses in order to eliminate the size effect by predicting the disparity that could be observed with smaller random samples (Foote, 1992; Neige, 2003).

The density metrics approximate the distribution of observations. They are referred to as dissimilarity, dispersion, or distances between observations (Foote, 1993b; Ciampaglio et al., 2001; Gerber, 2019). Here we are using the R package of Guillerme (2018) to compute disparity metrics and therefore decided to use his nomenclature (i.e. size, density and position metrics). Counter-intuitively, the metrics of density we are using are measuring the dispersion, being the distances between observations. Thus, as dispersion increases, the metrics of density will increase (observations being further from each other), whereas one could have expected the opposite by using the word "density" in its usual meaning for density metrics, that is to say an increase of density when observations are closer to each other. In other words, here we use density metrics which increase with increasing dispersion between observations and decrease with an increasing concentration of observations.

The density metrics computed here are the sum of variances, the median pairwise distances and the average nearest neighbour distances. The sum of variances is commonly used in paleontology (Ciampaglio et al., 2001; Villier and Eble, 2004; Wills et al., 1994). It is the sum of the variances of all PC axes. This estimates is known to be robust, less sensitive to sample size except for small samples, due to uncertainty inflation (Ciampaglio et al., 2001; Foote, 1992; Villier and Korn, 2004). However it can be biased when several clusters occur in the morphospace; that is to say, when species are grouped in several distinct areas in the morphospace (Villier and Eble, 2004; Neige, 2003; Foote, 1993b).

The median pairwise distances is the median of euclidean distances in the morphospace between all possible pairs of species. This estimates is insensitive to sample size. It is therefore well suited for study with large changes in observed species richness. (Ciampaglio et al., 2001; Bapst et al., 2012).

The average nearest neighbour distances is the sum of the euclidean distances between

each species and the closest one in the morphospace, divided by the total number of species. It is representative of the density of pairs of species (Foote, 1992; Guillerme et al., 2020).

The position is quantified by the average displacement. This estimate has been proposed by Guillerme et al. (2020). It is defined as the ratio between the subset species positions from their centroid and the center of the global morphospace (a value of 1 indicates that the subset species centroid is the center of the morphospace). It can inform us on change of areas occupied within the morphospace.

The use of these three types of estimates is needed to understand changes in morphospace occupation. These estimates are complementary and inform us on different aspects of disparity. The size estimate can reveal a change in group size (radiation for example), the density a change in distribution (niche specialization if increase for example) and the position can reveal a new occupation of the morphospace such as different niches (Ciampaglio et al., 2001; Guillerme et al., 2020).

Chapter 3

Odonata disparity in Ile-de-France

Contents

3.1	Introduction	49
3.2	Material & Methods	52
3.2.1	Sites selection	52
3.2.2	Landscape structure	52
3.2.3	Diversity	55
3.2.4	Disparity	56
3.3	Results	58
3.3.1	Sensitivity analysis and choice of parameters	61
3.3.2	Disparity & Diversity	67
3.3.3	Landscape structure	70
3.3.4	Forecast of diversity loss in urban environments	72
3.4	Discussion & Conclusion	74
3.4.1	Robustness of the Steli data and parametrisation of disparity analyses	74
3.4.2	Diversity and disparity patterns	74
3.4.3	Perspectives	77

3.1 Introduction

In respect of the five major crises that affected biodiversity over the last 500 million years (Alroy, 2008), the recent alarming loss of species, induced by human activities, has led to the proclamation of a sixth one (Myers and Knoll, 2001). Alteration of natural

habitats is the most important trigger of biodiversity loss at the global scale, which is well documented on freshwater habitats (Sala et al., 2000).

Odonata are known to be good bio-indicators in both aquatic and terrestrial habitats, being sensitive to the alteration and pollution of water bodies and the surrounding areas. Odonate species can be used as bio-indicators of environmental disturbance (Dutra and De Marco, 2015; Valente-Neto et al., 2016), either as individual species or combinations of species. Overall species richness may be maintained but species composition is affected by anthropogenic land alterations (Jeanmougin et al., 2014; Goertzen and Suhling, 2019; Rocha-Ortega et al., 2019, 2020).

Increased vegetation cover has been shown to be associated with increased odonate species richness in several countries, including France, and the city of Paris (Jeanmougin et al., 2014; Villalobos-Jimenez et al., 2016). For this city, Jeanmougin et al. (2014) found no correlation between species pond assemblages and a urban gradient, in the contrary of what is known for other species (butterflies, pollinators, etc.). They assume that this is related to the good dispersal ability of odonates, allowing them to colonize urban ponds even in the core of the city. In Paris, this might be linked to a high density of ponds resulting from favourable environmental policies. The density of building, the occurrences of open landscapes and of forest around the ponds impact diversity. The degree of urbanization surrounding ponds, rather than the urban gradient per se, might provide more relevant insights. This is the choice we made using buffer around sites to summarize environmental conditions within the usual territory of adult odonates.

Urban areas may have a negative effect on species dispersal and on reproduction cycles wherever suitable water bodies are missing. Thus, one can expect species richness to decrease with urban development and that relative contribution to diversity of tolerant species should increase (Villalobos-Jimenez et al., 2016). Indeed, some Odonata species may be more tolerant to urban stressors, and some may even reproduce in polluted water (Villalobos-Jimenez et al., 2016; Boudot et al., 2017). Generalist species are abundant in cities but some specialist species are also known to occur in such environment, including threatened ones, even in Ile-de-France (Houard and Merlet, 2014; Villalobos-Jimenez et al., 2016).

Most studies in conservation biology focus on taxonomic richness, whereas other metrics are available and can be used to investigate the response of organisms to different pressures. Disparity has often been used in palaeontology to describe the patterns of extinction selectivity or other biodiversity changes. However, some studies suggested to investigate temporal or spatial variations in nature thanks to disparity, and to use this metric in addition to species richness for conservation decisions (Roy et al., 2001; Neige, 2003; McClain et al., 2004; Neustupa et al., 2009). Both Roy et al. (2001) and Neustupa et al. (2009) found little relationship between diversity (species richness) and disparity. High diversity values for a given locality can be associated to low species richness, and

localities with high species richness are not necessarily linked to higher disparity values. Contrasted patterns of diversity and disparity have been described in the fossil record. It has been theorized for long that decoupling of diversity and disparity is relevant to investigate the severity and selectivity of extinctions (Foote, 1992, 1993b).

Some studies on Odonata conservation already took into account key traits such as body-size, climatic tolerance or breeding habitats to infer vulnerability to local extirpation (Rocha-Ortega et al., 2020). Indeed, trait-based approaches could be favoured for insects given the difficulties of sampling and lack (or heterogeneity) of abundance data (Cardoso et al., 2020; Rocha-Ortega et al., 2020).

Studies on evolution of insect wing shape have shown to be linked to natural and sexual selection pressures (Outomuro et al., 2012, 2013). Studies on odonates wing morphology investigated whether there is an adaptation in wing shape related to habitat variation, based on the hypothesis that wing shape is linked to flight dispersal ability (Outomuro et al., 2013). Outomuro et al. (2013) found no significant effect of water bodies but a difference between forested and open landscape. They have found evidence of natural but also sexual selection on wing shape (Outomuro et al., 2013, 2016).

Here we focused on wing disparity. In details, three type of disparity estimates are computed: size, density and position. If artificialization act as a selective pressure on odonates, we expect to see, from the most natural and diversified to the most artificialized sites, a decrease in size, revealing a loss of specific morphologies and also a decrease in density, revealing a potential loss of niche specialists. The position can also be predicted to change between those sites, revealing shifts in niches occupation (Guillerme et al., 2020).

Herein we investigate the disparity of Ile-de-France odonates wings thanks to an exploratory approach, allowing us to determine the optimal parameters to study this group in an urbanised area.

We expect wing morphology to reveal generalist vs. specialist morphologies more or less tolerant to landscape artificialization. Disparity changes could reflect changes in species assemblages. We expect to see different responses for Zygoptera and Anisoptera. The latter have a higher dispersal ability and are more adapted to different habitats than Zygoptera. The impact of threatened species loss on the disparity of the group in Ile-de-France is also inferred. Indeed, disparity is often used to study mass extinction events properties. Here we will try to predict a potential response to a sixth extinction crisis. In case of a morphologically selective extinction, with the decrease of diversity we expect to see a drop of disparity. In contrast, if disparity remains constant or increases it could reflect a morphologically non-selective crisis or more complex ecological triggers (Foote, 1993b).

3.2 Material & Methods

3.2.1 Sites selection

We based our study on standardized data of the Steli, a citizen science program for odonate species monitoring in France, which started in 2011. This monitoring program follows a strict protocol allowing the creation of a standardized database. The protocol identifies 3 periods during the flight period of odonates, the first one before the 15th June, the second between 15th June and 31st July and the third one after 31st July. Within each period, 3 monitoring sessions of at least 30 minutes in duration must be performed, before integration of the data into the database. The temporal gap between two sessions within a period should not exceed 21 days.

We focused our analyses on the Ile-de-France region, where forty sites have been monitored under the Steli framework. Among these sites, the monitoring protocol was strictly followed for at least one period in only 22 sites. To avoid comparing sites monitored during different periods, and thus comparing differences due to the time of season rather than the geography or the ecology of the sites, we choose to focus on only one period, the second one. This period is the one with the highest number of sessions and the highest species richness, corresponding to the reproduction period of most of odonates present in Ile-de-France (Boudot et al., 2017). However, among the 22 sites only 12 have been monitored during this period. We choose to add 5 sites that are at the margin of the protocol by extending by 4 days the beginning and end of the second period and by extending the temporal gap between two sessions to 24 days. Those 17 selected sites have been monitored at least once between 2013 and 2019. The location of the selected sites in Ile-de-France is reported in the Fig. 3.1. Three sites were monitored twice, two different years, so we ended up with a total of 20 sites, considering the different years as different sites.

3.2.2 Landscape structure

We gathered information from digitized land cover maps from the "Mode d'occupation du sol" (MOS) produced by the Institut Paris Region, in order to quantify the composition of landscapes surrounding each site. Eighty-one types of land cover are differentiated on the map. The 2017 map is taken as reference for the analyses but the map for 2012 was also considered in order to detect recent changes in land cover. We computed landscape composition within buffers of 500, 1000 and 2000 m radii around each site. Land cover types were grouped into three categories according to odonate ecology. Closed waters, streams and shorelines (land cover types 5, 11 and 12 of the MOS) are the category favourable to odonates, while urbanised and tilled areas (land cover types 6, 8, 9, 10, 19,

21, 24, 29 – 81) represent unfavourable conditions. Wetland and swamps were not taken into account in the favourable category because they are merged with herbaceous zones, wasteland and other areas, that are common environments not necessarily favourable to odonates. The other land cover types, such as grassland and forest, were considered neutral, neither favourable to odonates reproduction nor unfavourable to their presence. More detailed information on land cover types is available in Table 3.1. Maps of the buffer around each selected sites are available in Annex A.4. For each site, proportions of the three categories were computed by summing up surfaces of corresponding types within the buffer and then computing the percentage of the total buffer surface occupied by each.

Within the favourable category the impact of the diverse components of this category, lotic (i.e. bodies of moving water) and lentic (i.e. bodies of still, closed water) habitats, were investigated. Shorelines are present in a very reduced number of sites within the buffer of 1000 and 2000 m radii, and it is absent within the 500 m radius buffer. Therefore, the shoreline has not been discussed.

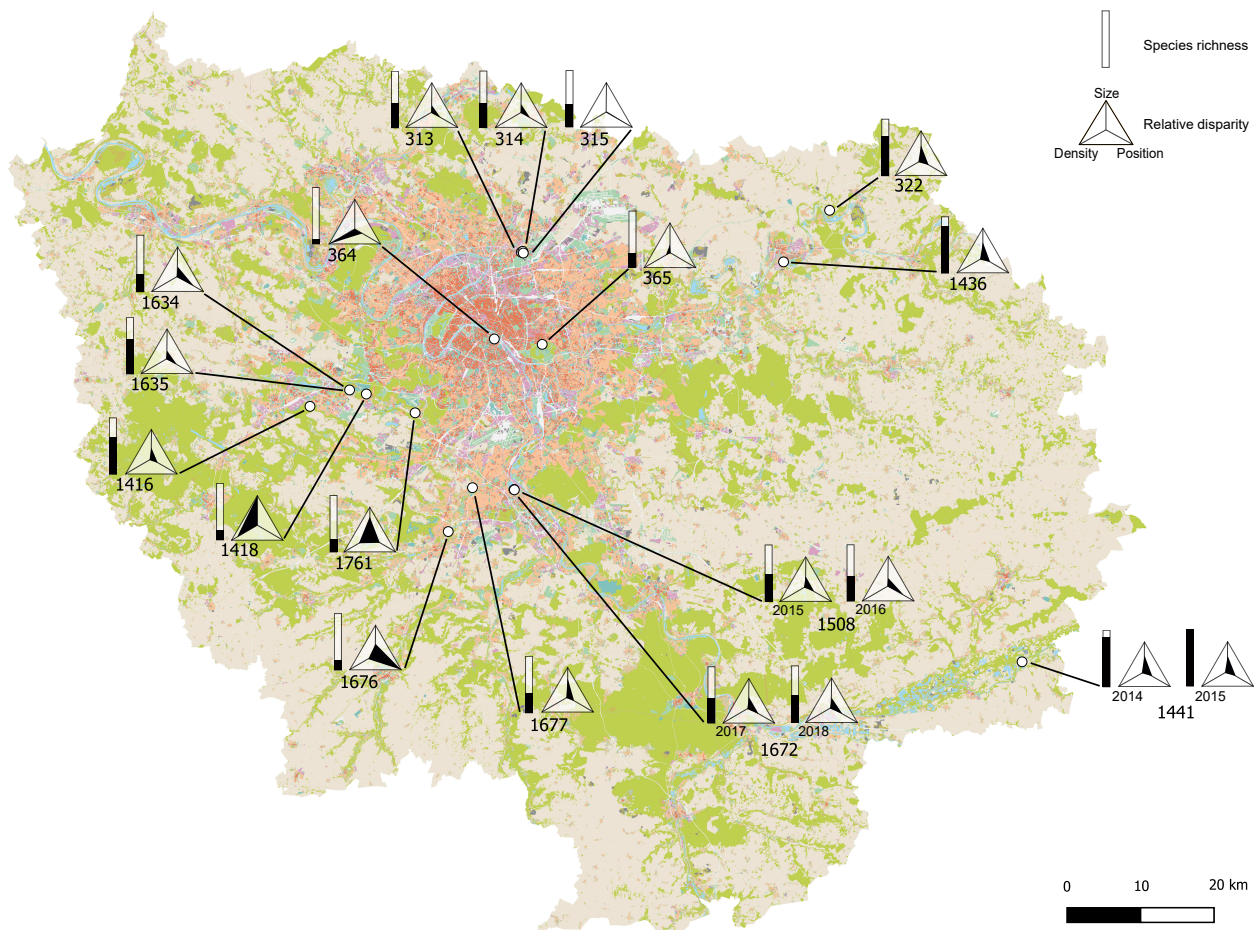


Figure 3.1 – Maps of the MOS 2017 of the Ile-de-France region. White dots correspond to the selected sites position. Sites numbering are the ones from the Steli database. Gauges represent species richness. Triangle-shaped graphs correspond to the proportion of size, density and position metrics for each site, minimum and maximum values of each metric axes correspond to the minimum and maximum values obtained among all the sites; represented density metric is the average nearest neighbour distances.

Table 3.1 – Nomenclature of the MOS 2017 in 81 land-cover types and the attributed category relative to odonate ecology.

MOS 2017	Land-cover type	Category
1	Woods or forests	Neutral
2	Clearings or logging areas in forests	Neutral
3	Poplar groves	Neutral
4	Open spaces with herbaceous or shrubby vegetation	Neutral
5	Shorelines	Favourable
6	Tilled land	Unfavourable
7	Grassland	Neutral
8	Fruit trees, nursery	Unfavourable
9	Market gardening, horticulture	Unfavourable
10	Intensive greenhouse cultivation	Unfavourable
11	Closed water (ponds, lakes. . .)	Favourable
12	Streams	Favourable
13	Parks and gardens	Neutral
14	Kitchen gardens	Neutral
15	Individual housing garden	Neutral
16	Rural housing garden	Neutral
17	Continuous low housing garden	Neutral
18	Outdoor sports fields	Neutral
19	Open tennis court	Unfavourable
21	Sports equipment evolution park	Unfavourable
22	Golf courses	Neutral
24	Camping, caravanning	Unfavourable
25	Parks related to leisure activities except castle parks	Neutral
26	Cemeteries	Neutral
27	Grassed area with or without shrubs	Neutral
28	Vacant land	Neutral
29	Individual housing	Unfavourable
30	Identical individual housing units	Unfavourable
31	Rural housing	Unfavourable
32	Low continuous housing	Unfavourable
33	Continuous high collective housing	Unfavourable
34	Discontinuous collective housing	Unfavourable
36	Other housing	Unfavourable
37	Water production	Unfavourable
38	Sanitation	Unfavourable
39	Electricity	Unfavourable
42	Other infrastructures	Unfavourable
43	Activities in mixed urban fabric	Unfavourable
44	Large industrial rights-of-way	Unfavourable
45	Economic activity zones	Unfavourable
46	Open-air storage	Unfavourable
47	Logistics warehouses	Unfavourable

Table 3.1 – *Continued on next page*

Table 3.1 – *Continued from previous page*

MOS 2017	Land-cover type	Category
48	Large commercial areas	Unfavourable
49	Other businesses	Unfavourable
51	Gas station	Unfavourable
52	Offices	Unfavourable
53	Indoor sports facilities	Unfavourable
54	Equestrian centre	Unfavourable
55	Indoor swimming pools	Unfavourable
56	Outdoor swimming pools	Unfavourable
58	Primary education	Unfavourable
59	Secondary education	Unfavourable
60	Higher education	Unfavourable
61	Other education	Unfavourable
62	Hospitals, clinics	Unfavourable
63	Other health equipment	Unfavourable
64	Large congress and exhibition centres	Unfavourable
65	Cultural and leisure facilities	Unfavourable
66	Seats of territorial administrations	Unfavourable
67	Main offices of territorial administrations	Unfavourable
68	Limited public access facilities	Unfavourable
69	Town Halls	Unfavourable
70	Permanent markets	Unfavourable
71	Places of worship	Unfavourable
72	Other local facilities	Unfavourable
73	Rail transport rights-of-way	Unfavourable
74	Ways with a right-of-way of more than 25 m	Unfavourable
75	Surface car parks	Unfavourable
76	Multi-storey car parks	Unfavourable
77	Bus stations, bus depots	Unfavourable
80	Discharges	Unfavourable
81	Construction sites	Unfavourable

3.2.3 Diversity

For each site, the abundance and species richness was calculated by summing the data of 3 monitoring sessions of the second period of the Steli timescale. The available abundance data were not uniform, three different types of abundance information were provided by the volunteers: (1) presence data, (2) a range (from 1 to 10, 11 to 50 and more than 51) or (3) exact counts. To make them comparable, abundance data were gathered in 4 categories, each with a standardized abundance value, (i) a value of 0 for absence, (ii) a value of 5 for species noted present or with exact counts ranging from 1 to 10, (iii) a value of 30 for occurrence count ranging from 11 to 50 and (iv) a value of 100 for all species reported with more than 51 individuals.

If localities with reduced species richness are associated to degraded ecosystems, then they may be relevant to investigate selectivity of species loss. Diversity was quantified at two different taxonomic levels, namely species and families. Data remained too uneven for abundance-based diversity indexes. We used the standardized abundance data to assess the rarity of monitored species. Species were assigned to categories according to their overall abundance. Relative rarity was also investigated from the number of sites where each species is present. Species were divided in 3 groups, as follows: present in more than 50% of sites (common species), less than 10% (rare species) and in-between (Table 3.2). For both approaches of species rarity, a permutation test has been realised to compare the means of common and rare species for each disparity estimates (Ludbrook and Dudley, 1998). The impact of the number of bootstraps on the obtained p-value was tested (Annex A.5).

Rarity of species defined as occurrence in locality is independent of population size. A given species can be present in a very limited number of localities but be very common where present and, conversely, species occurring in many localities may be locally very rare. The vulnerability of species is defined from abundance data and the changes of population size through time (Houard and Merlet, 2014). The vulnerability of odonate species was extracted from the regional redlist of odonates for Ile-de-France (Houard and Merlet, 2014 ; Table 3.2). Monitored species were clustered in two groups: threatened and non-threatened. Species classified as threatened are those listed in the categories "Critically Endangered" (CR), "Vulnerable" (VU) and "Near Threatened" (NT) in the red list, and non-threatened species the "Least Concerned" (LC) one.

Disparity and diversity were computed considering the entire dataset, i.e. all the species present in Ile-de-France, or data subsets: rare vs common species, threatened vs non-threatened, or at the scale of individual sites.

3.2.4 Disparity

A global morphospace was generated including all species monitored under the Steli framework in mainland France, which includes 79 species. The species monitored at each site can be plotted on this global morphospace, in order to visualize and compare the morphospace occupation by each site (Annex A.6).

Disparity can be described by three, different and complementary types of measurements, namely size, density and position. We computed several disparity estimates from the PC scores of the PCA, the sum of ranges for the size, the sum of variances, the mean pairwise distances and the average nearest neighbour distances for density and the average displacement (Guillerme et al., 2020) for position.

Table 3.2 – List of species monitored in Ile-de-France under the Steli framework with their associated regional Red List categories. The abundance category correspond to the rarity of the species assessed based on the standardized abundance data. Site frequency category correspond to the rarity assessed base on the number of sites the species are present.

Species	Red List categories	Abbreviations	Abundance category	Site frequency category
<i>Sympetrum danae</i>	Critically Endangered	CR	Rare	Rare
<i>Aeshna isoceles</i>	Vulnerable	VU	Rare	Rare
<i>Ceriagrion tenellum</i>	Vulnerable	VU	Rare	Rare
<i>Leucorrhinia caudalis</i>	Vulnerable	VU	Rare	Rare
<i>Oxygastra curtisii</i>	Vulnerable	VU	Rare	Rare
<i>Somatochlora metallica</i>	Vulnerable	VU	Rare	Rare
<i>Aeshna grandis</i>	Near threatened	NT	Rare	in between
<i>Calopteryx virgo</i>	Near threatened	NT	Common	in between
<i>Cordulia aenea</i>	Near threatened	NT	Rare	in between
<i>Erythromma najas</i>	Near threatened	NT	Common	in between
<i>Onychogomphus forcipatus</i>	Near threatened	NT	Rare	Rare
<i>Aeshna cyanea</i>	Least concern	LC	Common	Rare
<i>Aeshna mixta</i>	Least concern	LC	Rare	in between
<i>Anax imperator</i>	Least concern	LC	Common	Common
<i>Anax parthenope</i>	Least concern	LC	Common	Common
<i>Calopteryx splendens</i>	Least concern	LC	Common	in between
<i>Chalcolestes viridis</i>	Least concern	LC	Common	in between
<i>Coenagrion puella</i>	Least concern	LC	Common	Common
<i>Crocothemis erythraea</i>	Least concern	LC	Common	Common
<i>Enallagma cyathigerum</i>	Least concern	LC	Common	Common
<i>Erythromma lindenii</i>	Least concern	LC	Common	in between
<i>Erythromma viridulum</i>	Least concern	LC	Common	in between
<i>Gomphus pulchellus</i>	Least concern	LC	Rare	Rare
<i>Ischnura elegans</i>	Least concern	LC	Common	Common
<i>Libellula depressa</i>	Least concern	LC	Rare	in between
<i>Libellula fulva</i>	Least concern	LC	Common	in between
<i>Libellula quadrimaculata</i>	Least concern	LC	Rare	in between
<i>Orthetrum brunneum</i>	Least concern	LC	Rare	Rare
<i>Orthetrum cancellatum</i>	Least concern	LC	Common	Common
<i>Platycnemis pennipes</i>	Least concern	LC	Common	Common
<i>Pyrrhosoma nymphula</i>	Least concern	LC	Rare	in between
<i>Sympecma fusca</i>	Least concern	LC	Rare	Rare
<i>Sympetrum fonscolombii</i>	Least concern	LC	Rare	Rare
<i>Sympetrum meridionale</i>	Least concern	LC	Rare	Rare
<i>Sympetrum sanguineum</i>	Least concern	LC	Common	Common
<i>Sympetrum striolatum</i>	Least concern	LC	Common	in between

Disparity metrics were computed for each sites on R using the package `dispRity` (Guillerme, 2018). Some metrics such as the sum of ranges are sensitive to the number of dimensions and the number of observations.

All metrics were rarefied to a minimal sample size of 7 species using bootstrap estimates, except for 5 sites (364, 365, 1418, 1676 and 1761) where the number of monitored species is too low, and for which the raw disparity values are given.

Measures of disparity were computed from mean PC scores obtained from the Principal components analysis of the reference specimens of all the species. The 6 first principal

components (PCs) were used. The number of PCs to be used has been tested regarding the impact of the number of PC on the total disparity values (Annex A.7). Ten PCs would have been the best option, but disparity cannot be computed for sites with less species than PCs so that increasing morphospace dimensions reduces the number of sites to be considered. The PCs after PC6 explain less than 1% of the variation. To take into account as much sites as possible with the rarefaction of 7 we choose to use only 6 PCs. This way only 5 sites were not rarefied, against 13 if we had taken 10 PCs.

To assess the impact of the number of species accounted for on bootstrapped estimates of disparity, we compared means and variance of bootstrap sets for sampling quota varying from 3 to 11 species for each sites. Except for the sum of ranges and the average nearest neighbour distances, the species quota does not affect much disparity estimates. The sum of ranges values increase with the number of species and tends quickly towards a plateau. The average nearest neighbour distances values decrease with the number of species and also tends to a plateau. The more species are present and more the distance to the nearest neighbour have chances to be reduced. For both estimates, the plateau can be considered as reached with 7 species. The choice of 7 species and 6 PCs, allowing to maximise the sites that can be bootstrapped, thus seems to be a good compromise. Values for sites with fewer species than the quota of seven seem to express slightly higher values than bootstrapped values (Annexes A.8–A.12).

We computed disparity estimates for each site, first considering all odonate species, and then considering species subsets. Species of Anisoptera and Zygoptera occurring in France constitute very distinctive groups in terms of shape (see Fig. 2.9). Zygoptera families occupies really different parts of the morphospace, in particular the Calopterygidae, which are well-separated from any other groups. Disparity estimates were computed for Anisoptera and Zygoptera separately, then summed. It was not possible to analyse Calopterygidae separately from the other Zygoptera because the family is represented by a single species at most sites where it occurs. Disparity metrics could not be computed either for the site 364 for the subdivision in two groups, as it contains only 2 observed species, one Anisoptera and one Zygoptera.

3.3 Results

Out of the 79 Odonata species monitored in France by Steli, 47 have been reported in Ile-de-France, and, among these, 36 in the second period. The morphospace built from these only 36 occurring species is very similar to the global morphospace established for France as a whole. PC scores are strongly correlated for the co-occurring species pool. Anisoptera and Zygoptera occupy distinct areas. Within Zygoptera, the Calopterygidae, Lestidae and Coenagrionidae+Plactycnemididae occupy distinct areas (Fig. 3.2). Diversity and disparity values for each sites are given in Table 3.3 (and see Fig. 3.1).

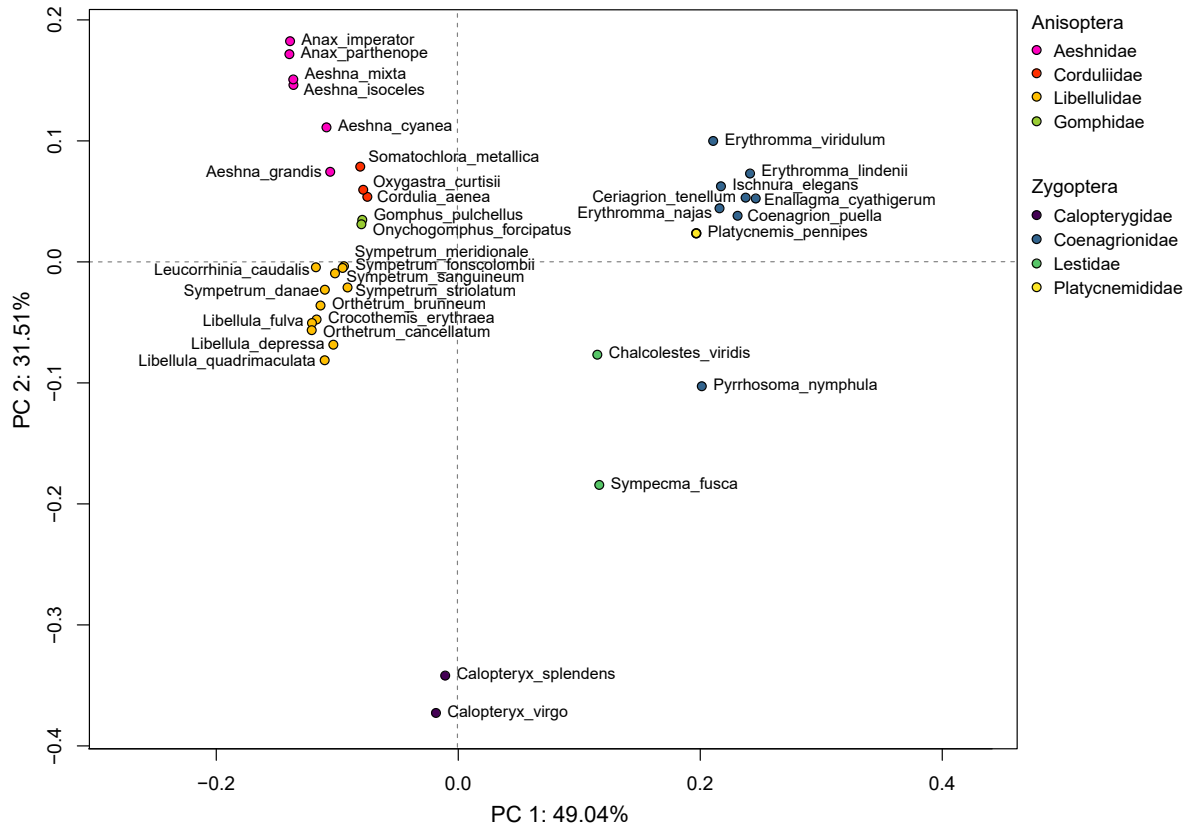


Figure 3.2 – Plot of the two first axes of PCA that summarize morphospace of odonates monitored under the Steli framework in mainland France. Only the species present in the selected sites of Ile-de-France during the second protocol period are represented.

Table 3.3 – Estimates of disparity for each sites in Ile-de-France and associated number of species and families. The value for disparity estimates correspond to the mean of the rarefied bootstrapped result except for the sites 364, 365, 1418, 1676 and 1761 for which rarefaction could not be computed. For those sites disparity estimates were directly calculated without resorting to bootstrap.

Sites	Number of species	Number of Families	sum of ranges	sum of variances	median pairwise distances	average nearest neighbour distances	average displacement
313	10	4	0,8480	0,0356	0,2665	0,0539	1,2188
314	10	4	0,8280	0,0402	0,2854	0,0427	1,2144
315	9	3	0,7666	0,0313	0,2338	0,0458	1,4620
322	16	7	0,9806	0,0423	0,2962	0,0812	1,2322
364	2	2	0,6776	0,0795	NA	0,3988	1,2124
365	6	3	0,8345	0,0411	0,3218	0,0954	1,0313
1416	15	5	0,8743	0,0361	0,2615	0,0655	1,2284
1418	4	4	1,2352	0,0853	0,3716	0,3205	1,0113
1436	19	6	0,9422	0,0411	0,2913	0,0764	1,2733
1634	7	4	0,8380	0,0430	0,2756	0,0449	1,4230
1635	14	4	0,8197	0,0390	0,2766	0,0468	1,2980
1676	4	3	0,8864	0,0530	0,2481	0,1391	1,6982
1677	8	5	1,0528	0,0567	0,3440	0,0639	1,1642
1761	5	4	1,0570	0,0529	0,3406	0,1909	1,2788
1441_2014	20	6	0,9365	0,0424	0,2918	0,0692	1,2261
1441_2015	23	7	0,9519	0,0439	0,2847	0,0726	1,2589
1508_2015	11	6	0,8535	0,0346	0,2571	0,0599	1,2577
1508_2016	10	5	0,8259	0,0378	0,2530	0,0475	1,4231
1672_2017	10	5	0,8984	0,0419	0,2911	0,0615	1,2612
1672_2018	11	5	0,8787	0,0404	0,2838	0,0556	1,2043

Different tests were performed on the results to identify the most suitable parameters for our analysis, and for the different disparity estimates. The impact of the sites with less than 7 species, the division of Anisoptera into subgroups, the land cover categories, and the size of the buffer radius has been investigated. Spearman correlation tests were computed between each diversity and disparity metrics (Fig. 3.3).



Figure 3.3 – Pairwise correlations between the five disparity estimates, the percentage of favourable and unfavourable areas within a 500 m radius buffer and the number of species and families. Figures on the upper right corner are the Spearman correlations. ***, ** and * correspond respectively to p-value between 0 and 0.001, 0.001 and 0.01, and 0.01 and 0.05. Red crosses indicate sites with less than 7 monitored species ; red figures indicate Spearman correlations for the 15 sites with more than 6 monitored species.

3.3.1 Sensitivity analysis and choice of parameters

Disparity estimates

To quantify disparity, only one size estimate and one position estimate have been used whereas three have been computed for the density. Among density estimates the distances, such as the median pairwise distances and the average nearest neighbour distances, are thought to be less sensitive to sample size than the very commonly used sum of variances (Foote, 1992). The distances metrics are supposed to be more revealing of species clustering in the morphospace. Several metrics were therefore considered, susceptible to be more sensitive to different aspects of the species distribution.

We retrieved a strong correlation, with a significant p-value (<0.01), between the different density metrics, which is an expected outcome, since they all represent the species distribution in the morphospace. The sum of ranges is also strongly correlated to density metrics except for the average nearest neighbour distances with which the correlation is moderate. The average displacement, the position metric, is moderately correlated to the other estimates except for the median pairwise distances, with which it is strongly correlated.

The density metrics are also correlated when considering only sites with at least 7 species. Given the correlation between these three metrics we refer to them as the density metrics for the rest of this chapter. They carry the same information on species distribution within the morphospace, so there is no need to discuss the correlation of each with other variables.

Sites with less than seven species

The sum of ranges is known to be sensitive to sample size, as the sum of variances to a lesser extent (Foote, 1992; Ciampaglio et al., 2001). Moreover, values obtained for sites with fewer species than the quota of seven seem to express slightly higher values than bootstrapped values (Fig. 3.4). Therefore we tested the impact of these sites on the obtained correlation between variables.

There is a weak or no correlation between the number of species and families and disparity estimates. Only the sum of ranges is moderately correlated to the number of families. Disparity estimates are quite constant with the increase in the number of species, except for the sites with less than 7 species for the sum of ranges, and the density.

The correlation between disparity estimates are stronger when the sites with low diversity are excluded, possibly due to their extreme values. Then, there is a very strong to moderate correlation (p-value <0.001 to <0.005) between the density metrics and the number of species and families, and a moderate negative one between the average displacement and the number of species and families.

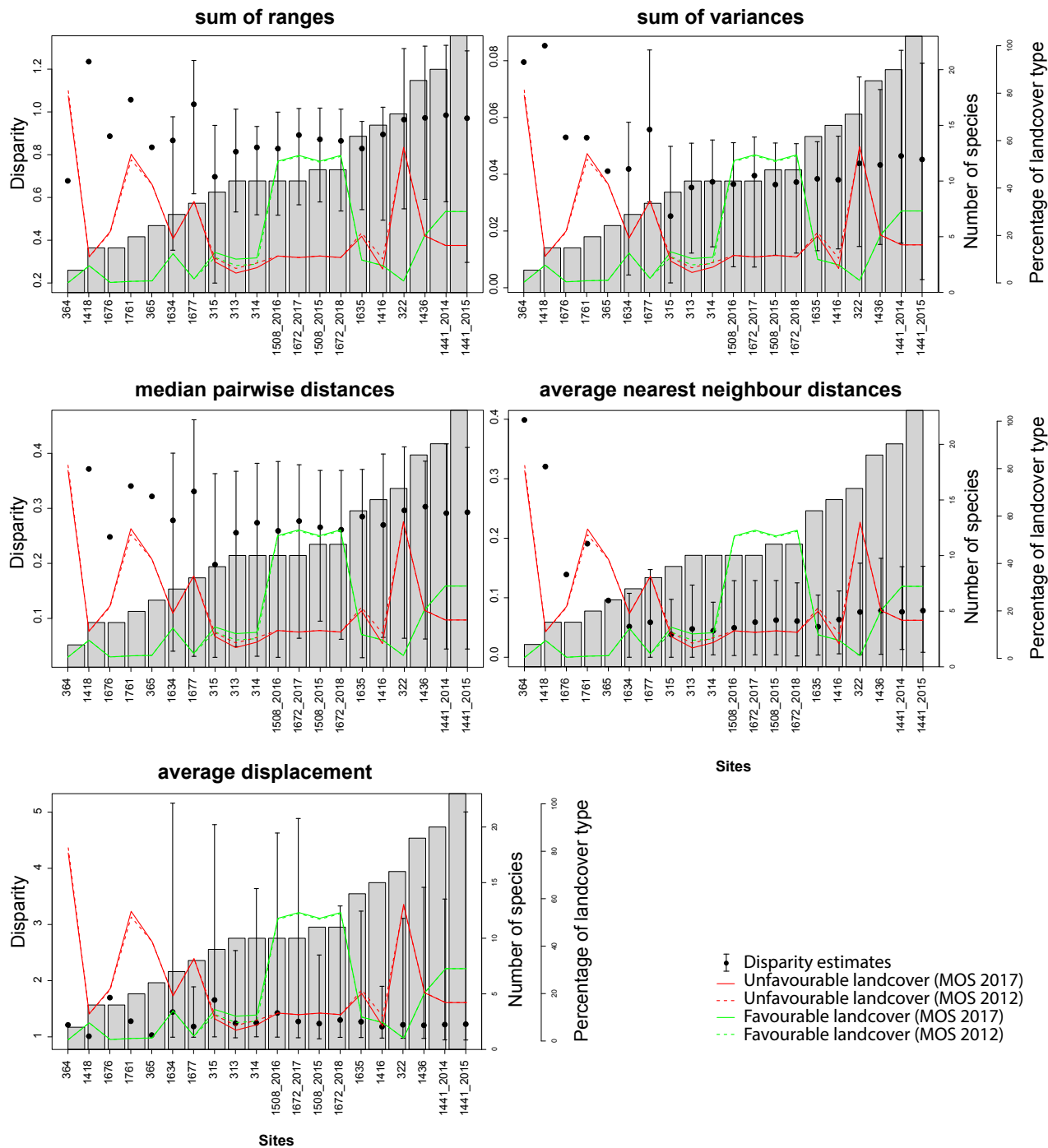


Figure 3.4 – Five disparity estimates for each of the 20 sites. Composed names indicate a site number and the year it was monitored. Sites are ordered by species richness. Grey barplots represent the number of species. Red continuous line represents the percentage of unfavourable land cover within a 500m radius buffer around each site using the MOS 2017, red dotted one using the MOS 2012. Green continuous line represents the favourable land cover in the buffer using the MOS 2017, green dotted line using the MOS 2012.

Disparity metrics tend to have higher and more variable values when there are few species. The distances between species in the morphospace are larger when few scattered species occur. The moderate negative correlation of the average displacement implies that this value tends to decrease with the increase in the number of species. In sites

with more species there is more chance to have extreme morphologies represented, hence a lower average displacement. In contrast, in the sites with few species, the values of this metric are more variable, depending on how the observations are dispersed in the morphospace. This could explain the correlations obtained when sites with less than 7 species are removed.

The sites with few species have an impact on disparity and its correlation to diversity. They could add noises but removing them would led to important reduction of sample size.

Anisoptera and Zygoptera subgroups

Some disparity metrics such as the sum of variances can be biased when several clusters occur (Foote, 1993b; Neige, 2003; Villier and Eble, 2004), which is the case here: Anisoptera and Zygoptera occupy well distinct areas in the morphospace. Thus, we tested the impact of considering subgroups by summing the disparity computed for each (Anisoptera+Zygoptera).

In contrast with the outcome obtained when using odonates as a single group, the sum of ranges is moderately correlated to the sum of variances (and no longer correlated to the three other metrics) when using subgroups. The sum of variance is now negatively correlated to the average displacement. When the variance within species increases then the centroid of each subgroup is closer to the centre of the morphospace. For Zygoptera alone, similar correlations are found for the density metrics. The sum of ranges is strongly correlated with two of these density metrics. The average displacement is negatively correlated to the other disparity metrics. For Anisoptera alone the sum of ranges is strongly negatively correlated to the average nearest neighbour distances (p-value < 0.001) and moderately negatively to the average displacement. The sum of variances is correlated to the median pairwise distances but there is no correlation between the density metrics. The average displacement is moderately positively correlated to the average nearest neighbour distances whereas it is negatively correlated for the odonates as a single group. The correlation of Zygoptera alone are consistent with the ones found for the odonates as a single group, highlighting their impact on computed disparity. This impact seems to be diminished using Anisoptera+Zygoptera.

There is a moderate correlation between the sum of ranges when using a single group and when the two subgroups (Anisoptera+Zygoptera) are summed. Moreover, for this metric, there is a strong correlation between the odonates as a single group and the Zygoptera alone (p-value < 0.01), and a very weak correlation with the Anisoptera alone. With the Anisoptera+Zygoptera the correlation is very strong with the Zygoptera (p-value < 0.001) and strong with Anisoptera (p-value < 0.05), increasing the impact of Anisoptera on total disparity of odonates.

There is a strong to weak correlation between the density metrics of odonates and of

Anisoptera+Zygoptera. For Anisoptera, there is no correlation with the density metrics of odonates as a single group. However, there is a very strong correlation with a density metric of Anisoptera+Zygoptera. For Zygoptera, there is a strong to moderate correlation with density metrics of odonates as a single group. Moreover, there is a very strong to moderate one with the density metrics of Anisoptera+Zygoptera. This highlights, again, the impact of Zygoptera on the total disparity of odonates. Taking Anisoptera+Zygoptera increases the impact of Anisoptera, in particular on the average nearest neighbour distances, which could be explained by the proximity of this species subgroup within the morphospace. The computed density metrics are most of the case lower when considering Anisoptera+Zygoptera instead of odonates as a single group.

The average displacement is the most impacted metric by the subgroup division. There is no correlation for this metric between odonates as a single group and Anisoptera+Zygoptera, neither with Anisoptera and Zygoptera alone. There is a strong and very strong correlation between Anisoptera+Zygoptera and Anisoptera alone and between Anisoptera+Zygoptera and Zygoptera alone, respectively (p-value <0.01 and <0.001). This metric has higher values with the subgroup division, which compares the centroid of each subgroup to the centre of the morphospace containing the two, reflecting the distinct areas occupied by each.

Except for the sum of range, for which the correlation is moderate (p-value <0.5), there is no correlation between the disparity estimates of Anisoptera and Zygoptera. This correlation could reflect the increase of both subgroups within sites with more species, which is congruent with the moderate correlation between the number of Anisoptera and Zygoptera species and their respective correlation with the total number of species.

Anisoptera seems to be better accounted for when using Anisoptera+Zygoptera disparity values. However disparity is computed on fewer species when considering the two groups separated, and we previously show that sites with few species may impact disparity correlation with other variables. Some disparity metrics are more sensitive to sample size as the sum of ranges. The sum of variances can also be more variable. For some sites, such as the 1418, the sum of range is significantly lower. This could be explained by the few number of species furthermore divided. With this division the site is composed of two subgroups, each including only two species (Fig. 3.5). Another example is the site 1676, for which four species are from the same subgroup and therefore occupy the same part of the morphospace. As a consequence, the size metric was already low. The same goes for the site 1761, with a single Anisoptera species, the disparity of this subgroup can not be computed so the total disparity is just the one from Zygoptera. For the site 315 it is the disparity of Zygoptera that can not be computed with only one species. The disparity of the site 364, with only one representative of each subgroup, can not be computed at all. Thus, using Anisoptera+Zygoptera seems to be a better option, Anisoptera are more accounted for, but, doing so, disparity values might be biased for sites with few represen-

tatives of the subgroups.

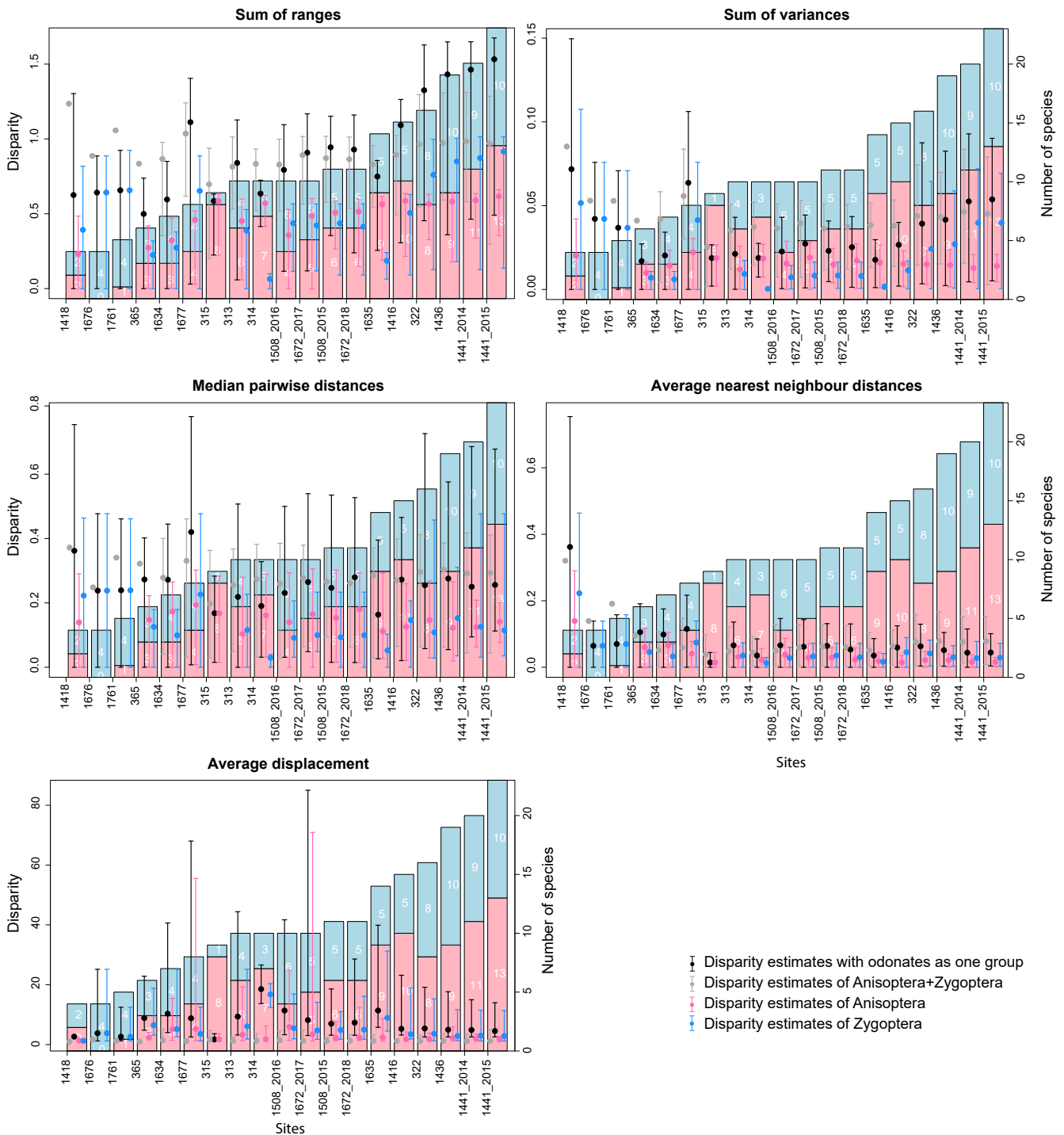


Figure 3.5 – Five disparity estimates for each of the 19 sites with subgroup division in Anisoptera+Zygoptera. Composed names indicate a site number and the year it was monitored. Sites are ordered by total species richness. Pink and blue barplots represent the number of Anisoptera and Zygoptera species respectively; number of species of each group is indicated in white. Grey dots represent disparity estimates for Odonates as one group; black dots, Anisoptera+Zygoptera disparity estimates; pink dots, Anisoptera disparity estimates; blue dots, Zygoptera disparity estimates.

Radius size of the land cover buffers

The change in land cover around the selected sites is negligible between 2012 and 2017 (Fig. 3.4). The correlation between diversity and disparity metrics and the land cover has been made with the MOS 2017.

For the three different buffer radii there is a moderate positive correlation (p-value <0.05) between the favourable land cover and the number of species and families. The number of species increases with the proportion of favourable land cover. However when we removed sites with less than 7 species, the correlation becomes weak for the number of species and moderate for the number of families, with a p-value between 0.05 and 0.1. Sites with few species have a really low proportion of favourable land cover that could explain the found correlation and its loss when they are not considered. The number of families reaches the maximal value in the majority of the sites, so that the sampling is complete or almost complete in each site independently of the amount of favourable land cover. There is no or a weak correlation with unfavourable land cover in any of the tested cases.

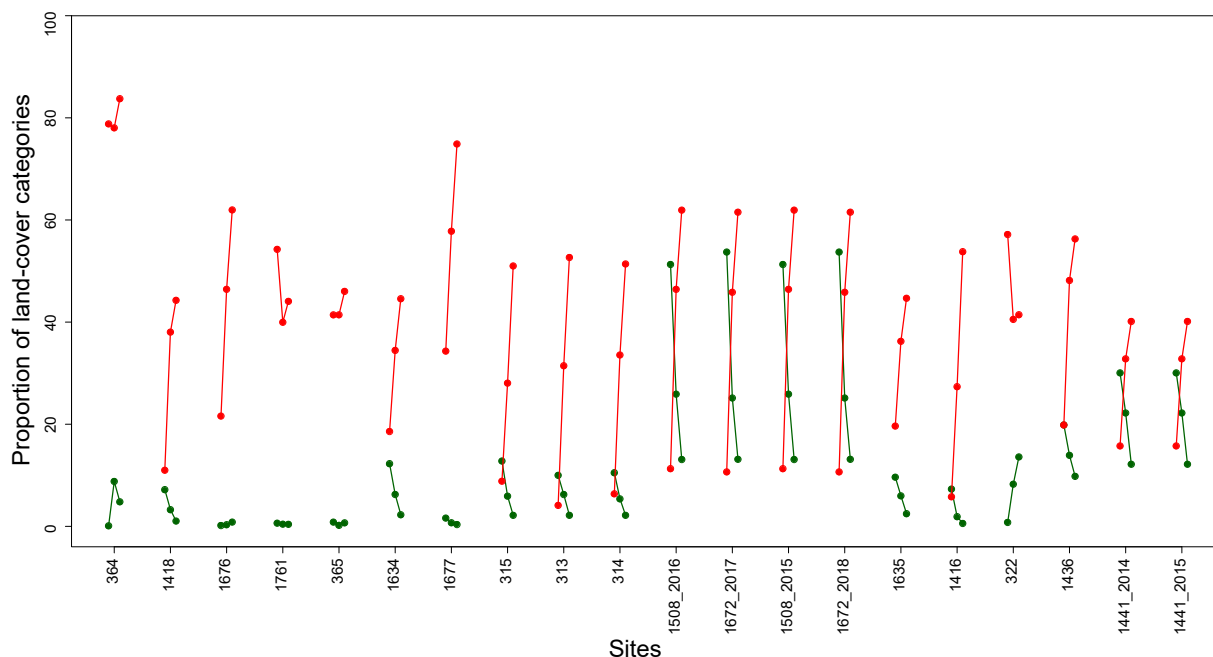


Figure 3.6 – Percentage of favourable and unfavourable areas for each sites within buffers of, in order, 500m, 1000m and 2000m radii. Green dots represent favourable areas; red dots, unfavourable ones. Lines connect for each site the percentage of each of the two areas for the 3 different radii (for each site, from left to right, 500m, 1000m and 2000m radii).

There is a weak or no correlation between the two categories of land cover and the different metrics of disparity with the 1000m radius buffer. With a buffer radius of 2000m the percentage of surface unfavourable for odonates is globally higher and the favourable lower. Taking a wider buffer probably adds too much noise because the area favoured for field inventories are usually much smaller. Moreover, there is no correlation between the

unfavourable areas of the 2000m radius buffer and the 500m one. This could reflect an over-representation of unfavourable areas when using a 2000m radius buffer, especially given the small size of the water bodies. With a 500m radius buffer, the percentage of unfavourable and favourable areas for each sites are much more different. Except for two sites (1761 and 322) the unfavourable area is smaller than under the two other radii, and the favourable areas higher. As it could be expected, the difference between the land cover of nearby sites, such as 313, 314 and 315, and 1508 and 1672, is amplified (Fig.3.6).

As for the 1000m radius, no correlation was found between almost all disparity metrics and the percentages of favourable and unfavourable land cover with the 2000m radius. Also, no correlation was found between the two categories of areas.

Given the observed differences between the three radii, we decided, from now on, to focus on the 500m radius buffer, which seems to be the optimal of the three to investigate land cover around the sites.

3.3.2 Disparity & Diversity

When considering all the sites there is only a moderate correlation between the size metric (sum of ranges) and the number of family, and no correlation with the number of species (these correlations become strong and moderate when removing sites with less than 7 species). This could be explained by the low number of families and by their different position in the morphospace. Indeed families are well separated in the morphospace and most of them correspond to extremes. Thus, with the increasing number of families, the morphospace occupation increases in size.

When using Anisoptera+Zygoptera, there is a very strong correlation (p-value <0.001) between the size metric and the total number of species. The distinctiveness of the morphospace area occupied by each species is better accounted for when using subgroups. Indeed, with odonates treated as a single group the position of a particular species had a lesser impact, being minimised by the stronger differences separating the two subgroups. The size metric of Anisoptera is more strongly correlated with the total number of species than for Zygoptera. Each of the subgroups has a strong correlation between this metric and the number of species within it. The number of Zygoptera and Anisoptera species are, respectively, very strongly and strongly correlated to the sum of ranges of Anisoptera+Zygoptera (p-value <0.001 and <0.01).

Therefore, there is a moderate to strong positive correlation between taxonomic richness and the size metric. This correlation is stronger when considering Anisoptera+Zygoptera.

The density metrics are not correlated to the number of species or families when considering all the sites but they are strongly to moderately correlated with the number

of families when removing sites with less than 7 species. One density metric is even correlated to the number of species.

The disparity estimates are quite constant with the increase in the number of species, except for the sites with less than 7 species and the site 1677 for the size and density (Fig. 3.4). The site 1677 contains only few species of each extreme of the morphospace, which could explain why density metrics reach higher values than for sites with more than 7 species.

Calopterygid species occupy an extreme position of the morphospace and disparity is often higher for the sites with limited diversity but that sample Calopterygidae. Good examples are the sites 364 and 1418, for which, monitored species occupy a large part of the morphospace, with only few representatives of each extreme (Annex A.6). The sites 1676 and 1761, even with high values (Fig. 3.4), have a smaller values than those sites, with several species occupying a same area of the morphospace, decreasing the distance with the nearest neighbour and therefore density.

When considering two subgroups, the site 1677 has a higher density value than when considering a single group, while it is the opposite for the other sites. This could reflect the distribution within each subgroup for this particular site, with the occurring species occupying extreme positions within each subgroup. This value obtained for the site 1677 is close to the one of the site 1418 with also equal number of representatives for each subgroup and on the extreme of the morphospace of each (see Fig. 3.5; Annex A.6).

When considering two subgroups, density metrics are not correlated and reflect different responses to the increase of diversity. The sum of variances is moderately correlated with the number of families and the average nearest neighbour distances is strongly negatively correlated with the total number of species. This negative correlation is also found for each subgroup. The same correlation for the average nearest neighbour distances is found for each subgroup with the number of species within each. The number of Anisoptera species is negatively correlated with the average nearest neighbour distances of Anisoptera+Zygoptera (p-values <0.001) whereas the number of Zygoptera species is not. This negative correlation can be explained by the smaller part of the morphospace occupied by the subgroup. It's morphology is less widespread than the Zygoptera one. This change of trend reflects that when the number of odonate species increase, species tend to be more widespread considering a single group rather than two subgroups, distances being calculated across the subgroups.

Therefore, correlation of density with diversity is not obvious, strongly impacted by the consideration of subgroups. Altogether, there is a positive correlation of density with the number of families, probably reflecting their distinct distribution within the morphospace.

The position metric is negatively correlated with the number of species and families (this correlation is weak when considering all the sites). With the increase in diversity,

the area occupied is closer to the centre of the morphospace. The position metric of Anisoptera+Zygoptera is not correlated to the total number of species neither to the number of Anisoptera species. There is only a moderate correlation (p-value between 0.05 and 0.1) of the average displacement with the number of Zygoptera species. However, there is no correlation between this metrics for Anisoptera or Zygoptera alone and any number of species.

The number of species of Anisoptera is moderately correlated with the number of species of Zygoptera. Anisoptera species are in average monitored in 5 sites and Zygoptera species in 7.5 sites. There is no significant difference between the two.

Therefore, change in diversity does impact the position of the area occupied in the morphospace when considering one group, but not when using subgroups, each subgroup occupying distinct areas not covering the centre of the morphospace.

For density metrics, there are significant differences (p-value of the permutation test) between species considered as common and rare focusing on the sites presence frequency and the cumulated abundance. The differences are not significant for size. There is a significant difference for the average displacement when focusing on cumulated abundance but not when considering sites presence frequency (Fig.3.7).

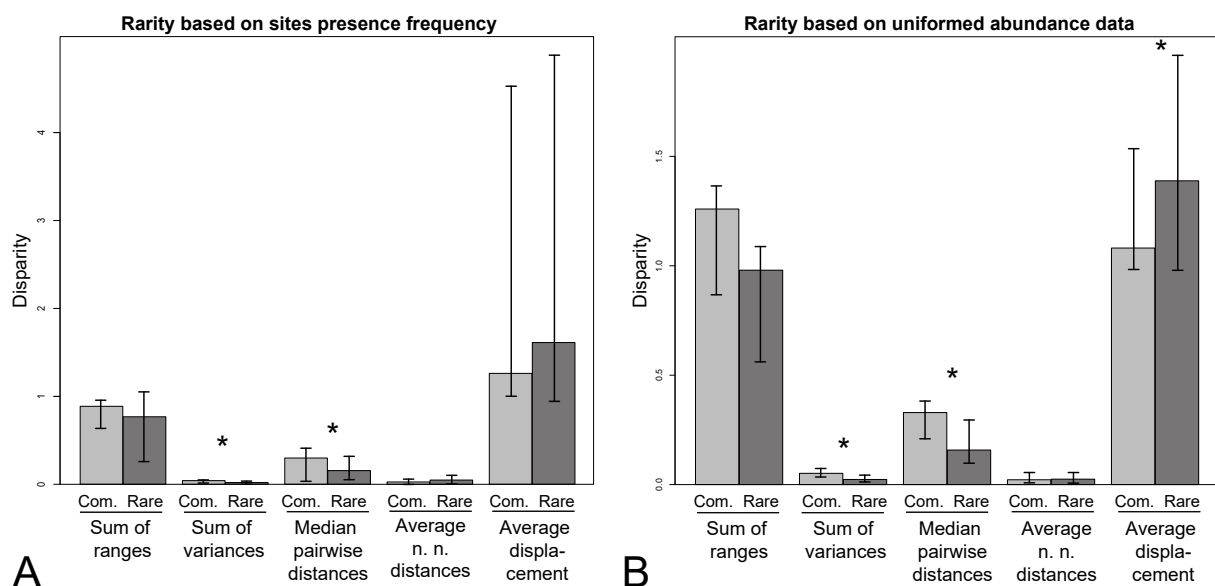


Figure 3.7 – Mean of five disparity estimates for species considered common or rare. **A**, rarity based on presence on site frequency (>50% and <10% of the sites); **B**, rarity based on cumulated abundance of the species. * correspond respectively to p-value below 0.05 computed with a permutation test. Com. =Common; n. n. =nearest neighbour.

3.3.3 Landscape structure

Relation between land cover and disparity

There is a negative correlation with a p-value <0.01 between the favourable and unfavourable land cover proportion indicating that while the proportion of favourable area increases, the unfavourable decreases. The ratio between favourable and unfavourable areas is, as the two areas, correlated with the density metrics of the morphospace occupation (moderate negative correlation with the median pairwise distances and the average nearest neighbour distances and a strong negative correlation with the sum of variances).

There is no correlation between the size metric and either of the two land cover categories when considering all the sites. There is a moderate negative correlation between the favourable (and positive one with the unfavourable) land cover percentage and the density metrics. Thus, the species become more scattered within the morphospace when the proportion of unfavourable area increases and the favourable one decreases.

The sites with less than 7 species (sites 364, 365, 1418, 1676 and 1761) and the sites 1634 and 1677, with 7 and 8 species respectively (Fig. 3.4) are among the highest density values. These values might be linked to the low numbers of species and to the fact that the occurring species occupy extreme positions in the morphospace. These sites have a low proportion of favourable land cover. It is concordant with the positive correlation between the number of species and families and the favourable proportion of land cover, which is lost when removing sites with less than 7 species. The site 315 is the one with the lowest density values, with most of the occurring species clustered in the morphospace (Annex A.6). These sites have isolated, small portions of water within otherwise residential areas.

Without considering the sites with less than 7 species, there is only a weak negative correlation between the proportion of favourable areas and the disparity metrics. For the proportion of unfavourable areas, however, the correlation is strong for the size and density. When looking at the relation between the density metrics and the proportion of unfavourable areas, only the site 322 is a complete outlier (Fig. 3.3).

In summary, the most notable result is the positive correlation between unfavourable proportion of land cover and density metrics. We can see the same results for the sum of ranges, with a moderate correlation when all the sites are considered and a stronger one when removing sites with few species (Fig. 3.3).

Sites with the lowest density values are the ones without Calopterygidae. The occurrence of Calopterygidae increases disparity. Indeed, these odonates have a very specific wing shape, translating into the occupation of a particular area of the global morphospace (Fig.3.2). Given our results, Calopterygidae species seem more susceptible to be found in areas with a higher proportion of unfavourable land cover. However, they are known to live along running water (Boudot et al., 2017) and this results could be linked to the type of water bodies present on sites.

Impact of the types of water bodies

The favourable land cover category is composed of several water bodies, streams and closed water. The closed water proportion is very strongly correlated with the favourable land cover proportion and strongly negatively correlated with the unfavourable one (p-value <0.001 and <0.01 respectively). The streams proportion is, on the contrary, not correlated with the favourable land cover, reflecting the higher proportion of closed water within favourable areas around the sites.

The closed water proportion is negatively correlated to the density metrics. The running water proportion is moderately positively correlated to the density metrics (Fig. 3.3). Thus density metrics are impacted by the type of water bodies. They decrease with closed water and increase with running water.

When the 5 sites with less than seven species are removed, the correlation with closed water is weaker. However there is a positive correlation between size and density metrics and the running water proportion. There is a moderate negative correlation between the position metric and the running water proportion, and a positive one with closed water proportion (p-value $<0,05$). Size and density metrics increase with the increase of running water proportion while position decreases (meaning that the area occupied in the morphospace becomes closer to the global morphospace occupation). The presence of running waters could therefore be favourable to more disparate assemblages of odonates, widespread over the morphospace.

There is also a correlation between the number of species and families, and the running water, when considering sites with more than 7 species. In contrast, a same correlation is found but with closed water when considering all the sites. This can be linked to the fact that sites with few species are sites with closed water.

The correlation between the running water and the size metric, and one of the density metrics, is also found when considering Anisoptera+Zygoptera (p-value <0.01). These metrics of Anisoptera and Zygoptera alone are both correlated to the proportion of running water. These correlations are more important for Zygoptera. The density metrics of Zygoptera alone are negatively correlated to the closed water proportion. Disparity of Zygoptera is therefore negatively impacted by closed water, which is not the case for Anisoptera.

The position metric is not correlated with closed water for Anisoptera+Zygoptera. This metric is also not correlated with the running water. For Zygoptera alone, there is a negative correlation between the position metric and the running water. The position of this subgroup in the morphospace is therefore impacted by the running water proportion, with a centroid being closer to the centre of the morphospace. This can be explained by the presence of Calopterygidae when there is running water (Fig. 3.2).

In summary, all the disparity metrics, size, density and position, are correlated to the

running water proportion. These correlations seem to be strongly linked to Zygoptera and thus to the presence of Calopterygidae. The results suggest that a wide range of morphologies is susceptible to be found around running water, more than around ponds in Ile-de-France.

3.3.4 Forecast of diversity loss in urban environments

The disparity estimates, for the whole Ile-de-France, are equivalent with and without the threatened species (Fig. 3.8). The disparity is constant, whereas the taxonomic diversity decreases with the loss of 11 species and 1 family, the Corduliidae. Therefore, for odonates, in Ile-de-France, selective loss of the threatened species would not lead to much loss of morphological diversity.

When looking at the impact on disparity for each sites (Fig. 3.9), there is no change, except for the site 1418. *Calopteryx virgo* is one of the threatened species and is monitored on only 3 sites, 1418, 1441_2014 and 1441_2015. In the two latter sites, *Calopteryx splendens* which is not threatened, is also monitored, so the disparity is not impacted. For the site 1418 with only 4 species monitored and now 3 (when focusing on not threatened ones), the occupation of the morphospace without Calopterygidae is impacted and disparity is thus lower for every metrics.

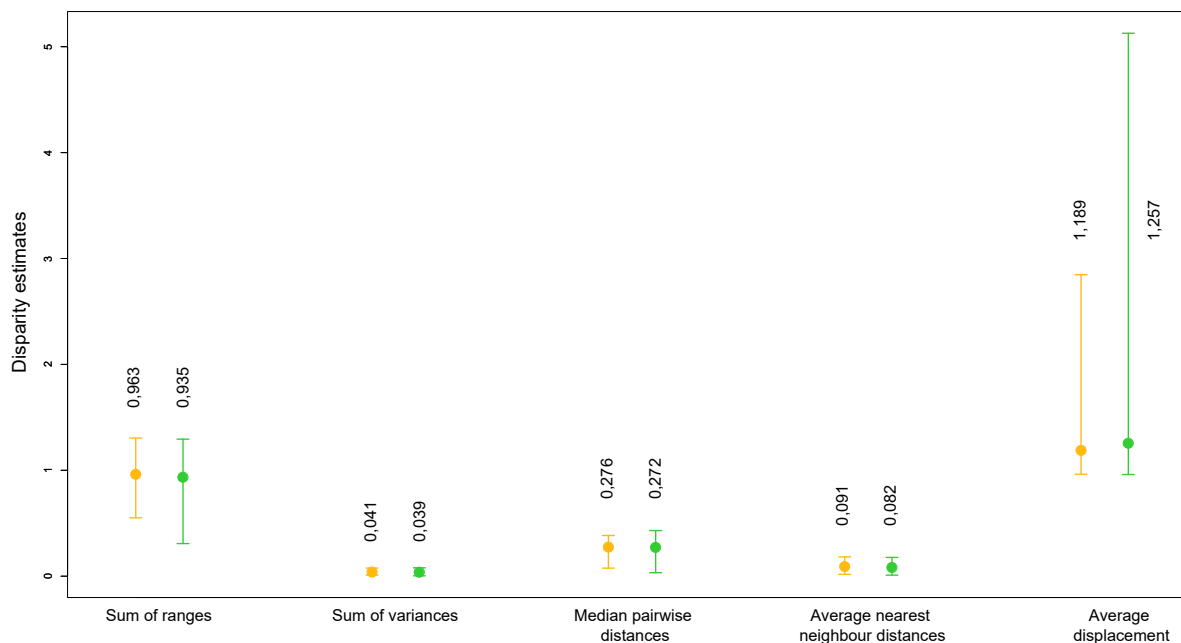


Figure 3.8 – Five disparity estimates for all species monitored in Ile-de-France (on the studied sites). Composed names indicate a site number and the year it was monitored. Sites are ordered by species richness. Orange dots represent disparity estimates for all monitored species; green dots, disparity estimates without threatened species. Figures are the mean value of each disparity estimates.

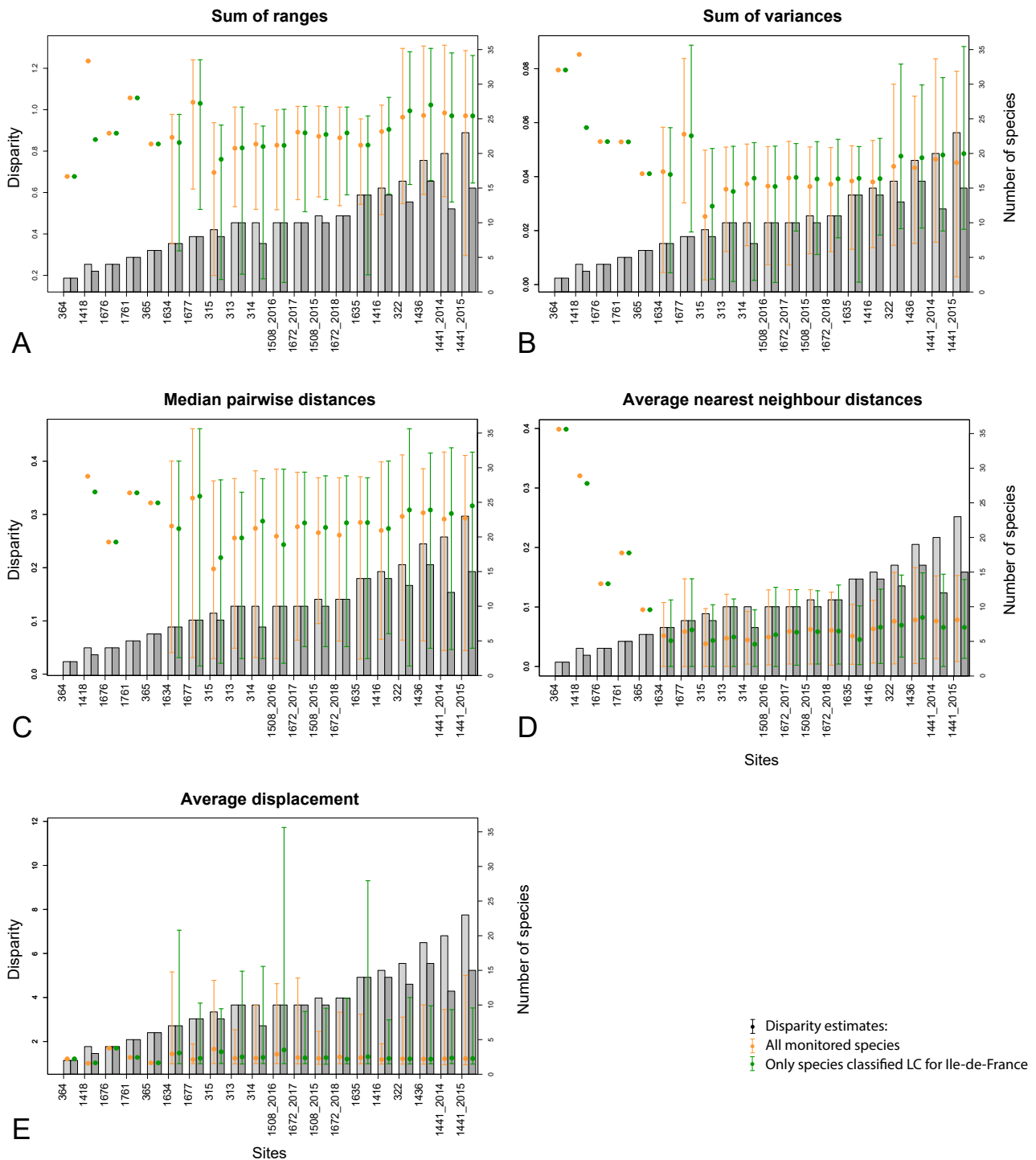


Figure 3.9 – Five disparity estimates for each of the 20 sites. Composed names indicate a site number and the year it was monitored. Sites are ordered by species richness. Light grey and dark grey bar-plots represent the number of species with and without the threatened ones, respectively. Orange dots represent disparity estimates for all monitored species; green dots, disparity estimates without threatened species.

3.4 Discussion & Conclusion

3.4.1 Robustness of the Steli data and parametrisation of disparity analyses

The citizen sciences program Steli provided excellent data for analytical research on diversity of the Odonates, mostly because of the standardised data acquisition. The exploratory approach allows identifying the optimal process and parameters to study diversity and disparity in urbanised region such as Ile-de-France. Results suggest that a size of 500m for the buffer radius is optimal to describe the land cover around the sampled localities, only the areas directly adjacent to the water bodies being taken into account.

The site 322 was identified as an outlier for the relationship between the two first density metrics (i.e. sum of variances and median pairwise distances) and the unfavourable areas proportion. With the 500m radius, the site 322 has almost no favourable land cover and the proportion of unfavourable land cover increases considerably. This site is documented as a residential area with no obvious water area on the map. There is still a doubt on the reliability of GPS coordinates of the monitoring area.

Calopterygidae are known to be found close to running water, however, according to the used MOS data, 4 of the sites where they have been monitored (1418, 1676, 1761 and 322) do not have running water in their buffer. The GPS coordinates might not be precise enough (for the site 322 for example) or this could be due to streams lacking in the land cover data. The MOS is based on aerial photography, some small streams might not be visible, covered by vegetation or even temporary and therefore not represented. Thus, they might be an underestimation of running water proportion. Disparity cannot be treated consistently in the sites with few species (less than 7). However, removal of the sites with low diversity is not a satisfying solution. All sites sampled in Paris city centre have a low diversity. They represent the most urban and degraded conditions, so that excluding them from the analysis would result in a loss of information. There is no significant difference in the species richness of Anisoptera and Zygoptera, with a mean of 5 and 7.5 species per site. Considering both subgroups independently when computing disparity seems to be optimal. However, the average displacement in morphospace might be more difficult to interpret, and the disparity of sites with few representatives of each subgroups cannot be computed.

3.4.2 Diversity and disparity patterns

The occupation of the morphospace (size metrics) is positively correlated to the diversity. However, the correlation of diversity with the density metrics is not so obvious, varying with the analytical parameters. As for Roy et al. (2001) and Neustupa et al. (2009), we

found high disparity values for sites with low species richness and also high disparity for sites with high species richness. Roy et al. (2001) found an increase in morphospace size with the increase of species richness and, therefore, that species tend to be preferentially added to the margin of the morphospace. The size metric does not change much above a minimal amount of species. They also suggest another explanation, that the observed results only reflect what could be expected from sample size alone. In this case, the range is expected to increase with diversity and the variance should be more variable at low sample size and stable with higher species richness. This could be our case here. However, we also used other disparity metrics, in particular, two other density estimates that are less sensitive to sample size. Sample size impact might have been diminished when considering only sites with at least 7 species. On the other hand Neustupa et al. (2009) found, as our results also suggest, that a few or even a single species were driving high values of disparity in low-diversity localities. This is the case, here, for the Calopterygidae. This, therefore, could be an argument to use disparity in addition to species richness for conservation decisions, highlighting specific sites which might not be taken in consideration for conservation measures given their low diversity.

The positive correlations between the unfavourable land cover proportion and the size and density metrics suggest that the artificialization of sites in Ile-de-France is not associated to a selective loss of odonate species. We found a moderate correlation between the favourable land cover proportion and the number of species. Thus, there is no major drop of diversity in highly artificialized landscape, neither as drop of disparity, within odonates (or within Zygoptera or Anisoptera). There is no selection of specialised species for such habitats and there is no evidence of wing morphologies linked to specialisation, except on the type of water bodies.

We have found that there is a positive correlation between disparity and unfavourable areas proportion. The sites with the highest proportion of unfavourable areas are the sites 322, 364, 365, 1677 and 1761. These sites (except 322) have among the lowest number of species and the highest density values. They have isolated, small portions of water within otherwise residential areas (Annex A.4). The species composition differs between each site and therefore do not highlight peculiar species susceptible to be more tolerant to such unfavourable areas. Almost every extreme of the morphospace are represented. Almost all the monitored species within these sites are considered common considering their presence frequency on sites and/or their abundance (Table 3.2). Only *Pyrrhosoma nymphula* (Sulzer, 1776) on the site 1761 and 365 is neither rare nor common in any case. Also, *Aeshna cyanea* (Müller, 1764), on site 365, is considered common due to its abundance but is rare due to its frequency, being observed only on this site. *Libellula depressa* Linnaeus, 1758, also on site 365, is considered rare due to its abundance and is only present on 3 sites.

Most common species in the study sites are known to be tolerant to environmental stress, including urbanization, such as *Anax parthenope* (Leach, 1815), *Orthetrum cancellatum* (Linnaeus, 1758), *Platycnemis pennipes* (Pallas, 1771), *Ishnura elegans* (Vander Linden, 1820) and *Erythromma lindenii* (Selys, 1840) (Villalobos, Ferreras Girgin, Solimoni). They represent a wide range of morphologies encounter in the morphospace (Fig. 3.2). Disparity, therefore, does not seem impacted by artificialization.

Odonates are good dispersers, and could be able to colonize urban water bodies, even in urbanised area (Jeanmougin et al., 2014; Goertzen and Suhling, 2019). Some studies even show that urbanization can provide higher quality habitats for some insect species (Goertzen and Suhling, 2013; Banaszak-Cibicka et al., 2018).

Jeanmougin et al. (2014) already highlight the importance of ponds and their surroundings for Odonata diversity in Paris area. Streams artificialization (Houard and Merlet, 2014) is also another issue for conservation of Odonata diversity. Our results suggest that the running water, in Ile-de-France, are conducive to odonates disparity. A wider range of morphology is susceptible to be found around running water than around ponds. Zygoptera are more impacted by the water bodies than Anisoptera. The positive correlation of Zygoptera with running water is probably due to the Calopterygidae species, which have a huge impact on the disparity and live around running water. Calopterygidae species can however survive along minor streams in areas with a high proportion of unfavourable land cover.

Among the 11 species listed as threatened only 3 are Zygoptera. All the species classified CR and VU are found rare (frequency and abundance) in the study sites. Among the species classified NT, *Onychogomphus forcipatus* (Linnaeus, 1758) is found rare for both measures of rarity. The other species classified NT are found rare for at least one of the measure (except *Erythromma najas* (Hansemann, 1823), see Table 3.2). Among the threatened species, three are more often found around running water: *Calopteryx virgo*, *Onychogomphus forcipatus* and *Oxygastra curtisii*. The latter species is protected in France (Houard and Merlet, 2014; Boudot et al., 2017). Assandri (2020) highlighted disappearance of *Calopteryx virgo* and *Onychogomphus forcipatus* in the alpine region linked to anthropization, notably with the loss of lotic habitats. The species, recognized as threatened, mostly suffer from water pollution, deterioration of aquatic vegetation and physical alterations of water bodies (van Strien et al., 2013). However they exhibit a wide range of lifestyle and very disparate morphology. We did not found evidence that wing morphology might help recognized specialised or generalist species. The variety of ecology of threatened species also indicate a pressure of artificialization not specifically linked to water body types. Our results corroborate the ones of Outomuro et al. (2013) who studied wing margin of odonates and found no significant effect of water body types on wing shape.

3.4.3 Perspectives

In case of future loss of threatened species, the disparity should not be impacted. Therefore, a drop in diversity would be linked to a constant disparity for every metrics (Fig. 3.8; and see Fig. 1F,G). This is an evidence for a potential morphologically non-selective crisis on wing morphology. Other traits might be taken into account for disparity, wings might not be the most relevant structures for characterizing specialisation. Climate change, given the scale we are working on, could impact all sites in a homogeneous way. Study on a temporal scale, as Assandri (2020), highlight changes in community over the last century and inform on the sensitivity of odonates to environmental changes. Specialised species may have already disappeared from Ile-de-France and only quite tolerant and generalist ones preserved. Exploration at the scale of the entire France country may help understanding the significance of regional results. A study at a wider geographic scale, such as France, might be relevant to also include less artificialized sites, further away from big metropolis. The impact of climate on disparity could then also be investigated.

Roy et al. (2001) suggest that, on a regional scale, distribution of species in morphospace may, at least partially, be constrained by phylogenetic relationships. This might be the case here given the distribution of species. Blanke (2018) have, moreover, shown a phylogenetic signal in Anisoptera wing shape variations. It would be more robust, in further studies, to consider phylogeny in disparity estimates computation.

Chapter 4

Odonata disparity during the Permian and the Triassic

Contents

4.1	Introduction	79
4.2	Fossils species selection	83
4.3	New data on Triassic odonates	83
4.3.1	New gondwanian Triassic material	83
4.3.2	A new Zygophlebiida from Molteno reconstructed	84
4.3.3	Reconstruction of <i>Moltenagrion koningskroonensis</i>	98
4.3.4	Completing Triassic dataset with retro-deformed Madygen material	99
4.4	Disparity analysis	101
4.4.1	Material & Method	101
4.4.2	Results	104
4.4.3	Discussion	107

4.1 Introduction

Most investigations on the evolution of diversity and disparity during the Permian and the Triassic, and in particular across the end-Permian mass extinction (EPME) focused on marine organisms. This is the case of studies on brachiopods or amonoids that aimed at understanding the properties of this event (Ciampaglio, 2004; Villier and Korn, 2004; Erwin, 2007). These studies highlighted a decrease in disparity during the Permian resulting on low disparity before the EPME. Diversity decreased but disparity post and

pre-extinction have equivalent values, as is the volume of morphospace occupied. Viller and Korn (2004) conclude to a morphologically non-selective extinction. They also highlight a steady or slightly increasing disparity in the Early Triassic while diversity increased.

The effect of the EPME on terrestrial life is less consensually accepted. Vertebrates experienced a huge decrease in species richness (Benton and Newell, 2014). Disparity has been investigated for some vertebrate groups, such as anomodont therapsids (Ruta et al., 2013), for which disparity and diversity were decoupled. Diversity severely dropped but disparity declined steadily from the beginning of the Permian and was not impacted by the EPME. Studies in parareptiles, in the contrary, showed a drop of disparity and a steady diversity through the EPME then a decline of diversity during the Triassic (MacDougall et al., 2019). On the other hand plants and insects seem to have been less impacted than other terrestrial organisms, less than one-third of the number of insects families disappeared (Benton and Newell, 2014; Ponomarenko, 2016).

An unsampled temporal gap, approximated to 5 myrs, spanning from the Late Permian to the Early Triassic render difficult to investigate the impact of this crisis on insects (Béthoux et al., 2005; Shcherbakov, 2008). However, a recent study investigated the impact of the EPME thanks to new fossil material from intertrappean deposits recording the terminal Permian and conclude that a drop of insect diversity does occur but that the scale of extinction was lower than usually accepted (Ponomarenko, 2016).

The EPME is the only period when several insect orders disappeared concurrently, including all the rostropalaeopteran orders, very prominent during the Palaeozoic (Carpenter, 1992). Holometabolan insects, which were rare during the Palaeozoic (Nel et al., 2007), seem to have experienced an important diversification after the EPME. For example, the fossil record indicates that an important increase in the abundance of Diptera took place during the Triassic (Blagoderov et al., 2007), as for Coleoptera (Ponomarenko, 2016). Among stem-Orthoptera, groups under-represented during the Palaeozoic became dominant during the Triassic, while more typical Permian groups disappeared (Béthoux et al., 2005).

A similar pattern characterizes the Odonata (Fig. 4.1). Most notably, the Meganisoptera (here provisionally considered to include *Lapeyria magnifica* Nel et al., 1999b), abundant and widely distributed during the Palaeozoic (Brongniart, 1893; Nel et al., 2009; Li et al., 2013), no longer occurred during the Triassic. The Permian Protanisoptera and Permagrionoidea had the same fate (Béthoux et al., 2005; Nel et al., 2012). The opposite pattern characterizes the Triadophlebiomorpha, represented by only two species during the Permian (Nel et al., 2001) but diverse and widely distributed during the Triassic (Pritykina, 1981; Nel et al., 2001; Zheng et al., 2017a). To a lesser extent, this is also the case of the Panodonata, including the Lobodonata (themselves including the Tarsophlebiidae and crown-Odonata) and triasolestids (Tierney et al. 2020). These odonates are very

rare during the Permian (Nel et al., 1999c) but more common during the Triassic. Finally, the Archizygoptera are the only odonate group to have been diversified during both periods, with several lineages crossing the EPME. Within Archizygoptera, Terskejoptera appeared and diversified from the Triassic.

Even though Odonata were greatly diversified and widespread during this two periods there seems to be a change in odonates fauna. However, there is no record of odonates during the Lower Triassic, making it difficult to appreciate the impact the EPME had on it. Moreover there are still uncertainties of systematic relevance, such as the monophyly of Meganisoptera (Li et al., 2013). Therefore, taxonomic diversity alone might not be the best approach to understand the evolution of odonates through this period. Disparity of this group might be the solution to better apprehend and quantify the change in fauna composition.

Despite its potential to address macro-evolutionary aspects, disparity has seldom been applied to insects (Labandeira et al., 2000; Nel et al., 2018). Nel et al. (2018) found that the last three major crises (Permian-Triassic, Triassic-Jurassic and Cretaceous-Cenozoic) had no evident impact on mouthparts disparity. At the contrary, according to Labandeira (2019), the number of mouthpart classes experienced an elevated increase (138%) from the Permian to the Triassic. However, even if mouthparts bear crucial information on feeding strategies evolution (Labandeira et al., 2000), they can only be investigated with sufficient detail in a few specimens (except for the comparatively recent amber-embedded material). These limited data are complemented by data derived from extant forms and inferred for fossil relatives. As a consequence, all studies resorted to large temporal intervals, making it difficult to relate the observed data to the EPME.

Compared to mouthparts, fossil insect wings are easier to investigate and are more abundant. Their shape and venation underwent an intense evolution in several groups, such as odonates (see Chapter 1). During the Permian this group is represented by a wide range of shapes and sizes: the Meganisoptera, lacking the distinctive nodus and pterostigma (Nel et al., 2009) and covering an extreme range of sizes (50 to 210 mm in wing length), co-occurred with a number of lineages possessing petiolated wings, including small Stigmoptera (Nel et al., 2012). The distinctive petiole was then lost by Triassic Lobodonata (Tierney et al., 2020). Additionally, some Permian and Triassic forms possessed very unusual features in their wing venation, such as the seemingly forked RP3+4 of the Triadophlebiomorpha (Pritykina, 1981), and the fusion of RP2 with $Irp_{1+2}-rp_{3+4}$, which evolved convergently within Terskejoptera and some Triadophlebiomorpha (Deregnaucourt et al., 2019a, and see subsection 4.3.2).

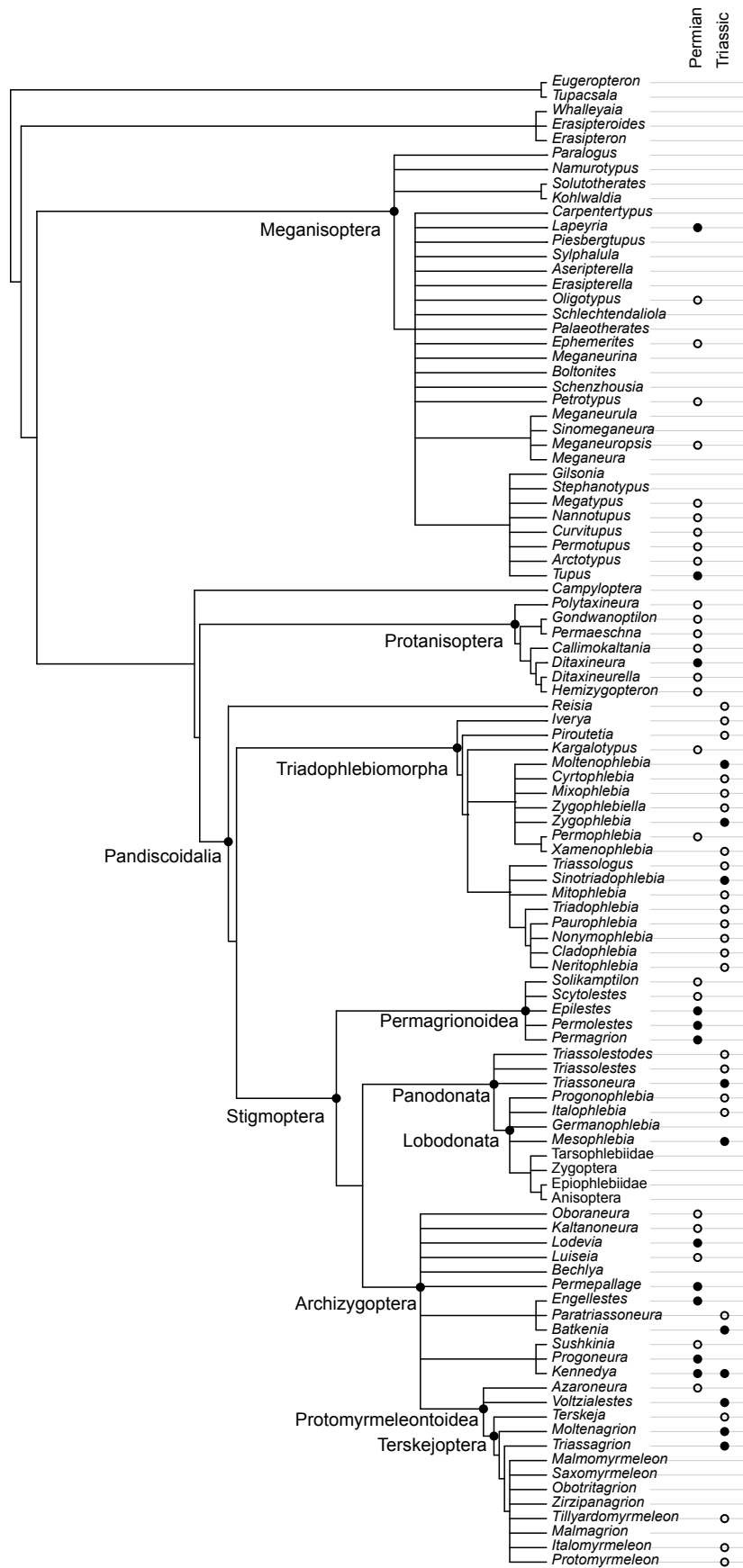


Figure 4.1 – Non-exhaustive summarized phylogeny of Odonata. Dots correspond to genera present during the Permian and/or the Triassic. Empty dots correspond to genera absent from the analysis and full dots to the ones present. This phylogeny is based on Bechly (2007), Nel et al. (2001), Nel et al. (2012), Deregnaucourt et al. (2019), and Tierney et al. (2020).

In summary, odonate wing disparity may have been very high during both Permian and Triassic times. As for others groups impacted by the EPME, odonates could undergo a loss of diversity but maintain steady disparity, highlighting a morphologically non-selective extinction. At the contrary, disparity of the group might have been altered during the EPME, at least in relation with the extinction of the Meganisoptera. Therefore we could expect a change in morphospace occupation with a decrease of disparity. This would be revealing of a selective extinction on extreme shapes.

Herein we investigated the evolution of odonate disparity during the Permian and the Triassic. We quantified wing morphology in the known fossils suitable for such approach and applied commonly used disparity metrics.

4.2 Fossils species selection

A pattern of vein homologies that could be applied to the entire odonates was adopted for the morphometric analyses. This pattern can only be applied on complete to sub-complete wings. Seventy-two Permian species have been sorted, among them 20 were considered sufficiently completes. For the Triassic 63 species have been sorted and only 4 were considered sufficiently completes. The low ratio of usable Triassic odonates for our analysis is essentially due to the fact that most of known fossils for that period were found at Madygen, where specimens endured important tectonic deformation (Sharov, 1968, 1971; Voigt et al., 2006). As a consequence, these specimens, cannot be used in their current state in morphometric analyses. To address the issue of the low number of Triassic odonates, we described or used unpublished data on new material, mainly from the Molteno Formation (Karoo Basin, South Africa), and developed reproducible methods to complement missing parts of a fossil, based on the morphology of its known relatives. Additionally, several lineages occur during the Permian and the Triassic and are represented by complete wings. However, they are only represented by Permian species in our analysis, Triassic ones being from Madygen and thus deformed. Retro-deformations of this uniformly deformed specimens has therefore been performed.

4.3 New data on Triassic odonates

4.3.1 New gondwanian Triassic material

Two new species from Molteno Formation, remaining to be formally described, were added to the dataset. The first one, referred to as "Odonata sp. 1", is known by the specimen BP/2/20950, composed of 4 wings. Three of these wings (including two forewings and a hindwing) are sufficiently complete to be included in the analysis. The few missing parts of each wing were completed by hand based on parts preserved on the other two wings. The

species belongs most probably to the Triadophlebiomorpha. The second species, referred to as "Odonata sp. 2", is known based on the specimen PRE/F/10442, consisting of a small, complete and well-preserved petiolated wing. We believe it to be a Panodonata, closely related to triassolestids.

Data on two gondwanian Lobodonata species were published by Tierney et al. (2020). A new specimen, from Australia, was assigned to *Mesophlebia antinodalis* Tillyard, 1916, greatly complementing the available data on this species. Another specimens, from the Molteno Formation, could be assigned to the same genus but to a new species, namely *Mesophlebia elegans* Deregnaucourt, Anderson, Wappler and Béthoux 2020 in Tierney et al. (2020). Parts missing in one specimen were completed by hand based on parts preserved in the other specimen, on the drawing of the holotype of *M. antinodalis* by Tillyard and Dunstan (1916, ;Plate 4, Fig.2), and on the morphology of related species known from Madygen (Pritykina, 1981).

We also described two new species from the Molteno Formation. These two species are considered as second category ones. However, they have been completed thanks to a standardized repeatable method we developed under R so they could be added to the geometry morphometrics analysis. The description and reconstruction of these two species are presented below.

4.3.2 A new Zygothlebiida from Molteno reconstructed

This part consists of a paper manuscript submitted to *Arthropod Structure and Development*. Reports from reviewers were obtained and a revised version will be prepared accordingly.

The wing venation of a new fossil species, reconstructed using geometric morphometrics, adds to the rare fossil record of Triassic Gondwanian Odonata

Deregnaucourt, I., Bardin, J., Anderson, J. M. and Béthoux, O.

Abstract

Probably, the most common rock imprint fossil insect remain is an incomplete, isolated wing. This pitfall has been traditionally addressed by manually reconstructing missing parts, which is not ideal to comprehend long-term evolutionary trends in the group, in particular for morphological diversity (i.e., disparity) approaches. Herein we describe a new Triassic relative of dragon- and damselflies (Odonata), *Moltenophlebia lindae* gen. et sp. nov., from the Molteno Formation (Karoo Basin, South Africa), on the basis of three incomplete, isolated wings. In order to provide a reconstruction of the complete wing venation of the species, we formalized and applied a repeatable method aiming at inferring

the missing parts of a given specimen. It is based on homologous veins automatically identified thanks to a standardized color-coding. The dedicated script can be applied broadly to the fossil record of insect wings. The species occurs to be a member of the Zygophlebiida, within the Triadophlebiomorpha. This discovery therefore represents the first ascertained occurrence of the latter group in Gondwana, an area where the fossil record of Odonata is depauperate.

Keywords: Wing venation – Molteno Formation – Stem-Odonata – Reconstruction

Introduction

Although the fossil record of Odonata (dragon- and damselflies, and their stem-relatives) is composed of about a thousand species (Paleobiology Database, 2019), many of the known fossils are represented by incomplete wings. Moreover, particular periods and geographical areas remain under-studied. This situation makes it difficult to comprehend long-term evolutionary trends in the group, using either taxonomic or morphological diversity (i.e., disparity) approaches.

Herein we describe a new species from the Molteno Formation (Triassic, South Africa). The species is represented by three incomplete, isolated wings. In order to provide a reconstruction of the entire wing venation of the species, we formalized and applied a standardized and repeatable method aiming at reconstructing missing parts. We used Thin Plate Splines (TPS), mathematical basis for deformation grids (Bookstein, 1989), to deform a reference shape onto a target shape using homologous landmarks and semi-landmarks subsampled along veins identified thanks to a standardized color-coding.

The new species adds to the fossil record of Odonata during the Triassic. Indeed it represents the first well ascertained occurrence of Triadophlebiomorpha in the Southern Hemisphere, a group previously known from Europe and Asia only (Pritykina, 1981; Nel et al., 2001; Zheng et al., 2017a).

Materials and methods

Documentation of fossil material

The studied specimens are housed at the Evolutionary Studies Institute (PRE/F/; formerly ‘Bernard Price Institute for Palaeontology’), University of the Witwatersrand, Johannesburg, South Africa.

Draft drawings were prepared with the aid of a Zeiss SteREO Discovery V8 Stereomicroscope equipped with a pair of W-PL 10x/23 eye pieces, a Plan Apo S 1.0x FWD objective, and a drawing tube (Jena, Germany). Photographs were taken using a Canon EOS 5D Mark III equipped with Canon 50 mm or MP-E 65 mm macro lenses. The light-mirror technique was used to provide positive views of the specimens. Photographs were optimized using Adobe Photoshop CS6 (Adobe Systems, San Jose, CA, USA). Draft

drawings were inked using Adobe Illustrator CS6 (Adobe Systems, San Jose, CA, USA) using both scanned draft drawings and photographs.

Reconstruction of missing parts

In the literature, reconstructing non-conserved part of a fossil, for example a wing, is usually achieved following the author's appreciation, i.e., a non-repeatable, unstandardized method. The material at hand, composed of several conspecific wings preserving different areas, was suitable for exploring methodologies aiming at reconstructing missing parts.

Several standardized reconstruction methods have already been developed in palaeoanthropology for 3D models of cranium (Gunz et al., 2009; Ogihara et al., 2015), involving bilateral symmetry, multivariate regression and/or thin-plate spline (TPS) interpolation. Bilateral symmetry is not appropriate for our model (there is no inner symmetry in an isolated wing). Multivariate regression requires a sample of complete specimens, which is not available for our case. We therefore resorted to semi-landmarks and TPS deformation.

TPS deformation mimics the deformation of an infinitely thin metal plate (Bookstein, 1989). Therefore it minimizes the bending energy of the transformation from a reference shape (here the wing used to infer the missing parts of the incomplete one) to a targeted shape (the wing to be reconstructed). As a consequence, the whole plan of the reference shape will be deformed. In practice, the entire reference drawing will be affected by the deformation in such a way that the placed points of reference (landmarks and semi-landmarks) fit perfectly the ones on the targeted shape. Thus, the missing parts of the targeted shape will be inferred by those deformed from the reference shape.

The two most complete specimens of *Moltenophlebia lindae*, PRE/F/20522 and PRE/F/10626 (Fig. 4.3A, B), have largely overlapping parts. Therefore, each can be used as reference shape to infer the missing parts of the other (Fig. 4.2A). Unfortunately, both specimens lack the wing apex. Thus, a second TPS deformation was performed using data on *Zygophlebia ramosa* Pritykina, 1981, the closest relative known from a complete wing, to reconstruct the missing apex (Fig. 4.2B).

For details, the missing parts of the specimen PRE/F/20522 (light lines in Fig. 4.3A) were inferred based on the specimen PRE/F/10626 (dark lines in Fig. 4.3B), and vice-versa. A drawing of the main veins and wing margin was first vectorized with Adobe Illustrator CS6. A specific color-code was applied to each vein. The vector files were then imported on R using grImport v.0.9-1 (Murrell, 2009).

Selection of sliding semi-landmarks was then performed (orange block in Fig. 4.2A). Fourteen homologous vein portions present on both specimens were automatically selected thanks to their color-coding. They were then sub-sampled to generate sets of landmarks with geomorph v.3.0.7 (Adams and Otárola-Castillo, 2013). For details, for each curve, the subsampling procedure generates two landmarks (considered homologous) at its beginning

and end, and 3 to 49 semi-landmarks between them (proportionally to the curve's length and complexity). Semi-landmarks were allowed to slide using the minimum Bending Energy criterion. This method is more suitable than minimizing Procrustes distances when there is large shape variation (Gunz and Mitteroecker, 2013; Schlager, 2017), which is the case for the second step of the reconstruction (see below; Fig. 4.2B). The actual disposition of landmarks and the rationale for placing them are provided as Supplemental Data 1 (Annex A.15).

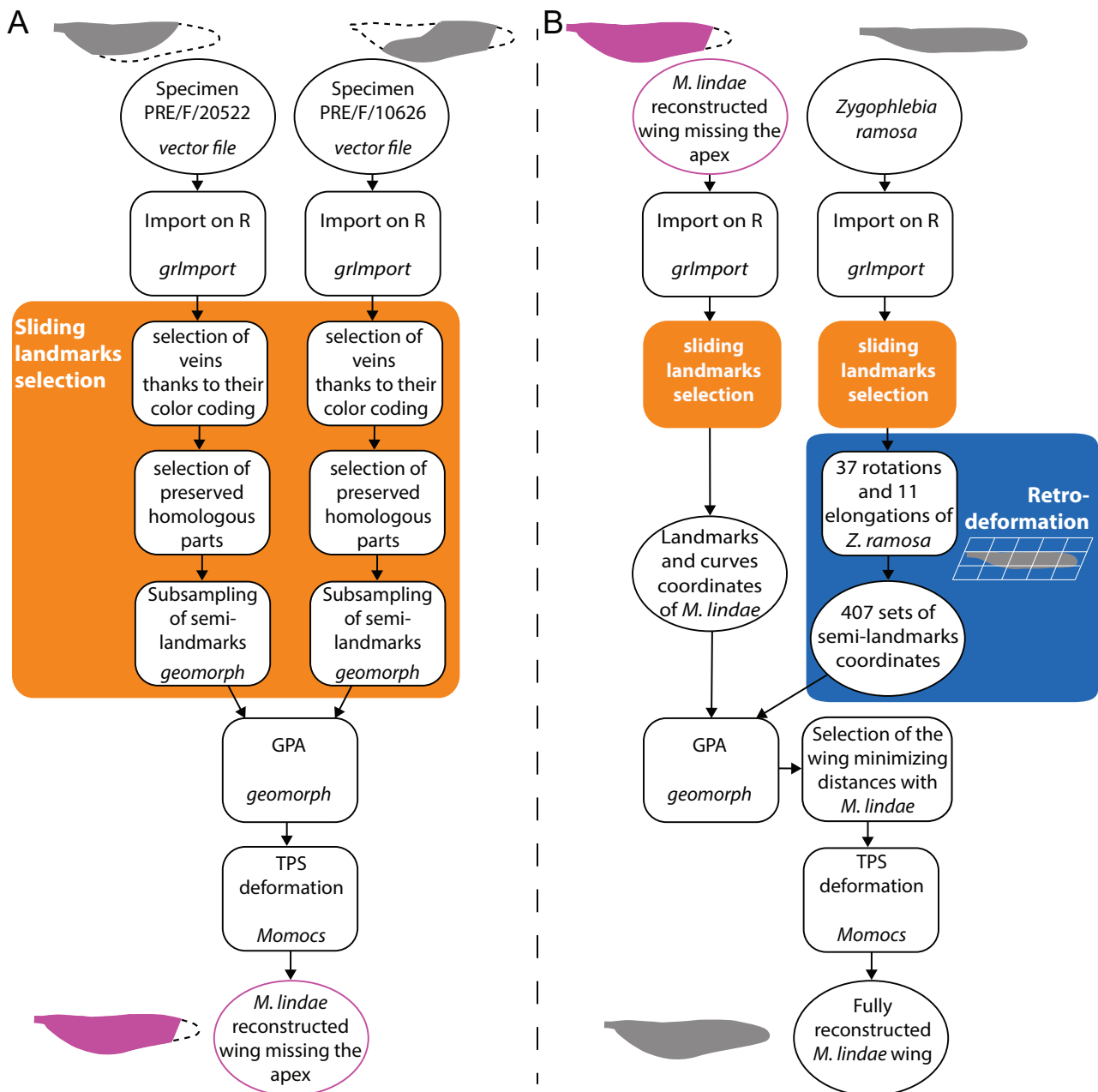


Figure 4.2 – Flow-chart explaining the standardized method used to reconstruct the wing of specimen PRE/F/20522. **A**, first step, reconstruction of specimen PRE/F/20522 with specimen PRE/F/10626. **B**, second step, reconstruction of the firstly reconstructed wing of specimen PRE/F/20522 with the holotype of *Zygophlebia ramosa* PIN 2785/20. GPA = generalised Procrustes analysis; TPS = thin plate splines; squares correspond to process and circles to data.

A Procrustes superimposition (GPA) was then performed to correct for the effects of rotation, translation and size (Rohlf and Slice, 1990). Finally, a TPS deformation was applied to the specimen PRE/F/10626 (reference shape) so that its homologous points' coordinates fit those of the specimen PRE/F/20522 (targeted shape). The same deformation is applied to each pixel of the original drawing in order to obtain the image of PRE/F/20522 complemented by PRE/F/10626 original parts. The wing was almost completely reconstructed at that point, except for the apex.

To reconstruct this last area we applied the same procedure using data on *Zygophlebia ramosa* which, among the Zygophlebiida, to which *Moltenophlebia lindae* belongs (see Systematic Paleontology section), is the only species represented by a complete wing (Fig. 4.2B). However this specimen, like others excavated in the corresponding locality, is assumed to have been uniformly deformed by tectonics (Sharov, 1968, 1971; Voigt et al., 2006). To take that bias into account, we added a 'retrodeformation' step (blue block in Fig. 4.2B): the wing of *Zygophlebia ramosa* was submitted to 37 rotations (over 180°) and 11 elongations (from 100% to 200%) to create 407 retro-deformed wings. The Procrustes superimposition was then performed. The retro-deformed drawing selected for reconstruction was the one minimizing distances between landmarks coordinates and those of the previously reconstructed wing (purple wing in Fig. 4.2). The TPS deformation was then realized on this retro-deformed wing so that its homologous points' coordinates fit those of the previously reconstructed wing (penultimate step in Fig. 4.2B). A fully reconstructed wing was then obtained (main script, functions and functions description are available as Supplemental Data 2, 3 and 4 respectively, Annexes A.13 – A.16).

The same procedure was used to reconstruct the wing of the specimen PRE/F/10626 (but using the specimen PRE/F/20522 as reference shape for the first step).

Nomenclature and abbreviations

We follow the serial insect wing venation ground pattern (Lameere, 1922, 1923). The corresponding wing venation nomenclature is repeated for convenience: ScP, posterior Subcosta; R, Radius; RA, anterior Radius; RP, posterior Radius; RP1+2, anterior branch of RP (to be further divided into RP1 and RP2); RP3+4, posterior branch of RP (to be further divided into RP3 and RP4); MA, anterior Media; MP, posterior Media; Cu, Cubitus; CuA, anterior Cubitus; CuP, posterior Cubitus; AA, anterior Analis (used in text only). Based on this ground pattern we follow homology conjectures for total-Odonata proposed by Riek and Kukalová-Peck (1984, Bechly, 1996; Béthoux, 2015; and see references therein). We follow Deregnaucourt et al. (2017) for the terminology to apply to intercalary veins. In details, Irp_1-rp_2 is the intercalary vein occurring between RP1 and RP2 (also termed 'IR1'), and $Irp_{1+2}-rp_{3+4}$ that occurring the RP1+2 and RP3+4 (also termed 'IR2'). In addition to this standard terminology, we propose to use additional terms, as follows. For the strongly convex, oblique cross-vein located between MA and

MP and aligned with RP+MA/MA, we propose the term ‘pons’ (‘bridge’ in Latin; also termed ‘MAB’, e.g. by Nel et al., 1996; for the strongly convex and aligned cross-veins located between MP and the posterior wing margin, or CuA and the posterior wing margin, we propose the term ‘pillar’. Whether its portion located between CuP and the posterior wing margin AA (or one of its branches) or a strengthened cross-vein is addressed in the Discussion.

Systematic paleontology

Order **Odonata** Fabricius, 1793

Taxon **Pandiscoidalia** Nel et al., 2001

Taxon **Discoïdalia** Bechly, 1996

Taxon **Triadophlebiomorpha** Pritykina, 1981

Taxon **Zygophlebiida** Nel et al., 2001

Emended diagnosis. RP2 and Irp_{1+2} - rp_{3+4} fused for some distance shortly after the origin of the former, and Irp_1 - rp_2 and RP2 fused for some distance; CuA without posterior branches; and, occurrence of a pillar (ranging either from CuA to the posterior wing margin, or from MP to the posterior wing margin).

Included families. Zygophlebiidae, Xamenophlebiidae, Permophlebiidae and Kargalotypidae.

Remarks. Nel et al. (2001) listed six character states as diagnostic of the taxon Zygophlebiida. Two of them relate to the particular organisation of Irp_1 - rp_2 , RP2, and Irp_{1+2} - rp_{3+4} . We provide a tentative interpretation of the corresponding area (Fig. 4.3) consistent with statements made by Bechly (1996) and Nel et al. (2001), positing that (1) in the basal part, RP2 briefly fuses with Irp_{1+2} - rp_{3+4} , and, (2) in the distal part, Irp_1 - rp_2 , briefly fuses with RP2. These two states might have been acquired concurrently as a consequence of the relocation of the bases of Irp_1 - rp_2 , RP2, and Irp_{1+2} - rp_{3+4} towards the wing base. Therefore we propose to treat them as a single character state, which is obviously derived, as it is absent in the most remote stem-Odonata (Riek and Kukalová-Peck, 1984). Note that, as indicated by Nel et al. (2001), this character state was acquired convergently within Protomyrmeleontidae, belonging to the Stigmoptera (Deregnacourt et al., 2019a, and references therein), a group therefore only remotely related to the Zygophlebiida.

Other character states listed by Nel et al. (2001) are present in various other Pandiscoidalia, such as the Triadotypomorpha (Nel et al., 2001; Deregnacourt et al., 2017). In other words, these states form a corpus relevant only if observed jointly. The most relevant is ‘CuA simple’, allowing Zygophlebiida to be distinguished from other Triadophlebiomorpha. However, it might represent the apomorphy of a larger group, including all extant

forms.

Whether the posterior-most portion of the pillar is composed of AA (or one of its branches) or a strengthened cross-vein, as favoured herein, is addressed in the Discussion. Regardless of its nature, the occurrence of the pillar itself is a putative diagnostic trait of Zygophlebiida, or of a subset within this group, as pointed out by Nel et al. (2001).

Family uncertain

Genus *Moltenophlebia* gen. nov.

Type species. *Moltenophlebia lindae* gen. et sp. nov.

Diagnosis. By monotypy, as for the type species

Etymology. The name derives from that of the geological Formation and from ‘phlebia’, itself derived from the Ancient Greek ‘phlebos’ (vein).

Remarks. The genus *Moltenophlebia* can be confidently assigned to the Discoidalia owing to the occurrence of the pons. It can be further assigned to the Zygophlebiida owing to the occurrence of the diagnostic character states of this taxon (see above).

Moltenophlebia lindae gen. et sp. nov.

(Figs. 4.3–4.5)

Type specimens. Holotype: PRE/F/20522 (negative imprint). Paratypes: PRE/F/10626 (negative and positive imprints), PRE/F/10615 (negative and positive imprints).

Diagnosis. CuA-CuP fork located basal to the pillar (i.e., CuP not capturing the pillar; putative plesiomorphy within Zygophlebiida); RP4 branched (putative plesiomorphy within Zygophlebiida).

Occurrence. All the specimens are from Aasvoëlberg locality (locality code "Aas 411"; see Anderson and Anderson, 1984), Karoo Basin, South Africa; Molteno Formation; Carnian, Triassic (Anderson et al., 1998).

General description. Wing total length and maximum width unknown, about 98 mm, and 23 mm respectively; wing broad with numerous small cells, slightly petiolate, narrowing from the second third of the wing to the apex; ScP fused with the anterior wing margin at the first third of the wing; many antenodal cross-veins; RA parallel to the anterior wing margin distal to the nodus, with a single row of cell between the two; RP+MA diverging obliquely from RA basal to the second antenodal cross-vein; RP+MA divided

in RP and MA distal to the second antenodal cross-vein; RP divided into RP1+2 and RP3+4 basal to the nodus (inferred from preserved parts of the holotype); Irp_1-rp_2 , RP2 and $Irp_{1+2}-rp_{3+4}$ fused for some distance, forming a ‘rectilinear convex stem’ parallel to RP1 and seemingly diverging from this vein just distal to the nodus; Irp_1-rp_2 and RP2 diverging shortly after the wing mid-length; $Irp_{1+2}-rp_{3+4}$ diverging obliquely from the ‘rectilinear convex stem’ at wing mid-length; RP2 diverging obliquely from the ‘rectilinear convex stem’ further distally; areas between RP1 and Irp_1-rp_2 , and between RP2 and $Irp_{1+2}-rp_{3+4}$ with a single row of cells; RP2 with at least two branches (some of the concave veins located between Irp_1-rp_2 and RP2, visible in PRE/F/10626, might actually be branches of RP2, as in Zygophlebiidae); RP3+4 divided in RP3 and RP4 at the two-third of the wing length, each with at least two branches; area between RP4 and MA with a single row of cells; MA with a strong angle when dividing from RP; presence of a convex pons aligned with the RP+MA and the basal portion of MA; MA and MP close and parallel to each other basal to the nodus, diverging distal to it, and converging close to their endings; area between MA and MP ranging from one row of cells up to four; a cross-vein occurring in the area between R+MA and MP, basal to the first antenodal cross-vein; MP with no evident fork, but delimiting a large area filled with several concave branches (intercalaries?) and convex intercalaries, subparallel; Cu close to the posterior wing margin at the end of the petiole; Cu divided into CuA and CuP at the level of the point of divergence of RA and RP+MA; CuA and CuP parallel with one row of cells between them, occasionally two; CuP with no evident fork, but delimiting an area filled with several concave branches (intercalaries?) and convex intercalaries, subparallel.

Specimen description.

Holotype specimen PRE/F/20522 (Figs. 4.3A and 4.4A): Left wing, almost complete, apex and posterior wing margin missing; preserved length 79.6 mm, maximum width 19.6 mm; CuA and CuP more bent than in the specimen PRE/F/10626.

Paratype specimen PRE/F/10626 (Figs. 4.3B, 4.4B): Two-third of a right wing, antero-basal third and apex missing; preserved length 74.7 mm, maximum width 20.6 mm; posterior wing margin and distal portions of RP2, RP3 and RP4 branches preserved.

Paratype specimen PRE/F/10615 (Figs. 4.3C, 4.4C): Two broken segments of a left wing, the base and a part of the third quarter; preserved length 19.2 mm, maximum width 34 mm.

Etymology. The name is dedicated to Linda Terblanche, who allowed access to the site where the fossils were discovered.

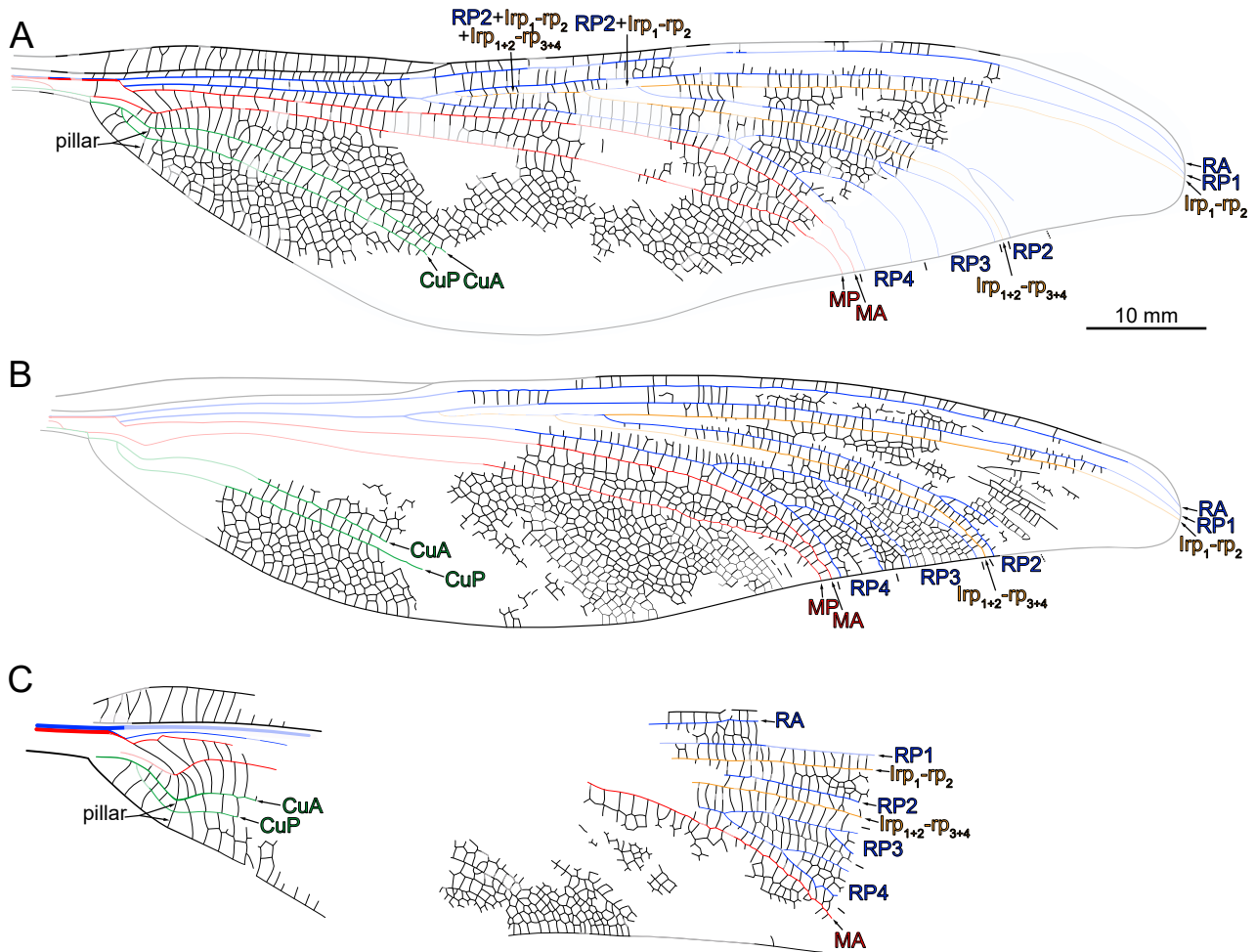


Figure 4.3 – *Moltenophlebia lindae* gen. et sp. nov., from Carnian (Triassic) of Aasvoëlberg locality, Molteno Formation, Karoo Basin, South Africa, line drawings. **A**, specimen PRE/F/20522 (left wing; holotype). **B**, specimen PRE/F/10626 (right wing; paratype). **C**, specimen PRE/F/10615 (left wing). RA = anterior Radius; RP = posterior Radius; RP1+2 = anterior branch of RP (to be further divided into RP1 and RP2); RP3+4 = posterior branch of RP (to be further divided into RP3 and RP4); Irp₁-rp₂ = intercalary vein between RP1 and RP2; Irp₁₊₂-rp₃₊₄ = intercalary vein between RP1+2 and RP3+4; MA = anterior Media; MP = posterior Media; CuA = anterior Cubitus; CuP = posterior Cubitus. Light lines were reconstructed.

Remarks. There is virtually no doubt that the specimens PRE/F/20522 (holotype) and PRE/F/10626 (paratype) are conspecific. Our reconstruction suggests that the former is slightly broader, but this could represent differences between a hind wing and a forewing, and/or sexual dimorphism. The specimen PRE/F/10615 can be attributed to the same species thanks to the presence of a convex pons aligned with the RP+MA and the basal portion of MA, and also the CuA-CuP split located basally (at the level of the point of divergence of RA and RP+MA). It is also very similar in size with the two other specimens.

The occurrence of a cross-vein in the area between R+MA and MP near the wing base, observed in the holotype specimen is unusual for the group. It is not unlikely that it represents a rare, uncommon feature for the species (it could then be an atavism).

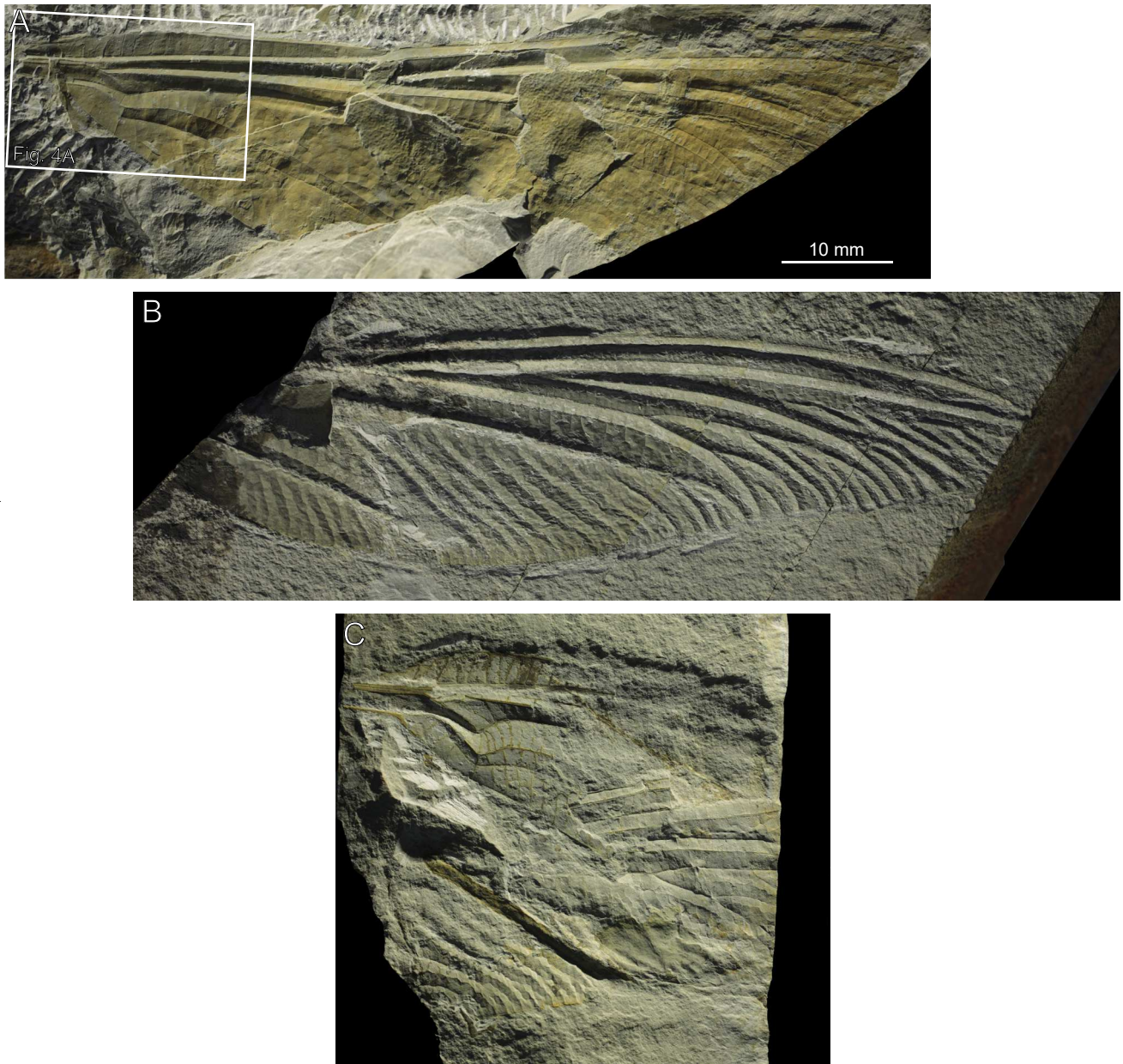


Figure 4.4 – *Moltenophlebia lindae* gen. et sp. nov., from Carnian (Triassic) of Aasvoëlbërg locality, Molteno Formation, Karoo Basin, South Africa, photographs. **A**, specimen PRE/F/20522, left wing (light-mirrored; holotype). **B**, specimen PRE/F/10626a, right wing (light-mirrored, flipped horizontally; paratype). **C**, specimen PRE/F/10615a left wing (flipped horizontally). White frame refers to Fig. 4.5A.

In the Zygophlebiida and more generally in Triadophlebiomorpha MP is distinct from Cu at the wing base (the two veins then remaining fused for some distance). This character state is plesiomorphic, being observed in early odonates. In our reconstruction we therefore assumed that *Moltenophlebia lindae* displayed this state. Within the Zygophlebiida, the new species can neither be attributed to the Xamenophlebiidae nor to the Permophlebiidae, as it lacks the diagnostic characters of these families as delimited by Nel et al. (2001). The family Zygophlebiidae currently lacks a diagnosis (Bechly, 1996; Nel et al., 2001). The family currently contains four genera, from which *Moltenophlebia*

lindae differs in many aspects, including a RP2 branched close to the posterior wing margin (whereas RP2 is widely developed in known Zygophlebiidae genera). Also, in the new species both RP3 and RP4 are branched. The resulting wide area (between RP3 and RP4) is also present in *Mixophlebia mixta* Pritykina, 1981, but RP4 is simple in this species. The observed differences justify the erection of a new genus. However, given uncertainties on the occurrence of several character states in various genera of Zygophlebiidae, and on the polarity of several character states, we refrained from erecting a new family to accommodate *Moltenophlebia*.

Discussion

Nature of the pillar

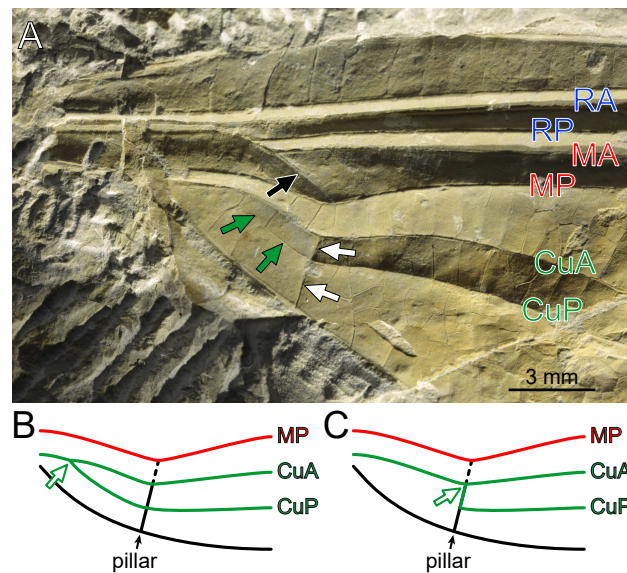


Figure 4.5 – Detail of the area of the pillar. **A**, *Moltenophlebia lindae* gen. et sp. nov., detail of specimen PRE/F/20522, left wing base (light-mirrored; holotype). **B–C**, schemes of the respective positions of CuP and of the pillar in **B**, *Moltenophlebia lindae* gen. et sp. nov and **C**, as assumed for Zygophlebiidae. RA = anterior Radius; RP = posterior Radius; MA = anterior Media; MP = posterior Media; CuA = anterior Cubitus; CuP = posterior Cubitus; large black arrow in **A** indicates the pons; white arrows in **B** indicate the pillar; green arrows (grey in grayscale version) in **A** indicate the portion of CuP basal to the pillar (and see Fig. 4.4A); small white arrows (bordered in green -gray in grayscale version) in **B** indicate the CuA-CuP split.

In Zygophlebiidae, the portion of the pillar located between CuP and the posterior wing margin is interpreted as a branch of AA by Pritykina (1981) and Bechly (1996), and AA by Nel et al. (2001) and Zheng et al. (2017). It implies that CuP and AA (or one of its branches) form a composite stem. However, the condition displayed by *Moltenophlebia lindae*, previously undocumented for Zygophlebiida, provides a new perspective on this particular aspect of wing venation homologies. Instead of possessing a single, convex stem in the area delimited by MP, the pillar and the posterior wing margin, *Moltenophlebia lindae* displays a convex stem but also another, conspicuously concave one

(green arrows in Fig. 4.5A; and see Fig. 4.4C), the latter likely being CuP free from any other vein (a configuration similar to that of Archizygoptera; Nel et al., 2012). It follows that the pillar, in *Moltenophlebia lindae*, is exclusively composed of strengthened cross-veins (as represented in Fig. 4.5B). Assuming the same for Zygophlebiidae, it can then be hypothesized that the CuA-CuP split is located more distally in these insects than in *Moltenophlebia lindae*, to the point where CuP fuses with the portion of the pillar previously located between it and CuA (i.e., CuP captures the pillar), as represented in Fig. 4.5C. The pillar being overall convex, it likely imposed this elevation to CuP. In these insects, AA would fuse with the posterior wing margin at the level of the petiole and would remain fused with it. Indeed, in the petiole of *Zygophlebia tongchuanensis* Zheng et al., 2017 (see original description), a short vein-like element occurs in the area between the posterior wing margin and the vein immediately anterior to it, between the point of fusion of MP with Cu+AA and the point of divergence of MP. This is likely the actual AA.

Reconstruction of the missing part

Several sets of main veins were tested for reconstruction. Notably, the pertinence of using semi-landmarks on RP2, for the second part of the process (aiming at reconstructing the wing apex; Fig. 4.2B), was examined. Indeed, the area between RP3 and the anterior branch of RP2 is very dissimilar in the reference and targeted shapes: RP2 is branched more basally than RP3+4 in *Zygophlebia ramosa* whereas in *Moltenophlebia lindae* RP2 is forked close to the posterior wing margin. Additionally, RP3+4 has many more branches in *Moltenophlebia lindae*. In a first attempt, RP2 was not used because of this important variation between the two wing shapes. However the obtained reconstructed wing was not realistic: it was very elongated and the apex had a marked posterior bending. This reconstructed wing could have hardly flown.

In a second attempt, semi-landmarks were placed on the portion of RP2 before its first split on each wing shape, assuming that this variable area would be more constrained so as to better fit the targeted shape. The obtained reconstruction, more realistic, is the one presented here (Fig. 4.3A). However, given the remarkable differences in this area between the two wings (viz. the reconstructed *Moltenophlebia lindae* and the retro-deformed *Zygophlebia ramosa*), the TPS deformation generated unrealistic distortions of some vein portions. These distortions were not taken into account for the final reconstruction because they affected parts which were preserved in the targeted shape. The proposed reconstruction (Fig. 4.3A) is therefore a smoothed version of the R output to fit the fossil's preserved parts.

Unrealistic distortions were probably due to shape differences too important to be managed by the method. Indeed, semi-landmarks are allowed to slide along a curve, while only the first and last points are homologous landmarks (i.e., are not allowed to slide). Some semi-landmarks slid away from the original curve, not fitting anymore the

original wing shape, probably because of the constraint induced by the use of RP2 curve for such a different area. The use of a more closely related species as reference shape might fix this issue. An additional improvement would be to consider more than one closely related species as reference shapes. Indeed, Gunz et al. (2009) used several references to reconstruct their target and obtained different results. However, for now, there is no other complete wing appropriate for such a reconstruction.

Other issues can also be mentioned. It was not always possible to delimit vein portions based on well-defined points such as vein branching. We therefore resorted to a manual pre-alignment of the two sub-complete wings, inducing some degree of subjectivity. As arose by Gunz et al. (2009) and Ogihara et al. (2015), other parameters are susceptible to lead to differing reconstructions, such as the number of landmarks and semi-landmarks. In our case, a minimal number of semi-landmarks is needed to faithfully quantify a vein curvature, but too many render the sliding computation more complicated, time-consuming and prone to generate unrealistic crossings of semi-landmarks (due to their proximity).

Also, we ignore whether the two specimens of *Moltenophlebia lindae* used in the first step (Fig. 4.2A) belonged to homologous thoracic segments (i.e., were both forewings, or hind wings), or to individuals of the same sex. Some of the observed differences could reflect fore- vs. hind wing differentiation and/or sexual dimorphism, both variations occurring among extant Odonata. Indeed, i.e., hind wings are commonly broader and shorter than forewings in these insects. This differentiation is much less conspicuous in those possessing petiolated wings (Zygoptera and Anisozygoptera; i.e., damselflies and *Epiophlebia* spp., respectively), as *Moltenophlebia lindae* does. In Calopterygidae (i.e., broad-winged damselflies) females commonly have wings more elongated than those of males. However, leaving apart purely shape-related aspects, the main veins pattern remains essentially unchanged, especially in the distal two-thirds of the wing. This general appreciation was confirmed by Blanke (2018) who, on the basis of a broad-scale morphometric analysis of Anisoptera wing venation, demonstrated that fore- and hind wings correlate with each other in their shape variation. It can then be expected that our reconstruction method will satisfactorily account for fore- vs. hind wing differentiation and/or sex-related shape differences. This is indeed exemplified by the fact that the obtained reconstruction of the specimen PRE/F/20522 (Fig. 4.3A) is broader than the used reference shape, which likely represents a genuine differentiation.

The obtained reconstructions are hypotheses based on a standardized repeatable method as less subjective as possible. This method could be used on any wing that needs to be reconstructed for comparative analysis, or any fossil equivalent to a 2D model lacking bilateral symmetry. However, the sensitivity of the method itself will need further testing. This could be achieved by simulating missing parts on extant species and comparing the obtained reconstructions with the original wing shape. The number and distribution of missing areas, as well as their extents, likely are critical elements. For example, the recon-

struction of a wing apex, as we endeavoured herein, is likely to be less reliable than that of an inner part. Indeed, we performed an extrapolation, i.e., constraints were only applied on one side of the reconstructed part. That could explain why the firstly reconstructed wing apex was unrealistically elongated. In contrast, the reconstruction of a part located in the middle of a wing could be more accurate because it is an interpolation, i.e., with constraints on several sides. Also, phylogenetic closeness between the reference and target shapes is likely another prevalent factor to be tested. The number of landmarks and semi-landmarks also needs to be tested. Ultimately, the error induced by the reconstruction could be tested against intra-specific variability, within an inter-specific framework (Gunz et al., 2009). Considering additional constraints, for example in relation with flight biomechanics (Wootton and Kukalová-Peck, 2000), and developmental modelling (Hoffmann et al., 2018), could further help obtaining more reliable reconstruction.

Triassic Gondwanian Odonata

Within early-diverging stem-Odonata (and, more specifically, within the Discoidalia), the Triadophlebiomorpha were greatly diversified and widely distributed across Europe and Asia during the Triassic (Pritykina, 1981; Nel et al., 2001; Zheng et al., 2017a). The new species, *Moltenophlebia lindae*, can be confidently assigned to one of the main lineages of this taxon, namely the Zygophlebiida. It therefore represents the first ascertained occurrence of the Triadophlebiomorpha in the Gondwana. This discovery concurs with previous accounts suggesting that major groups of Triassic Odonata had a world-wide distribution. The Triassic, Australian *Iverya averyi* Béthoux and Beattie, 2010, initially regarded as a Triadotymomorpha (see original description) but which actually occupies an uncertain position within the Discoidalia (Deregnacourt et al., 2017), already indicated similarities between Laurasian and Gondwanian faunas of stem-Odonata. Moreover, a representative of another group of stem-Odonata, the Triadotymomorpha, well-documented from Europe and Asia (Reis, 1909; Laurentiaux-Vieira et al., 1952; Pritykina, 1981; Bechly, 1997; Béthoux et al., 2009) also occurred at Molteno (Deregnacourt et al., 2017). Even the gracile, damselfly-like Protomyrmeleontoidea Handlirsch, 1906, which dispersal capabilities might have been more limited than those of larger, contemporaneous stem-Odonata, have been documented from Triassic outcrops in Australia (Tillyard, 1922; Henrotay et al., 1997) and also from Molteno (Deregnacourt et al., 2019a). In summary, this South African outcrop testifies to a great diversity of Triassic Odonata in the Gondwana, and to a widespread distribution of the main lineages of Odonata during this period.

4.3.3 Reconstruction of *Moltenagrion koningskroonensis*

Moltenagrion koningskroonensis, described in Chapter 1, belongs to the Archizygoptera and more specifically to the Terskejoptera. Its wing morphology is peculiar, it is the sister-group of Protomyrmelontidae (forming the Moltenoptera), represented in our analysis by the only Triassic specimen consisting of a complete wing, *Triassagrion australiense* Riek, 1976. Three other species are found in the Triassic but the specimens are too fragmentary (*Ferganagrion kirghiziensis* Nel et al., 2005, *Italomyrmeleon bergomensis* Bechly, 1997 and *Tillyardomyrmeleon petermilleri* Henrotay et al., 1997).

To be able to add *Moltenagrion koningskroonensis* to a morphometric analysis, it is essential to reconstruct the missing apex. However, at the contrary of *Moltenophlebia lindae*, it is represented by only one specimen. Therefore, we used the closest relatives represented by a complete wing. All Protomyrmeleontidae genera with at least one specimen consisting of a complete wing have been considered. These specimens are specimens of *Protomyrmeleon brunonis* Nel and Henrotay, 1992 (Jurassic), *Saxomyrmeleon keatingei* Nel and Jarzembowski, 1998 (Cretaceous), *Mongolagrion shartengensis* Nel et al., 2005 (Jurassic), *Triassagrion australiense* (Triassic) and *Obotritagrion petersi* Zessin, 1991 (Jurassic).

The used specimen of *Protomyrmeleon brunonis*, is a specimen previously considered as the holotype of *Protomyrmeleon bascharagensis* and synonymized by Ansorge (1996). It is held at the Museum National d'Histoire Naturelle, Paris: MNHN.F.A40897. This specimen has been redrawn and then drawn in vector lines. The other species are only represented by the holotype. Thus, vector line drawings were made directly based on the illustrations available in the original descriptions (Fig. 4.6).

Landmarks has been placed on portions of main veins corresponding to the ones conserved on *Moltenagrion koningskroonensis*, except on Irp_1 - rp_2 which is not conserved in *Saxomyrmeleon keatingei*. A GPA has then been realised on the 6 wings. The euclidean distances between the landmarks of the incomplete specimens and the 5 complete wings has been computed. The wing minimising these distances is the one of *Obotritagrion petersi*. The latter has therefore been used to complete the missing apex thanks to a TPS deformation. The method used to complete the wing is the same than the one used to reconstruct *Moltenophlebia lindae* in the previous section. This method is automated and incomplete portions of vein can directly be selected (by a click) on each complete wings under R.

This reconstructed wing of *Moltenagrion koningskroonensis* can now be used in morphometric analyses. We consider that such a repeatable method minimise the disparity added in the analysis, even if in this case the wing used to reconstruct the apex is not in our analysis.

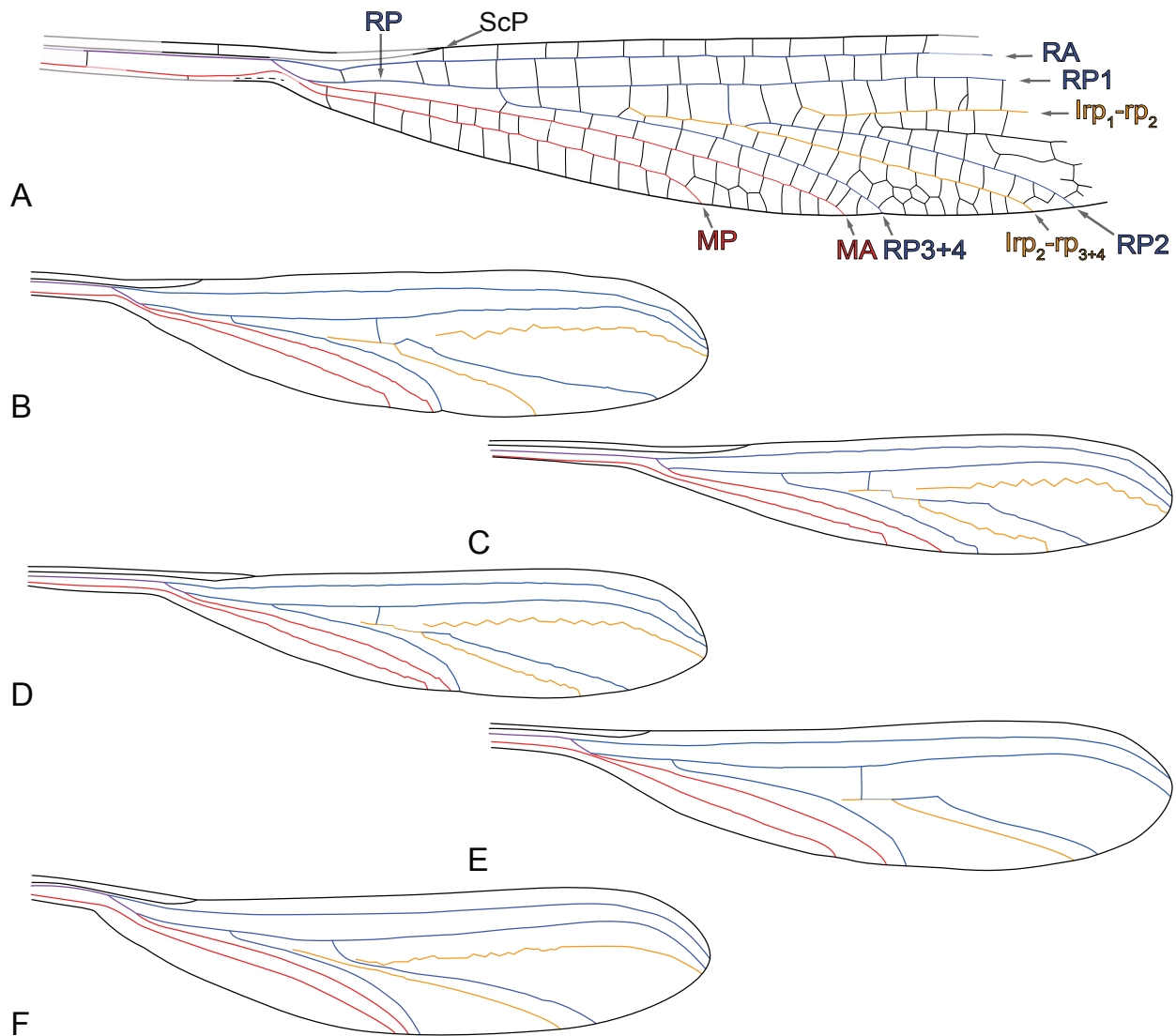


Figure 4.6 – Vector line drawings of *Moltenagrion koningskroonensis* (A) and Protomyrmeleonidae used to reconstruct its apex. B, *Mongolagrion shartengensis*; C, *Obotritagrion petersi*; D, *Protomyrmeleon brunonis*; E, *Saxomyrmeleon keatingei*; F, *Triassagrion australiense*.

4.3.4 Completing Triassic dataset with retro-deformed Madygen material

Triadophlebiomorpha are known from the Permian and the Triassic. However in our dataset we only have representatives dated from the Triassic. Only two specimens are known from the Permian, *Permophlebia uralica* Nel et al. 2001 and *Kargalotypus kargalensis* (Martynov, 1932) previously considered as Meganisoptera and placed within Triadophlebiomorpha by Nel et al. (2001). These two specimens are too incomplete to be added to our analyses. Archizygoptera are known from the Permian and the Triassic. In our dataset 4 families of Archizygoptera are represented for the Permian. Five families of Archizygoptera are represented for the Triassic, among them 3 belongs to the Pro-

tomyrmeleontoidea. The other two are Kennedyidae and Batkeniidae, also represented in the Permian. Protomyrmeleontoidea are known since the Triassic except *Azaronaura permiana* Nel et al. (2012) dated from the Permian but too incomplete to be added to the analyses. Terskejoptera, within Protomyrmeleontoidea, appeared during the Triassic and are the only group of Archizygoptera which are still found, with new representatives, after the Triassic. Panodonata (including extant species) are scarcely present from the Permian with only two representatives from Lodève, France, Saxonagrionidae Nel et al., 1999a and Huangiopteridae Prokop et al., 2015. These two taxa contain specimens too fragmentary to be used in morphometric analyses. Panodonata from the Triassic are considered, some belongings to the Lobodonata and the others probably sister-group of the latter.

Within Archizygoptera *Kennedyya* Tillyard, 1925 are found during Permian and Triassic. However, the specimens of *Kennedyya* spp. dated from the Triassic are found in Madygen. *Kennedyya carpenteri* Pritykina, 1981 and *Kennedyya gracilis* Pritykina, 1981 are complete but deformed wings from this formation. To take in count the morphological information carried by this genus during the Triassic we therefore computed a probable retro-deformation of these two genera. To do so we performed a Procrustes superimposition, with all the complete Permian *Kennedyya* (Table 4.1). A consensus shape of Permian *Kennedyya* has thus been computed. Then, each Triassic *Kennedyya* were retro-deformed following the same process than the retro-deformation of *Zygophlebia ramosa* Pritykina, 1981 presented in subsection 4.3.2. They have been rotated and elongated several time, resulting in 408 possible retro-deformations. The chosen retro-deformation of each Triassic *Kennedyya* is the one minimising the euclidean distances with the consensus shape of Permian *Kennedyya*. We consider this retro-deformations to be the most probable and the ones adding the least disparity within the analyses.

The Batkeniidae, an Archizygoptera family present during the Permian and the Triassic is represented for the Permian by *Engellestes cherkadensis* Nel et al., 2012 and during the Triassic by a fragmentary wing, *Paratriassoneura primitiva* (Pritykina, 1981) and a specimen composed of 3 wings (two complete and one almost complete), *Batkenia pusilla* Pritykina, 1981, both from the Madygen formation. To take into account a Triassic representative of this family, as for *Kennedyya*, we computed several possible retro-deformations of the two complete wings of *Batkenia pusilla* and considered the ones minimising the distances with *Engellestes cherkadensis* as the most probable and therefore the ones to use in morphometric analyses.

The retro-deformed *Zygophlebia ramosa* presented in the following section is also added to the analyses. Fourteen different species can, therefore, be used in the geometric morphometrics analyses for the Triassic, instead of four.

4.4 Disparity analysis

4.4.1 Material & Method

Fossil selection

Thirty-four fossils species have been selected. Twenty for the Permian and 14 for the Triassic (see Table 4.1). We considered the two periods Permian and Triassic and not the epoch within. Indeed, the selected Triassic species are all from the Upper Triassic except for *Voltzialestes triassicus* Nel et al., 1996, preventing the consideration of time bins smaller than periods.

Each species is represented by at least one wing. *Moltenophlebia lindae* is represented by two wings from different specimens. The yet undetermined Triadophlebiomorpha (BP/2/20950) from the Molteno formation is represented by 3 wings from a single specimen. *Batkenia pusilla* is represented by two wings from a single specimen.

As detailed in Chapter 2 each main veins and the outline has been drawn in vector line. The source of the pictures on which the fossils drawings are based are specified in Table 4.1. The undescribed specimens of the Molteno formation and the specimen used for *Triassoneura andersoni* Riek, 1976 are drawn based on drawings made by Olivier Béthoux using the same equipment as for the draft drawings of *Moltenophlebia lindae* (see subsection 4.3.3). The specimen of *Triassoneura andersoni* used is not the published holotype but a more complete wing also from the Molteno formation and not yet published.

Landmarks set

The set of landmarks used for this analysis differ from that presented in Chapter 2 regarding wing outline. Indeed, important differences between wing shapes led to an unrealistic distortions of deformation grids (indicating change in shapes from a given shape to a reference one, here axes extremes versus center of the morphospace). These distortions might be due to crossings between semi-landmarks sliding along the wing margin and the end of main veins, which themselves varied a lot between species. To correct this issue we divided the wing margin in different portions, delimited by the ends of two successive main veins or intercalaries. However the portions delimited by the ends of RA and RP1, and by the ends of RP1 and Irp_1-rp_2 , proved too short to allow the placement of semi-landmarks along them. These portions were therefore ignored. Each portion has a different color coding. These portions are numbered "O1" to "O10" starting antero-basally to postero-basally. The number of semi-landmarks on each veins and portions of veins is therefore of 17 for O1, 26 for O2, 2 for O5, 2 for O6, 2 for O7, 2 for O8, 2 for O9, 29 for O10, 17 for ScP, 36 for RA, 6 for RP, 10 for RP1+2, 17 for RP1, 15 for RP2, 21 for RP3+4, 13 for Irp_1-rp_2 , 19 for $Irp_{1+2}-rp_{3+4}$, 24 for MA and 29 for MP.

Table 4.1 – List of fossil specimens used in the morphometric analysis. Source correspond to the source of pictures vector lines drawings are based on. Institutional acronyms: BP, Bernard Price Institute for Palaeontology (Pretoria, South Africa), material actually housed at the Evolutionary Studies Institute, University of the Witwatersrand (Johannesburg, South Africa); IGLP, Institut de Geologie, Université Louis Pasteur (Strasbourg, France); Ld LAP, Lapeyre collection, Musée Fleury (Lodève, France); MCZ, Museum of Comparative Zoology (Harvard, USA); NIGP, Nanjing Institute of Geology and Palaeontology, Chinese Academy of Sciences (Nanjing, China); NRPS, Paleozoology, Naturhistoriska Riksmuseum (Stockholm, Sweden); PRE, Bernard Price Institute for Palaeontology (Pretoria, South Africa), material actually housed at the Evolutionary Studies Institute, University of the Witwatersrand (Johannesburg, South Africa); PIN, Arthropod Laboratory, Palaeontological Institute, Russian Academy of Science (Moscow, Russian Federation); QMF, Geosciences Collection, Queensland Museum (Hendra, Australia); GQS, Queensland Geological Survey (Brisbane, Australia); WU, University of Wichita (Wichita, USA); UT, University of Texas (Austin, USA).

Period	Taxa	Family	Species	Locality	Collection number	Source
Permian	Archizygoptera	Bakteniidae	<i>Engelletes chekardensis</i>	Koshelevka, Urals, Russia	PIN 1700/3250	Nel et al. (2012)
Permian	Archizygoptera	Kennedyidae	<i>Kennedyia azari</i>	Koshelevka, Urals, Russia	PIN 1/276	Nel et al. (2012)
Permian	Archizygoptera	Kennedyidae	<i>Kennedyia fraseri</i>	Midco, Noble Co., Okla., USA	MCZ PALE-4793	Carpenter (1947)
Permian	Archizygoptera	Kennedyidae	<i>Kennedyia ivensis</i>	Arkhangelsk, European Russia	PIN 15/117	Nel et al. (2012)
Permian	Archizygoptera	Kennedyidae	<i>Kennedyia minabilis</i>	Elmo, Kansas, USA	MCZ PALE-3971	Carpenter (1939)
Permian	Archizygoptera	Kennedyidae	<i>Kennedyia pritykinae</i>	Arkhangelsk, European Russia	PIN 3353/76	Nel et al. (2012)
Permian	Archizygoptera	Kennedyidae	<i>Kennedyia tillyardi</i>	Elmo, Kansas, USA	MCZ PALE-3970	Carpenter (1939)
Permian	Archizygoptera	Kennedyidae	<i>Progoneura nobilis</i>	Midco, Noble Co., Okla., USA	MCZ PALE-4768	Carpenter (1947)
Permian	Archizygoptera	Lodeviidae	<i>Lodevia longialata</i>	Salagou, Lodèvois, France	Ld LAP 111	Nel et al. (1999c)
Permian	Archizygoptera	Permepellagidae	<i>Permepallage angustissima</i>	Koshelevka, Urals, Russia	PIN 65/117	Nel et al. (2012)
Permian	Meganisoptera	Meganeuridae	<i>Tupus gracilis</i>	Midco, Noble Co., Okla., USA	MCZ PALE-4819,	MCZbase
Permian	Meganisoptera	Meganeuridae	<i>Tupus permianus</i>	Elmo, Kansas, USA	UT Sellards coll. 630	Sellards (1906) and unpubl. photo. (R. Beckemeyer, pers. com. to O. Béthoux)
Permian	Nodialata	Lapeyriidae	<i>Lapeyria magnifica</i>	Salagou, Lodèvois, France	Ld LAP 316	Nel et al. (1999b)
Permian	Permagnionoidea	Permagnionidae	<i>Epilestes gallica</i>	Salagou, Lodèvois, France	Ld LAP 110	Nel et al. (1999c)
Permian	Permagnionoidea	Permagnionidae	<i>Epilestes kargalensis</i>	Orenburg, Urals, Russia	PIN 100/0	Nel et al. (2012)
Permian	Permagnionoidea	Permagnionidae	<i>Permagnion falklandicum</i>	Bodie Creek Head, Falkland\newline newline Islands, Argentina	NRPS Ar 2168	Nel et al. (2012)
Permian	Permagnionoidea	Permagnionidae	<i>Permolestes gracilis</i>	Arkhangelsk, European Russia	PIN 2455/1	Nel et al. (2012)
Permian	Permagnionoidea	Permagnionidae	<i>Permolestes soyanaensis</i>	Arkhangelsk, European Russia	PIN 3353/63	Nel et al. (2012)
Permian	Protanisoptera	Ditaxineuridae	<i>Ditaxineura anomalostigma</i>	Elmo, Kansas, USA	MCZ PALE-3046,	Carpenter (1931)
Permian	Protanisoptera	Ditaxineuridae	<i>Ditaxineura cellulosa</i>	Elmo, Kansas, USA	WU Tasch coll. 1025	Tasch and Zimmerman (1962)

Continued on next page

Continued from previous page

Period	Taxa	Family	Species	Locality	Collection number	Source
Triassic	Archizygoptera	Bakteniidae	<i>Bakhenia pusilla</i> Pritykina, 1981	Madygen, Kyrgyzstan	PIN 2785/22	Pritykina (1981) and unpubl. photo. (D. Vasilenko, pers. com.)
Triassic	Archizygoptera	Kennedyidae	<i>Kennedyia carpenteri</i> Pritykina, 1981	Madygen, Kyrgyzstan	PIN 2785/2	Pritykina (1981)
Triassic	Archizygoptera	Kennedyidae	<i>Kennedyia gracilis</i> Pritykina, 1981	Madygen, Kyrgyzstan	PIN 2785/23	Pritykina (1981)
Triassic	Archizygoptera	Moltenagrionidae	<i>Moltenagrion koningskroonenensis</i> Deregnacourt et al. 2019	Molteno, South Africa	PRE/F/10334	Deregnacourt et al. (2019)
Triassic	Archizygoptera	Protomyrmeleontidae	<i>Triassagrion australiense</i> Tillyard, 1922	Ipswich, Queensland, Australia	QGS 290a	Tillyard (1922)
Triassic	Archizygoptera	Voltzialestidae	<i>Voltzialestes triassicus</i> Nel et al., 1996	Adamswiller quarry, Vosges, France	IGLP coll. Grauvogel et Gall 9041	Nel et al. (1996)
Triassic	Lobodonata	Mesophlebiidae	<i>Mesophlebia antinodalis</i> Tillyard, 1916	Burnett, Queensland, Australia	QMF 58847	Tierney et al. (2020)
Triassic	Lobodonata	Mesophlebiidae	<i>Mesophlebia elegans</i> Deregnacourt et al., 2020	Molteno, South Africa	PRE/F/20242	Tierney et al. (2020)
Triassic	Panodonata	Triassolestidae	<i>Triassoneura andersoni</i> Riek, 1976	Molteno, South Africa	PRE/F/11872	Unpubl. hand drawings and photo., O. Béthoux
Triassic	Panodonata	undetermined	"Odonata sp. 2"	Molteno, South Africa	PRE/F/10442	Unpubl. hand drawings and photo., O. Béthoux
Triassic	Triadophlebiomorpha	Sinotriadophlebiidae	<i>Sinotriadophlebia lini</i> Zheng et al., 2017	Baijiantan, Xinjiang, China	NIGP I63160	Zheng et al. (2017a)
Triassic	Triadophlebiomorpha	uncertain	<i>Moltenophlebia lindae</i> n. sp.	Molteno, South Africa	PRE/F/20522, PRE/F/10626	Unpubl. hand drawings and photo., O. Béthoux
Triassic	Triadophlebiomorpha	undetermined	"Odonata sp. 1"	Molteno, South Africa	BP/2/20950	Unpubl. hand drawings and photo., O. Béthoux
Triassic	Triadophlebiomorpha	Zygophlebiidae	<i>Zygophlebia ramosa</i> Pritykina, 1981	Madygen, Kyrgyzstan	PIN 2785/20	Pritykina (1981)

Once *Moltenophlebia lindae* and *Moltenagrion koningskroonensis* reconstructed and *Batkenia pusilla*, *Kennedya carpenteri*, *Kennedya gracilis* and *Zygophlebia ramosa* retro-deformed, allowing the use of 6 more Triassic species, a GPA has been performed to correct for the effects of size, rotation and translation. A PCA was then performed for all the 38 fossil wings. For the three species with more than one wings a mean shape has been computed by taking the mean of the PC scores of each specimens. Each species is thus represented by only one point in the morphospace.

Disparity metrics

Principal components 1 to 13 were used to compute disparity metrics with 500 bootstraps rarefied to 14 species. The considered metrics belong to 3 different categories, namely size (sum of ranges), density (sum of variances, median pairwise distance and average nearest neighbour distance) and position (average displacement).

A non-parametric MANOVA was performed on the PC scores (residuals of the MANOVA not being uniformly distributed) to test for differences between Permian and Triassic odonate assemblages, thanks to the R package *vegan* (Oksanen et al., 2016) . Permutations were performed in order to compare each disparity metric between the two periods. A thousand permutations have been performed on 1000 bootstraps for each metric. A p-value was then computed, comparing the disparity obtained with our dataset to the ones obtained with the random set created by the permutations (Ludbrook and Dudley, 1998). The impact of the number of bootstraps on each p-value as been tested (Annex A.17).

4.4.2 Results

Morphospace structure

The 13 first PCs used in the disparity studies accounts for 99% of the total shape variation. The first 3 axes of the PCA illustrate a substantial amount of shape variation (84%), and segregate the main clades according to their wing shapes (Fig.4.7; interactive 3D plot in Annex A.18). Permian griffenflies such as the two *Tupus* species and *Lapeyria magnifica* occupy a distinct area of the morphospace, with extremely low scores on PC1 and PC2 but high scores on PC3. *Ditaxineura* spp., that represent the Permian Protanisoptera, also occupies a distinct area of the morphospace with medium scores on PC1, low scores on PC2 and high scores on PC3. The different species of Permagrionoidea share high scores on PC2 and PC3 and mid scores on PC1. They are found close to the Archizyoptera.

Triadophlebiomorpha, a large group of mostly Triassic species, is widespread in the morphospace, likely because there is a wide range of venation patterns within the group. *Moltenophlebia lindae* and *Zygophlebia ramosa* are located in extreme position of PC1

and PC2. They represent a sub-clade of Triadophlebiomorpha, the Zygophlebiida, characterized by the fusion for some distance of RP2 and $Irp_{1+2}-rp_{3+4}$ and also of Irp_1-rp_2 and RP2. *Sinotriadophlebia lini* and the still undescribed taxon from the Molteno formation, "Odonata sp. 1", belong to the Triadophlebiida, a group of Triadophlebiomorpha that does not exhibit the vein fusions of Zygophlebiida. Their wing shapes are found closer to Archizygoptera.

Archizygoptera, are the most represented group of the analysed species pool. They are known from both the Permian and the Triassic and they occupy a large part of the morphospace. The Kennedyidae (*Kennedyia* spp. and *Progoneura nobilis*) are gathered, on the two first axes, with extreme values of PC1. *Permepallage angustissima*, the only representative of the family Permepallagidae, is found close to the Kennedyidae. The Terskejoptera are Triassic species with a wing structure close to the non-Zygophlebiida Triadophlebiomorpha. *Lodevia longialata* belongs to a distinct family and it is placed in the morphospace between the Kennedyidae and Terskejoptera. Batkeniidae, represented by the Triassic *Batkenia pusilla* and the Permian *Engellestes chekardensis*, are close to each other and occupy a distinct area of the morphospace, with low scores on PC2 and PC3, far from the other Archizygoptera.

Panodonata, are gathered in the middle of the morphospace. They are represented by the Triassic species, *Triassoneura andersoni*, "Odonata sp.2" (undetermined fossil from the Molteno formation) and the *Mesophlebia* species.

The variations explained by PC1 seems to be linked to the positions of the division of RP into RP3+4 and RP1+2 and the division of RP1+2 in RP1 and RP2 relative to the position of the end of ScP. This is why the Zygophlebiida have extreme values for the PC1 with a division of RP1+2 occurring more basally than in other species. The variation explained by PC2 seems to be impacted by the position of MP relative to MA. This explains why Meganisoptera and Permagrionoidea have values on PC2 close to that of the small petiolated Batkeniidae. For Meganisoptera MA is well developed with posterior branches, and MP is far away from the anterior branch of MA. For the Batkeniidae, the wing is very slender, and thus, MP is a lot reduced and end closer to the wing base, far from the end of MA. The variation explained by PC3 seems to be linked to the size of the wing. Small, petiolated wings with reduced venation, especially at the wing base, have low values. The size of the postero-proximal portion of the outline ("O10") is a lot reduced and closer to the course of MP. It reflects the reduction of MP and, indirectly, also of CuA and CuP (which are not considered in the analysis). The higher values of this axis represent wings with a well developed postero-basal area such as griffenflies and the Triadophlebiomorpha. Thus, Batkeniidae and griffenflies occupy opposite, extreme positions along this axis.

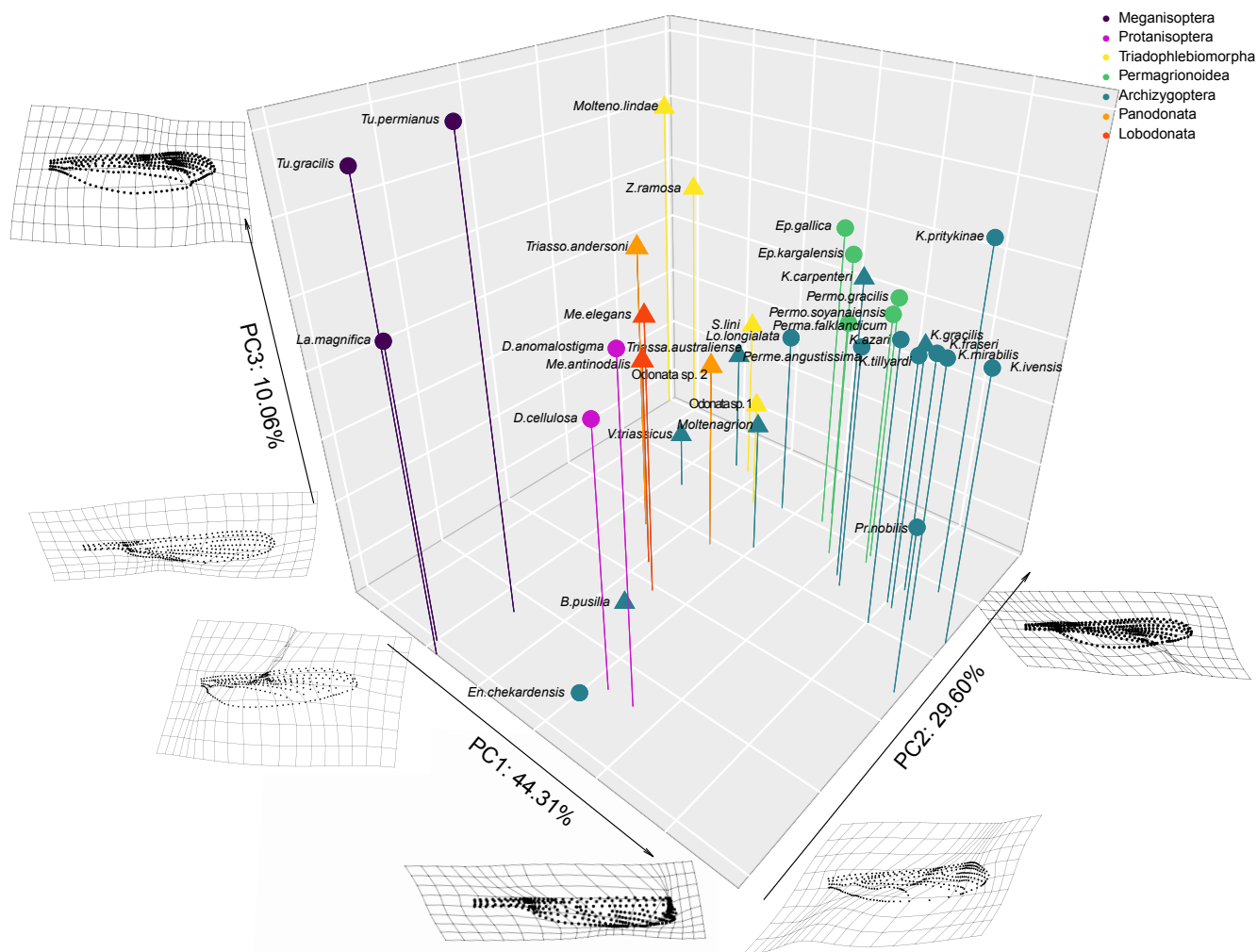


Figure 4.7 – First 3 axes of the principal component analysis of the 34 fossil species and wing shapes and deformation grids associated to extremes of each axes. Triangles represent the Triassic species and points the Permian ones. Species are coloured by taxa. Interactive 3D plot of the first three axes of this PCA available in Annex A.18.

Changes in morphospace occupation between the Permian and the Triassic

The R^2 obtained with the non-parametric MANOVA is equal to 0.16 meaning that only 16% of the morphological variation is explained by the differences between Permian and Triassic. However the obtained p-value of 0.003 reflects significant differences between the two morphospaces occupied by Permian and Triassic odonates. In other words, morphospace occupation changes little during the Permo-Triassic transition, but changes significantly.

The disparity metrics is given in Table 4.2. All the disparity values seem smaller in the Triassic, although there is no significant differences according to the permutation tests (Fig. 4.8). However, given the morphospace observable on the first 3 PCs, there is a modification of the occupation of the morphospace. The volume of the morphospace occupied is not significantly different between the two periods, but the morphospace structure changes (Fig. 4.7).

Table 4.2 – Estimates of disparity for Permian and Triassic and p-value issued for a permutation test. The values correspond to the mean of the 500 bootstraps.

Disparity	Permian	Triassic	p-values
sum of ranges	1.951	1.873	0.739
sum of variances	0.058	0.045	0.420
median pairwise distances	0.301	0.271	0.603
average nearest neighbour distances	0.071	0.061	0.810
average displacement	1.271	1.166	0.243

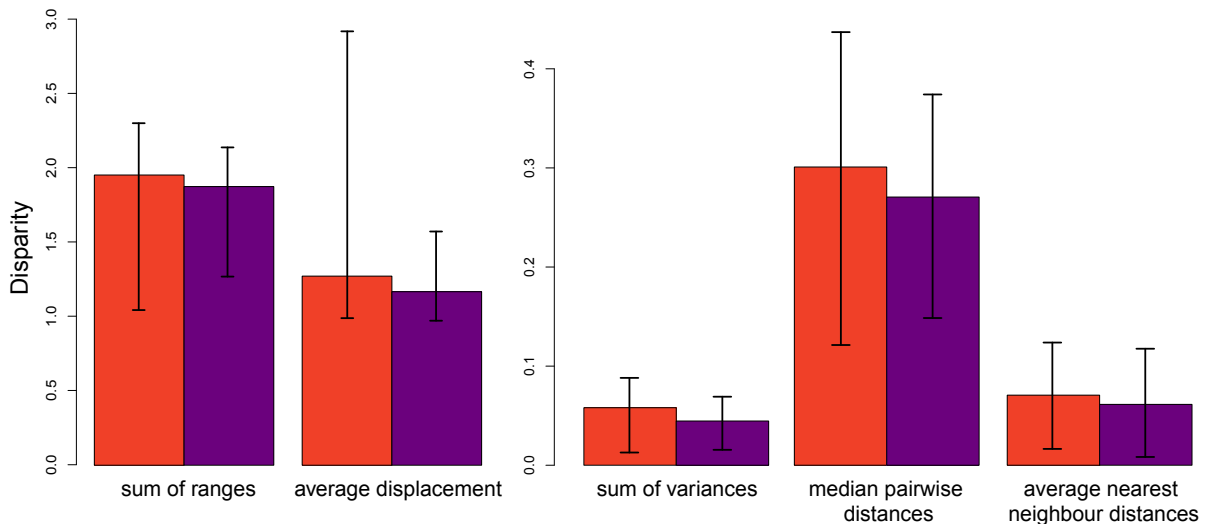


Figure 4.8 – Mean of the 500 bootstraps of five disparity estimates for the Permian and the Triassic. Red barplots correspond to the Permian and violet to the Triassic. Black segments represent the minimum and maximum of bootstraps for each estimates.

The loss of extreme shapes of the Permian period (Meganisoptera, Permagrionoidea, some Archizygoptera families) is compensated by emergence of new morphologies during the Triassic, especially within the Triadophlebiomorpha and Panodonata. The density estimates reflect an even distribution of the species within the Triassic and Permian morphospaces. The replacement of taxa, which implies the loss of some Permian groups and the emergence of new Triassic ones, is not associated with a significant shift in morphospace occupation (position metric). Triassic species such as Panodonata seem, however, to be more concentrated in the middle of the morphospace. For both periods species are widespread all over the morphospace. Griffenflies for the Permian and Zygophlebiida for the Triassic are the one driving the observed change in morphospace occupation, even if there is no significant differences.

4.4.3 Discussion

A morphospace highly constrained by phylogeny and biased by fossil preservation

The species of a given family or of a higher taxa are usually found close to each other in the morphospace. The chosen landmarks reflect the morphological characters already used

to elaborate odonates phylogeny. A match between the phylogeny and the morphospace could be expected.

Only Archizygoptera are extremely widespread, due to the distinct venation patterns expressed among the families, but not to their geological age. We tried to sample each major group present during the Permian and the Triassic (Fig. 4.1). The sampling remains limited, and the addition of a few species with restored wing shapes strongly impacted the margin of the morphospace. As an example, inclusion of *Moltenophlebia* (Zygophlebiida: Triadophlebiomorpha) added an outlier to the Triassic morphospace. The Permian Triadophlebiomorpha are not represented in the analysis and could slightly change our results. However *Kargalotypus kargalensis* does not display the fusion of the intercalary veins with RP2, typical of the Zygophlebiida. Nel et al. (2001) who placed *Kargalotypus kargalensis* into Triadophlebiomorpha consider it might be the sister-group of the Zygophlebiida. Given that the Zygophlebiida represented in our analysis occupy an extreme of the morphospace because of the vein fusion, *Kargalotypus kargalensis* should be found in a more central position, close to the Triadophlebiida and should not drastically change the morphospace occupied during the Permian. *Permophlebia uralica* is another Permian Zygophlebiida described with vein fusion, (Nel et al., 2001) but the specimen is too incomplete to be added to the analysis. A reconstruction of additional specimens would be required for a proper description of the Triadophlebiomorpha disparity.

Triassic species, in our analysis, are represented by 4 retro-deformed and 2 completed wings out of the 14 used. The retro-deformed species fall close to the relatives used as references for the retro-deformation. Such a conservative approach may reduce the shape variations and consequently the disparity metrics. A bigger issue might be the Zygophlebiida, for which the wing shape of one species is reconstructed and another species is retro-deformed. The sensitivity of this reconstruction method still need to be tested in order to evaluate the reliability of the obtained apex of *Moltenophlebia lindae*. Even more, the effects of reconstructions and retro-deformation on morphospace and disparity estimates have to be investigated.

Once this method tested, a lot of fossils could be added to this analysis by completing the missing parts, if complete close relatives are known. A good example might be the Permian Meganisoptera often missing a piece of apex. The ones from Lodève might also be added by re-drawing the collection specimens. Some really complete specimens are not drawn and the photography was not allowing a vector line drawing. Others were drawn but there was no photo available. With further use of the retro-deformation, most of the Triassic complete specimens found in Madygen, about 20, could also be added to the analysis.

The position of Panodonata in the middle of the morphospace is really interesting. Stem-Odonata less closely related to extant species are at the extreme of the morphospace. This could reflect a loss of wing morphologies through Odonata history. The fossil record,

from the Jurassic to the extant species, should be added in such an analysis to investigate the changes in morphospace occupation led by disappearance of these stem-odonates and the emergence of new ones.

Disparity patterns and the putative record of an end-Permian mass extinction in odonates

There is no significant change between the size, density and position metrics of the Permian and the Triassic. However, the morphospcae occupied is slightly different (Fig. 4.7). There seems to be a slight reduction of the size and density metrics and also a slight change in position. In parallel, there is no notable loss of species richness between the Permian and the Triassic, with 72 and 63 species in the fossil record, respectively.

There is a gap in the fossil record, no odonates are known from the Lower Triassic. Therefore, the impact of the EPME on odonates might not be depicted by our data. Considering that insects experienced a drop in diversity during the EPME, as deduced from family- to ordinal-level counts (Nicholson et al., 2015; Ponomarenko, 2016), it can be assumed that odonates may have experienced a drop in species richness during this event. There is no significant drop of disparity monitored, whereas a change in the morphospace occupation is observable. The Triassic species available and used in our analyses could reflect the odonates fauna after a recuperation. A diversification may have occurred for example with the Terskejoptera or the Panodonata species.

Therefore, there is several possible scenarios. The disparity might have stayed constant through the EPME. This scenario would be revealing of a morphologically non-selective extinction which is consistent with what have been found for this event in other groups (Villier and Eble, 2004), and also with the steady or increasing insects mouth parts disparity (Nel et al., 2018; Labandeira, 2019). The size metric would have therefore been constant as the position and the density could have been steady or slightly increasing, depending on the morphological dispersion of the disappearing species (see Fig. 1F). Such disparity trends could also reflect a selection on intermediate morphologies. In this case, range and position are not impacted, but an increase in density should be observed (see Fig. 1G). If different clusters are derived from such a selection, then density of each cluster with little dispersion within the cluster might compensate the wide dispersion between the cluster and density metric would therefore not reveal this change. We decided to estimate disparity with three complementary types of metrics but the recognition of clusters and corresponding interpretation could be a promising avenue.

However, our results tend to show a decrease in disparity and especially a disappearance of extreme morphologies such as the Meganisoptera. Therefore, another scenario that might be more probable is a decrease in disparity during the EPME. The values of disparity we are monitoring might be the ones after a recomposition event and diversification of the surviving groups. A selection on extreme morphologies is therefore plausible.

In this scenario, the size metric would decrease while density and position stay constant (Fig. 1D). This selection could also target a wide specific part of the morphospace (Fig. 1E), and therefore a change in position. It seems plausible given the morphospace occupation (Fig. 4.7), however it is not monitored by our analysis. This last scenario would imply that during the Triassic, new species colonized the morphological areas of the morphospace left empty by the disappearance of other forms. This could be the case of Zygophlebiida colonizing the niches left empty by the Meganisoptera. However these two morphological groups are separated by the second axes of the PCA, explaining about 30% of the morphological variations. Moreover, the disappearance of other groups such as Permagrionidae and Protanisoptera through the EPME could favour the first scenario of selection on extreme morphologies.

These last two scenarios of loss of disparity through the EPME imply a diversification during the Triassic. This diversification would have been coupled with an increase in disparity. This increase in disparity might have occur early in the Triassic, before an increase in taxonomic diversity. Such a scenario would be revealed by a strong increase of size metric then steady or slightly increasing and a strong increase of density metrics then steady or slightly decreasing (Fig. 1B). Disparity and diversity may also have increase more or less concordantly. In that case, density and position would have been constant while size metric increased. However, the time resolution of the odonates fossil record does not allow to favour a scenario over the other.

A last scenario could be that there was no drop of diversity or disparity through the EPME for odonates. In other words, odonates might have not been impacted by the EPME.

A better temporal resolution of odonates fossil record is essential to better understand the impact of the EPME. The different occupation of the morphospace and the disappearance and appearance of extreme morphologies led to think that EPME did have an impact on odonates. The addition of missing taxa is also necessary to ensure a good quantification of disparity for both period. Reconstruction of incomplete fossils as well as retro-deformation would allow addition of many fossil for both periods.

General conclusion

The challenge of comparing Recent and fossil biodiversity

To be able to compare extant and fossil odonates we focused on a structure predominantly found in the fossil record, the wing. However, wing morphology has to be accurately quantified, based on well-ascertained homologies. Notable structures found in extant species such as the nodus or pterostigma are not observed in all fossil species. This wide diversity of wing morphology led us to erect a basic pattern of wing venation homologies applicable to extant and fossil species and best quantifying all odonates wing morphologies. This basic pattern can be applied to all extant and fossil species, not just French and Permo-Triassic ones.

The automated selection of semi-landmarks under R, as well as the reconstruction script and retro-deformation, are applicable to all extant and fossil odonate species and would allow completion of the datasets in a short amount of time. Moreover, these methods can be applied not only to odonates but also to any other insects wings or 2D shapes characterized by curves.

The sliding semi-landmarks method using minimizing BE criterion as shown to be the best suited for our analyses and bear nearly equivalent morphological information for extant species than landmarks set specifically designed for extant species. Therefore an optimal landmarks set have been designed, for fossil and extant species and having the best balance between sliding method and number of sliding semi-landmarks. Disparity quantified for fossil and extant species should therefore be comparable.

To quantify disparity we used several complementary metrics. When analysing Ile-de-France sites disparity, size metric was found to be correlated with diversity but this was not the case of density metrics. The density metrics might be impacted by the low dispersion among the different monitored clusters (Fig. 3.2). In particular, the average nearest neighbour distances might be less impacted by distances between the clusters. That could explain why it shows correlation slightly different than the other two density metrics with diversity. It is revealing of the importance of using several complementary disparity metrics. Also, the recognition of clusters and corresponding interpretation could

be a promising avenue.

Could the effect of landscape artificialization be compared to the effects of the major mass extinction of the Permo-Triassic transition, 250 My ago?

Artificialization of landscape in Ile-de-France is believed to have triggered major depletion of species richness. However, the sampled morphological disparity displays limited variations among sites. Some sites with low diversity even display high values of disparity. This is revealing of the usefulness of disparity to highlight sites with low diversity but high disparity, on which conservation efforts could be made. The highest values of disparity, however, seem to be linked to environments with running water, which could be explained by the extreme position in the morphospace occupied by the Calopterygidae, which are more susceptible to be found close to this type of water bodies.

The situation would keep the same in case of future loss of the threatened species recorded in Ile-de-France. Species loss would not have a significant impact on disparity. This decoupling of the loss of diversity and steady disparity is a pattern often recognized in the fossil record of mass extinctions (Foote, 1993b, 1995, 1997a; Lupia, 1999; Eble, 2000a; Villier and Korn, 2004; Bapst et al., 2012; Halliday and Goswami, 2016). This steady disparity could be explained by two scenarios: either the main driver of extinction is not selective on characters of wing outline and venation (Fig. 1F) or extinction is selective, negatively impacting intermediate morphologies and positively impacting marginal and specialized morphologies (Fig. 1G). Given that threatened species are sparsely distributed in the morphospace (Fig. 3.2) the first scenario of non selective species loss is more plausible.

Although substantial, with thousands of occurrences, the fossil record of odonates remain unevenly distributed in time and space. A major consequence is that description of Permo-Triassic crisis required merging all Permian and all Triassic data for comparisons. Such a coarse temporal resolution precludes the effects of species loss and recovery to be distinguished in the overall species richness. On average, both the species richness and morphological diversity are at a similar level in the Permian and the Triassic. Some extreme morphologies of the Permian morphospace were lost with the demise of Meganisoptera or Permagrionoidea, impacting disparity. New morphologies appeared during the Triassic that compensate for the end-Permian loss. The selectivity of the mass extinction cannot be analysed properly assuming that the Permian would cumulate the effects of conjoint causes of diversity loss, as recorded at that time in other groups of organisms, either marine or terrestrial (Stanley and Yang, 1994; Villier and Korn, 2004; Retallack et al., 2006; Bond et al., 2010; Day et al., 2015).

Our results suggest that the current crisis could be comparable in its effect to the past mass extinction events. However, Ile-de-France is a very limited sample of the whole odonates diversity. Exploration of odonates at a wider scale, such as the entire France country, providing a higher diversity of environmental conditions, may help understanding the significance of regional results, including artificialized sites but also more natural ones. Climatic impact could also be investigated. A study of the evolution of disparity of extant odonates over the last century would also be relevant. Their dispersion could be investigated and disappearance of species sensitive to land-cover artificialization might be monitored.

The approach developed in the thesis should be broadened to compare the impact on odonates of the current crises to the one of historical crises with a better accuracy. They are about 6000 species of odonates monitored worldwide, and investigation of their disparity may help understanding the respective impact of biogeographic pattern and phylogenetic trigger, whether they suffer or not from an anthropogenic impact. A better sampling of the fossil record of the Triassic and Permian species and a refinement of the time scale would clearly improve our understanding of the extinctions properties. The comparison with other mass extinctions would also be relevant. The fossil record of odonates becomes higher in the Mesozoic and more refined analyses would be welcome.

Perspectives

Our results for extant and fossil species suggest that an important variation of wing morphologies could be explained by phylogeny. Therefore, phylogenetic signal should be tested in both analyses and corrected for. This is essential to have a better signal of ecological impact on wing morphology.

To better apprehend the EPME, known species should be added to the analysis, by being reconstructed or retro-deformed. The reconstruction method sensitivity needs therefore to be tested. However, the fossil record is quite incomplete, for example we have no record of the Lower Triassic. They might be an important under-estimation of disparity during intervals with limited fossil record. To answer this issue, we could complete our dataset by modelling missing morphologies. These modellings should be based on phylogenetic relationships, presumed age and morphologies of observed taxa.

On another note, quantification of wing morphology could be refined. The addition of a character matrix could allow inclusion of important discrete morphological characters that are not taken into account with our analyses, such as the nodus and pterostigma. Moreover, it would be relevant to compute an index of uniqueness for each species. This index could be used as a criterion of species selection for conservation plan, reflecting the rarity of its morphology.

The impact of biological crises on odonate wing disparity is not yet resolved. An

analysis comprising all the fossil record from the Carboniferous to the extant species included would allow the study of global evolution of odonates wing disparity. Odonates are widespread and well diversified since the Carboniferous. The fossil record is rich and data on extant species are available. Non-complete fossil wings can be reconstructed, once the method presented here tested, and deformed ones can be retro-deformed. Such a study is therefore achievable and would allow a better understanding of odonates wing shape evolution and help identified which events or pressure led to the observed changes in wing morphologies, in particular by exploring phylogenetic signal.

Bibliography

- Adams, D. C. and Otárola-Castillo, E. (2013). geomorph: an R package for the collection and analysis of geometric morphometric shape data. *Methods in Ecology and Evolution*, 4(4):393–399.
- Adams, D. C., Rohlf, F. J., and Slice, D. E. (2004). Geometric morphometrics: Ten years of progress following the ‘revolution’. *Italian Journal of Zoology*, 71(1):5–16.
- Alroy, J. (2008). Dynamics of origination and extinction in the marine fossil record. *Proceedings of the National Academy of Sciences of the United States of America*, 105(suppl. 1):11536–11542.
- Anderson, J. M. and Anderson, H. M. (1984). The fossil content of the Upper Triassic Molteno Formation, South Africa. *Palaeontologia Africana*, 25:39–59.
- Anderson, J. M., Anderson, H. M., and Cruickshank, A. R. I. (1998). Late Triassic Ecosystems of the Molteno/Lower Elliot Biome of Southern Africa. *Palaeontology*, 41(3):387–421.
- Assandri, G. (2020). Anthropogenic-driven transformations of dragonfly (insecta: Odonata) communities of low elevation mountain wetlands during the last century. *Insect Conservation and Diversity*.
- Banaszak-Cibicka, W., Fliszkievicz, M., Langowska, A., and Żmihorski, M. (2018). Body size and wing asymmetry in bees along an urbanization gradient. *Apidologie*, 49(3):297–306.
- Bapst, D. W., Bullock, P. C., Melchin, M. J., Sheets, H. D., and Mitchell, C. E. (2012). Graptoloid diversity and disparity became decoupled during the Ordovician mass extinction. *Proceedings of the National Academy of Sciences*, 109(9):3428–3433.
- Barour, C. and Baylac, M. (2016). Geometric morphometric discrimination of the three African honeybee subspecies *Apis mellifera intermissa*, *A. m. sahariensis* and *A. m. capensis* (Hymenoptera, Apidae): Fore wing and hind wing landmark configurations. *Journal of Hymenoptera Research*, 52(52):61–70.

- Bechly, G. (1995). Morphologische Untersuchungen am Flügelgeäder der rezenten Libellen und deren Stammgruppenvertreter (Insecta; Pterygota; Odonata) unter besonderer Berücksichtigung der Phylogenetischen Systematik und des Grundplanes der Odonata. *Petalura*, special volume 1:1–341.
- Bechly, G. (1996). Morphologische Untersuchungen am Flügelgeäder der rezenten Libellen und deren Stammgruppenvertreter (Insecta; Pterygota; Odonata) unter besonderer Berücksichtigung der Phylogenetischen Systematik und des Grundplanes der Odonata [revised edition including appendix in English]. *Petalura*, Special Volume 2:1–402.
- Bechly, G. (1997). New fossil odonates from the Upper Triassic of Italy, with a redescription of *Italophlebia gervasuttii*, and a reclassification of Triassic dragonflies (Insecta: Odonata). *Rivista del Museo civico di Scienze Naturali "Enrico Caffi"*, 19:31–70.
- Benton, M. J. and Newell, A. J. (2014). Impacts of global warming on Permo-Triassic terrestrial ecosystems. *Gondwana Research*, 25(4):1308–1337.
- Blagoderov, V., Grimaldi, D. A., and Fraser, N. C. (2007). How time flies for flies: Diverse Diptera from the Triassic of Virginia and early radiation of the order. *American Museum Novitates*, 3572:1–39.
- Blanke, A. (2018). Analysis of modularity and integration suggests evolution of dragonfly wing venation mainly in response to functional demands. *Journal of The Royal Society Interface*, 15:20180277.
- Bode, A. (1953). Die Insektenfauna des Ostniedersächsischen Oberen Lias. *Palaeontographica A*, 103:1–375.
- Bond, D., Wignall, P., Wang, W., Izon, G., Jiang, H.-S., Lai, X.-L., Sun, Y.-D., Newton, R., Shao, L.-Y., Védrine, S., and Cope, H. (2010). The mid-Capitanian (Middle Permian) mass extinction and carbon isotope record of South China. *Palaeogeography, Palaeoclimatology, Palaeoecology*, 292(1):282–294.
- Bookstein, F. (1989). Principal warps: thin-plate splines and the decomposition of deformations. *IEEE Transactions on Pattern Analysis and Machine Intelligence*, 11(6):567–585.
- Bookstein, F. L. (1991). *Morphometric Tools for Landmark Data: Geometry and Biology*. Cambridge University Press.
- Boudot, J.-P., Grand, D., Wildermuth, H., and Monnerat, C. (2017). *Les libellules de France, Belgique, Luxembourg & Suisse*. Biotope, Mèze (Collection Parthénope), 2nd edition.

- Briggs, D., Fortey, R., and Wills, M. (1992). Morphological disparity in the Cambrian. *Science*, 256:1670–1673.
- Brongniart, C. (1893). Recherches pour servir à l’histoire des insectes fossiles des temps primaires précédées d’une étude sur la nervation des ailes des insectes. *Bulletin de la Société d’Industrie Minérale de Saint-Etienne* (3), 7:124–615.
- Béthoux, O. (2015). The Late Carboniferous *Triplosoba pulchella* is not a fly in the ointment but a stem-mayfly. *Systematic Entomology*, 40(2):342–356.
- Béthoux, O. and Beattie, R. (2010). *Iverya averyi* gen. nov. & sp. nov., a new triadotypomorph species from the Middle Triassic at Picton, New South Wales, Australia. *Acta Geologica Sinica*, 84(4):688–692.
- Béthoux, O., Horra, R. d. l., Benito, M. I., Barrenechea, J. F., Galán, A. B., and López-Gómez, J. (2009). A new triadotypomorph insect from the Anisian (Middle Triassic), Buntsandstein facies, Spain. *Journal of Iberian Geology*, 35(2):179–184.
- Béthoux, O., Llamosi, A., and Toussaint, S. (2016). Reinvestigation of *Protelytron permianum* (Insecta; Early Permian; USA) as an example for applying reflectance transformation imaging to insect imprint fossils. *Fossil Record*, 20:1–7.
- Béthoux, O., Papier, F., and Nel, A. (2005). The Triassic radiation of the entomofauna. *Comptes Rendus Palevol*, 4(6):609–621.
- Cardoso, P., Barton, P. S., Birkhofer, K., Chichorro, F., Deacon, C., Fartmann, T., Fukushima, C. S., Gaigher, R., Habel, J. C., Hallmann, C. A., Hill, M. J., Hochkirch, A., Kwak, M. L., Mammola, S., Ari Noriega, J., Orfinger, A. B., Pedraza, F., Pryke, J. S., Roque, F. O., Settele, J., Simaika, J. P., Stork, N. E., Suhling, F., Vorster, C., and Samways, M. J. (2020). Scientists’ warning to humanity on insect extinctions. *Biological Conservation*, 242(108426):1–12.
- Carpenter, F. M. (1931). The Lower Permian insects of Kansas. Part 2. The orders Palaeodictyoptera, Protodonata, and Odonata. *American Journal of Science* (5), 21(5):97–139.
- Carpenter, F. M. (1939). The Lower Permian insects of Kansas. Part 8. Additional Megasecoptera, Protodonata, Odonata, Homoptera, Psocoptera, Protelytroptera, Plecoptera, and Protoperlaria. *Proceedings of the American Academy of Arts and Sciences*, 73(3):29–70.
- Carpenter, F. M. (1947). Lower Permian insects from Oklahoma. Part 1. Introduction and the orders Megasecoptera, Protodonata, and Odonata. *Proceedings of the American Academy of Arts and Sciences*, 76(2):25–54.

- Carpenter, F. M. (1992). Superclass Hexapoda. In Kaesler, R. L., editor, *Treatise on Invertebrate Paleontology*, volume 4, pages xxii+655. The Geological Society of America and the University of Kansas.
- Ciampaglio, C. N. (2004). Measuring changes in articulate brachiopod morphology before and after the Permian mass extinction event: do developmental constraints limit morphological innovation? *Evolution and Development*, 6(4):260–274.
- Ciampaglio, C. N., Kemp, M., and McShea, D. W. (2001). Detecting changes in morphospace occupation patterns in the fossil record: characterization and analysis of measures of disparity. *Paleobiology*, 27(4):695–715.
- Clavel, J., Julliard, R., and Devictor, V. (2011). Worldwide decline of specialist species: toward a global functional homogenization? *Frontiers in Ecology and the Environment*, 9(4):222–228.
- Day, M. O., Ramezani, J., Bowring, S. A., Sadler, P. M., Erwin, D. H., Abdala, F., and Rubidge, B. S. (2015). When and how did the terrestrial mid-Permian mass extinction occur? Evidence from the tetrapod record of the Karoo Basin, South Africa. *Proceedings of the Royal Society B: Biological Sciences*, 282(1811):20150834.
- Deregnacourt, I., Wappler, T., Anderson, J. M., and Béthoux, O. (2017). A new triadotypid insect from the Late Triassic of South Africa. *Acta Palaeontologica Polonica*, 62(3):613–618.
- Deregnacourt, I., Wappler, T., Anderson, J. M., and Béthoux, O. (2019a). The wing venation of the Protomyrmeleontidae (Insecta: Odonatoptera) reconsidered thanks to a new specimen from Molteno (Triassic; South Africa). *Historical Biology*.
- Deregnacourt, I., Wappler, T., Anderson, J. M., and Béthoux, O. (2019b). Data from: The wing venation of the Protomyrmeleontidae (Insecta: Odonatoptera) reconsidered thanks to a new specimen from Molteno (Triassic; South Africa). Dryad Digital Repository, doi:10.5061/dryad.jh3m624.
- Dijkstra, K.-D. B. (2015). *Guide des libellules de France et d'Europe*. Delachaux & Niestlé, 3rd edition.
- Dijkstra, K.-D. B., Bechly, G., Bybee, S. M., Dow, R. A., Dumont, H. J., Fleck, G., Garrison, R. W., Hämäläinen, M., Kalkman, V. J., Karube, H., May, M. L., Orr, A. G., Paulson, D. R., Rehn, A. C., Theischinger, G., Trueman, J. W. H., van Tol, J., von Ellenrieder, N., and Ware, J. (2013). The classification and diversity of dragonflies and damselflies (Odonata). *Zootaxa*, 3703(1):36–45.

- Dommanget, J.-L. (1999). La conservation des couleurs et la préparation des libellules destinées à la collection de référence. *Insectes*, 114(3):25–28.
- Dutra, S. and De Marco, P. (2015). Bionomic differences in odonates and their influence on the efficiency of indicator species of environmental quality. *Ecological Indicators*, 49:132–142.
- Eble, G. J. (2000a). Contrasting evolutionary flexibility in sister groups: Disparity and diversity in Mesozoic atelostomate echinoids. *Paleobiology*, 26(1):56–79.
- Eble, G. J. (2000b). Theoretical morphology: State of the art. *Paleobiology*, 26(3):520–528.
- Erwin, D. H. (2007). Disparity: morphological pattern and developmental context. *Palaeontology*, 50(1):57–73.
- Fabricius, J. C. (1793). *Entomologia systematica emendata et aucta. Secundum classes, ordines, genera, species adjectis synonymis, locis, observationibus, descriptionibus. Tome 2*. Proft, C. G., Copenhagen.
- Foote, M. (1992). Rarefaction analysis of morphological and taxonomic diversity. *Paleobiology*, 18(1):1–16.
- Foote, M. (1993a). Contribution of individual taxa to overall morphological disparity. *Paleobiology*, 19:403–419.
- Foote, M. (1993b). Discordance and concordance between morphological and taxonomic diversity. *Paleobiology*, 19(2):185–204.
- Foote, M. (1995). Morphological diversification of paleozoic crinoids. *Paleobiology*, pages 273–299.
- Foote, M. (1997a). The evolution of morphological diversity. *Annual Review of Ecology and Systematics*, 28:129–152.
- Foote, M. (1997b). Sampling, taxonomic description, and our evolving knowledge of morphological diversity. *Paleobiology*, 23(2):181–206.
- Foote, M. (2001). Inferring temporal patterns of preservation, origination, and extinction from taxonomic survivorship analysis. *Paleobiology*, 27(4):602–630.
- Garrison, R. W., von Ellenrieder, N., and Louton, J. A. (2010). *Damselfly genera of the New World*. John Hopkins University Press.
- Geinitz, F. (1887). Neue Aufschlüsse der Flözformation Mecklenburgs. IX. Beiträg zur Geologie Mecklenburgs. IV. Jura. *Archiv des Vereins der Freunde Naturgeschichte Mecklenburg*, 41:194–208.

- Gerber, S. (2019). Use and misuse of discrete character data for morphospace and disparity analyses. *Palaeontology*, 62(2):305–319.
- Goertzen, D. and Suhling, F. (2013). Promoting dragonfly diversity in cities: major determinants and implications for urban pond design. *Journal of Insect Conservation*, 17(2):399–409.
- Goertzen, D. and Suhling, F. (2019). Urbanization versus other land use: Diverging effects on dragonfly communities in Germany. *Diversity and Distributions*, 25(1):38–47.
- Gould, S. J. (1989). *Wonderful life: the Burgess Shale and the nature of history*. Norton.
- Grand, D., Boudot, J.-P., and Doucet, G. (2014). *Cahier d'identification des Libellules de France, Belgique, Luxembourg & Suisse*. Biotope, Mèze.
- Grimaldi, D. and Engel, M. S. (2005). *Evolution of the Insects*. Cambridge University Press, New York.
- Guillerme, T. (2018). dispRity: A modular R package for measuring disparity. *Methods in Ecology and Evolution*, 9(7):1755–1763.
- Guillerme, T., Puttick, M. N., Marcy, A. E., and Weisbecker, V. (2020). Shifting spaces: Which disparity or dissimilarity measurement best summarize occupancy in multidimensional spaces? *Ecology and Evolution*, 10(14):7261–7275.
- Gunz, P. and Mitteroecker, P. (2013). Semilandmarks: a method for quantifying curves and surfaces. *Hystrix, the Italian Journal of Mammalogy*, 24(1):103–109.
- Gunz, P., Mitteroecker, P., Neubauer, S., Weber, G. W., and Bookstein, F. L. (2009). Principles for the virtual reconstruction of hominin crania. *Journal of Human Evolution*, 57(1):48–62.
- Halliday, T. J. D. and Goswami, A. (2016). Eutherian morphological disparity across the end-Cretaceous mass extinction. *Biological Journal of the Linnean Society*, 118(1):152–168.
- Handlirsch, A. (1906). *Die fossilen Insekten und die Phylogenie der rezenten Formen. Ein Handbuch für Paläontologen und Zoologen*. Wilhelm Engelmann, Berlin.
- Henrotay, M., Nel, A., and Jarzembowski, E. A. (1997). New Protomyrmeleontidae damselflies from the Triassic of Australia and the Liassic of Luxembourg. *Odonatologica*, 26(4):395–404.
- Hoffmann, J., Donoughe, S., Li, K., Salcedo, M. K., and Rycroft, C. H. (2018). A simple developmental model recapitulates complex insect wing venation patterns. *Proceedings of the National Academy of Sciences*, 115(40):9905–9910.

- Hopkins, M. and Gerber, S. (2017). Morphological disparity. In Nuño de la Rosa, L. and Müller, G., editors, *Evolutionary Developmental Biology*, pages 1–12. Springer International Publishing.
- Houard, X. and Merlet, F. (2014). *Liste rouge régionale des libellules d’Île-de-France*. Natureparif, Office pour les insectes et leur environnement, Société française d’Odonatologie, Paris.
- Jacquelin, L., Desutter-Grandcolas, L., Chintauan-Marquier, I., Boistel, R., Zheng, D., Prokop, J., and Nel, A. (2018). New insights on basiventral sclerites using 3D tools and homology of wing veins in Odonatoptera (Insecta). *Scientific Reports*, 8(1):238.
- Jeanmougin, M., Leprieur, F., Lois, G., and Clergeau, P. (2014). Fine-scale urbanization affects Odonata species diversity in ponds of a megacity (Paris, France). *Acta Oecologica*, 59:26–34.
- Korkmaz, S., Goksuluk, D., and Zararsiz, G. (2014). Mvn: An r package for assessing multivariate normality. *The R Journal*, 6(2):151–162.
- Kukalová-Peck, J. (1991). Fossil History and the Evolution of Hexapod Structures. In Naumann, I. D., Crane, P. B., Lawrence, J. F., Nielsen, E. S., Spradbery, J. P., Taylor, R. W., Whitten, M. J., and Littlejohn, M. J., editors, *The Insects of Australia, a textbook for students and researchers*, volume 1, pages 141–179. Melbourne University Press, Melbourne, 2nd edition.
- Labandeira, C. C. (2019). The fossil record of insect mouthparts: Innovation, functional convergence, and associations with other organisms. In Krenn, H. W., editor, *Insect Mouthparts: Form, Function, Development and Performance*, pages 567–671. Springer International Publishing, Cham.
- Labandeira, C. C., Eble, G. J., et al. (2000). The fossil record of insect diversity and disparity. In Anderson, J., Thackeray, F., Van Wyk, B., and De Wit, M., editors, *Gondwana alive: biodiversity and the evolving biosphere*, page 54 pp. Witwatersrand University Press.
- Lameere, A. (1922). Sur la nervation alaire des insectes. *Bulletin de la Classe des Sciences de l’Académie Royale de Belgique*, 8:138–149.
- Lameere, A. (1923). On the wing-venation of insects. *Psyche*, 30:123–132.
- Laurentiaux-Vieira, F., Ricour, J., and Laurentiaux, D. (1952). Un Protodonate du Trias de la Dent de Villard. *Bulletin de la Société Géologique de France*, (6), 1:319–324.

- Li, Y., Béthoux, O., Pang, H., and Ren, D. (2013). Early Pennsylvanian Odonatoptera from the Xiaheyuan locality (Ningxia, China): new material, taxa, and perspectives. *Fossil Record*, 16(1, 2):117–139, 244.
- Ludbrook, J. and Dudley, H. (1998). Why permutation tests are superior to t and f tests in biomedical research. *The American Statistician*, 52(2):127–132.
- Lupia, R. (1999). Discordant morphological disparity and taxonomic diversity during the Cretaceous angiosperm radiation: North American pollen record. *Paleobiology*, 25(1):1–28.
- MacDougall, M. J., Brocklehurst, N., and Fröbisch, J. (2019). Species richness and disparity of parareptiles across the end-permian mass extinction. *Proceedings of the Royal Society B*, 286(1899):20182572.
- MacLeod, N. (2011). Palaeomath 101: Semilandmarks and radial fourier analysis. *Palaeontology Newsletter*, 76:25–42.
- Martínez-Delclós, X. and Nel, A. (1996). Discovery of a new Protomyrmeleontidae in the Upper Jurassic from Germany (Odonatoptera, Odonata, Archizygoptera). *Archaeopteryx*, 14:67–73.
- Martynov, A. V. (1927). Jurassic fossil insects from Turkestan. 7. Some Odonata, Neuroptera, Thysanoptera. *Bulletin de l'Académie des Sciences de l'URSS. VI série*, 21(5):757–768.
- McClain, C. R., Johnson, N. A., and Rex, M. A. (2004). Morphological disparity as a biodiversity metric in lower bathyal and abyssal gastropod assemblages. *Evolution*, 58(2):338–348.
- McGhee, G. R. (1999). *Theoretical morphology: the concept and its applications*. Columbia University Press.
- Murrell, P. (2009). Importing vector graphics: The grImport package for R. *Journal of Statistical Software*, 30(4):1–37.
- Myers, N. and Knoll, A. H. (2001). The biotic crisis and the future of evolution. *Proceedings of the National Academy of Sciences of the United States of America*, 98(10):5389–5392.
- Needham, J. G. (1903). A genealogical study of dragonfly wing venation. *Proceedings of the United States National Museum*, 26:703–764 + pls 31–54.
- Neige, P. (2003). Spatial patterns of disparity and diversity of the Recent cuttlefishes (Cephalopoda) across the Old World. *Journal of Biogeography*, 30(8):1125–1137.

- Nel, A., Bechly, G., Prokop, J., Béthoux, O., and Fleck, G. (2012). Systematics and evolution of Palaeozoic and Mesozoic damselfly-like Odonatoptera of the 'Protozygopteran' grade. *Journal of Paleontology*, 86(1):81–104.
- Nel, A., Béthoux, O., Bechly, G., Martínez-Delclòs, X., and Papier, F. (2001). The Permo-Triassic Odonatoptera of the "protodonate" grade (Insecta: Odonatoptera). *Annales de la Société Entomologique de France (N.S.)*, 37(4):501–525.
- Nel, A., Fleck, G., Garrouste, R., Gand, G., Lapeyrie, J., Bybee, S. M., and Prokop, J. (2009). Revision of Permo-Carboniferous griffenflies (Insecta: Odonatoptera: Meganisoptera) based upon new species and redescription of selected poorly known taxa from Eurasia. *Palaeontographica Abteilung A*, 289(4–6):89–121.
- Nel, A., Gand, G., Fleck, G., Béthoux, O., Lapeyrie, J., and Garric, J. (1999a). *Saxonagrion minutus* nov. gen. et sp., the oldest damselfly from the upper permian of france (odonatoptera, panodonata, saxonagrionidae nov. fam.). *Geobios*, 32(6):883–888.
- Nel, A., Gand, G., and Garric, J. (1999b). A new family of odonatoptera from the continental upper permian: the lapeyriidae (lodève basin, france). *Geobios*, 32(1):63–72.
- Nel, A., Gand, G., Garric, J., and Lapeyrie, J. (1999c). The first recorded protozygopteran insects from the upper permian of france. *Palaeontology*, 42(1):83–97.
- Nel, A., Garrouste, R., and Schubnel, T. (2019). Response to Trueman and Rowe (2019) 'The wing venation of Odonata. International Journal of Odonatology'. *International Journal of Odonatology*, 22(2):115–119.
- Nel, A. and Henrotay, M. (1992). Les Protomyrmeleontidae (Odonatoptera: Odonata, Archizygoptera stat. rest.): état actuel des connaissances. *Annales de Paléontologie*, 78(1):1–47.
- Nel, A. and Jarzembowski, E. A. (1998). New protomyrmeleontid dragonflies from the Lower Cretaceous of southern England (Insecta, Odonata, Archizygoptera). *Cretaceous Research*, 19:393–402.
- Nel, A., Papier, F., Stamm-Grauvogel, L., and Gall, J.-C. (1996). *Voltzialestes triasicus*, gen. nov., sp. nov., le premier Odonata Protozygoptera du Trias inférieur des Vosges (France). *Paleontologia Lombarda, (N.S.)*, 5:25–36.
- Nel, A., Petrulevičius, J. F., and Martínez-Delclòs, X. (2005). New Mesozoic Protomyrmeleontidae (Insecta: Odonatoptera: Archizygoptera) from Asia with a new phylogenetic analysis. *Journal of Systematic Palaeontology*, 3(2):1–15.

- Nel, A., Rocques, P., Nel, P., Prokop, J., and Steyer, J. S. (2007). The earliest holometabolous insect from the carboniferous: a "crucial" innovation with delayed success (insecta protomeropina protomeropidae). *Annales de la Société Entomologique de France (N.S.)*, 43(3):349–355.
- Nel, P., Bertrand, S., and Nel, A. (2018). Diversification of insects since the devonian: a new approach based on morphological disparity of mouthparts. *Scientific Reports*, 8(3516):1–10.
- Neustupa, J., Černá, K., and Štátný, J. (2009). Diversity and morphological disparity of desmid assemblages in Central European peatlands. *Hydrobiologia*, 630:243–256.
- Nicholson, D. B., Mayhew, P. J., and Ross, A. J. (2015). Changes to the Fossil Record of Insects through Fifteen Years of Discovery. *PLOS ONE*, 10(7):1–61.
- Nordhausen, K., Sirkia, S., Oja, H., and Tyler, D. (2018). Icsnp: Tools for multivariate nonparametrics, version 1.1-1. *R package*. [Available online at <http://CRAN.R-project.org/web/packages/ICSNP/>].
- Ogihara, N., Amano, H., Kikuchi, T., Morita, Y., Hasegawa, K., Kochiyama, T., and Tanabe, H. C. (2015). Towards digital reconstruction of fossil crania and brain morphology. *Anthropological Science*, 123(1):57–68.
- Oksanen, J., Blanchet, F. G., Friendly, M., Kindt, R., Legendre, P., McGlinn, D., Minchin, P. R., O'hara, R., Simpson, G. L., Solymos, P., et al. (2016). *vegan: Community ecology package*. r package version 2.4-3. *Vienna: R Foundation for Statistical Computing*.
- Outomuro, D., Bokma, F., and Johansson, F. (2012). Hind wing shape evolves faster than front wing shape in calopteryx damselflies. *Evolutionary Biology*, 39(1):116–125.
- Outomuro, D., Dijkstra, K.-D. B., and Johansson, F. (2013). Habitat variation and wing coloration affect wing shape evolution in dragonflies. *Journal of Evolutionary Biology*, 26(9):1866–1874.
- Outomuro, D., Söderquist, L., Nilsson-Örtman, V., Cortázar-Chinarro, M., Lundgren, C., and Johansson, F. (2016). Antagonistic natural and sexual selection on wing shape in a scrambling damselfly. *Evolution*, 70(7):1582–1595.
- Paleobiology Database (2019). The Paleobiology Database (www.paleobiodb.org) accessed on 22.11.2019.
- Perez, S. I., Bernal, V., and Gonzalez, P. N. (2006). Differences between sliding semi-landmark methods in geometric morphometrics, with an application to human craniofacial and dental variation. *Journal of anatomy*, 208(6):769–784.

- Perrard, A., Villemant, C., Carpenter, J. M., and Baylac, M. (2012). Differences in caste dimorphism among three hornet species (Hymenoptera: Vespidae): forewing size, shape and allometry. *Journal of Evolutionary Biology*, 25(7):1389–1398.
- Petrulevičius, J. F. and Gutiérrez, P. R. (2016). New basal Odonatoptera (Insecta) from the lower Carboniferous (Serpukhovian) of Argentina. *Archivos Entomológicos*, 16:341–358.
- Ponomarenko, A. G. (2016). Insects during the time around the Permian—Triassic crisis. *Paleontological Journal*, 50(2):174–186.
- Pritykina, L. N. (1981). Novye triasovye strekozy srednej azii. In Vishniakova, V. N., Dlussky, G. M., and Pritykina, L. N., editors, *Novye iskopaemye nasekomye s Terrotorii SSSR*, pages 5–42. Trudy Paleontologicheskogo instituta, Akademiya Nauk SSSR, 183.
- Prokop, J., Szwed, J., Lapeyrie, J., Garrouste, R., and Nel, A. (2015). New Middle Permian insects from Salagou Formation of the Lodève Basin in southern France (Insecta: Pterygota). *Annales de la Société entomologique de France (N.S.)*, 51(1):14–51.
- R Core Team (2018). *R: A Language and Environment for Statistical Computing*. R Foundation for Statistical Computing, Vienna, Austria.
- Redtenbacher, J. (1886). Vergleichende studien über das flügelgeäder der insekten. *Annalen des Kaiserlich-Königlichen Naturhistorischen Hofmuseums*, 1:153–232 + pl. 9–20.
- Reis, O. M. (1909). *Handlirschia gelasii* nov. gen. et spec. aus dem Schaumkalk Frankens. *Abhandlungen der Koeniglich Bayerischen Akademie der Wissenschaftern, Mathematisch-Physikalischen Klasse*, 23:659–694.
- Retallack, G. J., Metzger, C. A., Greaver, T., Jahren, A. H., Smith, R. M., and Sheldon, N. D. (2006). Middle-late permian mass extinction on land. *Geological Society of America Bulletin*, 118(11):1398–1411.
- Riek, E. F. and Kukalová-Peck, J. (1984). A new interpretation of dragonfly wing venation based upon Early Upper Carboniferous fossils from Argentina (Insecta, Odonatoidea) and basic character states in pterygota wings. *Canadian Journal of Zoology*, 62(6):1150–1166.
- Rocha-Ortega, M., Rodríguez, P., Bried, J., Abbott, J., and Córdoba-Aguilar, A. (2020). Why do bugs perish? Range size and local vulnerability traits as surrogates of Odonata extinction risk. *Proceedings of the Royal Society B: Biological Sciences*, 287(1924):20192645.

- Rocha-Ortega, M., Rodríguez, P., and Córdoba-Aguilar, A. (2019). Can dragonfly and damselfly communities be used as bioindicators of land use intensification? *Ecological Indicators*, 107:105553.
- Rohdendorf, B. (1962). Podklass pterygota, krilatye nasekomye [subclass pterygota, winged insects]. In Rohdendorf, B., editor, *Osnovy Paleontologii [Fundamentals of Palaeontology]*. Izdatel'stvo Akademii Nauk SSSR, Moscow.
- Rohlf, F. J. and Corti, M. (2000). Use of Two-Block Partial Least-Squares to study covariation in shape. *Systematic Biology*, 49(4):740–753.
- Rohlf, F. J. and Slice, D. (1990). Extensions of the Procrustes method for the optimal superimposition of landmarks. *Systematic Biology*, 39(1):40–59.
- Romano, M., Brocklehurst, N., and Fröbisch, J. (2017). Discrete and continuous character-based disparity analyses converge to the same macroevolutionary signal: a case study from captorhinids. *Scientific Reports*, 7(17531):1–9.
- Roy, K., Balch, D. P., and Helberg, M. E. (2001). Spatial patterns of morphological diversity across the Indo-Pacific: analyses using strombid gastropods. *Proceedings of the Royal Society B, Biological Sciences*, 268(1485):2503–2508.
- Ruta, M., Angielczyk, K. D., Fröbisch, J., and Benton, M. J. (2013). Decoupling of morphological disparity and taxic diversity during the adaptive radiation of anomodont therapsids. *Proceedings of the Royal Society B: Biological Sciences*, 280(1768):20131071.
- Sala, O. E., Chapin, F. S., Armesto, J. J., Berlow, E., Bloomfield, J., Dirzo, R., Huber-Sanwald, E., Huenneke, L. F., Jackson, R. B., Kinzig, A., Leemans, R., Lodge, D. M., Mooney, H. A., Oesterheld, M., Poff, N. L., Sykes, M. T., Walker, B. H., Walker, M., and Wall, D. H. (2000). Global biodiversity scenarios for the year 2100. *Science*, 287(5459):1770–1774.
- Schlager, S. (2017). Morpho and Rvcg – Shape analysis in R. In Zheng, G., Li, S., and Székely, G., editors, *Statistical Shape and Deformation Analysis*, pages 217–256. Elsevier.
- Sellards, E. H. (1906). Types of Permian insects. Part 1: Odonata. *American Journal of Science (4)*, 22(4):249–258.
- Sharov, A. G. (1968). Filogeniya orthopteroidnykh nasekomykh. *Trudy Paleontologicheskogo instituta, Akademiya Nauk SSSR*, 118:1–216.
- Sharov, A. G. (1971). *Phylogeny of the Orthopteroidea*. Israel Program for Scientific Translations, Jerusalem.

- Shcherbakov, D. E. (2008). Insect recovery after the Permian/Triassic crisis. *Alavesia*, 2:125–131.
- Stanley, S. M. and Yang, X. (1994). A double mass extinction at the end of the Paleozoic era. *Science*, 266(5189):1340–1344.
- Stockmeyer-Lofgren, A., Plotnick, R. E., and Wagner, P. J. (2003). Morphological diversity of Carboniferous arthropods and insights on disparity patterns through the Phanerozoic. *Paleobiology*, 29(3):349–368.
- Tasch, P. and Zimmerman, J. R. (1962). The *asthenohymen-delopterum* bed: A new Leonardian insect horizon in the Wellington of Kansas and Oklahoma. *Journal of Paleontology*, 36(6):1319–1333.
- Tierney, A., Deregnaucourt, I., Anderson, J. M., Tierney, P., Wappler, T., and Béthoux, O. (2020). The Triassic Mesophlebiidae, a little closer to the crown of the Odonata (Insecta) than other ‘triassolestids’. *Alcheringa: An Australasian Journal of Palaeontology*, 44(2):279–285.
- Tillyard, R. J. (1922). Mesozoic insects of Queensland. No. 9. Orthoptera, and additions to the Protorthoptera, Odonata, Hemiptera and Plannipennia. *Proceedings of the Linnean Society of New South Wales*, 47:447–470.
- Tillyard, R. J. (1925). Kansas Permian insects. Part 5. The order Protodonata and Odonata. *American Journal of Science (5)*, 10:41–73.
- Tillyard, R. J. and Dunstan, B. (1916). Mesozoic and tertiary insects of queensland and new south wales. descriptions of the fossil insects. *Queensland Geological survey*, 253:11–64.
- Tillyard, R. J. and Fraser, F. C. (1938). A reclassification of the order Odonata based on some new interpretations of the venation of the dragonfly wing. *The Australian Zoologist*, 9:125–169.
- Trueman, J. W. H. and Rowe, R. J. (2019a). The wing venation of Odonata. *International Journal of Odonatology*, 22(1).
- Trueman, J. W. H. and Rowe, R. J. (2019b). Reply to Nel, Garrouste, and Schubnel (2019) “The wing venation of Odonata. International Journal of Odonatology”. *International Journal of Odonatology*, 22(3-4):167–172.
- Valente-Neto, F., de Oliveira Roque, F., Rodrigues, M. E., Juen, L., and Swan, C. M. (2016). Toward a practical use of neotropical odonates as bioindicators: Testing congruence across taxonomic resolution and life stages. *Ecological Indicators*, 61:952–959.

- van Strien, A. J., Termaat, T., Kalkman, V., Prins, M., De Knijf, G., Gourmand, A.-L., Houard, X., Nelson, B., Plate, C., Prentice, S., Regan, E., Smallshire, D., Vanapelghem, C., and Vanreusel, W. (2013). Occupancy modelling as a new approach to assess supranational trends using opportunistic data: a pilot study for the damselfly *Calopteryx splendens*. *Biodiversity and Conservation*, 22(2):673–686.
- Villalobos-Jimenez, G., Dunn, A. M., and Hassall, C. (2016). Dragonflies and damselflies (Odonata) in urban ecosystems: A review. *European Journal of Entomology*, 113:217–232.
- Villier, L. and Eble, G. J. (2004). Assessing the robustness of disparity estimates: the impact of morphometric scheme, temporal scale, and taxonomic level in spatangoid echinoids. *Paleobiology*, 30(4):652–665.
- Villier, L. and Korn, D. (2004). Morphological disparity of ammonoids and the mark of Permian mass extinctions. *Science*, 306(5694):264–266.
- Voigt, S., Haubold, H., Meng, S., Krause, D., Buchantschenko, J., Ruckwied, K., and Götz, A. E. (2006). Die Fossil-Lagerstätte Madygen: ein Beitrag zur Geologie und Paläontologie der Madygen-Formation (Mittel- bis Ober-Trias, SW-Kirgisistan, Zentralasien). *Hallesches Jahrbuch für Geowissenschaften*, 22:85–119.
- Wills, M. A. (1998). Cambrian and recent disparity: The picture from priapulids. *Paleobiology*, 24(2):177–199.
- Wills, M. A., Briggs, D. E. G., and Fortey, R. A. (1994). Disparity as an evolutionary index: A comparison of Cambrian and Recent arthropods. *Paleobiology*, 20(2):93–130.
- Wootton, R. J. and Kukalová-Peck, J. (2000). Flight adaptations in Palaeozoic Palaeoptera. *Biological Review*, 75:129–167.
- Zessin, W. (1991). Die Phylogenie der Protomyrmeleontidae unter einbeziehung neuer oberliassischer Funde (Odonata: Archizygoptera sens. nov.). *Odonatologica*, 20(1):97–125.
- Zheng, D. R., Nel, A., Wang, B., Jarzembowski, E. A., Chang, S.-C., and Zhang, H. C. (2017a). The first Triassic ‘Protodonatan’ (Zygophlebiidae) from China: stratigraphical implications. *Geological Magazine*, 154(1):169–174.
- Zheng, G., Li, S., and Székely, G. (2017b). *Statistical shape and deformation analysis: methods, implementation and applications*. Elsevier.

Annex A.1

Tierney, A., Deregnaucourt, I., Anderson, J. M., Tierney, P., Wappler, T., and Béthoux, O. (2020). The Triassic Mesophlebiidae, a little closer to the crown of the Odonata (Insecta) than other ‘triassolestids’. *Alcheringa: An Australasian Journal of Palaeontology*, 44(2) :279–285.

The Triassic *Mesophlebiidae*, a little closer to the crown of the Odonata (Insecta) than other 'triassoletids'

Ayla Tierney, Isabelle Deregnacourt, John M. Anderson, Paul Tierney, Torsten Wappler, and Olivier Béthoux

ABSTRACT

Two new, subcomplete forewings belonging to the 'triassoletid assemblage', a group of Triassic stem-relatives of dragon- and damselflies (Odonata), are described. One, recovered from Australia (Aranbanga Volcanic Group), belongs to *Mesophlebia antinodalis* Tillyard, 1916, previously documented on the basis of two very incomplete wings. The other, recovered from South Africa (Molteno Formation), is assigned to a new species, *Mesophlebia elegans* sp. nov. The new data allow a reconsideration of the diagnosis of the genus *Mesophlebia* Tillyard, 1916 and a re-instatement of the family *Mesophlebiidae* Tillyard, 1916. Notably, the new specimens possess, near the wing base, a posterior lobe absent in most 'triassoletid' genera, but present in crown-Odonata and a number of their stem-relatives. *Lobodonata* tax. nov. is erected to accommodate odonates possessing this lobe. The nature of the 'vein-like' element anteriorly delimiting this lobe is discussed. We submit that it might have been initially composed of an invagination of the posterior wing-margin ('fibula'), which was later captured by AA, imposing its course on CuP.

ARTICLE HISTORY

Received 5 September 2019
Revised 28 January 2020
Accepted 13 February 2020

KEYWORDS

Stem-Odonata; Aranbanga volcanic group; Molteno Formation; Australia; South Africa

Ayla Tierney [ayla.tierney@qm.qld.gov.au], Queensland Museum, PO Box 3300, South Brisbane BC, Queensland 4101, Australia; Isabelle Deregnacourt [isabelle.deregnacourt@edu.mnhn.fr], Sorbonne Université, MNHN, CNRS, Centre de recherche sur la paléontologie – Paris (CR2P), 57 rue Cuvier, CP38, F-75005 Paris, France; John M. Anderson [jmanderson.gondwana@gmail.com], Evolutionary Studies Institute, Witwatersrand University, 1 Jan Smuts Ave., Braamfontein, Johannesburg 2000, South Africa; Paul Tierney [paul.tierney@qm.qld.gov.au], Queensland Museum, PO Box 3300, South Brisbane BC, Queensland 4101, Australia; Torsten Wappler [torsten.wappler@hmd.de], Hessisches Landesmuseum Darmstadt, Friedensplatz 1, 64283 Darmstadt, Germany; Olivier Béthoux [obethoux@mnhn.fr], Sorbonne Université, MNHN, CNRS, Centre de recherche sur la paléontologie – Paris (CR2P), 57 rue Cuvier, CP38, F-75005 Paris, France.

DURING the Triassic, dragon- and damselflies (i.e., Odonata) were represented by stem-groups exhibiting a wide range of wing morphologies, indicating, at least in part, their distant phylogenetic relationships (Tillyard 1925, Pritykina 1981, Bechly 1996, 1997, Nel *et al.* 2001, 2002, Deregnacourt *et al.* 2017, *in press*; among others). Among these stem-odonatans, the 'triassoletid assemblage' most likely includes the stem-groups that are the closest relatives of crown-Odonata at the time. However, this assemblage is documented based only on a few species, most often known from fragmentary wing remains.

Herein the Australian species *Mesophlebia antinodalis* Tillyard, 1916 is redescribed on the basis of a new, subcomplete forewing. A new, closely related, South African species is also described on the basis of another subcomplete forewing. The new data allow a reconsideration of the diagnosis of the genus *Mesophlebia* Tillyard, 1916, and of the status and position of the *Mesophlebiidae* Tillyard, 1916 with respect to other 'triassoletids'.

Material and methods

The Australian specimen investigated herein is housed at the Queensland Museum (Geosciences Collection, Hendra). It bears the specimen number QMF 58847 (positive imprint; Fig. 1A, B). It was collected from a new locality provisionally

numbered 'QLM 1307' near the town of Wondai, in the Burnett region of southeastern Queensland. The wing was preserved in a tuff together with plants (*Dicroidium* spp. and Calamitales) and spinicaudatans. As for its stratigraphic position, a minimum age constraint of 226.5 ± 1.6 Ma was derived for the Aranbanga Volcanic Group based on U–Pb zircon dating of the intruding Mungore Granite (see Donchak *et al.* 2013 and references therein). Therefore, it is likely of Carnian, or possibly lowermost Norian, age.

The South African specimen investigated herein bears the number PRE/F/20242 (positive imprint; Fig. 1C, D). Even though its number includes an acronym (viz. 'PRE') referring to the National Botanical Institute (now the South African National Biodiversity Institute; Pretoria, South Africa), it is currently housed at the Evolutionary Studies Institute (School of Geosciences, University of the Witwatersrand, Johannesburg). It was collected from the Molteno Formation (considered of lower Carnian age; Anderson *et al.* 1998), the geology of which has been reviewed in detail elsewhere (Deregnacourt *et al.* 2017).

Other specimens mentioned in the text are housed at the Natural History Museum (London, UK; acronym 'NHMUK') and the Australian Museum (Sydney, Australia; acronym 'AM').

Hand-drawn sketches were prepared with the aid of a Zeiss SteREO Discovery V8 stereomicroscope, equipped with a pair of W-PL 10×/23 eye pieces, a Plan Apo S 1.0× FWD objective, and a drawing tube (all Jena, Germany).

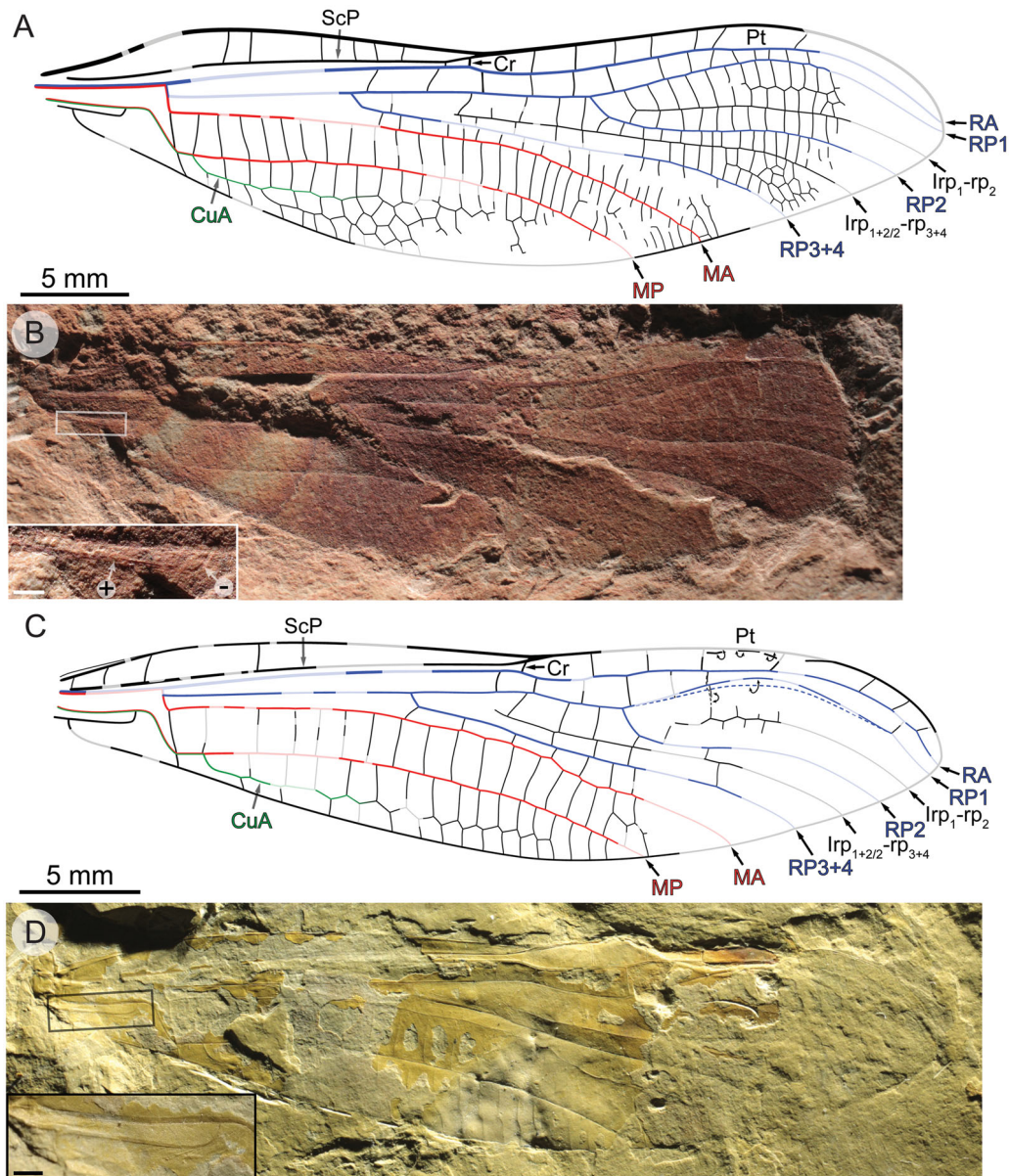


Figure 1. Representatives of Mesophlebiidae Tillyard, 1916: **A, B**, *Mesophlebia antinodalis* Tillyard, 1916, specimen QMF 58847, left forewing; **A**, drawing of wing venation; **B**, photograph (positive imprint, flipped horizontally), with habitus and detail of the vein-like element delimiting the posterior lobe highlighted (inset, scale bar 500 μ m); **C, D**, *Mesophlebia elegans* Deregnaucourt, Anderson, Wappler & Béthoux sp. nov., specimen PRE/F/20242, left forewing; **C**, drawing of wing venation (adjustments indicated by double-headed arrows, adjusted vein portion indicated by dashed line); **D**, photograph (positive imprint, flipped horizontally), with habitus of the vein-like element delimiting the posterior lobe highlighted (inset, scale bar 500 μ m).

Photographs were taken using a Canon EOS 5D Mark III equipped with Canon 50 mm or MP-E 65 mm macro lenses (all Tokyo, Japan). Photographs were optimized using Adobe Photoshop CS6 (Adobe Systems, San Jose, CA, USA). Final drawings were inked using Adobe Illustrator CS6 (Adobe Systems) integrating both the scanned hand-drawn sketches and photographs. RTI files of specimen QMF 58847 were produced following the procedure detailed by Béthoux *et al.* (2016), and are made available in an online Dryad Digital Repository (Tierney *et al.* 2019).

We follow the so-called ‘serial insect wing venation groundplan’ (Lameere 1922, 1923). Within this paradigm, we follow the Odonata wing-venation groundplan elaborated by Riek & Kukalová-Peck (1984) and its successive implementations, relevant at various levels of inclusiveness (Nel

et al. 1993, Bechly 1996, Béthoux 2015). The corresponding nomenclature is repeated for convenience, with indication of color coding used in the figures: ScP, posterior Subcosta; R, Radius (blue, including its branches); RA, anterior Radius; RP, posterior Radius; RP1 + 2, anterior branch of RP; RP1, anterior branch resulting from the second fork of RP; RP2, posterior branch resulting from the second fork of RP; RP3 + 4, posterior branch of RP; MA, anterior Media (red); MP, posterior Media (red); Cu, Cubitus (green, including its branches); CuA, anterior Cubitus; CuP, posterior Cubitus; AA, anterior Analis (purple; only on Fig. 2); Cr, nodal cross-vein; Sn, subnodal cross-vein; Pt, pterostigma. We follow Deregnaucourt *et al.* (2017) for the intercalary vein terminology. The area we propose to term the ‘posterior lobe’ is colored orange (in Fig. 2).

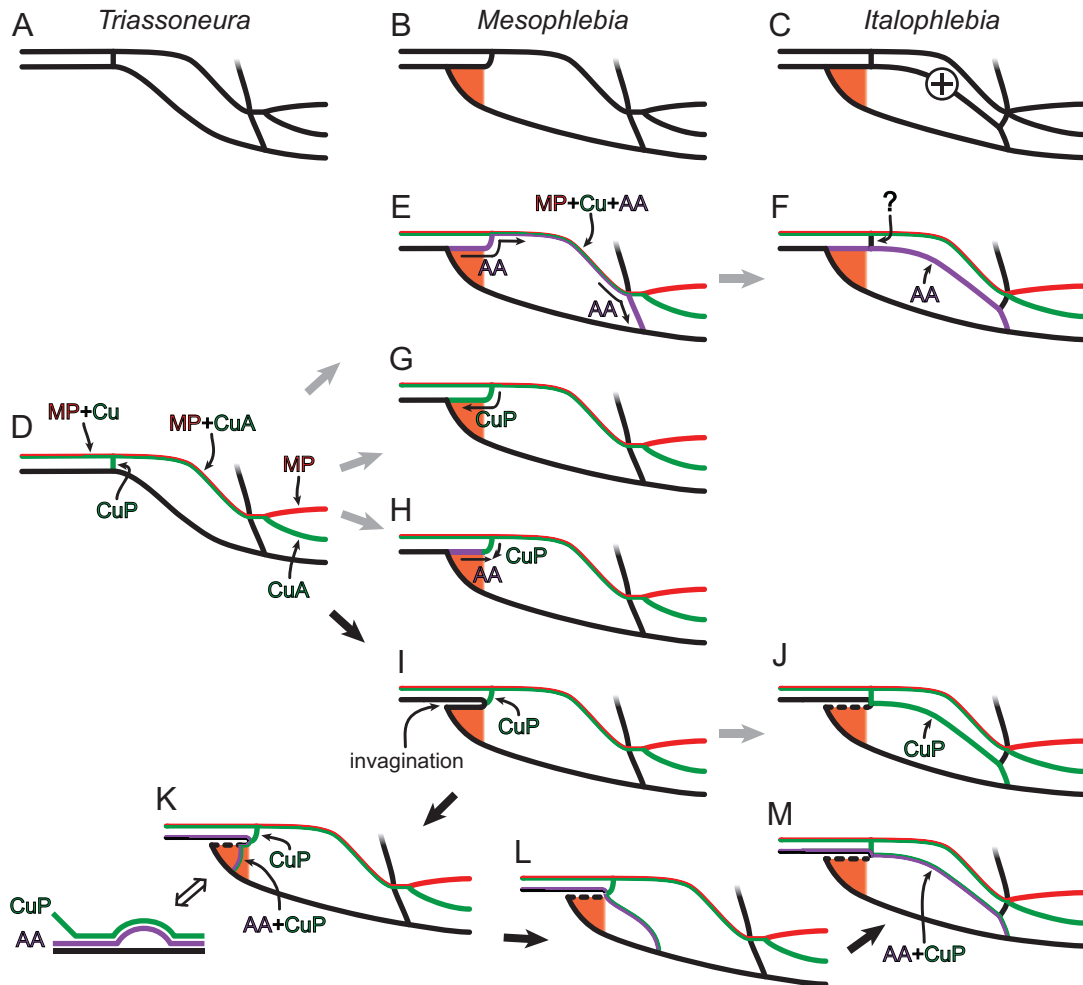


Figure 2. Theoretical topological homologues of the forewing base among 'triassoletids' (arrows in black, as opposed to gray, indicate the favored scenario; see text for details): A–C, blank patterns of A, 'Triassoneura-like', B, 'Mesophlebia-like', and C, 'Italophlebia-like' venation; D, Triassoneura-like pattern assuming 'archizygoteran' homologues; E, Mesophlebia-like pattern assuming an emergence of AA from the posterior wing-margin; F, Italophlebia-like pattern under the same assumption; G, Mesophlebia-like pattern assuming a backwards-directed CuP; H, Mesophlebia-like pattern assuming CuP and AA converge; I, Mesophlebia-like pattern assuming an invagination of the posterior margin ('fibula'); J, Italophlebia-like pattern under the same assumption and with a developed CuP; K, intermediate pattern assuming a brief emergence of CuP + AA (with explanatory scheme assuming a rectilinear posterior margin); L, intermediate pattern assuming a more developed CuP + AA; M, Italophlebia-like pattern assuming an even more strongly developed CuP + AA.

Systematic palaeontology

Order ODONATA Fabricius, 1793

Taxon STIGMOPTERA Bechly, 1996

Taxon LOBODONATA Béthoux, tax. nov.

Diagnosis. In the forewing, presence of an area ('posterior lobe', colored orange in Fig. 2) located between the posterior margin and a vein-like element, parallel to the main axis of the wing in its basal portion and located posteriorly to MP + Cu (see Discussion on the nature of the 'vein-like element').

Etymology. A combination of 'lobos', meaning 'the lobe of the ear' in ancient Greek, referring to the location and shape of the area diagnostic of the taxon (here used as prefix); and 'Odonata', a noun commonly used in the higher systematics of dragon- and damselflies.

Composition. Mesophlebiidae, *Germanophlebia* Nel *et al.*, 2002, *Italophlebia* Whalley, 1986, *Progonophlebia* Tillyard,

1925, most fossil 'Anisozygotera' (as reviewed by Nel *et al.* 1993; see below), and Anisozygotera, Anisoptera and Zygotera.

Remarks. Original data on triassoletid genera were gathered using references listed in Nel *et al.* (2002) and Barth *et al.* (2013). The fore- and hindwing morphology of *Italophlebia gervasutti* Whalley, 1986 (see revision in Bechly 1997) suggests that the posterior lobe first appeared in the forewing, and was later acquired in the hindwing.

The position of the genus *Triassoletes* Tillyard, 1918 remains uncertain to some extent, because most of the forewing, including its base, is unknown. However, available data suggest that this genus is extremely similar to *Triassoneura* Riek, 1976, which can be excluded from the Lobodonata due to the lack of a posterior lobe. The same applies to the genera *Triassoneura* Riek, 1976, *Triassoletodes* Pritykina, 1981 and *Triassothemis* Carpenter, 1960, which were previously regarded as closely related to *Mesophlebia* (Nel *et al.* 2002). In other words, a part of the triassoletid assemblage as previously delimited can be considered

relatives of the Lobodonata, whereas others can be directly assigned to this taxon.

As for the species *Sogdopteron legibile* Pritykina, 1980, we question the relevance of assigning it to a genus distinct from *Sogdopteron leve* Pritykina, 1980 and of recognizing it as a triassolestid on the basis of vein organization at the wing base, as suggested by Nel *et al.* (2002). Indeed, the two species, as far as documented, are extremely similar, and the observed minor differences could well be accounted for by fore- vs hindwing dimorphism. Moreover, both species were recovered from the Lower to Middle Jurassic Sagul locality (Rasnitsyn & Zherikhin 2002), a time when no triassolestids are documented.

Family MESOPHLEBIIDAE Tillyard, 1916 stat. rest.

Diagnosis. RA–RP1 area very narrow opposite the pterostigma.

Type genus. *Mesophlebia* Tillyard, 1916 (monotypic family).

Remarks. Due to the incompleteness of previously known specimens, uncertainties regarding the organization of venation at the wing base in the type genus remained, leaving some doubt as to its affinities and the status of the family. The new specimens we describe confirm that the type genus belongs to the ‘triassolestid assemblage’ as previously delimited (Nel *et al.* 2002), but that this assemblage is paraphyletic. An emendation of the type genus diagnosis and reinstatement of the family Mesophlebiidae therefore appear justified. The review of the status of the family provided by Nel *et al.* (2002) is exhaustive and remains up to date, and therefore does not need to be repeated here.

Mesophlebia Tillyard, 1916

Type species. *Mesophlebia antinodalis* Tillyard, 1916.

Other species. *Mesophlebia elegans* sp. nov.

Diagnosis. RA–RP1 area very narrow opposite the pterostigma.

Description. Nodal cross-vein short and strong; RA markedly bent posteriorly distal to nodus; RP1 + 2 bent posteriorly opposite its first fork, with RP2 diverging very obliquely; RP1 + 2 fork located well distal of nodus; within a median band along the wing’s main axis, areas between RP2, $Irp_{1+2/2-rp_{3+4}}$, RP3 + 4 and MA narrow; MA with a more or less sudden inflection slightly distal of nodus; width of the MA–MP area constant; basalmost cross-vein connecting MA and MP + CuA aligned with basalmost cross-vein connecting MP + CuA and the posterior margin; posterior lobe without (cross-)veins.

Remarks. The narrowness of the RA–RP1 area is unique to *Mesophlebia*, whereas the other traits listed in the description are shared with other taxa.

Mesophlebia antinodalis Tillyard, 1916 (Fig. 1A, B; and Tierney *et al.* 2019)

Annotated diagnosis. Cross-veins numerous (in particular, in the area between MP and posterior wing-margin, which is more than three cells wide at its broadest); first fork of RP and nodus located more basally than in *M. elegans*.

Type material. Holotype NHMUK In.33279 (negative imprint, specimen ‘3b’ in Tillyard 1916; current location of the positive imprint, ‘3a’ in Tillyard 1916, unknown), left wing, likely a hindwing; paratype (‘heautotype’ in Tillyard, 1922) composed of AM F39270 (positive imprint, specimen ‘127a’ in Tillyard 1922) and NHMUK In.33397 (negative imprint, specimen ‘127b’ in Tillyard 1922), right wing, presumably a hindwing.

Other material. QMF 58847 (positive imprint), left wing, likely a forewing.

Type locality and horizon. Holotype and paratype from Denmark Hill, Ipswich, Queensland, Australia; Blackstone Formation; Carnian (possibly lowermost Norian).

Other locality and horizon. Specimen QMF 58847 from ‘QML 1307’ site (register of the Queensland Museum) near Wondai, Burnett region, Queensland, Australia; Aranbanga Volcanic Group; Carnian (possibly lowermost Norian).

Description of new material. Isolated wing, preserved length 37.8 mm (complete length about 41.9 mm), width at mid-length about 9.7 mm; apex and median portion of posterior margin missing, basal portion of RA and RP not preserved, crease along RP3 + 4; area between anterior margin and ScP very broad along its basal third; nodus located slightly basal to wing mid-length; in the RA–RP area, two oblique cross-veins basal to the nodus, and slightly stronger, straight cross-vein distal to the nodus (possibly Sn); first fork of RP located well basal of the second fifth of wing length; at least one supplementary intercalary between RP1 and Irp_1-rp_2 ; area between MP and posterior margin broad, with a network of cross-veins into which CuA vanishes; CuA possibly branched; posterior lobe incomplete, preserved portion without visible (cross-)vein.

Remarks. There has been some confusion around whether the type specimens are the positive and negative imprints of the same individual. Contrary to the statement by Nel *et al.* (2002), specimen NHMUK In.33397 (not ‘In.3397’) is not the negative imprint of the holotype (NHMUK In.33279), but rather the negative imprint of the paratype, AM F39270. This is confirmed by the original numbering mentioned in Tillyard’s accounts and still visible on the NHM specimens (‘3b’ on NHMUK In.33279, and ‘127b’ on NHMUK In.33397; red paint), and based on the fact that both are negative imprints. The number ‘127a’ is visible on the specimen AM F39270 (red paint). Incidentally, this explains

discrepancies between the drawings provided by Nel *et al.* (2002), as they document distinct individuals.

We observed only a few differences between the known specimens of *M. antinodalis* and the new specimen QMF 58847. The distance between the RP1 + 2/RP3 + 4 and RP1/RP2 forks is greater than the wing width opposite the nodus in QMF 58847, whereas this distance is much shorter in the holotype. However, such differences have been observed among fore- and hindwing of the same species in extant Zygoptera (see Garrison *et al.* 2006 among others), and also in *Epiophlebia superstes* (de Selys Longchamps, 1889) (Bridges 1994, OB pers. obs. 2019), consensually regarded as a sister group to Anisoptera (Bechly 1996, Dumont *et al.* 2010, Blanke *et al.* 2013; among others). As this distance is observed to be shorter in the hindwing within these species, we suggest that QMF 58847 is a forewing (which is corroborated by its morphological features), whereas the holotype, and probably the paratype, are hindwings.

Mesophlebia elegans Deregnaucourt, Anderson, Wappler & Béthoux sp. nov. (Fig. 1C, D)

Annotated diagnosis. Cross-veins not numerous (in particular, in the area between MP and posterior wing-margin, two cells only at its broadest); first fork of RP and nodus located more distally than in *M. antinodalis*.

Etymology. Referring to the relative paucity of cross-veins in wings of this species.

Type material. Holotype: PRE/F/20242 (positive imprint), left wing, likely a forewing.

Type locality and horizon. Birds River (locality code 'Bir 111'; see Anderson & Anderson 1984), South Africa; Molteno Formation; lower Carnian, Upper Triassic (Anderson & Anderson 1993).

Specimen description. Isolated wing, length 36.9 mm, width at mid-length 8.4 mm; imprint extends across several sedimentary layers, presumably including positive imprint of dorsal side of the wing on one layer and negative imprint of ventral side of the wing on another; venation in most of posterodistal area not decipherable; creases affecting the pterostigmatic area; area between anterior margin and ScP gradually tapering; nodus located distal to wing mid-length; in the RA–RP area, a straight cross-vein distal to the nodus (possibly Sn); first fork of RP located opposite the second fifth of wing length; area between MP and posterior margin not particularly broad, with two rows of cross-veins into which CuA vanishes; CuA simple; posterior lobe without (cross-)veins.

Remarks. The wing of the holotype is creased in several areas. We propose some adjustments to account for these creases (indicated by double-headed arrows and dashed line on Fig. 1C).

Discussion

The posterobasal area in forewings of *Mesophlebia* displays a configuration previously unknown. The area between MP + Cu and the posterior margin is crossed by a rectilinear 'vein-like' element terminating on MP + Cu (or MP + CuA) after an ultimate sharp bend (Fig. 1B, D insets). The nature of this element is not evident, so we devised several conjectural topological homologies, taking into account venation patterns documented for forewings of *Triassoneura* (Fig. 2A), *Mesophlebia* (Fig. 2B) and *Italophlebia* (Fig. 2C), all previously considered members of the same, triasolestid, assemblage. Considering *Triassoneura* as a starting point and assuming 'archizygopteran' wing-venation homologies (Fig. 2D), the 'vein-like element' (in *Mesophlebia*) can be regarded as AA emerging from the posterior margin, fusing with MP + Cu, and then diverging from it to recombine with the posterior margin (Fig. 2E). This interpretation can be easily applied to *Italophlebia* (Fig. 2F), but does not account for the presence of a cross-vein between MP + Cu and AA ('?' on Fig. 2F). Note that our 'CuP' in *Triassoneura* can also be interpreted as AA diverging from the posterior margin and then fusing with MP + Cu (Bechly 1997, Nel *et al.* 2002). However, this interpretation requires a major modification with respect to other Archizygoptera and is contradicted by the fact that this vein is concave in *Triassoneura andersoni* Riek, 1976 (ID & OB, pers. obs. 2019).

Another option is to consider the 'vein-like element' as CuP directed backwards (Fig. 2G). However, major modifications of this pattern would be required to explain the venation observed in *Italophlebia* (not included on Fig. 2). An alternative scenario can also be imagined where both CuP, diverging from MP + Cu, and AA, diverging from the posterior margin, converge (Fig. 2H). We consider this interpretation highly unlikely because the tracheae filling insect wing-veins tend to run parallel to one another, and there are no known cases of tracheae converging toward each other.

We then submit that the 'vein-like element' could be composed of an invagination of the posterior wing-margin (Fig. 2I). This is consistent with our observations of the 'vein-like' element in specimen QMF 58847, in which the rectilinear portion is convex and the terminal, bent portion is concave (Fig. 1B, inset; Tierney *et al.* 2019), and can therefore be interpreted as CuP. This proposal also explains the sharp angle formed by the (then apparent) posterior margin opposite the origin of the 'vein-like element'. If this invagination was indeed occurring, it would be represented by a single stem-like element, without space separating its two borders. We propose to term this supposed invagination the 'fibula' (after the name of an antique garment safety-pin; referring to the loop shared by both structures).

It is then possible to interpret *Italophlebia* as possessing a long portion of free CuP re-diverging from the posterior margin (Fig. 2J), but this is contradicted by the convexity of the corresponding structure (based on an observation of the corresponding vein in extant species). We then submit that within the posterior lobe, AA emerges from the posterior

margin, imposes its course on CuP, and shortly re-fuses with the margin (Fig. 2K). This pattern is consistent with the venation documented in the hindwing of *Germanophlebia* (see original description of the type species). The vein AA would completely capture the fibula, and the composite vein CuP + AA would develop (Fig. 2L; hypothetical), eventually reaching the cross-vein previously connecting MP + CuA and the posterior margin (Fig. 2M). Assuming that AA (convex) dominates CuP (concave), this interpretation is consistent with the convexity of the vein posterior to MP + CuA, as assumed for *Italophlebia* (Fig. 2C).

In summary, the scenario involving an invagination of the posterior margin best explains the observed patterns. Among other aspects, it makes it unnecessary to advocate for a disappearance of CuP in ‘triastolestids’ (Nel *et al.* 2002). Regardless of the actual nature of the ‘vein-like element’, it delimits an area, the posterior lobe, present in a subset of Stigmoptera including all extant forms and some of their closest fossil relatives, termed here the Lobodonata (erected above).

Acknowledgements

We are grateful to two anonymous reviewers and to the editorial board of *Alcheringa* (and in particular S. Martin) for constructive comments and for improving the readability of the paper. We are grateful to Heidi M. Anderson (Honorary Research Associate, Evolutionary Studies Institute, Johannesburg), and often the Anderson kids, for having helped build the Molteno fossil insect collection. We are grateful to K. Spring (QM, Hendra) for allowing a loan of QMF 58847; to C. Mellish (NHM, London), P. Smith (AM, Sydney) and A. Rix (University of Queensland, Brisbane) for providing information and/or photographs of the type material of *M. antinodalis*; and to A. Rasnitsyn (PIN, Moscow) for assistance with access to Russian literature. We also acknowledge M. Saul, who brought the existence of insects at ‘QML 1307’ to the attention of AT & PT. Data on the ‘Anderson collection’ and the new fossil species in particular were collected during two visits to the Evolutionary Studies Institute (Wits University; Johannesburg; 2014, 2015). We are grateful to M. Bamford and T. Scott-Turner for their help during these visits.

Disclosure statement

No potential conflict of interest was reported by the author(s).

Funding

Visits to the Evolutionary Studies Institute were supported by two grants from the ‘Action Transversale Muséum Emergences’ (O. Béthoux, 2014, 2015) and by a grant from the DFG [WA 1492/9-1; T. Wappler and O. Béthoux, 2014].

References

- ANDERSON, J.M. & ANDERSON, H.M., 1984. The fossil content of the Upper Triassic Molteno Formation, South Africa. *Palaeontologia Africana* 25, 39–59.
- ANDERSON, J.M. & ANDERSON, H.M., 1993. Terrestrial flora and fauna of the Gondwana Triassic: Part 1 — Occurrences. In *The Nonmarine Triassic*. LUCAS, S.G. & MORALES, M., eds, New Mexico Museum of Natural History & Science, Bulletin 3, Albuquerque, 3–12.
- ANDERSON, J.M., ANDERSON, H.M. & CRUICKSHANK, A.R.I., 1998. Late Triassic ecosystems of the Molteno/Lower Elliot Biome of Southern Africa. *Palaeontology* 41, 387–421.
- BARTH, G., NEL, A. & FRANZ, M., 2013. Two new odonate-like insect wings from the latest Norian of northern Germany. *Polish Journal of Entomology/Poliskie Pismo Entomologiczne* 82, 127–142.
- BECHLY, G., 1996. Morphologische Untersuchungen am Flügelgeäder der rezenten Libellen und deren Stammgruppenvertreter (Insecta; Pterygota; Odonata) unter besonderer Berücksichtigung der Phylogenetischen Systematik und des Grundplanes der Odonata. *Petalura special volume 2*, 1–402. (Revised edition including appendix in English)
- BECHLY, G., 1997. New fossil odonates from the Upper Triassic of Italy, with a redescription of *Italophlebia gervasuttii*, and a reclassification of Triassic dragonflies (Insecta: Odonata). *Rivista Del Museo Civico di Scienze Naturali “Enrico Caffi”* 19, 31–70.
- BÉTHOUX, O., 2015. The Late Carboniferous *Triplosoba pulchella* is not a fly in the ointment but a stem-mayfly. *Systematic Entomology* 40, 342–356.
- BÉTHOUX, O., LLAMOSI, A. & TOUSSAINT, S., 2016. Reinvestigation of *Protelytron permianum* (Insecta; Early Permian; USA) as an example for applying reflectance transformation imaging to insect imprint fossils. *Fossil Record* 20, 1–7.
- BLANKE, A., GREVE, C., MOKSO, R., BECKMANN, F. & MISOF, B., 2013. An updated phylogeny of Anisoptera including formal convergence analysis of morphological characters. *Systematic Entomology* 38, 474–490.
- BRIDGES, C.A., 1994. *Catalogue of the Family-Group, Genus-Group and Species-Group Names of the Odonata of the World* (3rd ed.), The Author, Urbana, USA, 905 pp.
- CARPENTER, F.M., 1960. Studies on North American Carboniferous Insects 1. The Protodonata. *Psyche: A Journal of Entomology* 67, 98–110.
- DEREGNAUCOURT, I., WAPPLER, T., ANDERSON, J.M. & BÉTHOUX, O., 2017. A new triadotypid insect from the Late Triassic of South Africa. *Acta Palaeontologica Polonica* 62, 613–618.
- DEREGNAUCOURT, I., WAPPLER, T., ANDERSON, J.M. & BÉTHOUX, O., in press. The wing venation of the Protomyrmeleontidae (Insecta: Odonoptera) reconsidered thanks to a new specimen from Molteno (Triassic; South Africa). *Historical Biology*.
- DONCHAK, P.J.T., PURDY, D.J., WITHNALL, I.W., BLAKE, P.R. & JELL, P.A., 2013. New England Orogen. In *Geology of Queensland*. JELL, P.A., ed., Geological Survey of Queensland, Brisbane, Australia, 305–472.
- DUMONT, H.J., VIERSTRAETE, A. & VANFLETEREN, J.R., 2010. A molecular phylogeny of the Odonata (Insecta). *Systematic Entomology* 35, 6–18.
- FABRICIUS, J.C., 1793. *Entomologia Systematica Emendata et aucta. Secundum Classes, Ordines, Genera, Species Adjectis Synonymis, Locis, Observationibus, Descriptionibus*. Tome 2, C.G. Proft, Copenhagen, Denmark, viii + 519 pp.
- GARRISON, R.W., VON ELLENRIEDER, N. & LOUTON, J.A., 2006. *Dragonfly Genera of the New World*. John Hopkins University Press, Baltimore, USA, 368 pp.
- LAMEERE, A., 1922. Sur la nervation alaire des insectes. *Bulletin de la Classe des Sciences de l’Académie Royale de Belgique* 8, 138–149.
- LAMEERE, A., 1923. On the wing-venation of insects. *Psyche: A Journal of Entomology* 30, 123–132.
- NEL, A., BÉTHOUX, O., BECHLY, G., MARTÍNEZ-DELCLÓS, X. & PAPIER, F., 2001. The Permo-Triassic Odonoptera of the “protodonate” grade (Insecta: Odonoptera). *Annales de la Société Entomologique de France (N.S.)* 37, 501–525.
- NEL, A., MARIE, V. & SCHMEIßNER, S., 2002. Revision of the lower Mesozoic dragonfly family Triastolestidae Tillyard, 1918 (Odonata: Epiproctophora). *Annales de Paléontologie* 88, 189–214.
- NEL, A., MARTÍNEZ-DELCLÓS, X., PAICHELER, J.C. & HENROTAY, M., 1993. Les “Anisozygoptera” fossiles. Phylogénie et classification (Odonata). *Martinia Hors-Série* 3, 1–311.
- PRITYKINA, L.N., 1980. Novye strekozy iz nijneurskikh otlagienii srednei Azii [New odonates from Lower Jurassic strata of Middle Asia]. In *Iskopaemye Nacekomye Mesozoi [Fossil Insects of the Mesozoic]*. DOLIN, V.G., PANFILOV, D.V., PONOMARENKO, A.B., & PRITYKINA, L.N.,

- eds, Akademia Nauk Ukrainskoj SSR, Naukova Dumka, Kiev, Ukraine, 121–133. (Russian)
- PRITYKINA, L.N., 1981. Novye triasovye strekozy srednej Azii. In *Novye Iskopaemye Nasekomye s Terrotorii SSSR*. VISHNIAKOVA, V.N., DLUSSKY, G.M., & PRITYKINA, L.N., eds, Trudy Paleontologicheskogo Instituta, Akademiya Nauk SSSR, New York, 183, 5–42. (Russian)
- RASNITSYN, A.P. & ZHERIKHIN, V.V., 2002. Impression fossils. In *History of Insects*. RASNITSYN, A.P. & QUICKE, D.L.J., eds, Kluwer Academic Publishers, Dordrecht, The Netherlands, 437–444.
- RIEK, E.F., 1976. A new collection of insects from the Upper Triassic of South Africa. *Annals of the Natal Museum* 22, 791–820.
- RIEK, E.F. & KUKALOVA-PECK, J., 1984. A new interpretation of dragonfly wing venation based upon Early Upper Carboniferous fossils from Argentina (Insecta, Odonatoidea) and basic character states in pterygota wings. *Canadian Journal of Zoology* 62, 1150–1166.
- SELYS LONGCHAMPS, E.D., 1889. *Palaeophlebia*, nouvelle légion de Caloptérygines, suivi de la description d'une nouvelle Gomphine du Japon: *Tachopteryx pryeri*. *Comptes Rendus de la Société Entomologique de Belgique* 3, 153–154.
- TIERNEY, A., DEREGNAUCOURT, I., ANDERSON, J.M., TIERNEY, P., WAPPLER, T. & BÉTHOUX, O., 2019. Data from: The Triassic Mesophlebiidae, a little closer to the crown of Odonata (Insecta) than other 'triassolestids'. *Dryad Digital Repository*. doi:10.5061/dryad.5hqbzkh2f
- TILLYARD, R.J., 1916. Mesozoic and Tertiary insects of Queensland and New South Wales. Descriptions of the fossil insects. *Queensland Geological Survey, Publication* 253, 11–64.
- TILLYARD, R.J., 1918. Mesozoic insects of Queensland. 3. Odonata and Protodonata. *Proceedings of the Linnean Society of New South Wales* 43, 417–435.
- TILLYARD, R.J., 1922. Mesozoic insects of Queensland. No. 9. Orthoptera, and additions to the Protorthoptera, Odonata, Hemiptera and Plannipennia. *Proceedings of the Linnean Society of New South Wales* 47, 447–470.
- TILLYARD, R.J., 1925. *The British Liassic Dragonflies (Odonata)*. British Museum (Natural History), London, UK, 40 pp. + pls I–V.
- WHALLEY, P.E.S., 1986. Insects from the Italian Upper Trias. *Rivista Del Museo Civico di Scienze Naturali "Enrico Caffi"* 10, 51–60.

Annex A.2 – List of the specimens used in this study, their sexe and their location. MNHN = Muséum National d'Histoire Naturelle; ZSM = Zoologische Staatssammlung München; WC = working collection.

Suborder	Familles	Espèces	Female			Male			Total
			MNHN	ZSM	WC	MNHN	ZSM	WC	
Anisoptera	Aeshnidae	<i>Aeshna affinis</i>	2	0	0	1	0	0	3
		<i>Aeshna cyanea</i>	2	0	0	0	2	0	4
		<i>Aeshna grandis</i>	2	0	0	1	1	0	4
		<i>Aeshna isocles</i>	1	1	0	0	2	0	4
		<i>Aeshna juncea</i>	0	2	0	0	2	0	4
		<i>Aeshna mixta</i>	2	0	0	0	0	2	4
		<i>Aeshna subarctica</i>	0	1	0	0	2	0	3
		<i>Anax imperator</i>	0	2	0	0	1	1	4
		<i>Anax parthenope</i>	1	1	0	0	1	1	4
		<i>Boyeria irene</i>	1	1	0	0	1	1	4
		<i>Brachytron pratense</i>	2	0	0	0	2	0	4
		<i>Hemianax ephippiger</i>	2	0	0	2	0	0	4
		Gomphidae	<i>Gomphus graslinii</i>	0	1	0	0	1	1
	<i>Gomphus pulchellus</i>		1	0	1	2	0	0	4
	<i>Gomphus simillimus</i>		1	1	0	1	1	0	4
	<i>Gomphus vulgatissimus</i>		1	1	0	1	1	0	4
	<i>Onychogomphus forcipatus</i>		0	1	1	0	1	1	4
	<i>Onychogomphus uncatus</i>		1	1	0	1	1	0	4
	<i>Ophiogomphus cecilia</i>		0	2	0	0	2	0	4
	Cordulegastridae	<i>Cordulegaster bidentata</i>	1	1	0	1	1	0	4
		<i>Cordulegaster boltonii</i>	1	1	0	0	1	1	4
	Corduliidae	<i>Cordulia aenea</i>	2	0	0	0	2	0	4
		<i>Epithea bimaculata</i>	2	0	0	2	0	0	4
		<i>Oxygastra curtisii</i>	1	1	0	1	1	0	4
		<i>Somatochlora arctica</i>	1	1	0	1	1	0	4
		<i>Somatochlora flavomaculata</i>	0	2	0	0	2	0	4
		<i>Somatochlora metallica</i>	1	1	0	0	1	1	4
	Libellulidae	<i>Crocothemis erythraea</i>	0	1	1	0	2	0	4
		<i>Leucorrhinia albifrons</i>	0	2	0	0	2	0	4
		<i>Leucorrhinia caudalis</i>	0	2	0	0	2	0	4
		<i>Leucorrhinia dubia</i>	0	2	0	0	2	0	4
		<i>Leucorrhinia pectoralis</i>	0	2	0	0	2	0	4
		<i>Libellula depressa</i>	2	0	0	1	1	0	4
		<i>Libellula fulva</i>	2	0	0	0	0	2	4
		<i>Libellula quadrimaculata</i>	1	0	0	0	2	0	3
		<i>Orthetrum albistylum</i>	2	0	0	2	0	0	4
		<i>Orthetrum brunneum</i>	1	1	0	0	0	2	4
		<i>Orthetrum cancellatum</i>	0	0	2	0	1	1	4
		<i>Orthetrum coerulescens</i>	0	1	0	0	2	0	3
		<i>Sympetrum danae</i>	0	2	0	0	2	0	4
		<i>Sympetrum depressiusculum</i>	1	1	0	1	1	0	4
		<i>Sympetrum flaveolum</i>	0	1	0	1	1	0	3
		<i>Sympetrum fonscolombii</i>	1	1	0	1	1	0	4
<i>Sympetrum meridionale</i>		1	1	0	1	1	0	4	
<i>Sympetrum pedemontanum</i>		1	1	0	1	1	0	4	
<i>Sympetrum sanguineum</i>		0	0	7	0	0	13	20	
<i>Sympetrum striolatum</i>		0	0	7	0	0	8	15	
<i>Sympetrum vulgatum</i>	0	2	0	0	2	0	4		
<i>Trithemis annulata</i>	1	1	0	1	1	0	4		
Calopterygidae	<i>Calopteryx haemorrhoidalis</i>	0	0	2	0	0	2	4	
	<i>Calopteryx splendens</i>	0	0	2	0	2	0	4	
	<i>Calopteryx virgo</i>	0	0	2	0	1	1	4	

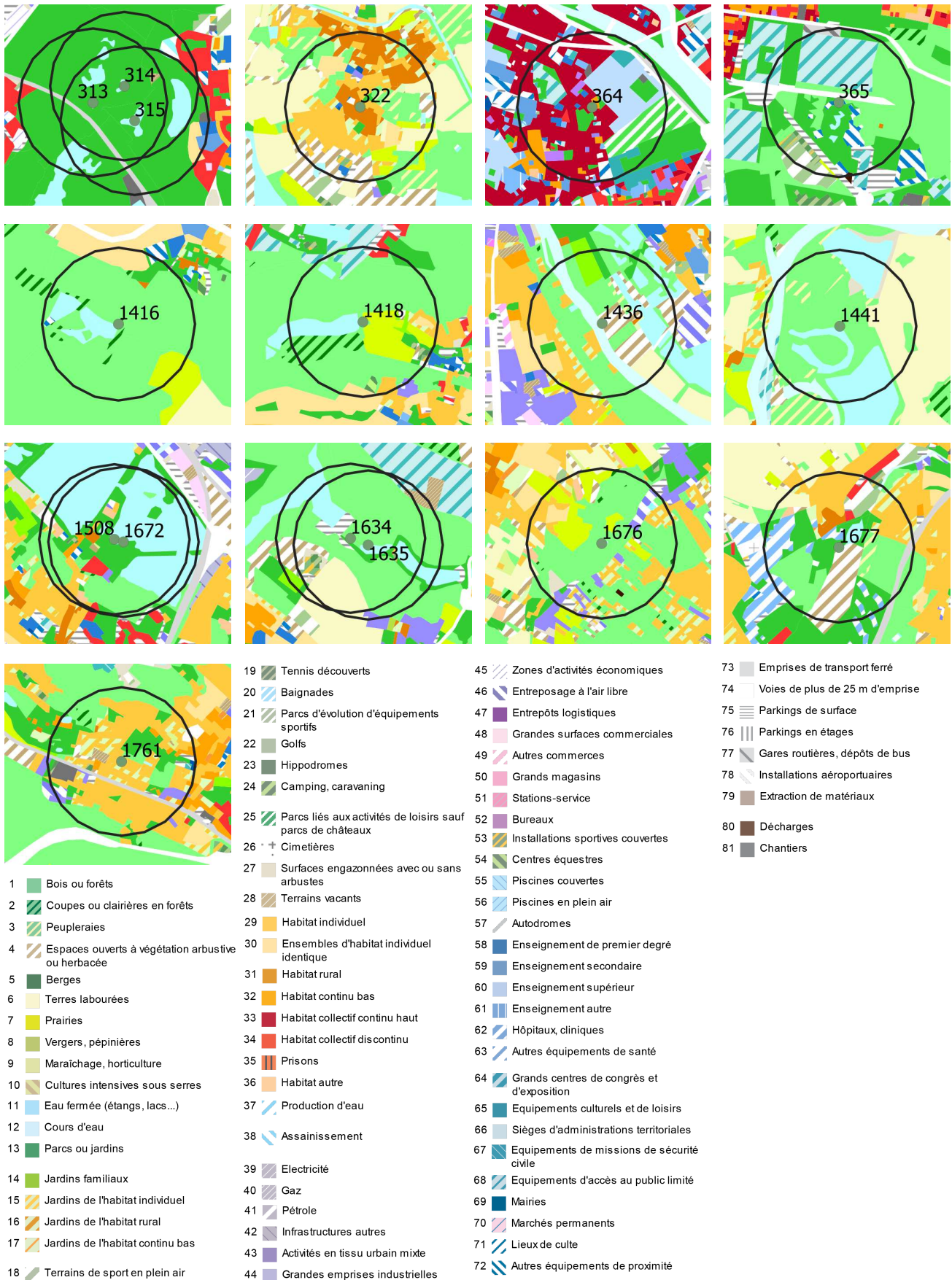
Annex A.2 – Continued on next page

Annex A.2 – Continued from previous page

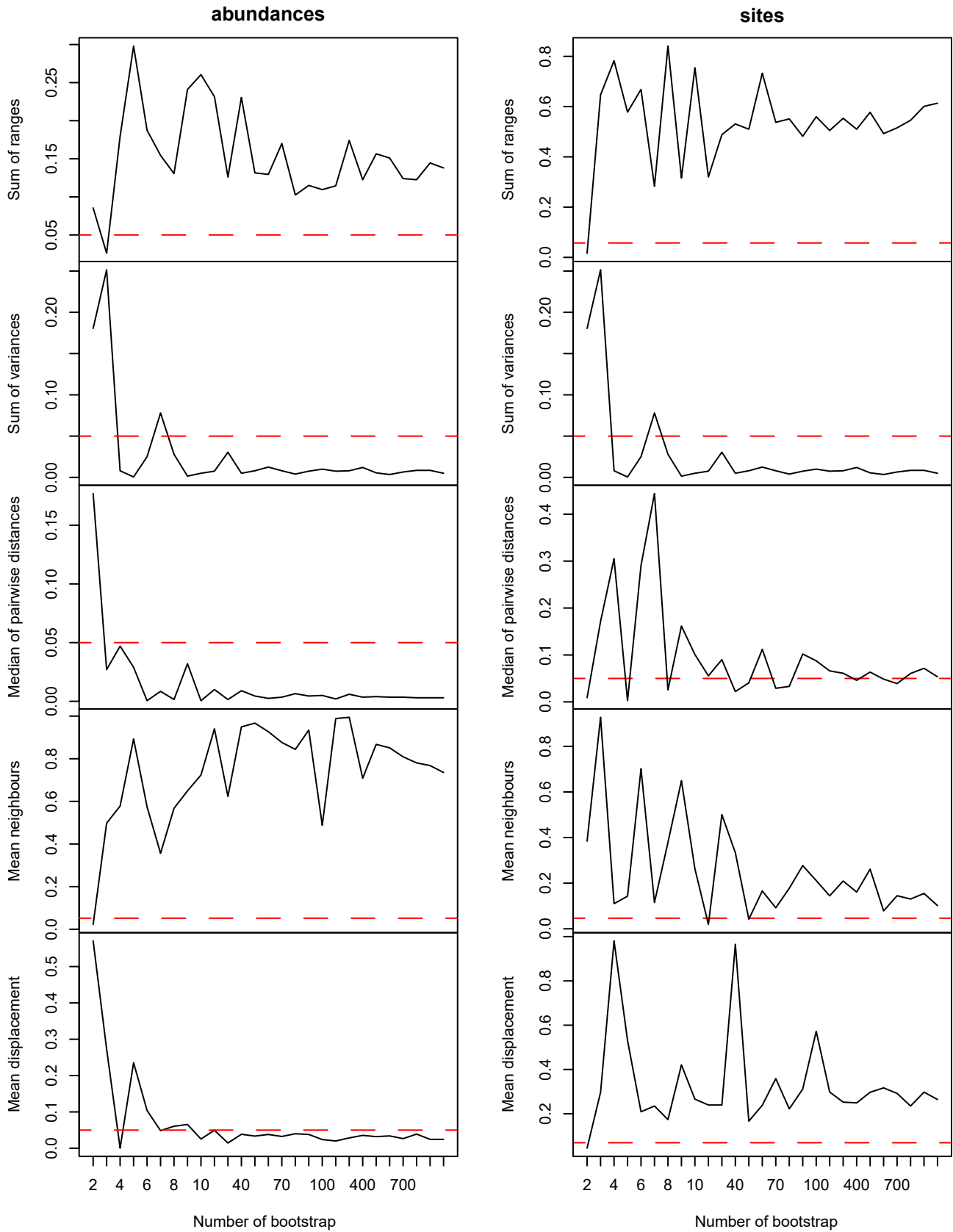
Suborder	Familles	Espèces	Female			Male			Total
			MNHN	ZSM	WC	MNHN	ZSM	WC	
		<i>Calopteryx xanthostoma</i>	0	0	4	0	0	4	8
	Lestidae	<i>Chalcolestes viridis</i>	0	0	2	0	0	2	4
		<i>Lestes barbarus</i>	2	0	0	1	0	1	4
		<i>Lestes dryas</i>	1	1	0	1	1	0	4
		<i>Lestes macrostigma</i>	1	1	0	1	1	0	4
		<i>Lestes sponsa</i>	0	2	0	0	2	0	4
		<i>Lestes virens</i>	0	2	0	0	2	0	4
		<i>Sympecma fusca</i>	0	1	1	0	0	2	4
	Platycnemididae	<i>Platycnemis acutipennis</i>	1	1	0	1	1	0	4
		<i>Platycnemis latipes</i>	0	0	2	0	0	2	4
		<i>Platycnemis pennipes</i>	0	1	1	0	1	1	4
	Coenagrionidae	<i>Ceriagrion tenellum</i>	0	0	2	0	0	2	4
		<i>Coenagrion caerulescens</i>	0	0	0	0	2	0	2
		<i>Coenagrion hastulatum</i>	0	1	0	0	2	0	3
		<i>Coenagrion lunulatum</i>	0	1	0	1	1	0	3
		<i>Coenagrion mercuriale</i>	0	2	0	0	2	0	4
		<i>Coenagrion ornatum</i>	2	0	0	1	1	0	4
		<i>Coenagrion puella</i>	2	0	0	0	2	0	4
		<i>Coenagrion pulchellum</i>	1	1	0	0	2	0	4
		<i>Coenagrion scitulum</i>	2	0	0	0	2	0	4
		<i>Enallagma cyathigerum</i>	0	0	2	0	1	1	4
		<i>Erythromma lindenii</i>	0	0	2	0	0	2	4
		<i>Erythromma najas</i>	2	0	0	0	2	0	4
		<i>Erythromma viridulum</i>	0	0	2	0	0	2	4
		<i>Ischnura elegans</i>	0	0	2	0	1	1	4
		<i>Ischnura pumilio</i>	1	1	0	0	1	0	3
	<i>Pyrrhosoma nymphula</i>	1	1	0	0	1	1	4	

Annex A.3 – Importance of the first 6 components of the PCA realised on the 79 species monitored in France by the Steli program during the interval 2011-2019, each represented by forewings and hindwings of 2 females and 2 males.

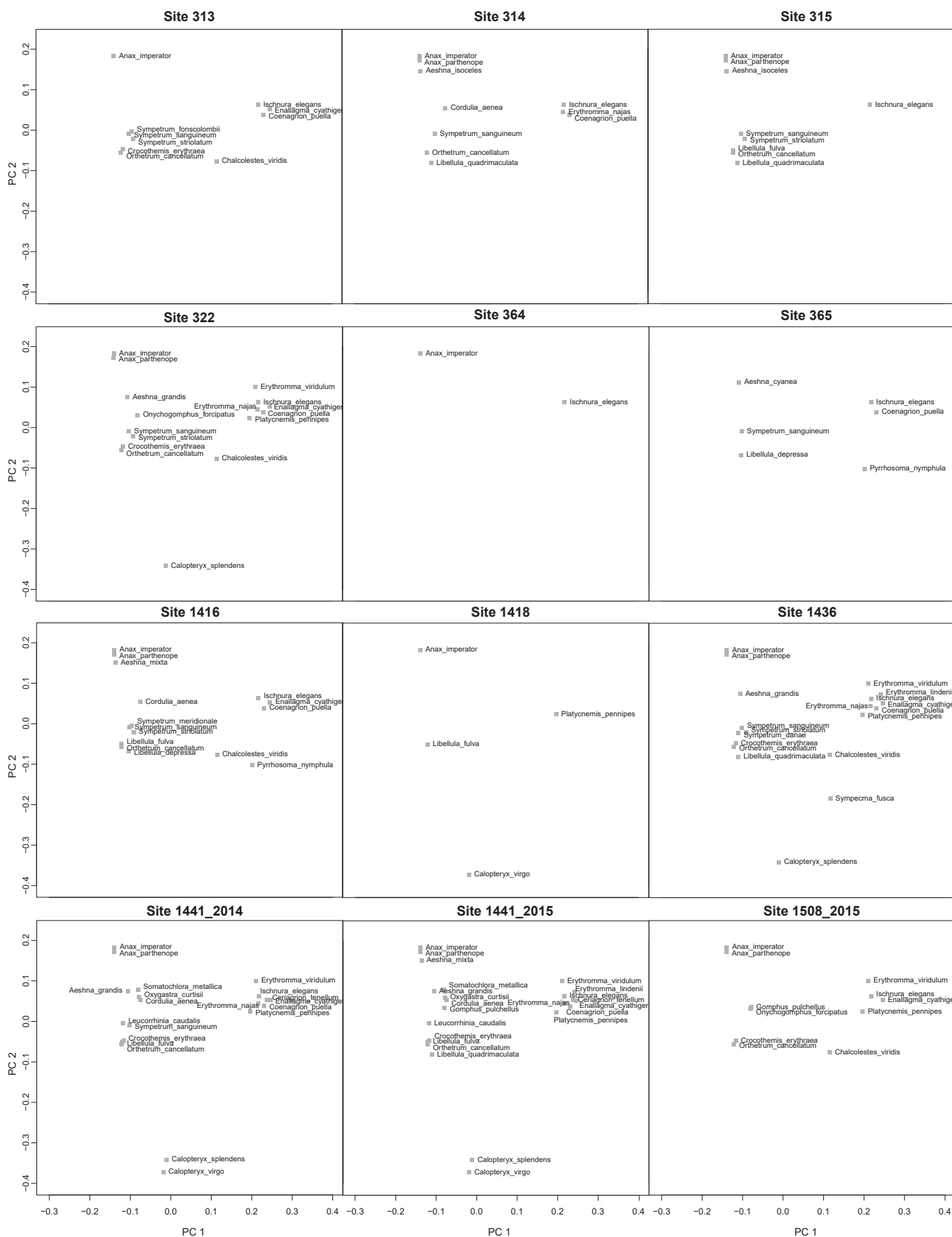
	PC1	PC2	PC3	PC4	PC5	PC6
Standard deviation	0.1472	0.1180	0.06523	0.04085	0.02687	0.02116
Proportion of Variance	0.4904	0.3151	0.09627	0.03776	0.01634	0.01013
Cumulative Proportion	0.4904	0.8056	0.90184	0.93961	0.95595	0.96608

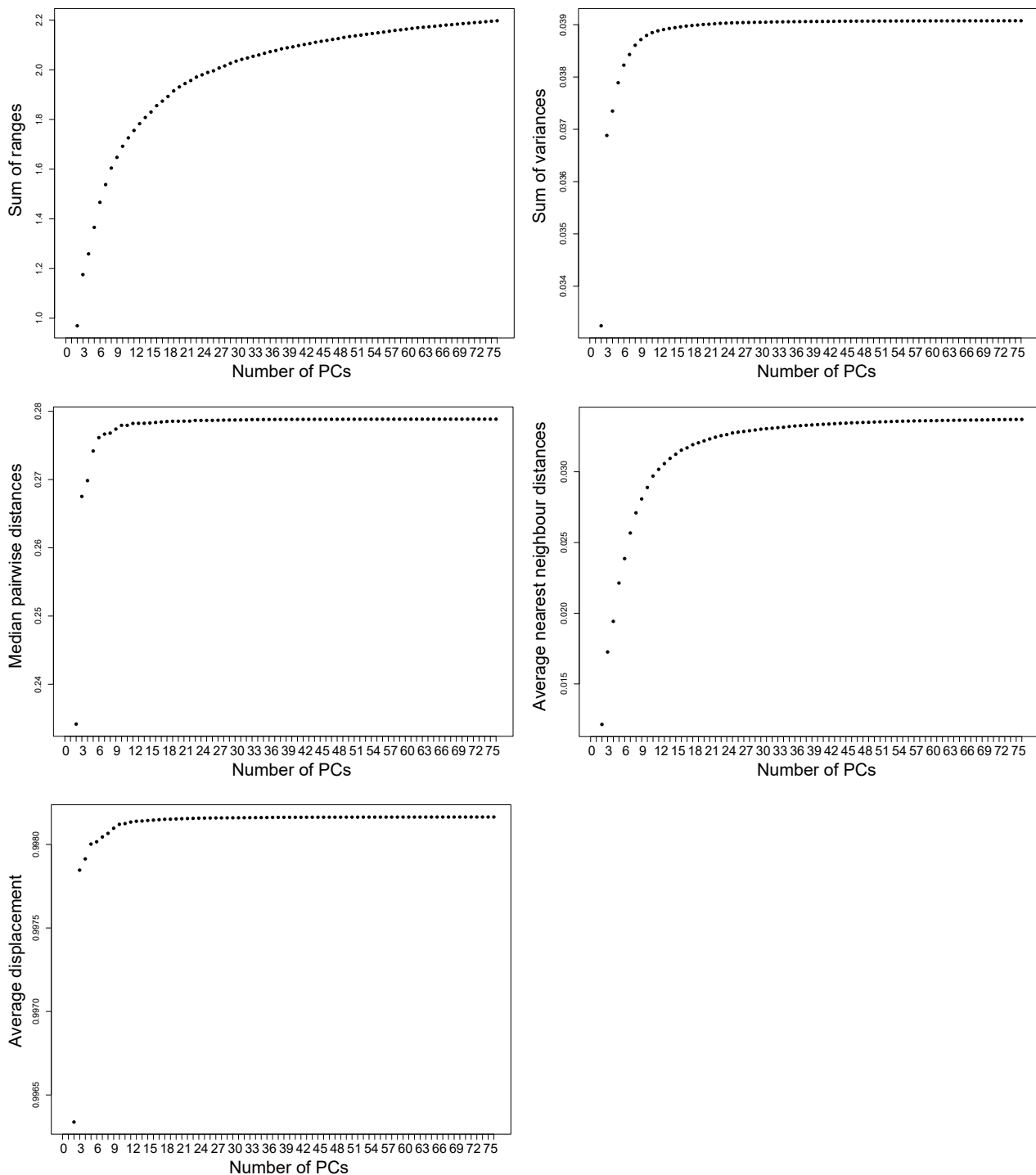


Annex A.4 – Maps of the 500m radius buffer around each sites considered in Ile-de-France. Legend correspond to the MOS 2017.

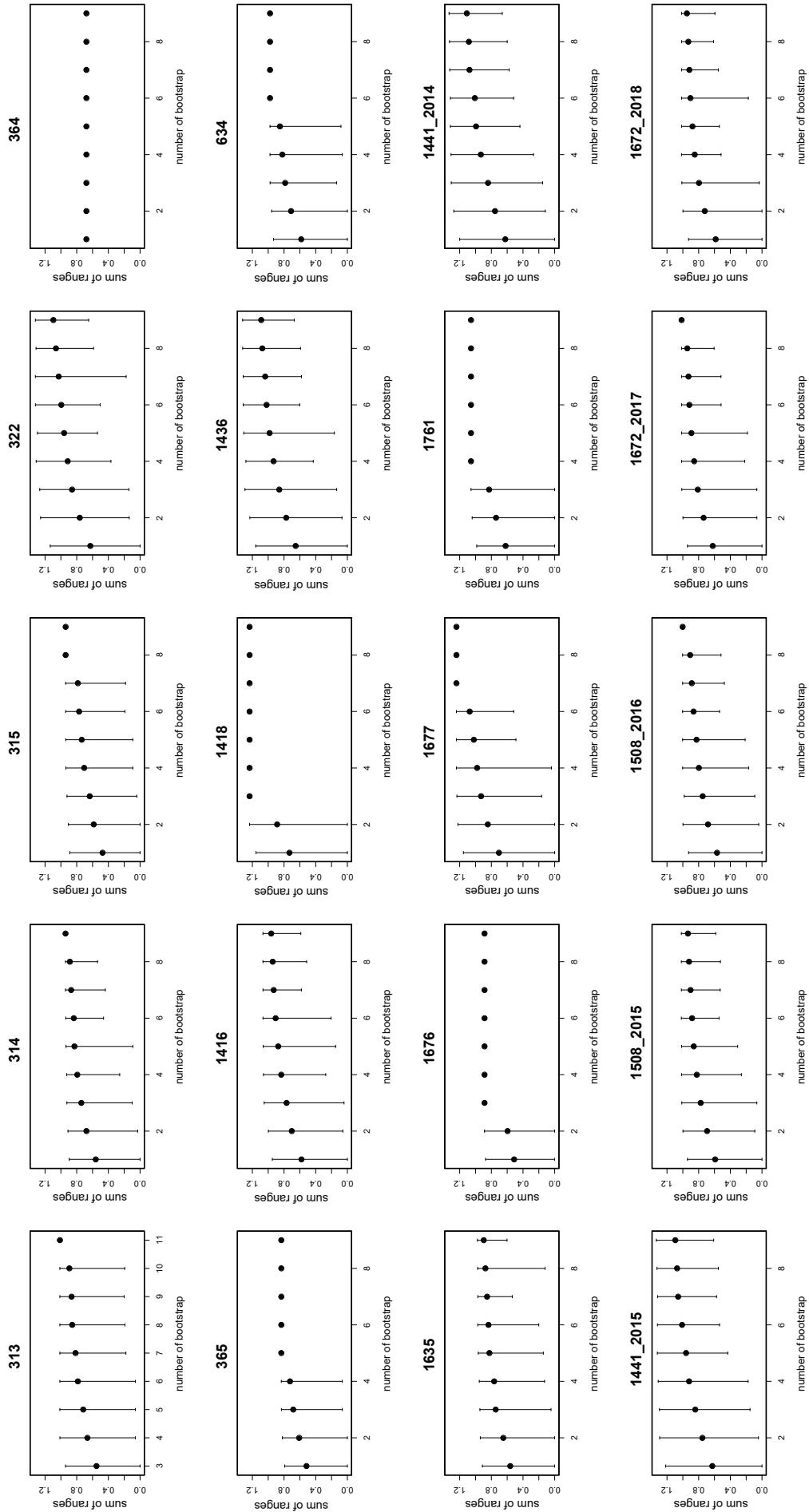


Annex A.5 – Test of the impact of the number of bootstraps on the p-value obtained by a permutation test, comparing common and rare species. Left column correspond to assessed rarity based on abundance of each species, right column correspond to assessed rarity based on site frequency of each species. Dotted red line correspond to a p-value of 0.05

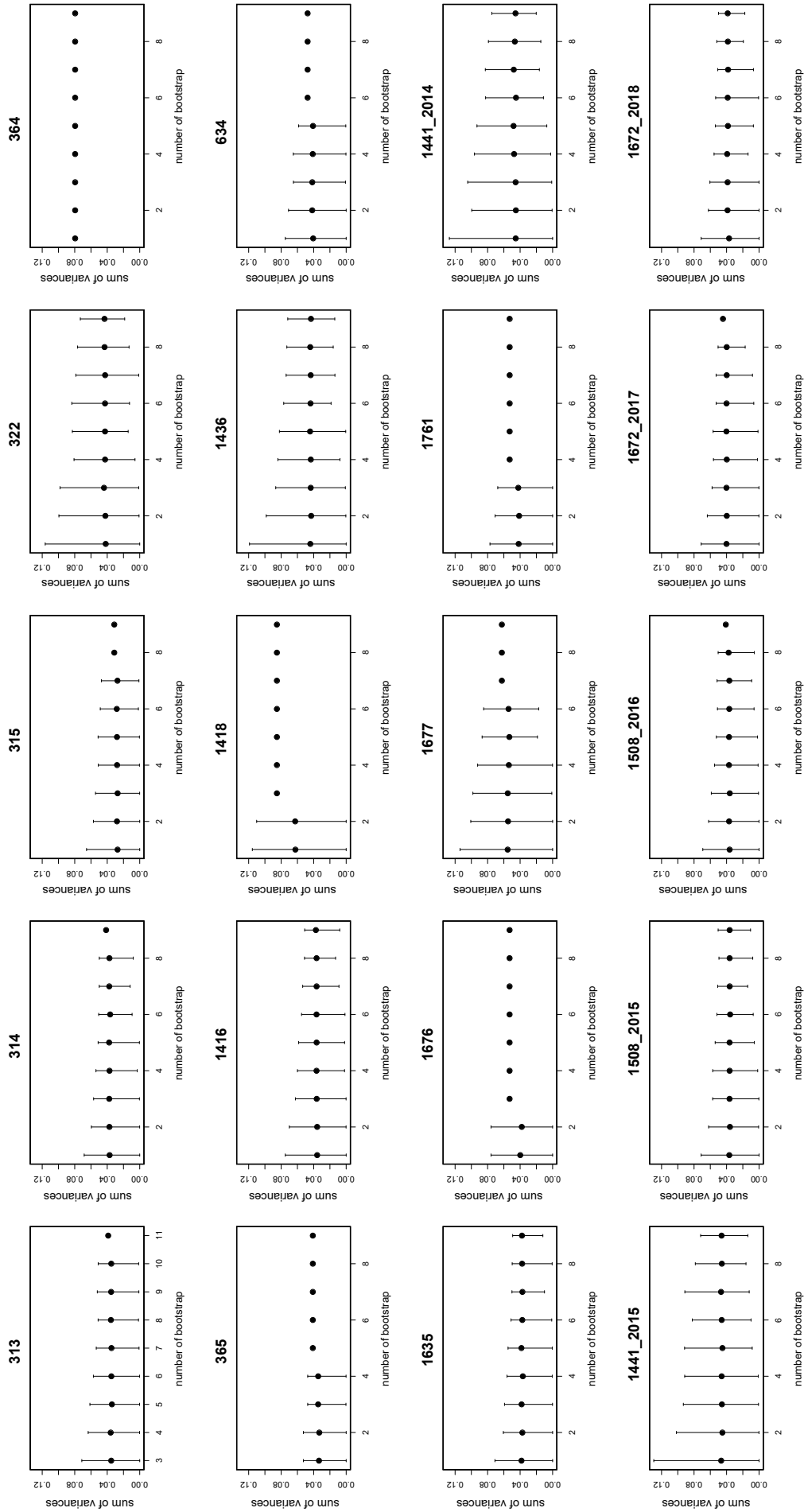




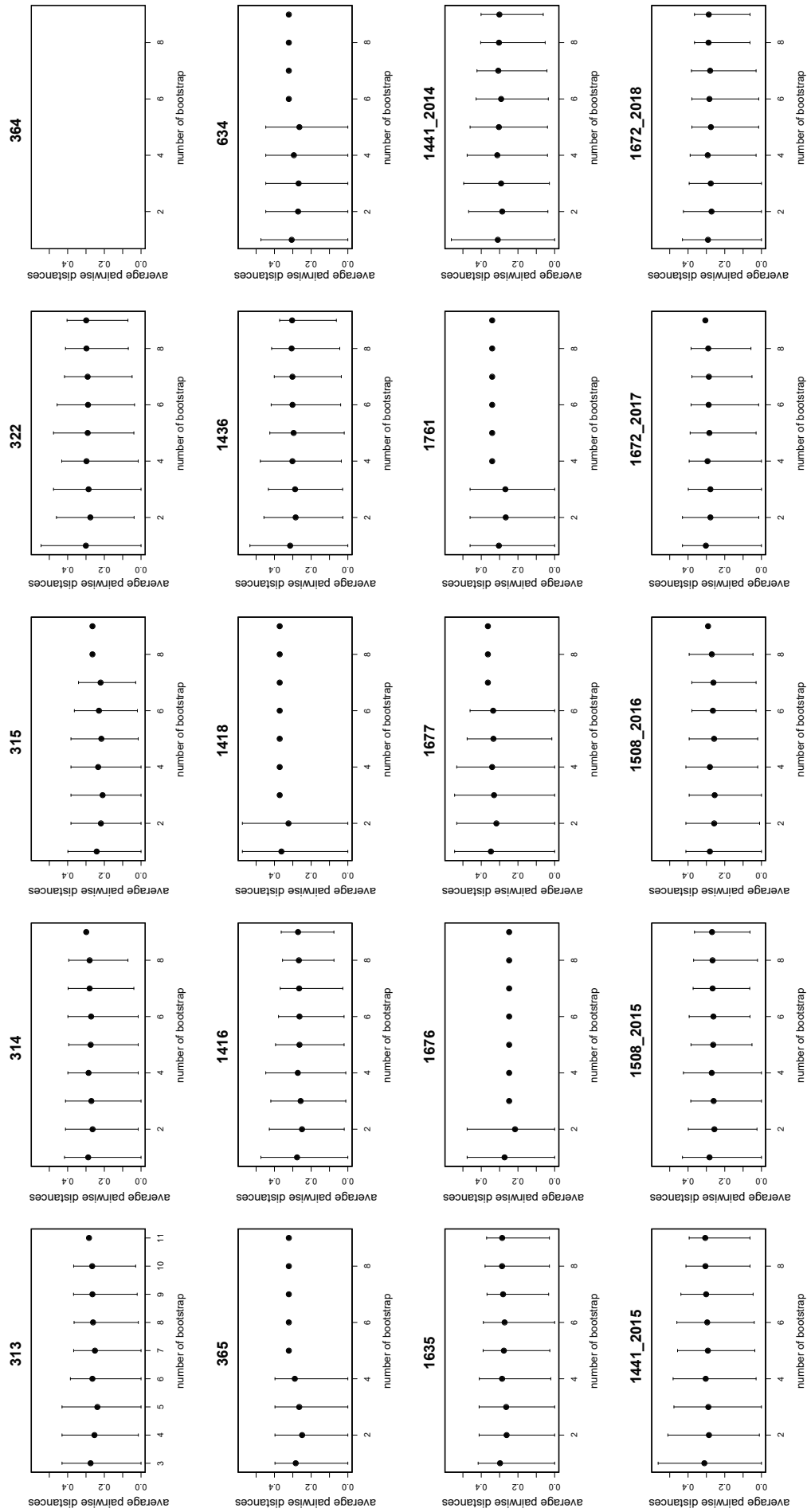
Annex A.7 – Five disparity estimates values computed on 1 to 76 PCs of the PCA realised on the 79 species monitored in France by the Steli program during the interval 2011-2019. The used PC scores are the mean values computed for the reference shape of each species.



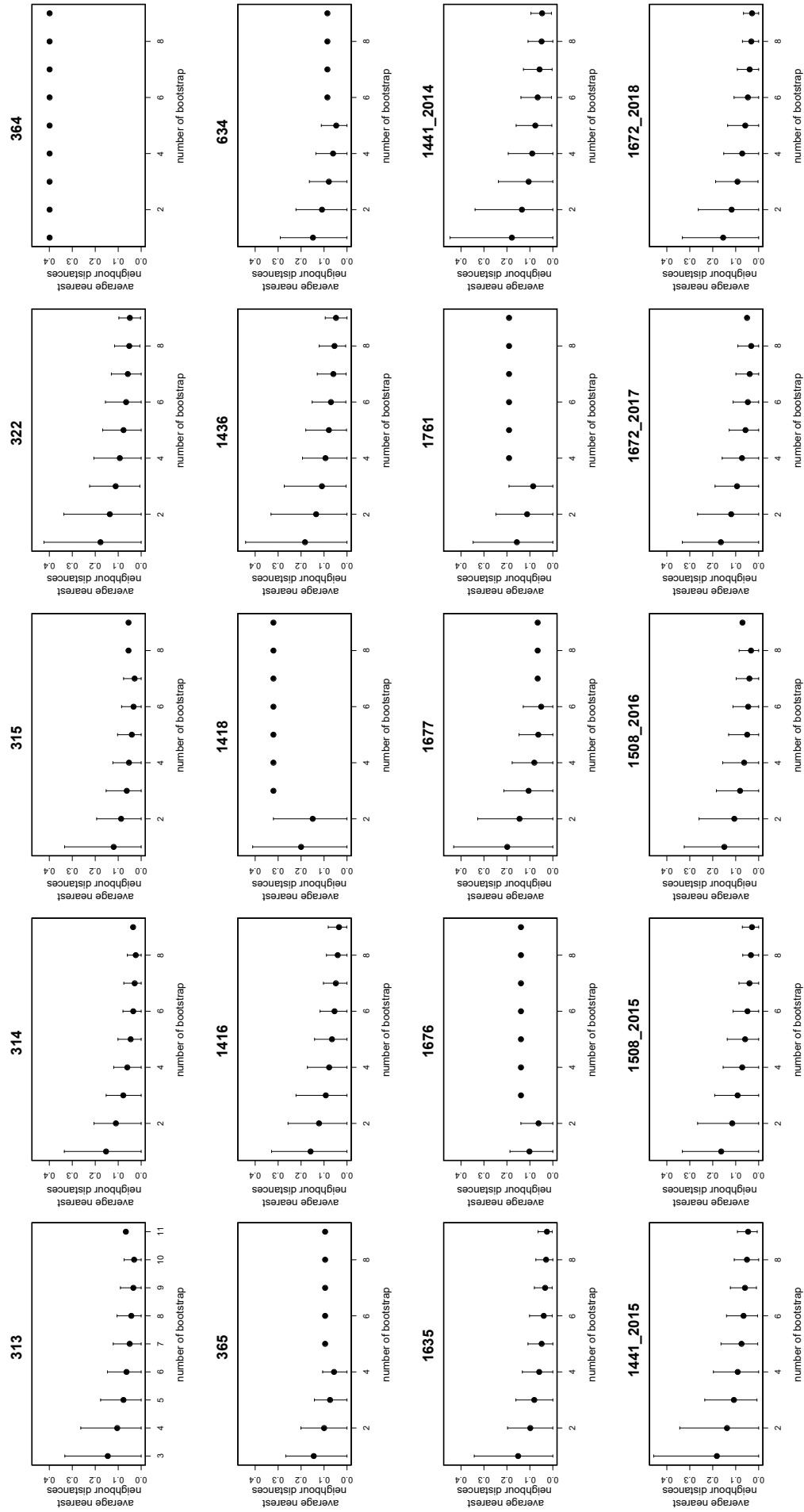
Annex A.8 – Values of the sum of ranges computed with bootstraps sets for sampling quota varying from 3 to 11 species for each site selected in Ile-de-France.



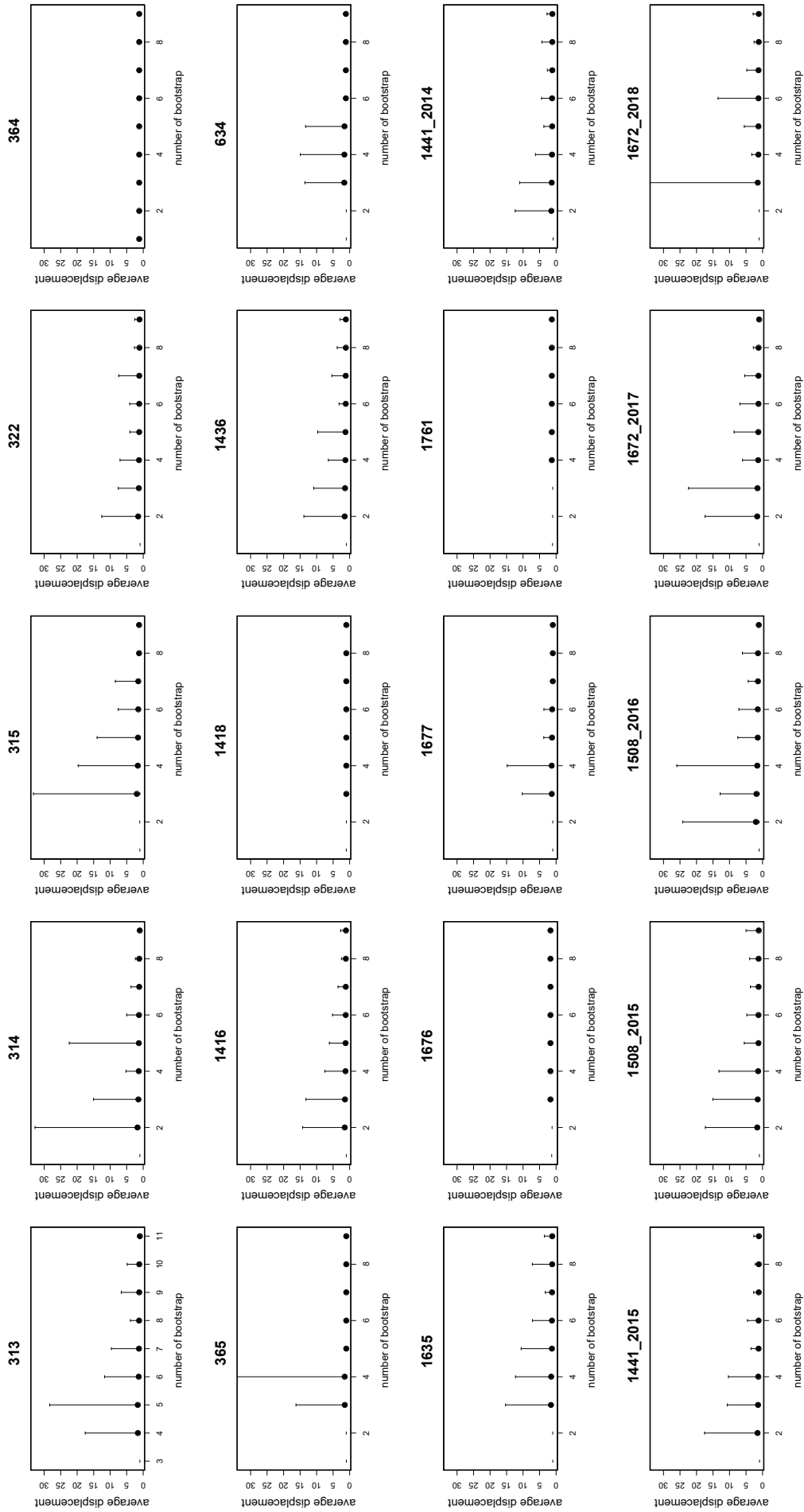
Annex A.9 – Values of the sum of variances computed with bootstraps sets for sampling quota varying from 3 to 11 species for each site selected in Ile-de-France.



Annex A.10 – Values of the average median pairwise distances computed with bootstraps sets for sampling quota varying from 3 to 11 species for each site selected in Ile-de-France.



Annex A.11 – Values of the average nearest neighbour distances computed with bootstraps sets for sampling quota varying from 3 to 11 species for each site selected in Ile-de-France.



Annex A.12 – Values of the average displacement computed with bootstrap sets for sampling quota varying from 3 to 11 species for each site selected in Ile-de-France.

The four following appendices (A.13 – A.16) are associated to the section 4.3.2 of Chapter 4, submitted to Arthropod Structure and Development and currently under review. Numbering within this appendices correspond to the one chosen for submission of the manuscript. Annexe A.13 and A.14 are available via the provided links. The perenity will be ensure at least until the thesis defence.

Annex A.13– Main R script used for wing reconstruction of *Moltenophlebia lindae*.
Available at: <https://www.dropbox.com/s/9cifm8z3j8kr6u7/Annexe .14.R?dl=0>.

Annex A.14– R script containing the R functions used in the main reconstruction R script.
Available at: <https://www.dropbox.com/s/9qtwqinzjg7hn4d/Annexe .15.R?dl=0>

Annex A.15

Moltenophlebia lindae gen. et sp. nov. reconstruction, detailed information on landmarks positioning. Includes Supplementary Figure 1 with landmarks positions and Supplementary Table 1 with detailed information on landmarks positioning (Supplemental Data 1).

&

Annex A.16

Description of the R functions associated with the wing reconstruction of *Moltenophlebia lindae* in Chapter 4 (Supplemental Data 4).

In: The wing venation of a new fossil species, reconstructed using geometric morphometrics, adds to the rare fossil record of Triassic Gondwanian Odonata

Supplemental Data 1: *Moltenophlebia lindae* gen. et sp. nov. reconstruction,
detailed information on landmarks positioning

Deregnacourt, I.^{*,1,2}, Bardin, J.¹, Anderson, J. M.³, and Béthoux, O.¹

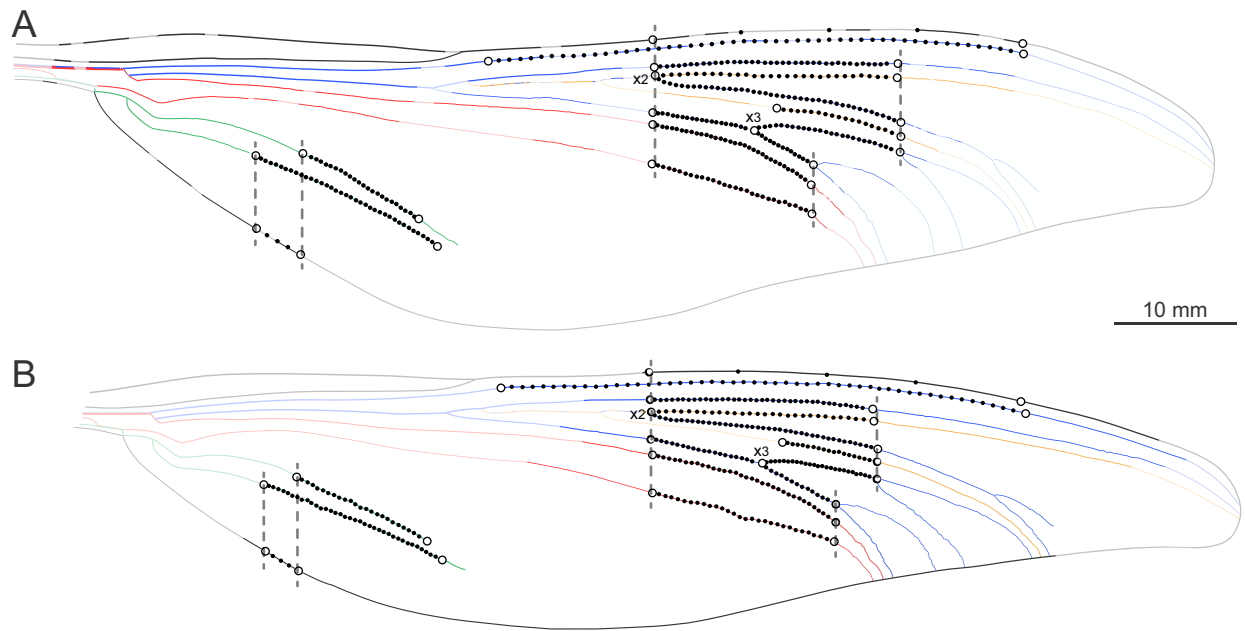
¹Centre de Recherche sur la Paléontologie – Paris (CR2P), Sorbonne Université, MNHN, CNRS, 57 rue Cuvier, CP38, F-75005 Paris, France

²Centre d'Ecologie et des Sciences de la Conservation (CESCO), Sorbonne Université, MNHN, CNRS, 43 rue Buffon, 75005, Paris, France

³Environmental Studies Institute, Witwatersrand University, 1 Jan Smuts Ave., Braamfontein, Johannesburg 2000, South Africa

To obtain a reconstruction of *Moltenophlebia lindae* gen. et sp. nov. we inferred missing parts of the specimen PRE/F/20522 (light lines in Fig. 2A in main document) based on the specimen PRE/F/10626 (dark lines in Fig. 2B in main document), and vice-versa. To do so we placed landmarks and semi-landmarks on fourteen homologous vein portions. The information about the placement of landmarks and semi-landmarks on each vein portion for each specimen is detailed in the Supplementary Figure 1 and Supplementary Table 1.

*Corresponding author: deregnacourt.isa@gmail.com



Supplementary Figure 1: *Moltenophlebia lindae* gen. et sp. nov. from Carnian (Triassic) of Aasvoëlberg locality, Molteno Formation, Karoo Basin, South Africa, line drawings of homologous vein portions used for reconstruction. **A**, specimen PRE/F/20522 (left wing; holotype). **B**, specimen PRE/F/10626 (right wing; paratype). White dots correspond to homologous points used as landmarks; small black dots correspond to semi-landmarks; "x2" and "x3" indicate where several landmarks are superimposed; dotted lines indicate particular alignments used to place landmarks (see Supplementary Table 1); light lines were reconstructed.

Supplementary Table 1: Information on the position of non-sliding landmarks (white dots in Supplementary Figure 1), considered as homologous points for the reconstruction of specimen PRE/F/20522 and PRE/F/10626 of *Moltenophlebia lindae* n. gen. n. sp., and number of associated sliding semi-landmarks placed for each homologous vein portion. LMs = landmarks; RA = anterior Radius; RP = posterior Radius; MA = anterior Media; MP = posterior Media; CuA = anterior Cubitus; CuP = posterior Cubitus.

			Specimen PRE/F/20522	Specimen PRE/F/10626
anterior wing margin	non-sliding LMs	first	opposite the point of origin of the free portion of RP2 (extrapolation based on preserved portions)	opposite the point of origin of the free portion of RP2
		last	end of the preserved section	manual pre-alignment, opposite the end of the preserved section in specimen PRE/F/20522
	number of sliding LMs		3	
RA	non-sliding LMs	first	manual pre-alignment, opposite the beginning of the preserved section in specimen PRE/F/10626	beginning of the preserved section
		last	end of the preserved section	manual pre-alignment, opposite the end of the preserved section in specimen PRE/F/20522
	number of sliding LMs		49	
RP1	non-sliding LMs	first	opposite the point of origin of the free portion of RP2 (extrapolation based on preserved portions)	opposite the point of origin of the free portion of RP2
		last	opposite the RP3 fork (RP3a-RP3b fork)	
	number of sliding LMs		38	
Irp₁-rp₂	non-sliding LMs	first	point of origin of the free portion of RP2 (extrapolation based on preserved portions)	point of origin of the free portion of RP2
		last	opposite the RP3 fork	
	number of sliding LMs		28	
RP2	non-sliding LMs	first	point of origin of the free portion of RP2 (extrapolation based on preserved portions)	point of origin of the free portion of RP2
		last	opposite the RP3 fork	
	number of sliding LMs		41	
Irp₁₊₂-rp₃₊₄	non-sliding LMs	first	manual pre-alignment, opposite the beginning of the preserved section in specimen PRE/F/10626	beginning of the preserved section
		last	opposite the RP3 fork	
	number of sliding LMs		17	
RP3+4	non-sliding LMs	first	opposite the point of origin of the free portion of RP2 (extrapolation based on preserved portions)	opposite the point of origin of the free portion of RP2
		last	RP3-RP4 fork	
	number of sliding LMs		19	

Table 1 – *Continued on next page*

Table 1 – *Continued from previous page*

RP3	non-sliding LMs	first	RP3-RP4 fork	
		last	RP3 fork	
	number of sliding LMs		25	
RP4	non-sliding LMs	first	RP3-RP4 fork	
		last	RP4 fork (RP4a-RP4b fork)	
	number of sliding LMs		13	
MA	non-sliding LMs	first	opposite the point of origin of the free portion of RP2 (extrapolation based on preserved portions)	opposite the point of origin of the free portion of RP2
		last	opposite the RP4 fork	
	number of sliding LMs		33	
MP	non-sliding LMs	first	opposite the point of origin of the free portion of RP2 (extrapolated based on preserved portions)	opposite the point of origin of the free portion of RP2
		last	opposite the RP4 fork	
	number of sliding LMs		28	
CuA	non-sliding LMs	first	manual pre-alignment, opposite the beginning of the preserved section in specimen PRE/F/10626	beginning of the preserved section
		last	manual pre-alignment, opposite the end of the preserved section in specimen PRE/F/10626	end of the preserved section
	number of sliding LMs		23	
CuP	non-sliding LMs	first	manual pre-alignment, opposite the beginning of the preserved section in specimen PRE/F/10626	beginning of the preserved section
		last	end of the preserved section	manual pre-alignment, opposite the end of the preserved section in specimen PRE/F/20522
	number of sliding LMs		36	
posterior wing margin	non-sliding LMs	first	manual pre-alignment, opposite the beginning of the preserved section of CuP in the specimen PRE/F/10626	opposite the beginning of the preserved section of CuP
		last	manual pre-alignment, opposite the beginning of the preserved section of CuA in the specimen PRE/F/10626	opposite the beginning of the preserved section of CuA
	number of sliding LMs		3	

In: The wing venation of a new fossil species, reconstructed using geometric morphometrics, adds to the rare fossil record of Triassic Gondwanian Odonata

Supplemental Data 4: Functions associated with the wing reconstruction

Deregnacourt, I.^{*,1,2}, Bardin, J.¹, Anderson, J. M.³, and Béthoux, O.¹

¹Centre de Recherche sur la Paléontologie – Paris (CR2P), Sorbonne Université, MNHN, CNRS, 57 rue Cuvier, CP38, F-75005 Paris, France

²Centre d'Ecologie et des Sciences de la Conservation (CESCO), Sorbonne Université, MNHN, CNRS, 43 rue Buffon, 75005, Paris, France

³Environmental Studies Institute, Witwatersrand University, 1 Jan Smuts Ave., Braamfontein, Johannesburg 2000, South Africa

Contents

full_landmarks_set	2
collect.landmarks.ps	3
collect.landmarks	4
define_sliders	4
liste_sliding_semiauto	4
partial_curves_delineation	5
retrodeformation	6
superposition	7
deformation	8

The main script "Supplemental_Data_2.R" calls several functions to perform the two steps of the wing reconstruction presented in the Fig. 1 of the manuscript. All these functions are available in "Supplemental_Data_3.R" script.

For details, the main function `full_landmarks_set` allows the placement of landmarks and semi-landmarks and the selection of vein portions. It also creates a matrix specifying the position of the semi-landmarks between which the sliding semi-landmarks are allowed to slide. To do so it calls the functions `collect.landmarks.ps` (itself calling `collect.landmarks`),

*Corresponding author: deregnacourt.isa@gmail.com

`define_sliders`, `liste_sliding_semiauto`, and `partial_curves_delineation`. The results can therefore be used to perform a Procrustes superimposition. A retro-deformation can be performed as needed before this last step. Finally the Thin Plate Spline deformation can be performed.

full_landmarks_set

Description

Imports Postscript files in 'Picture' object using the package `grimport` (Murrell 2009). Allows the placement of type I landmarks and automatically places semi-landmarks along selected curves with specific color-coding. Creates a matrix specifying the position of the semi-landmarks between which the sliding semi-landmarks are allowed to slide. Allows the selection of portions of vein.

Usage

```
full_landmarks_set(nblm, couleurs, nervation, coeff_nervation,  
                  nervure, nn, coeff_nervure, select, start=NA, sl)
```

Arguments

<code>nblm</code>	The number of type 1 landmarks to select.
<code>couleurs</code>	A numeric vector specifying the color-coding of each curves.
<code>nerivation</code>	A character vector specifying the name of each curves.
<code>coeff_nervation</code>	A numeric vector specifying the proportion of pixel to be used as semi-landmarks for each curve.
<code>nervure</code>	A character vector specifying the name of the veins from which only one or several portions will be used.
<code>nn</code>	A numeric vector containing the number of portions to select for each curve specified in 'nervure'
<code>coeff_nervure</code>	A numeric vector specifying the proportion of pixel to be used as semi-landmarks for each curve specified in 'nervure'.
<code>select</code>	A logical vector specifying which vein portion specified in 'nervure' already have homologous start and end coordinates. False if these coordinates have to be selected.
<code>start</code>	A list of matrices specifying start and end coordinates for vein portions specified in 'nervure'. NA as default value.
<code>sl</code>	The number of veins with sliding semi-landmarks.

Value

A list with the following components:

<code>wing_names</code>	A character vector specifying the name of each wing.
<code>wing_coordinates</code>	A list of matrices specifying the x and y coordinates of all the pixels of each wing.
<code>landmarks</code>	An array specifying the landmarks and semi-landmarks coordinates of each wing.
<code>sliders</code>	A matrix of 3 column ("before","slide","after") specifying the position of the semi-landmarks between which the sliding semi-landmarks will slide. To be used in the function <code>gpa-gen</code> (geomorph package) for example.
<code>start</code>	A list of matrices specifying start and end coordinates for vein portions selected.

References

Murrell P. 2009. Importing vector graphics: The `grImport` package for R. *Journal of Statistical Software* 30(4):1–37

`collect.landmarks.ps`

Description

Converts a 'Picture' object (package `grImport`, Murrell 2009) into matrix of x and y coordinates. Allows the placement of type I landmarks by calling the function `collecting.landmarks`.

Usage

```
collect.landmarks.ps(nblm, names.lm = paste("lm", 1:nblm, sep=""),
                    imgs= myWings, Wings=Wings)
```

Arguments

<code>nblm</code>	The number of type 1 landmarks to select.
<code>names.lm</code>	A character vector specifying landmarks names.
<code>imgs</code>	A character vector specifying the name of each wing.
<code>Wings</code>	A list of 'Picture' objects corresponding to each wing.

Value

A list with the following components:

<code>landmarks1</code>	An array specifying the x and y coordinates of the selected type I landmarks for each wing.
<code>wing_coordinates</code>	A list of matrices specifying the x and y coordinates of all the pixels of each wing.

References

Murrell P. 2009. Importing vector graphics: The `grImport` package for R. *Journal of Statistical Software* 30(4):1–37

collect.landmarks

Description

Allows the placement of type I landmarks.

Usage

```
collect.landmarks(numLands, names.lm, imgs)
```

Arguments

<code>numLands</code>	The number of type 1 landmarks to select.
<code>names.lm</code>	A character vector specifying landmarks names.
<code>imgs</code>	A character vector specifying the name of each wing.

Value

An array specifying the x and y coordinates of the selected type I landmarks for each wing.

define_sliders

Description

Creates a matrix specifying the sliding semi-landmarks position.

Usage

```
define_sliders(s1, nb_semi, nblm = 0)
```

Arguments

<code>s1</code>	The number of veins with sliding semi-landmarks.
<code>nb_semi</code>	A vector specifying the number of semi-landmarks for each curve.
<code>nblm</code>	The number of type I landmarks to select.

Value

A matrix of 3 column ("before","slide","after") specifying the position of the semi-landmarks between which the sliding semi-landmarks will slide.

liste_sliding_semiauto

Description

Selects each curve according to their color-coding and automatically places semi-landmarks along them.

Usage

```
liste_sliding_semiauto(couleurs, nervation, imgs=myWings, Wings=Wings,  
coeff)
```

Arguments

<code>couleurs</code>	A numeric vector specifying the color-coding of each curves.
<code>nervation</code>	A character vector specifying the name of each curves.
<code>imgs</code>	A character vector specifying the name of each wing.
<code>Wings</code>	A list of 'Picture' objects corresponding to each wing (package <code>grImport</code> , Murrell 2009).
<code>coeff</code>	A numeric vector specifying the proportion of pixel to be used as semi-landmarks for each curve.

Value

A list with the following components:

<code>InfoCurves</code>	A dataframe specifying information linked to each curve: curve index, color-coding, name and the wing index.
<code>Curves</code>	A list of matrices specifying the x and y coordinates of each curve.
<code>sampleCurves</code>	A list of matrices specifying the x and y coordinates of the semi-landmarks on each curve.
<code>nbsemi</code>	A vector specifying the number of semi-landmarks for each homologous curve specified in the argument 'nervation'.

References

Murrell P. 2009. Importing vector graphics: The `grImport` package for R. *Journal of Statistical Software* 30(4):1–37

`partial_curves_delineation`

Description

Allows the selection of start and end points for vein portions. Automatically places semi-landmarks along the portions.

Usage

```
partial_curves_delineation(nervure, nn, InfoCurves, Curves,  
                           imgs=myWings, coeff, select, start=NA)
```

Arguments

<code>nervure</code>	A character vector specifying the name of the veins to select a portion on.
<code>nn</code>	A numeric vector containing the number of portions to select for each curve specified in 'nervure'.
<code>InfoCurves</code>	A dataframe specifying information linked to each curve: curve index, color-coding, name and the wing index.
<code>Curves</code>	A list of matrices specifying the x and y coordinates of each curve.
<code>imgs</code>	A character vector specifying the name of each wing.
<code>coeff</code>	A numeric vector specifying the proportion of pixel to be used as semi-landmarks for each curve.
<code>select</code>	A logical vector specifying which vein portion specified in 'nervure' already have homologous start and end coordinates. False if these coordinates have to be selected.
<code>start</code>	list of matrices specifying start and end coordinates for vein portions specified in 'nervure'. NA as default value.

Value

A list with the following components:

<code>Landmarks_partial</code>	A list of matrices specifying the x and y coordinates of the semi-landmarks on each portion.
<code>nbsemi_partial</code>	A vector specifying the number of semi-landmarks for each portion.
<code>selection_partial</code>	A list of matrices specifying start and end coordinates for each portion selected.

retrodeformation

Description

Creates 407 retro-deformed wings, applying 37 rotations from -90° to 90° and 11 elongations from 100% to 200% and compiles them on a list also containing the information of the other wing (the one to be completed).

Usage

```
retrodeformation(landmarks, wing_corrdinates, a, b)
```

Arguments

<code>landmarks</code>	An array specifying the landmarks and semi-landmarks coordinates of each wing.
<code>wing_coordinates</code>	A list of matrices specifying the x and y coordinates of all the pixels of each wing.
<code>a</code>	The index of the wing to be completed by the one that will be retro-deformed.
<code>b</code>	The index of the wing to be retro-deformed.

Value

A list with the following components:

<code>landmarks</code>	An array specifying the landmarks and semi-landmarks coordinates of each wing, the wing indexed 'a' then the 407 retro-deformed wings 'b'.
<code>Info_def</code>	A list of matrices specifying the landmarks and semi-landmarks coordinates of each wing and the rotation and the elongation information for each wing.
<code>wings_coordinates</code>	A list of matrices specifying the x and y coordinates of all the pixels of each wing.

superposition

Description

Performs and plot the Procrustes superimposition by calling the function `gpagen` from the `geomorph` package (Adams and Otarola-Castillo 2013).

Usage

```
superposition(lm, sliders, Sliding=T, Bending=T, imgs)
```

Arguments

<code>lm</code>	An array specifying the landmarks and semi-landmarks coordinates of each wing.
<code>sliders</code>	A matrix of 3 column ("before", "slide", "after") specifying the position of the semi-landmarks between which the sliding semi-landmarks will slide.
<code>Sliding</code>	A logical value indicating whether or not the semi-landmarks are allowed to slide.
<code>Bending</code>	A logical value indicating if the bending energy method should be used to slide the semi-landmarks. If <code>FALSE</code> the Procrustes distances method is used.
<code>imgs</code>	A character vector specifying the name of each wing.

Value

An object of class `gpagen`. See `gpagen` function description.

References

Adams DC, Otarola-Castillo E. 2013. Geomorph: an R package for the collection and analysis of geometric morphometric shape data. *Methods in Ecology and Evolution* 4(4):393–399

deformation

Description

Performs a Thin Plate Spline deformation on all the pixels of a selected wing onto another wing by fitting the landmarks and semi-landmarks.

Usage

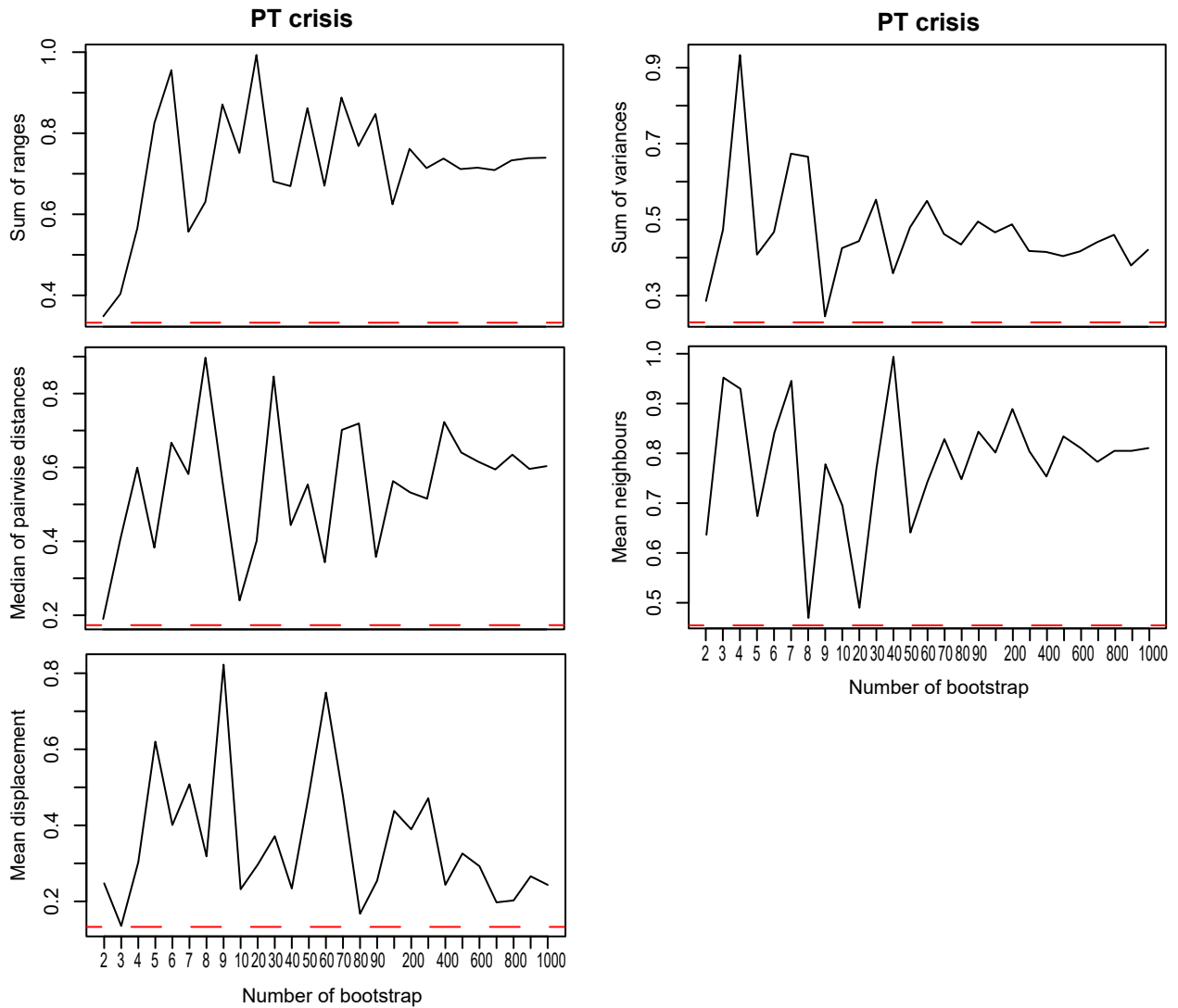
```
deformation(a, b, superpos, lm, px_coordinates )
```

Arguments

<code>a</code>	The index of the wing to be reconstructed.
<code>b</code>	The index of the wing used to reconstruct the wing 'a'.
<code>superpos</code>	An object of class <code>gpagen</code> resulting from the Procrustes superimposition of the wing 'a' and 'b'.
<code>lm</code>	An array specifying the landmarks and semi-landmarks coordinates of each wing.
<code>px_coordinates</code>	A list of matrices specifying the x and y coordinates of all the pixels of each wing.

Value

A matrix of x and y coordinates of all the pixels of the deformed wing.



Annex A.17 – Test of the impact of the number of bootstraps on the p-value obtained by a permutation test, comparing Permian and Triassic species. Dotted red line correspond to a p-value of 0.05

Annex A.18– First 3 axes of the principal component analysis of the 34 fossil species. Red dots correspond to the Permian species; Violet dots to the Triassic ones; convex hull represent the morphospace occupation of each period. This interactive 3D plot is available at: <https://www.dropbox.com/s/8944mf1yr1f8aua/Annexe .19.html?dl=0>. The perenity of the link will be ensure at least until the thesis defence. This .html file needs to be download and then open in a browser.

List of Figures

- 1 Idealized diversity histories (modified from Foote, 1993b, Fig. 1, p. 192) and the corresponding potential diversity and disparity curves over time. The evolution of three metrics of disparity is represented: size, dispersion and position. **A-C**, diversification events; **D-G**, extinction events. Dotted black line correspond to diversity; red line corresponds to size metric, orange line to dispersion and violet line to position; arrows (on **D-G**) indicate time of maximal taxonomic diversity. 3
- 1.1 *Megatypus schucherti* Tillyard, 1925 from the Elmo locality (Early Permian, Kansas, USA). **A, D**, wing venation interpretation according to Tillyard (1925), overview (**A**) and details of the base (**D**); **C, D**, wing venation interpretation according to Riek and Kukalová-Peck (1984), overview (**C**) and details of the base (**F**); **B**, photograph, overview; **E**, photograph of the wing base. Red arrow on D corresponds to the location of a supposed distinct MP according to Tillyard (1925). From Béthoux et al. (*in prep.*). . 10
- 1.2 †*Protomyrmeleon brunonis* Geinitz, 1887, specimen MNHN.F.A40897 (one of the two overlapping wings represented, left wing; all drawings flipped horizontally); Toarcian (Jurassic), Bascharage, Grand Duchy of Luxembourg. **A, B**, wing venation interpretation according to Zessin (1991), overview (**A**) and details of the radial area as located on **A** (**B**), main veins thickness increased for clarity; **C, D**, wing venation interpretation according to Nel and Henrotay (1992) , overview (**C**) and details of the radial area as located on **C** (**D**), main veins thickness increased for clarity; **E, F**, new interpretation, overview (**E**) and details of the radial area as located on **E** (**F**), main veins thickness increased for clarity. 13
- 1.3 Proposed terminology for paired intercalaries (pI), based on RTI extracts of extant Zygoptera wing apices, specular enhancement (see text for details; Rosser W. Garrison collection). **A**, right hindwing in dorsal view of a male *Dimeragrion percubitale* Calvert, 1913; **B**, right hindwing in dorsal view of a male *Heliocharis amazona* Selys, 1853. 14
- 1.4 Proposed summarized phylogeny of Protomyrmeleontoidea. 15

1.5	† <i>Terskeja pumilio</i> Pritykina, 1981, redrawn with minor modifications from Pritykina (1981: fig. 25).	16
1.6	† <i>Moltenagrion koningskroonensis</i> gen. et sp. nov., specimen PRE/F/10334 (right wing); Carnian (Triassic), Konings Kroon, Molteno Formation, Karoo Basin, South Africa. A , drawing, wing venation interpretation favoured herein; B , photograph; C–E , details of the radial area (drawings, main veins thickness increased for clarity); C , wing venation interpretation favoured herein; D , photograph, as located on B ; E , wing venation interpretation according to Zessin (1991); F , wing venation interpretation according to Nel and Henrotay (1992).	18
1.7	Hindwing base of a male <i>Calopteryx splendens</i> (Harris, 1780)	21
1.8	Hindwings apex of A , a male <i>Aeshna isoceles</i> (Müller, 1767) with a seemingly branched Irp_{1+2} - rp_{3+4} ; B , a female <i>Aeshna caerulea</i> (Störm, 1783) with a simple Irp_{1+2} - rp_{3+4} . Orange dotted line correspond to the seemingly anterior branch of Irp_{1+2} - rp_{3+4} , orange arrow indicate its end.	22
1.9	Forewing base of a male <i>Sympetrum flaveolum</i> (Linnaeus, 1758) with all the possible courses of CuA represented.	23
1.10	A , basic pattern of homologous main veins on odonates wings applied to: B , C , forewing and hindwing of a male <i>Libellula quadrimaculata</i> (Linnaeus, 1758; D , E , forewing and hindwing of a male <i>Onychogomphus forcipatus</i> (Linnaeus, 1758).	24
1.11	Basic pattern of homologous main veins on odonates wings applied to: A , hindwing of a male <i>Calopteryx virgo</i> (Linnaeus, 1758); B , hindwing of a female <i>Ceriagrion tenellum</i> (Villers, 1789); C , <i>Tupus gracilis</i> Carpenter, 1947, photo of the specimen PALE-4819 from the MCZbase; D , imprint of specimen PRE/F/10442a from the Molteno formation, apex completed by the counterprint PRE/F/10442b.	25
2.1	Mounting adapted from Perrard et al. (2012) used to picture odonate wings. Specimen in the picture is a pinned <i>Macromia splendens</i> (Pictet, 1843) male from the Zoologische Staatssammlung München.	30
2.2	Forewing of a male of <i>Anax parthenope</i> (Selys, 1839). Light orange structure is the supertriangle; dark orange structure is the triangle.	33
2.3	Forewing of a male of <i>Crocothemis erythraea</i> (Brullé, 1832). Photograph and vector line drawing of veins and vein portions with the associated color-code, followed by a flow-chart summarizing the steps of the R script designed to place landmarks and semi-landmarks automatically, based on color-code, to be further used for geometric morphometrics analyses. Violet frame on the wing: RGB color-codes.	34

2.4	Two Block-Partial Least Squares between two different landmarks datasets on the same 15 forewings of male Anisoptera. Along x axis: PLS scores of Blanke (2018) dataset of 60 landmarks; along y axis: PLS scores of our dataset with a maximum of sliding semi-landmarks and using sliding method minimizing Procrustes distances.	36
2.5	Illustration of the sliding methods. A. Minimum Bending Energy criterion: (a1) semi-landmarks slide along an outline tangent (a2) and are projected onto the outline after relaxation step. B. Minimum Procrustes distances criterion: semi-landmarks (b1) before and (b2) after sliding towards the line perpendicular to the edge of the corresponding semi-landmarks of the reference. Modified from Perez et al. (2006).	37
2.6	Thin plate Spline deformation of <i>Zygophlebia ramosa</i> Pritykina, 1981 onto <i>Moltenophlebia lindae</i> Deregnaucourt et al., <i>in review</i> after Procrustes superimposition sliding semi-landmarks under two different criteria: A. minimizing Procrustes distances, B. minimizing Bending Energy. Boxes correspond to zoom on areas showing unwanted distortion under the minimizing Procrustes distances criterion.	38
2.7	Principal component analyses and a representation of the placement of the landmarks and semi-landmarks on the anterior wing of <i>Aeshna affinis</i> for each tested coefficient defining the number of semi-landmarks. Unrealistic distortions appear starting from subfigure E (coefficient 0.002). A. coefficient of 0.0004, B. 0.0006, C. 0.0008, D. 0.001, E. 0.002, F. 0.003	40
2.8	Principal component analysis of the 304 wing pairs considered as reference for species monitored in mainland France by the Steli program. Observations are coloured by species. Coloured areas delimit families. Large and small triangles represent female forewings and hindwings, respectively, while large and small squares represent male forewings and hindwings, respectively.	44
2.9	Distribution of reference shape for each species in the global morphospace. Observations are coloured by species. Coloured areas as in Fig. 2.8 delimit the space occupied by each families prior to the computation of species reference shape.	46

3.1	Maps of the MOS 2017 of the Ile-de-France region. White dots correspond to the selected sites position. Sites numbering are the ones from the Steli database. Gauges represent species richness. Triangle-shaped graphs correspond to the proportion of size, density and position metrics for each site, minimum and maximum values of each metric axes correspond to the minimum and maximum values obtained among all the sites; represented density metric is the average nearest neighbour distances.	53
3.2	Plot of the two first axes of PCA that summarize morphospace of odonates monitored under the Steli framework in mainland France. Only the species present in the selected sites of Ile-de-France during the second protocol period are represented.	59
3.3	Pairwise correlations between the five disparity estimates, the percentage of favourable and unfavourable areas within a 500 m radius buffer and the number of species and families. Figures on the upper right corner are the Spearman correlations. ***,** and * correspond respectively to p-value between 0 and 0.001, 0.001 and 0.01, and 0.01 and 0.05. Red crosses indicate sites with less than 7 monitored species ; red figures indicate Spearman correlations for the 15 sites with more than 6 monitored species.	60
3.4	Five disparity estimates for each of the 20 sites. Composed names indicate a site number and the year it was monitored. Sites are ordered by species richness. Grey barplots represent the number of species. Red continuous line represents the percentage of unfavourable land cover within a 500m radius buffer around each site using the MOS 2017, red dotted one using the MOS 2012. Green continuous line represents the favourable land cover in the buffer using the MOS 2017,green dotted line using the MOS 2012. .	62
3.5	Five disparity estimates for each of the 19 sites with subgroup division in Anisoptera+Zygoptera. Composed names indicate a site number and the year it was monitored. Sites are ordered by total species richness. Pink and blue barplots represent the number of Anisoptera and Zygoptera species respectively; number of species of each group is indicated in white. Grey dots represent disparity estimates for odonates as one group; black dots, Anisoptera+Zygoptera disparity estimates; pink dots, Anisoptera disparity estimates; blue dots, Zygoptera disparity estimates.	65
3.6	Percentage of favourable and unfavourable areas for each sites within buffers of, in order, 500m, 1000m and 2000m radii. Green dots represent favourable areas; red dots, unfavourable ones. Lines connect for each site the percentage of each of the two areas for the 3 different radii (for each site, from left to right, 500m, 1000m and 2000m radii).	66

- 3.7 Mean of five disparity estimates for species considered common or rare. **A**, rarity based on presence on site frequency (>50% and <10% of the sites); **B**, rarity based on cumulated abundance of the species. * correspond respectively to p-value below 0.05 computed with a permutation test. Com. =Common; n. n. =nearest neighbour. 69
- 3.8 Five disparity estimates for all species monitored in Ile-de-France (on the studied sites). Composed names indicate a site number and the year it was monitored. Sites are ordered by species richness. Orange dots represent disparity estimates for all monitored species; green dots, disparity estimates without threatened species. Figures are the mean value of each disparity estimates. 72
- 3.9 Five disparity estimates for each of the 20 sites. Composed names indicate a site number and the year it was monitored. Sites are ordered by species richness. Light grey and dark grey bar-plots represent the number of species with and without the threatened ones, respectively. Orange dots represent disparity estimates for all monitored species; green dots, disparity estimates without threatened species. 73
- 4.1 Non-exhaustive summarized phylogeny of Odonata. Dots correspond to genera present during the Permian and/or the Triassic. Empty dots correspond to genera absent from the analysis and full dots to the ones present. This phylogeny is based on Bechly (2007), Nel et al. (2001), Nel et al. (2012), Deregnaucourt et al. (2019), and Tierney et al. (2020). 82
- 4.2 Flow-chart explaining the standardized method used to reconstruct the wing of specimen PRE/F/20522. **A**, first step, reconstruction of specimen PRE/F/20522 with specimen PRE/F/10626. **B**, second step, reconstruction of the firstly reconstructed wing of specimen PRE/F/20522 with the holotype of *Zygophlebia ramosa* PIN 2785/20. GPA = generalised Procrustes analysis; TPS = thin plate splines; squares correspond to process and circles to data. 87

- 4.3 *Moltenophlebia lindae* gen. et sp. nov., from Carnian (Triassic) of Aasvoëlberg locality, Molteno Formation, Karoo Basin, South Africa, line drawings. **A**, specimen PRE/F/20522 (left wing; holotype). **B**, specimen PRE/F/10626 (right wing; paratype). **C**, specimen PRE/F/10615 (left wing). RA = anterior Radius; RP = posterior Radius; RP1+2 = anterior branch of RP (to be further divided into RP1 and RP2); RP3+4 = posterior branch of RP (to be further divided into RP3 and RP4); Irp_{1-rp2} = intercalary vein between RP1 and RP2; Irp_{1+2-rp3+4} = intercalary vein between RP1+2 and RP3+4; MA = anterior Media; MP = posterior Media; CuA = anterior Cubitus; CuP = posterior Cubitus. Light lines were reconstructed. 92
- 4.4 *Moltenophlebia lindae* gen. et sp. nov., from Carnian (Triassic) of Aasvoëlberg locality, Molteno Formation, Karoo Basin, South Africa, photographs. **A**, specimen PRE/F/20522, left wing (light-mirrored; holotype). **B**, specimen PRE/F/10626a, right wing (light-mirrored, flipped horizontally; paratype). **C**, specimen PRE/F/10615a left wing (flipped horizontally). White frame refers to Fig. 4.5A. 93
- 4.5 Detail of the area of the pillar. **A**, *Moltenophlebia lindae* gen. et sp. nov., detail of specimen PRE/F/20522, left wing base (light-mirrored; holotype). **B–C**, schemes of the respective positions of CuP and of the pillar in **B**, *Moltenophlebia lindae* gen. et sp. nov and **C**, as assumed for Zygophlebiidae. RA = anterior Radius; RP = posterior Radius; MA = anterior Media; MP = posterior Media; CuA = anterior Cubitus; CuP = posterior Cubitus; large black arrow in **A** indicates the pons; white arrows in **B** indicate the pillar; green arrows (grey in grayscale version) in **A** indicate the portion of CuP basal to the pillar (and see Fig. 4.4A); small white arrows (bordered in green -gray in grayscale version) in **B** indicate the CuA-CuP split. . . . 94
- 4.6 Vector line drawings of *Moltenagrion koningskroonensis* (**A**) and Protomyrmeleontidae used to reconstruct its apex. **B**, *Mongolagrion shartengensis*; **C**, *Obotritagrion petersi*; **D**, *Protomyrmeleon brunonis*; **E**, *Saxomyrmeleon keatingei*; **F**, *Triassagrion australiense*. 99
- 4.7 First 3 axes of the principal component analysis of the 34 fossil species and wing shapes and deformation grids associated to extremes of each axes. Triangles represent the Triassic species and points the Permian ones. Species are coloured by taxa. Interactive 3D plot of the first three axes of this PCA available in Annex A.18. 106

4.8	Mean of the 500 bootstraps of five disparity estimates for the Permian and the Triassic. Red barplots correspond to the Permian and violet to the Triassic. Black segments represent the minimum and maximum of bootstraps for each estimates.	107
A.4	Maps of the 500m radius buffer around each sites considered in Ile-de-France. Legend correspond to the MOS 2017.	139
A.5	Test of the impact of the number of bootstraps on the p-value obtained by a permutation test, comparing common and rare species. Left column correspond to assessed rarity based on abundance of each species, right column correspond to assessed rarity based on site frequency of each species. Dotted red line correspond to a p-value of 0.05	140
A.6	Morphospace occupied by species present on each of the 20 sites considered in Ile-de-France within the two first axes of the global morphospace. Global morphospace is represented by the two first axes of the PCA of the 79 odonate species monitored under the Steli framework in mainland France. .	142
A.7	Five disparity estimates values computed on 1 to 76 PCs of the PCA realised on the 79 species monitored in France by the Steli program during the interval 2011-2019. The used PC scores are the mean values computed for the reference shape of each species.	143
A.8	Values of the sum of ranges computed with bootstraps sets for sampling quota varying from 3 to 11 species for each site selected in Ile-de-France. .	144
A.9	Values of the sum of variances computed with bootstraps sets for sampling quota varying from 3 to 11 species for each site selected in Ile-de-France. .	145
A.10	Values of the average median pairwise distances computed with bootstraps sets for sampling quota varying from 3 to 11 species for each site selected in Ile-de-France.	146
A.11	Values of the average nearest neighbour distances computed with bootstraps sets for sampling quota varying from 3 to 11 species for each site selected in Ile-de-France.	147
A.12	Values of the average displacement computed with bootstraps sets for sampling quota varying from 3 to 11 species for each site selected in Ile-de-France.	148
A.17	Test of the impact of the number of bootstraps on the p-value obtained by a permutation test, comparing Permian and Triassic species. Dotted red line correspond to a p-value of 0.05	162

List of Tables

- 2.1 RGB color-codes used for each vein or portion of vein on vector lines drawings. 33
- 2.2 Species observed in France from 2011 to 2019 in the STELI database . . . 41
- 2.3 Results of the paired Hotteling t^2 test realised on the scores of the 6 first principal components. The column "Group" indicate the group on which the test has been performed, the "Comparison" one the parameters that have been compared, the "MVN" one indicate the results of the Multivariate Normality tests. * refers to significant values. FW = forewing; HW =hindwing. 45
- 3.1 Nomenclature of the MOS 2017 in 81 land-cover types and the attributed category relative to odonate ecology. 54
- 3.2 List of species monitored in Ile-de-France under the Steli framework with their associated regional Red List categories. The abundance category correspond to the rarity of the species assessed based on the standardized abundance data. Site frequency category correspond to the rarity assessed base on the number of sites the species are present. 57
- 3.3 Estimates of disparity for each sites in Ile-de-France and associated number of species and families. The value for disparity estimates correspond to the mean of the rarefied bootstrapped result except for the sites 364, 365, 1418, 1676 and 1761 for which rarefaction could not be computed. For those sites disparity estimates were directly calculated without resorting to bootstrap. 59

4.1	List of fossil specimens used in the morphometric analysis. Source correspond to the source of pictures vector lines drawings are based on. Institutional acronyms: BP, Bernard Price Institute for Palaeontology (Pretoria, South Africa), material actually housed at the Evolutionary Studies Institute, University of the Witwatersrand (Johannesburg, South Africa); IGLP, Institut de Geologie, Université Louis Pasteur (Strasbourg, France); Ld LAP, Lapeyrie collection, Musée Fleury (Lodève, France); MCZ, Museum of Comparative Zoology (Harvard, USA); NIGP, Nanjing Institute of Geology and Palaeontology, Chinese Academy of Sciences (Nanjing, China); NRPS, Paleozoology, Naturhistoriska Riksmuseum (Stockholm, Sweden); PRE, Bernard Price Institute for Palaeontology (Pretoria, South Africa), , material actually housed at the Evolutionary Studies Institute, University of the Witwatersrand (Johannesburg, South Africa); PIN, Arthropod Laboratory, Palaeontological Institute, Russian Academy of Science (Moscow, Russian Federation); QMF, Geosciences Collection, Queensland Museum (Hendra, Australia); GQS, Queensland Geological Survey (Brisbane, Australia); WU, University of Wichita (Wichita, USA); UT, University of Texas (Austin, USA).	102
4.2	Estimates of disparity for Permian and Triassic and p-value issued for a permutation test. The values correspond to the mean of the 500 bootstraps.	107
A.2	List of the specimens used in this study, their sexe and their location. MNHN = Muséum National d'Histoire Naturelle; ZSM = Zoologische Staatssammlung München; WC = working collection.	137
A.3	Importance of the first 6 components of the PCA realised on the 79 species monitored in France by the Steli program during the interval 2011-2019, each represented by forewings and hindwings of 2 females and 2 males. . .	138

Résumé : Les organismes ont été, au cours du temps, fortement affectés par cinq crises majeures et les activités humaines mènent à une sixième. Il est difficile de comparer ces extinctions grâce à la richesse spécifique, en partie à cause de biais d'échantillonnage. La disparité, visant à quantifier la diversité morphologique, peut-être une approche pertinente. Le contraste entre la diversité taxonomique et morphologique a été utilisé pour étudier les propriétés des extinctions dans le registre fossile. La disparité a toutefois été rarement appliquée à la biologie de la conservation. Nous étudions, ici, l'impact sur la disparité des ailes d'Odonata (1) de l'artificialisation de l'occupation des sols et (2) de l'extinction de masse Permo-Triassique. Pour quantifier la morphologie alaire, nous avons élaboré un patron de base d'homologies de nervation alaire applicable aux espèces actuelles et fossiles. Nous avons, ensuite, utilisé la morphométrie géométrique et élaboré un set de landmarks et de semi-landmarks optimale. L'impact de l'artificialisation a été étudié sur des sites en Ile-de-France. L'artificialisation et la perte d'espèces n'a pas d'impact significatif sur la disparité, ce qui supporte un scénario d'extinction non-sélective sur la morphologie. Rien n'indique que la morphologie alaire puisse aider à identifier des espèces spécialistes ou généralistes. Aucune différences significatives n'ont été observées entre la disparité et la diversité du Permien et du Trias. Des morphologies extrêmes perdues durant le Permien ont pu être compensées par de nouvelles morphologies extrêmes durant le Trias. Etant donné la résolution temporelle, les effets de la perte et récupération d'espèces ne peuvent être distingués. Les crises actuelles pourraient être comparables, dans leurs effets, aux extinctions de masses passées. Cependant, les données sur les actuelles devraient être élargies à toutes les espèces recensées à travers le monde et la résolution de l'échantillonnage fossile affinée.

Mots clés : Disparité - Odonata - Crises - Artificialisation - Permo-Trias - Reconstruction des parties manquantes - Homologies de nervation alaire - Diversité morphologique - 6^{ème} crise

Disparity, an unified metric to compare the responses of biodiversity to past and current crises: a test with dragonfly wings

Abstract: Organisms through time have been strongly affected by five major crises and human activities are leading to a sixth one. It is difficult to compare these extinctions using species richness, due, in part, to sampling biases. Disparity, aiming at quantifying morphological diversity, might be a relevant approach. The contrast between morphological and taxonomic diversity has been used to address properties of extinction events in the fossil record. Disparity has, however, rarely been applied in conservation biology. Here we investigated the impact on Odonata wing disparity (1) of land cover artificialization and (2) of the Permo-Triassic mass extinction. To quantify wing morphology, we assessed a basic pattern of wing venation homologies applicable to extant and fossil species. We then used a morphometric geometric approach and elaborated an optimal set of landmarks and sliding semi-landmarks. Impact of artificialization has been investigated on sites in Ile-de-France. Artificialization and loss of species do not significantly impact disparity. This support a scenario of a non-morphologically selective extinction. We did not found evidence that wing morphology might help recognition of specialised or generalist species. No significant differences between disparity and diversity of the Permian and the Triassic were observed. Extreme morphologies lost in the Permian may have been compensated with new extreme morphologies during the Triassic. Given the temporal resolution, effects of species loss and recovery cannot be distinguished. Current crises could be comparable in their effects to past mass extinction. However, data on extant should be broadened to all the species monitored worldwide and resolution of fossil sampling refined.

Keywords: Disparity - Odonata - Crises - Artificialization - Permo-Triassic - Missing parts reconstruction - Wing venation homologies - Morphological diversity - 6th crisis